科技部補助專題研究計畫成果報告
期末報告

DnaT 與 DNA 結合性質之研究

計 畫 類 別 ：個別型計畫
計 畫 編 號 ：NSC 102-2320-B-040-019-
執 行 期 間 ：102 年 08 月 01 日至 103 年 07 月 31 日
執 行 單 位 ：中山醫學大學生物醫學科學學系（所）

計 畫 主 持 人：黃晟洋

計畫參與人員：碩士級-專任助理人員：黃彥華
碩士班研究生-兼任助理人員：黃育瑄
大專生-兼任助理人員：林敬傑
大專生-兼任助理人員：何芊儀
大專生-兼任助理人員：徐梁才

報 告 附 件 ：出席國際會議研究心得報告及發表論文

處 理 方 式 ：
1.公開資訊：本計畫可公開查詢
2.「本研究」是否已有嚴重損及公共利益之發現：否
3.「本報告」是否建議提供政府單位施政參考：否

中 華 民 國 103 年 10 月 30 日

中 文 摘 要 ： DnaT 是革蘭氏陰性菌所特有的蛋白質，其角色為複製重啟之引子合成體 (replication restart primosome)組裝與產生活性時所必需要的一員，已知若此活性遭到壓制將對細菌的生長造成極大影響。DnaT 的命名雖與 DNA 複製有關，然先前並不知道它有 DNA 結合的活性。在此計劃執行後，我們已證明 DnaT 擁有強的 DNA 結合活性，並且已進一步的研究了其詳細的 DNA 結合模式。總計這個為期一年的計畫在執行終了後共發表 5 篇 SCI 論文(含一篇 review)。希望這些結果在未來對各種抗藥性細菌包括克雷伯氏菌，能提供初步的標靶藥物設計之建議。

中文關鍵詞： 克雷伯氏肺炎桿菌，DnaT，蛋白質-DNA 交互作用。

英 文 摘 要 ： DnaT protein, only found in the Gram-negative bacteria, is required for assembly of the replication restart primosome. Activity of the replication restart primosome is essential for cell growth and survival. Although DnaT is involved in DNA replication, nothing is known about DNA binding activity of DnaT. In this project, we have showed that DnaT has a strong DNA binding ability relatively higher than those of other members in the primosome, and have detailed the DNA-binding mode. In this one-year project, we have published 5 SCI papers, of which 1 is a review article. We hope these results will provide a new target for drug design for bacterial antibiotics resistances, including Klebsiella pneumoniae.

英文關鍵詞： Klebsiella pneumoniae, DnaT, protein-DNA interactions.

目　　錄

一、計畫摘要

1a. 中文摘要

關鍵詞：克雷伯氏肺炎桿菌，DnaT，蛋白質-DNA 交互作用。

DnaT 是革蘭氏陰性菌所特有的蛋白質，其角色為複製重啟之引子合成體 (replication restart primosome)組裝與產生活性時所必需要的一員，已知若此活性遭到壓制將對細菌的生長造成極大影響。DnaT 的命名雖與 DNA 複製有關，然先前並不知道它有 DNA 結合的活性。在此計劃執行後，我們已證明 DnaT 擁有強的 DNA 結合活性，並且已進一步的研究了其詳細的 DNA 結合模式。總計這個為期一年的計畫在執行終了後共發表 5 篇 SCI 論文(含一篇 review)。希望這些結果在未來對各種抗藥性細菌包括克雷伯氏菌，能提供初步的標靶藥物設計之建議。

一、計畫摘要

1b. 英文摘要

Keywords: *Klebsiella pneumoniae*, DnaT, protein-DNA interactions.

DnaT protein, only found in the Gram-negative bacteria, is required for assembly of the replication restart primosome. Activity of the replication restart primosome is essential for cell growth and survival. Although DnaT is involved in DNA replication, nothing is known about DNA binding activity of DnaT. In this project, we have showed that DnaT has a strong DNA binding ability relatively higher than those of other members in the primosome, and have detailed the DNA-binding mode. In this one-year project, we have published 5 SCI papers, of which 1 is a review article. We hope these results will provide a new target for drug design for bacterial antibiotics resistances, including *Klebsiella pneumoniae*.

二、背景介紹

2a. 前言

2b. 研究目的

2c. 文獻探討

This report focuses on "**DnaT is a single-stranded DNA binding protein**."

The ability to reinitiate chromosomal DNA replication to maintain genetic integrity after encountering DNA damage is essential for bacterial survival (Cox *et al.* 2000; Cox 2001; McGlynn & Lloyd 2002). Given that the DNA replication machinery of all organisms may stall anywhere on the chromosome, the collapsed DNA replication forks must be reactivated through origin-independent reloading of the replisome for genome duplication. The replication restart primosome (Schekman *et al.* 1974; Marians 2000; Sandler 2000), a formidable enzymatic machine, is a protein–DNA complex that reactivates stalled DNA replication at repaired replication forks after DNA damage (Masai *et al.* 2010). It travels along the lagging strand template, unwinds the duplex DNA, and primes the Okazaki fragments that are required for replication fork progression (Patel *et al.* 2011; Zheng & Shen 2011). Contrary to the DnaA-directed primosome initiated at the unique *oriC* site (Mott & Berger 2007; Leonard & Grimwade 2011), the replication restart primosome preferentially recognizes three-way branched DNA structures possessing a leading strand (Tanaka *et al.* 2002; Mizukoshi *et al.* 2003; Sasaki *et al.* 2007; Tanaka *et al.* 2007). In *Escherichia coli*, the replication restart primosome includes seven essential proteins, namely, PriA helicase, PriB, PriC, DnaB helicase, DnaC, DnaT, and DnaG primase. At least two overlapping mechanisms are available for the reassembly of the replication forks, that is, initiation is induced by either the PriA helicase or PriC (Heller & Marians 2006a, 2006b). In a PriA-PriB-DnaT-dependent reaction, PriB and DnaT are the second and third proteins to be assembled in the protein-DNA complex, respectively. In addition, the association of DnaT with PriA is facilitated by PriB (Liu *et al.* 1996). The binding site on PriB for the ssDNA overlaps the binding sites for PriA and DnaT, suggesting a dynamic primosome assembly process, in which single-stranded DNA (ssDNA) is handed off from one primosome protein to another as the repaired replication fork is reactivated (Lopper *et al.* 2007). The binding of DnaT to PriA and PriB induces the dissociation of PriB from the ssDNA (Figure 1). However, the mechanism of PriA-PriB-DnaT in reloading the DnaC-DnaB complex and in the formation of the DnaB-DnaG complex at the forks remains unclear.

DnaT, formerly known as the "protein i" (Arai *et al.* 1981; Masai *et al.* 1986; Masai & Arai 1988), has been initially described as a key component for phage X174 (Marians 1992) and pBR322 plasmid replication, but not for R1 plasmid replication (Masai & Arai 1989). Genetic analysis for *E. coli* DnaT suggests an essential replication protein for bacterial cell growth because the *dnaT822* mutant shows colony size, cell morphology, inability to properly partition nucleoids, UV sensitivity, and basal SOS expression similar to *priA2::kan* mutants (McCool *et al.* 2004). DnaT is a homotrimer of ~22 kDa subunits (Arai *et al.* 1981). However, recent studies have also indicated that the protein exists in solution as a monomer-trimer equilibrium system (Szymanski *et al.* 2013). Although the role of DnaT in the recruitment of DnaB helicase has been proposed, little is known about the fundamental function of DnaT for the replication restart primosome assembly.

Currently, infections occur that are resistant to all antibacterial options. Few therapies are effective against the six antibiotic-resistant ESKAPE pathogens (*Enterococcus faecium*, *Staphylococcus aureus*, *Klebsiella pneumoniae*, *Acinetobacter baumannii*, *Pseudomonas aeruginosa*, and *Enterobacter species*) (Bush 2010). *K. pneumoniae* is a ubiquitous opportunistic pathogen that causes severe diseases such as septicemia, pneumonia, urinary tract infections, and soft tissue infections (Podschun & Ullmann 1998). Since DnaT is required for reinitiating chromosomal DNA replication in bacteria, blocking the activity of DnaT would be detrimental to

bacterial survival. In addition, because DnaT is not found in human, the *K. pneumoniae* DnaT protein may be a promising target in developing antibiotics.

The number of oligonucleotide/oligosaccharide-binding (OB)-fold proteins has grown rapidly over the past few years, and their mechanisms in interacting with ssDNA, including PriB and SSB, has been relatively understood (Flynn & Zou 2010). To date, little information on the ssDNA-binding mode of non-OB fold proteins is available, especially for a trimeric protein. In this study, we identified a trimeric DnaT that could form stable complex(es) with dT homopolymers of 25 bases (dT25) or longer using electrophoretic mobility shift analysis (EMSA). EMSA is a very popular and well-established approach in molecular biology that facilitates the observation of the protein-DNA complex (Cadman *et al.* 2005; Huang 2012). In addition, we also found that the ssDNA-binding affinity of DnaT was approximately 2-fold higher than that of PriB, an OB-fold protein. Based on the bioinformatic analyses of DnaT using ConSurf (Landau *et al.* 2005) and $(PS)^2$ (Chen *et al.* 2006, 2009), as well as the results from the biophysical and mutational studies, we proposed a binding model for the DnaT trimer-ssDNA complex. A previously proposed hand-off mechanism for primosome assembly (Lopper *et al.* 2007) in replication restart was discussed and modified.

三、研究方法

Materials

All restriction enzymes and DNA-modifying enzymes were purchased from New England Biolabs (Ipswich, MA, USA) unless explicitly stated otherwise. All chemicals were purchased from Sigma-Aldrich (St. Louis, MO, USA) unless explicitly stated otherwise. The *E. coli* strains TOP10F' (Invitrogen, USA) and BL21(DE3)pLysS (Novagen, UK) were used for genetic construction and protein expression, respectively.

Construction of the DnaT, DnaT26-179, and DnaT42-179 expression plasmids

The gene *KPN04812* encoding the putative DnaT was PCR-amplified using genomic DNA of *K. pneumoniae* subsp. *pneumoniae* MGH 78578 as template. The forward (5′-GAAGGGGCATATGTCTTCGCGAATTTTAACCTC-3′) and the reverse (5′-GGGGCTCGAGTCCTCGGAAACCTCGCGGAAT-3′) primers were designed to introduce unique NdeI and XhoI restriction sites (underlined) into DnaT, permitting insertion of the amplified gene into the pET21b vector (Novagen Inc., Madison, WI, USA) for protein expression in *E. coli*. The DnaT26-179 and DnaT42-179 expression plasmids were constructed using the same protocol for DnaT. The oligonucleotide primers for preparation of the DnaT26-179 and DnaT42-179 expression plasmids were: 5′-GGGCATATGAAATCGACTGACGGCACC-3′ and 5′-GGGCTCGAGTCCTCGGAAACCTCGCGG-3′ for DnaT26-179, and 5′-GGGCATATGTTCTATGCGCTGACGCCA-3′ and 5′-GGGCTCGAGTCCTCGGAAACCTCGCGG-3′ for DnaT42-179. The expected gene product expressed by these plasmids has a His tag, which is useful for purifying the recombinant protein.

Protein expression and purification

The recombinant DnaT proteins were expressed and purified using the protocol described previously for allantoinase (Ho *et al.* 2013), hydantoinase (Huang *et al.* 2009), dihydroorotase (Wang *et al.* 2010), PriB (Huang *et al.* 2012b), DnaB (Lin & Huang 2012), and SSB (Huang & Huang 2012). Briefly, *E. coli* BL21(DE3) cells were individually transformed with the expression vector and grown to OD_{600} of 0.9 at 37 ^{o}C in Luria-Bertani medium containing 250 μg/ml ampicillin with rapid shaking. Overexpression of the expression plasmids was induced by incubating with 1 mM isopropyl thiogalactoside (IPTG) for 3 h at 37 °C. The cells overexpressing the protein were chilled on ice, harvested by centrifugation, resuspended in Buffer A (20 mM Tris-HCl, 5 mM imidazole, and 0.5 M NaCl, pH 7.9) and disrupted by sonication with ice cooling. The protein purified from the soluble supernatant by Ni^{2+}-affinity chromatography (HiTrap HP; GE Healthcare Bio-Sciences, Piscataway, NJ, USA) was eluted with Buffer B (20 mM Tris-HCl, 250 mM imidazole, and 0.5 M NaCl, pH 7.9) and dialyzed against a dialysis

buffer (20 mM Tris-HCl and 100 mM NaCl, pH 8.0; Buffer C). Protein purity remained greater than 97 % as determined by Coomassie-stained SDS-PAGE (Mini-PROTEAN Tetra System; Bio-Rad, CA, USA).

Protein concentration

The protein concentration of the solutions was determined by the Bio-Rad Protein Assay using bovine serum albumin as a standard (Bio-Rad, CA, USA). The Bio-Rad Protein Assay is a dye-binding assay in which a differential color change of a dye occurs in response to various concentrations of protein.

Gel-filtration chromatography

Gel-filtration chromatography was carried out by the AKTA-FPLC system (GE Healthcare Bio-Sciences, Piscataway, NJ, USA). Briefly, purified protein (4 mg/ml) in Buffer C was applied to a Superdex 200 HR 10/30 column (GE Healthcare Bio-Sciences, Piscataway, NJ, USA) equilibrated with the same buffer. The column was operated at a flow rate of 0.5 ml/min, and 0.5-ml fractions were collected. The proteins were detected by measuring the absorbance at 280 nm. The column was calibrated with proteins of known molecular weight: thyroglobulin (670 kDa), γ-globulin (158 kDa), ovalbumin (44 kDa), and myoglobin (17 kDa). The K_{av} values for the standard proteins and the DnaT variants were calculated from the equation: $K_{av} = (V_e - V_o)/(V_c - V_o)$, where V_o is column void volume, V_e is elution volume, and V_c is geometric column volume.

Electrophoretic mobility shift assay (EMSA)

EMSA for the DnaT variants was carried out by the protocol described previously for DnaB (Lin & Huang 2012), PriB (Hsieh & Huang 2011; Huang *et al.* 2012a; Huang *et al.* 2012b), and SSB proteins (Huang *et al.* 2011; Jan *et al.* 2011; Huang & Huang 2012). Briefly, radiolabeling of various lengths of ssDNA oligonucleotides was carried out with [γ^{32}P]ATP (6000 Ci/mmol; PerkinElmer Life Sciences, Waltham, MA) and T4 polynucleotide kinase (Promega, Madison, WI, USA). DnaT, DnaT26-179, and DnaT42-179 (0, 0.35, 0.7, 1.4, 2.8, 5.6, 11.3, 22.5, 45, and 90 μM) were individually incubated for 30 min at 25 °C with 1.7 nM DNA substrates (dT20–55) in a total volume of 10 μl in 20 mM Tris-HCl pH 8.0 and 100 mM NaCl. Aliquots (5 μl) were removed from each of the reaction solutions, and added to 2 μl of gel-loading solution (0.25% bromophenol blue and 40% sucrose). The resulting samples were resolved on a native 8% polyacrylamide gel at 4 °C in TBE buffer (89 mM Tris borate and 1 mM EDTA) for 1–1.5 h at 100 V, and were visualized by autoradiography. Complexed and free DNA bands were scanned and quantified.

ssDNA-binding ability

The ssDNA binding ability ($[\text{Protein}]_{50}$; $K_{d,app}$) for the protein was estimated from the protein concentration that binds 50% of the input ssDNA (Huang 2012). Each $[\text{Protein}]_{50}$ is calculated as the average of at least three measurements ± SD.

Site-directed mutagenesis

Two DnaT mutants, DnaT42-179/W140A and DnaT42-179/W140A,K143A, were generated using a QuikChange Site-Directed Mutagenesis kit according to the manufacturer's protocol (Stratagene; LaJolla, CA, USA). The presence of the mutation was verified by DNA sequencing in each construct. The oligonucleotide primers for the preparation of mutants were: 5′-TTTCACCACGTGCAGGCGCAGCAGAAG-3′ and 5′-CAGCTTCTGCTGCGCCTGCACGTGGTG-3′ for DnaT42-179/W140A (the pET21b-DnaT42-179 as template); 5′-GTGCAGGCGCAGCAGGCGCTGGCACGTAGC-3′ and 5′-GCTACGTGCCAGCGCCTGCTGCGCCTGCAC-3′ for DnaT42-179/W140A,K143A (the pET21b-DnaT42-179/W140A as template). The underlined sequences denote the mutated amino acid(s).

Bioinformatics

The amino acid sequences of 29 sequenced DnaT homologs were aligned using ConSurf (Landau *et al.* 2005). The model of DnaT was built from the coordinate of 1GD9 (crystal structure of *Pyrococcus horikoshii* alpha-aminotransferase) by using $(PS)^2$ (Chen *et al.* 2006, 2009). The 25-mer ssDNA in the model of the ssDNA-DnaT complex was generated from the coordinate of 1EYG (crystal structure of the ssDNA-SSB complex) (Raghunathan *et al.* 2000), in which dC3-27 (25-mer ssDNA) was used. The structures were visualized by using the program PyMol.

四、結果與討論

Sequence analysis

Although DnaT has been identified as a component of the replication restart primosome, the fundamental function of DnaT in the replication restart primosome assembly has yet to be properly presented. The gene *KPN04812*, encoding *Klebsiella pneumoniae* DnaT, was initially found using a database search through the National Center for Biotechnology Information (NCBI). Based on the known nucleotide sequence, the predicted DnaT monomer protein has a length of 179 amino acid residues and a molecular mass of ~20 kDa. Figure 2 shows that the alignment consensus of 29 sequenced DnaT homologs by ConSurf (Landau *et al.* 2005; Ho *et al.* 2013) revealed the degree of variability at each position along the primary sequence. Amino acid residues that are highly variable are colored teal, whereas highly conserved amino acid residues are colored burgundy. A consensus sequence was established by determining which amino acid residue that is most commonly found at each position relative to the primary sequence of *K. pneumoniae* DnaT. In general, amino acid residues in the C-terminal region of DnaT are highly conserved.

Purification of DnaT

The gene *KPN04812* encoding the putative DnaT was PCR-amplified using genomic DNA of *K. pneumoniae* subsp. *pneumoniae* MGH 78578 as template. This amplified gene was then ligated into the pET21b vector for protein expression. *K. pneumoniae* DnaT protein was hetero-overexpressed in *E. coli* and then purified from the soluble supernatant by Ni^{2+}-affinity chromatography (Figure 3). Pure protein was obtained in this single chromatographic step with an elution of Buffer B (20 mM Tris–HCl, 250 mM imidazole, and 0.5 M NaCl, pH 7.9), and the dialyzed against a dialysis buffer (20 mM Tris-HCl and 100 mM NaCl, pH 8.0; Buffer C). Approximately >60 mg of purified protein was obtained from 1 L of a culture of *E. coli* cells. The truncated and mutant DnaT proteins were also purified according to the same protocol as that for the wild-type protein, and with very similar purification results.

DnaT has an ssDNA-binding activity

Aromatic stacking and electropositive interactions has an important role in ssDNA binding by proteins (Raghunathan *et al.* 2000; Huang *et al.* 2006). Given that DnaT contains 10 Arg, 5 Lys, and 18 aromatic amino acid residues (11 Phe, 4 Trp and 3 Tyr), we attempted to test whether DnaT has ssDNA-binding activity. We studied the binding of DnaT to ssDNA of different lengths with different protein concentrations using EMSA (Figure 4). EMSA is a well-established approach in studies of molecular biology, allowing the detection of the distinct protein-DNA complex(es) (Huang 2012). When we incubated DnaT with dT20, no significant band shift was observed, indicating that DnaT could not form a stable complex with this homopolymer (Figure 4A). To investigate the length of nucleotides sufficient for the formation of the DnaT-ssDNA complex, as well as the ssDNA-binding ability of DnaT, we further tested dT25 (Figure 4B), dT35 (Figure 4C), and dT50 (Figure 4D) to bind to DnaT. In contrast to dT20, longer dT homopolymers, dT25–50, produced a very significant band shift (C, complex). These findings confirm the ssDNA-binding activity of DnaT, which is strong enough to form a stable protein-DNA complex in solution. Furthermore, two different complexes for dT55 were formed by DnaT (Figure 4E). At lower protein concentrations, DnaT formed a single complex (C1) with

dT55, similar to that observed with dT50 (Figure 4D). However, when the DnaT concentration was increased, another slower-migrating complex (C2) was observed. The appearance of the second complex resulted from the increased DnaT concentration, suggesting that two DnaT proteins may be contained per oligonucleotide. Although dT55 is only 5 nt longer than dT50, the presence of an extra 5 nt in dT55 compared with that of dT50, provides enough interaction space for the binding of two DnaT trimers. Therefore, one DnaT protein occupies 25 (50/2 = 25) nt to 27.5 (55/2 = 27.5) nt of the ssDNA. These results from EMSA suggest that the length of an ssDNA (or the binding site size) (Huang 2012) required for DnaT binding is 26 ± 2 nt.

Design of the truncated DnaT proteins DnaT26-179 and DnaT42-179

The N-terminal region of the DnaT is revealed by an alignment consensus of 29 sequenced DnaT homologs (Figure 2), indicating that the function of DnaT can accommodate many different amino acids in the N-terminal region. Thus, the truncated DnaT proteins, DnaT26-179 (the N-terminal 25 aa was removed) and DnaT42-179 (the N-terminal 41 aa was removed), were constructed and purified (Figure 3) to investigate whether the N-terminal region is essential for ssDNA binding and oligomerization of DnaT.

DnaT26-179 bound to ssDNA

The binding of DnaT26-179 to dT20 (Figure 5A), dT25 (Figure 5B), dT35 (Figure 5C), dT50 (Figure 5D), and dT55 (Figure 5E) were examined using EMSA. As shown in Figure 5A, no significant band shift was observed when DnaT26-179 was incubated with dT20. However, DnaT26-179 bound to dT25-50 and formed a single complex. For dT55, two different complexes of DnaT26-179 appeared at high protein concentrations. Regardless of the efficient concentrations for the ssDNA binding, the stoichiometry of DnaT26-179 was nearly identical to that of the wild-type DnaT.

DnaT42-179 bound to ssDNA

The binding of DnaT42-179 to dT20 (Figure 6A), dT25 (Figure 6B), dT35 (Figure 6C), dT50 (Figure 6D), and dT55 (Figure 6E) were studied by EMSA. No significant band shift was observed when DnaT42-179 was incubated with dT20. DnaT42-179 could form a single complex with dT25-50 and form two distinct complexes with dT55, respectively. Although the efficient concentrations of DnaT42-179 for the complex(es) formation are higher than those of DnaT and DnaT26-179, their stoichiometries for ssDNA binding are very similar. These data indicate that deletion of the N-terminal 1-41 aa region does not influence the binding site size of DnaT.

Binding constants of the DnaT-ssDNA complexes determined from EMSA

To compare the ssDNA-binding abilities of DnaT, DnaT26-179, and DnaT42-179, the midpoint values for input ssDNA binding, calculated from the titration curves of EMSA and referred to as $[\text{Protein}]_{50}$, were quantified and are summarized in Table 1. Although the binding site size of these DnaT variants was very similar as previously discussed, their ssDNA-binding activities were different. The deletion of the N-terminal 1-25 aa region in the DnaT slightly affected the ssDNA binding (Table 1). DnaT42-179 had a 2.5- to 4-fold lesser affinity for binding to dT25-55 compared with those of DnaT.

The N-terminal region of DnaT was assumed to be not significant in the primosome assembly because this region was quite variable (Figure 2). Although the region aa 1-41 in DnaT does not contain highly conserved positively charged/aromatic residues for ssDNA interacting (except for F16), our EMSA results indicated that DnaT42-179 still had a defective ssDNA-binding ability compared with DnaT (Table 1). Thus, this region in DnaT may not be directly involved in ssDNA binding. Previous data have shown that the binding of SSB to long ssDNA results in a conformational change in the protein, making the glycine-rich region more easily accessible to the action of proteases (Curth *et al.* 1996). Although the flexible region in DnaT has not been identified yet, DnaT has been noted to contain 13 Pro and 11 Gly amino acid residues (Figure 2), which are important components of the flexible region. We speculate that the phenomenon for SSB may be applied to DnaT. The N-terminal region aa 1-41 may be involved in

some unknown conformational changes in DnaT, causing some ssDNA-binding sites to be more accessible to interact with ssDNA. Given the hand-off mechanism for the primosome assembly, we believe that some significant conformational changes in DnaT must occur during ssDNA binding (Lopper *et al.* 2007). Many bacteria do not contain a recognizable homologue of PriB (Dong *et al.* 2010) and other loading factors, such as PriC and DnaC. Thus, several regions that are important for protein-protein interaction and conformational change in DnaT are not necessarily conserved.

Oligomeric state of DnaT in solution

The analysis of purified DnaT protein (4 mg/ml; 204 μM) by gel filtration chromatography revealed a single peak with elution volume of 81.6 ml (Figure 7A). Assuming that DnaT has a shape and partial specific volume similar to the standard proteins, the native molecular mass of DnaT was estimated to be 60320 Da, calculated from a standard linear regression equation, $K_{av} = -0.3684$ (logMw) + 2.2707 (Figure 7B). The native molecular mass for DnaT is approximately thrice as much as that of a DnaT monomer (~20 kDa). In addition, a single peak with the same elution volume similar to that of 4 mg/ml was observed when 1 mg/ml (~50 μM) DnaT concentration was used. Therefore, we believe that DnaT, under these conditions, is a stable trimer in solution. In addition, this concentration (50 μM) used in estimating the DnaT trimer was also used in EMSA (Figure 4). Given the formation of a single complex with ssDNA (dT25-50), we speculate that only the trimeric form of DnaT, but not a mixture or other oligomeric form, is involved in the complex(es) formation.

Purified DnaT42-179 (4 mg/ml; 253 μM) was also analyzed by gel filtration chromatography to investigate the deletion effect in the oligomeric state of DnaT. The chromatographic result also showed a single peak (Figure 7A). The native molecular mass of DnaT42-179 was estimated to be 45982 Da (Figure 7B). Based on the molecular mass of the DnaT42-179 monomer (~16 kDa), we concluded that DnaT42-179 in the solution is a stable trimer, similar to DnaT. Thus, deletion of the N-terminal 1-41 aa region does not cause any change in the oligomeric state of DnaT.

Structure modeling of DnaT

To obtain an in-depth understanding of the structure-function relationship of DnaT, we decided to model its three-dimensional structure by homology modeling. No protein with amino acid sequence similar to DnaT was found in the structure databank. Hence, homology modeling for the DnaT structure by several homology-based programs was not successful. For example, when we pasted the DnaT amino acid sequence to SWISS-MODEL (http://swissmodel.expasy.org/) for modeling, no result was provided (Arnold *et al.* 2006). Thus, DnaT may form a novel fold for ssDNA binding.

We subsequently used another type of the bioinformatic program, $(PS)^2$ (Chen *et al.* 2006, 2009), for the structure modeling of DnaT. $(PS)^2$ (http://140.113.239.111/~ps2v2/docs.php) is an automatic homology modeling server that combines both sequence and secondary structure information to detect the homologous proteins with remote similarity and the target-template alignment. After pasting the amino acid sequence to the website of $(PS)^2$, one hit (Protein Data Bank entry: 1GD9), alpha-aminotransferase from *Pyrococcus horikoshii*, was suggested. The amino acid residue 14-165 in DnaT (pink) was matched in the alpha-aminotransferase (yellow) of aa 143-314, with 20% identity in amino acid sequence and 85% identity in the secondary structure (Figure 8A). This model shows that the N-terminal region in the modeled structure of DnaT is flexible, and the C-terminal region contains helices with several loops (Figure 8B). Given that the deletion in the N-terminal region did not cause any change in the oligomerization state of DnaT (Figure 7), the C-terminal region of DnaT may serve as the oligomerization/ssDNA-binding domain, similar to the N-terminal oligomerization/ssDNA-binding domain in SSB (Raghunathan *et al.* 2000; Chan *et al.* 2009). However, the sequence and structure fold between DnaT and SSB are quite different.

Trimeric DnaT structure model

Although the ssDNA-binding ability of DnaT has been identified in this study, the ssDNA-binding mode remains ambiguous. Considering that the oligomerization state and ssDNA-binding properties of DnaT42-179 are similar to those of DnaT, the region aa 42-179 could be defined as the oligomerization/ssDNA-binding domain in DnaT. Accordingly, a possible trimeric DnaT structure was manually built using 3-fold symmetry; each monomer is stabilized by two helices (Figure 8C). We found that the modeled DnaT trimer structure is ring-shaped. The ring-like structure of DnaT is slightly similar to that of the hexameric (consisted of three dimers) DnaC helicase from *Geobacillus kaustophilus*, a DnaB-like helicase (Lo *et al.* 2009). DnaT may bind to DnaB with a stoichiometry of 1:2, one DnaT monomer to a DnaB dimer. However, this DnaT structure is only a modeled structure, and these speculations must be further confirmed by additional biophysical studies.

ssDNA-binding mode of DnaT

Based on the structural model of DnaT, the positively charged (blue) and aromatic residues (green) located in the C-terminus of DnaT has been suggested to be involved in ssDNA binding: H136, H137, W140, K143, R146 and R151 (Figure 8D). In addition, these residues in DnaT are significantly conserved among the 29 sequenced DnaT proteins (Figure 2). F73 and F74 are also potential binding sites for ssDNA, but they are not conserved in DnaT family. These residues in DnaT create a shallow groove on the surface that can potentially be wrapped around by ssDNA. According to the structure-function relationship of DnaT, we manually added and superimposed the ssDNA dC25 from the crystal structure of *E. coli* SSB (Raghunathan *et al.* 2000) (Protein Data Bank entry: 1EYG) into the DnaT trimer structure (Figure 8E). DnaT could form a stable complex with 25-mer ssDNA (Figure 4B). In this modeled structure of DnaT-ssDNA complex, 25-mer ssDNA seems to suitably fit DnaT (Figure 8E). However, this DnaT complex structure is only a modeled structure, and this binding mode must be further confirmed by additional biophysical studies.

To test whether the proposed model is possible for forming the DnaT-ssDNA complex, alanine substitution mutant DnaT42-179/W140 and the double mutant DnaT42-179/W140,K143A were conducted and analyzed by EMSA. As shown in Figure 9A, although the band shift was still observed when DnaT42-179/W140 was incubated with dT35, significant smears and decreased ability for ssDNA binding were found. The $[\text{Protein}]_{50}$ for the binding of DnaT42-179/W140 to dT35 is 16 ± 3 μM, a value lower than that for DnaT42-179 (12 ± 2 μM). For the double mutant DnaT42-179/W140,K143A, it could not form a stable complex, indicating a dramatically impaired ability for ssDNA binding of this mutant (Figure 9B). Thus, residues suggested from the proposed model were involved in ssDNA binding of DnaT. Because of a trimer, mutation in these two residues (W140 and K143) may lead to loss of six binding sites in the C-terminal region of DnaT (Figure 9C).

DnaT is a novel ssDNA-binding protein

For the first time, the ssDNA-binding activity of DnaT was identified and assessed with a $K_{d,app}$ ($[\text{Protein}]_{50}$) of 5.6 ± 0.3 μM for dT25 binding and the binding site size of 26 ± 2 per DnaT trimer. To date, insufficient information on the ssDNA-binding mode for a trimeric protein is available. Although DnaT has been identified as a component of the replication restart primosome, the function of DnaT for DNA binding has yet to be properly presented. Although previous fluorescence anisotropy studies have indicated that DnaT has a very weak ssDNA-binding activity to determine its K_d (Lopper *et al.* 2007), with the use of EMSA, we showed in our study that the ssDNA-binding activity of DnaT is strong enough for forming a stable complex with ssDNA. This activity for ssDNA binding by DnaT, assayed in the same manner, is even higher than that of an OB-fold protein PriB (Table 1), another loading factor for primosome assembly (Huang *et al.* 2012b). EMSA is a useful technology in molecular biology and the use of radioactive DNA make it highly sensitive and allows to observation of the distinct complexes (Huang 2012). For 25-mer ssDNA or longer, stable DnaT-ssDNA complex(es) is clearly shown from EMSA (Figure 4). However, whether this significant disparity is due to inherent differences among the species, the use of different assay methods, or the effect of different investigators,

remains unknown. We also noted that these seemingly contradictory data may reconcile. In a previous study that used fluorescence anisotropy (Lopper *et al.* 2007), the ssDNA-binding ability of DnaT was assayed with 18-mer ssDNA, and a very weak activity of DnaT for ssDNA-binding was then observed and concluded. Similarly, DnaT could not bind to short ssDNA from our EMSA result (Figure 4A).

Comparison with PriB

Various single-stranded DNA binding proteins bind to ssDNA with some degree of positive cooperativity (Lohman & Ferrari 1994; Wold 1997; Huang *et al.* 2006). In this study, we found different EMSA behaviors between PriB and DnaT proteins. DnaT variants form multiple distinct complexes with ssDNA of different lengths (Figures 4–6), whereas binding of PriB to ssDNA dT20–dT60 forms a single complex only (Huang *et al.* 2012b). Considering their binding activities (Table 1), these findings suggest that DnaT binds to ssDNA with higher binding affinity but lower cooperativity than PriB. Although DnaT is not an OB-fold protein predicted from sequence analysis and structure modeling, DnaT has a higher ssDNA-binding activity than that of PriB, an OB-fold protein.

Insight into the hand-off mechanism: A modified version

A hand-off mechanism for primosome assembly (Lopper *et al.* 2007) has been proposed (Figure 1), where (i) PriA recognizes and binds to a replication fork; (ii) PriB joins to PriA to form a PriA-PriB-DNA ternary complex; and (iii) DnaT participates in this nucleocomplex to form a triprotein complex, in which, the recruitment of DnaT results in the release of ssDNA by PriB, and then loads the DnaB/C complex. In this study, we have identified DnaT as a kind of ssDNA-binding protein, and found that the ssDNA-binding activity of DnaT is ~2-fold higher than that of PriB. Thus, the hand-off mechanism for primosome assembly should be modified (Figure 10), such that (i) PriA recognizes and binds to a replication fork; (ii) PriB joins to PriA to form a PriA-PriB-DNA ternary complex; and (iii) DnaT interacts with ssDNA, PriA, and PriB, forces the release of ssDNA by PriB, and then the DnaB/C complex are loaded. This updated model explains the mechanism as to how DnaT binds to ssDNA and its partner proteins. However, the detailed action of DnaT in every key step for primosome assembly is still unclear. In addition, whether DnaT is a necessary factor for primosome assembly because many bacteria do not have a recognizable homolog of DnaT still remains to be explored. Furthermore, given that only one monomer of the PriB dimer can engage in interactions with the DNA and the partner protein(s) (Huang *et al.* 2006; Szymanski *et al.* 2010), whether the binding site on PriB for ssDNA is necessary to overlap the binding sites for PriA and DnaT should be determined. The more complex structures of PriB and DnaT are useful in helping our understanding of the primosome assembly mechanism(s).

References

Arai, K., McMacken, R., Yasuda, S. & Kornberg, A. (1981) Purification and properties of *Escherichia coli* protein i, a prepriming protein in phi X174 DNA replication. *J Biol Chem* **256**, 5281-5286.

Arnold, K., Bordoli, L., Kopp, J. & Schwede, T. (2006) The SWISS-MODEL workspace: a web-based environment for protein structure homology modelling. *Bioinformatics* **22**, 195-201.

Bush, K. (2010) Alarming beta-lactamase-mediated resistance in multidrug-resistant *Enterobacteriaceae*. *Curr Opin Microbiol* **13**, 558-564.

Cadman, C.J., Lopper, M., Moon, P.B., Keck, J.L. & McGlynn, P. (2005) PriB stimulates PriA helicase via an interaction with single-stranded DNA. *J Biol Chem* **280**, 39693-39700.

Chan, K.W., Lee, Y.J., Wang, C.H., Huang, H. & Sun, Y.J. (2009) Single-stranded DNA-binding protein complex from *Helicobacter pylori* suggests an ssDNA-binding surface. *J Mol Biol* **388**, 508-519.

Chen, C.C., Hwang, J.K. & Yang, J.M. (2006) $(PS)^2$: protein structure prediction server. *Nucleic Acids Res* **34**, W152-157.

Chen, C.C., Hwang, J.K. & Yang, J.M. (2009) $(PS)^2$-v2: template-based protein structure

prediction server. *BMC Bioinformatics* **10**, 366.
Cox, M.M. (2001) Recombinational DNA repair of damaged replication forks in *Escherichia coli*: questions. *Annu Rev Genet* **35**, 53-82.
Cox, M.M., Goodman, M.F., Kreuzer, K.N., Sherratt, D.J., Sandler, S.J. & Marians, K.J. (2000) The importance of repairing stalled replication forks. *Nature* **404**, 37-41.
Curth, U., Genschel, J., Urbanke, C. & Greipel, J. (1996) In vitro and in vivo function of the C-terminus of *Escherichia coli* single-stranded DNA binding protein. *Nucleic Acids Res* **24**, 2706-2711.
Dong, J., George, N.P., Duckett, K.L., DeBeer, M.A. & Lopper, M.E. (2010) The crystal structure of *Neisseria gonorrhoeae* PriB reveals mechanistic differences among bacterial DNA replication restart pathways. *Nucleic Acids Res* **38**, 499-509.
Flynn, R.L. & Zou, L. (2010) Oligonucleotide/oligosaccharide-binding fold proteins: a growing family of genome guardians. *Crit Rev Biochem Mol Biol* **45**, 266-275.
Heller, R.C. & Marians, K.J. (2006a) Replication fork reactivation downstream of a blocked nascent leading strand. *Nature* **439**, 557-562.
Heller, R.C. & Marians, K.J. (2006b) Replisome assembly and the direct restart of stalled replication forks. *Nat Rev Mol Cell Biol* **7**, 932-943.
Ho, Y.Y., Huang, Y.H. & Huang, C.Y. (2013) Chemical rescue of the post-translationally carboxylated lysine mutant of allantoinase and dihydroorotase by metal ions and short-chain carboxylic acids. *Amino Acids* **44**, 1181-1191.
Hsieh, H.C. & Huang, C.Y. (2011) Identification of a novel protein, PriB, in *Klebsiella pneumoniae*. *Biochem Biophys Res Commun* **404**, 546-551.
Huang, C.Y. (2012) Determination of the binding site-size of the protein-DNA complex by use of the electrophoretic mobility shift assay. In: Stoichiometry and Research – The Importance of Quantity in Biomedicine (ed. A. Innocenti), pp. 235 – 242. Rijeka, Croatia: InTech Press.
Huang, C.Y., Hsu, C.C., Chen, M.C. & Yang, Y.S. (2009) Effect of metal binding and posttranslational lysine carboxylation on the activity of recombinant hydantoinase. *J Biol Inorg Chem* **14**, 111-121.
Huang, C.Y., Hsu, C.H., Sun, Y.J., Wu, H.N. & Hsiao, C.D. (2006) Complexed crystal structure of replication restart primosome protein PriB reveals a novel single-stranded DNA-binding mode. *Nucleic Acids Res* **34**, 3878-3886.
Huang, Y.H. & Huang, C.Y. (2012) Characterization of a single-stranded DNA-binding protein from *Klebsiella pneumoniae*: mutation at either Arg73 or Ser76 causes a less cooperative complex on DNA. *Genes Cells* **17**, 146-157.
Huang, Y.H., Lee, Y.L. & Huang, C.Y. (2011) Characterization of a single-stranded DNA binding protein from *Salmonella enterica* Serovar Typhimurium LT2. *Protein J* **30**, 102-108.
Huang, Y.H., Lin, H.H. & Huang, C.Y. (2012a) A single residue determines the cooperative binding property of a primosomal DNA replication protein, PriB, to single-stranded DNA. *Biosci. Biotechnol. Biochem.* **76**, 1110-1115.
Huang, Y.H., Lo, Y.H., Huang, W. & Huang, C.Y. (2012b) Crystal structure and DNA-binding mode of *Klebsiella pneumoniae* primosomal PriB protein. *Genes Cells* **17**, 837-849.
Jan, H.C., Lee, Y.L. & Huang, C.Y. (2011) Characterization of a single-stranded DNA-binding protein from *Pseudomonas aeruginosa* PAO1. *Protein J* **30**, 20-26.
Landau, M., Mayrose, I., Rosenberg, Y., Glaser, F., Martz, E., Pupko, T. & Ben-Tal, N. (2005) ConSurf 2005: the projection of evolutionary conservation scores of residues on protein structures. *Nucleic Acids Res* **33**, W299-302.
Leonard, A.C. & Grimwade, J.E. (2011) Regulation of DnaA assembly and activity: taking directions from the genome. *Annu Rev Microbiol* **65**, 19-35.
Lin, H.H. & Huang, C.Y. (2012) Characterization of flavonol inhibition of DnaB helicase: real-time monitoring, structural modeling, and proposed mechanism. *J Biomed Biotechnol* **2012**, 735368.
Liu, J., Nurse, P. & Marians, K.J. (1996) The ordered assembly of the phiX174-type primosome. III. PriB facilitates complex formation between PriA and DnaT. *J Biol Chem* **271**, 15656-15661.
Lo, Y.H., Tsai, K.L., Sun, Y.J., Chen, W.T., Huang, C.Y. & Hsiao, C.D. (2009) The crystal

structure of a replicative hexameric helicase DnaC and its complex with single-stranded DNA. *Nucleic Acids Res* **37**, 804-814.
Lohman, T.M. & Ferrari, M.E. (1994) *Escherichia coli* single-stranded DNA-binding protein: multiple DNA-binding modes and cooperativities. *Annu Rev Biochem* **63**, 527-570.
Lopper, M., Boonsombat, R., Sandler, S.J. & Keck, J.L. (2007) A hand-off mechanism for primosome assembly in replication restart. *Mol Cell* **26**, 781-793.
Marians, K.J. (1992) Prokaryotic DNA replication. *Annu. Rev. Biochem.* **61**, 673-719.
Marians, K.J. (2000) PriA-directed replication fork restart in *Escherichia coli*. *Trends Biochem. Sci.* **25**, 185-189.
Masai, H. & Arai, K. (1988) Initiation of lagging-strand synthesis for pBR322 plasmid DNA replication in vitro is dependent on primosomal protein i encoded by dnaT. *J Biol Chem* **263**, 15016-15023.
Masai, H. & Arai, K. (1989) *Escherichia coli* dnaT gene function is required for pBR322 plasmid replication but not for R1 plasmid replication. *J Bacteriol* **171**, 2975-2980.
Masai, H., Bond, M.W. & Arai, K. (1986) Cloning of the *Escherichia coli* gene for primosomal protein i: the relationship to dnaT, essential for chromosomal DNA replication. *Proc Natl Acad Sci U S A* **83**, 1256-1260.
Masai, H., Tanaka, T. & Kohda, D. (2010) Stalled replication forks: making ends meet for recognition and stabilization. *Bioessays* **32**, 687-697.
McCool, J.D., Ford, C.C. & Sandler, S.J. (2004) A dnaT mutant with phenotypes similar to those of a *priA2::kan* mutant in *Escherichia coli* K-12. *Genetics* **167**, 569-578.
McGlynn, P. & Lloyd, R.G. (2002) Recombinational repair and restart of damaged replication forks. *Nat Rev Mol Cell Biol* **3**, 859-870.
Mizukoshi, T., Tanaka, T., Arai, K., Kohda, D. & Masai, H. (2003) A critical role of the 3' terminus of nascent DNA chains in recognition of stalled replication forks. *J Biol Chem* **278**, 42234-42239.
Mott, M.L. & Berger, J.M. (2007) DNA replication initiation: mechanisms and regulation in bacteria. *Nat Rev Microbiol* **5**, 343-354.
Patel, S.S., Pandey, M. & Nandakumar, D. (2011) Dynamic coupling between the motors of DNA replication: hexameric helicase, DNA polymerase, and primase. *Curr Opin Chem Biol* **15**, 595-605.
Podschun, R. & Ullmann, U. (1998) *Klebsiella* spp. as nosocomial pathogens: epidemiology, taxonomy, typing methods, and pathogenicity factors. *Clin Microbiol Rev* **11**, 589-603.
Raghunathan, S., Kozlov, A.G., Lohman, T.M. & Waksman, G. (2000) Structure of the DNA binding domain of *E. coli* SSB bound to ssDNA. *Nat Struct Biol* **7**, 648-652.
Sandler, S.J. (2000) Multiple genetic pathways for restarting DNA replication forks in *Escherichia coli* K-12. *Genetics* **155**, 487-497.
Sasaki, K., Ose, T., Okamoto, N., Maenaka, K., Tanaka, T., Masai, H., Saito, M., Shirai, T. & Kohda, D. (2007) Structural basis of the 3'-end recognition of a leading strand in stalled replication forks by PriA. *EMBO J* **26**, 2584-2593.
Schekman, R., Weiner, A. & Kornberg, A. (1974) Multienzyme systems of DNA replication. *Science* **186**, 987-993.
Szymanski, M.R., Jezewska, M.J. & Bujalowski, W. (2010) Interactions of the *Escherichia coli* primosomal PriB protein with the single-stranded DNA. Stoichiometries, intrinsic affinities, cooperativities, and base specificities. *J Mol Biol* **398**, 8-25.
Szymanski, M.R., Jezewska, M.J. & Bujalowski, W. (2013) The *Escherichia coli* Primosomal DnaT Protein Exists in Solution as a Monomer-Trimer Equilibrium System. *Biochemistry* **52**, 1845-1857.
Tanaka, T., Mizukoshi, T., Sasaki, K., Kohda, D. & Masai, H. (2007) *Escherichia coli* PriA protein, two modes of DNA binding and activation of ATP hydrolysis. *J Biol Chem* **282**, 19917-19927.
Tanaka, T., Mizukoshi, T., Taniyama, C., Kohda, D., Arai, K. & Masai, H. (2002) DNA binding of PriA protein requires cooperation of the N-terminal D-loop/arrested-fork binding and C-terminal helicase domains. *J Biol Chem* **277**, 38062-38071.

Wang, C.C., Tsau, H.W., Chen, W.T. & Huang, C.Y. (2010) Identification and characterization of a putative dihydroorotase, KPN01074, from *Klebsiella pneumoniae*. *Protein J* **29**, 445-452.
Wold, M.S. (1997) Replication protein A: a heterotrimeric, single-stranded DNA-binding protein required for eukaryotic DNA metabolism. *Annu Rev Biochem* **66**, 61-92.
Zheng, L. & Shen, B. (2011) Okazaki fragment maturation: nucleases take centre stage. *J Mol Cell Biol* **3**, 23-30.

Figure legends

Figure 1 A hand-off mechanism for the replication restart primosome assembly. (i) PriA recognizes and binds to a replication fork; (ii) PriB joins to PriA to form a PriA-PriB-DNA ternary complex; and (iii) DnaT participates in this nucleocomplex to form a triprotein complex, in which, the recruitment of DnaT results in the release of ssDNA by PriB, and then loads the DnaB/C complex. This figure is adapted from the published assembly mechanism presented earlier by Lopper *et al*. 2007.

Figure 2 Amino acids sequence alignment of *K. pneumoniae* DnaT. An alignment consensus of 29 sequenced DnaT homologs by ConSurf (Landau *et al.* 2005) reveals the degree of variability at each position along the primary sequence. Amino acid residues that are highly variable are colored teal, while highly conserved amino acid residues are colored burgundy. A consensus sequence was established by determining the amino acid residue that is most commonly found at each position relative to the primary sequence of *K. pneumoniae* DnaT. In general, amino acid residues in the C-terminal region of DnaT are highly conserved.

Figure 3 Protein purity. Coomassie Blue-stained SDS-PAGE (12%) of the purified DnaT (lane 1; 5.5 μg), DnaT26-179 (lane 2; 4.8 μg), DnaT42-179 (lane 3; 4.4 μg) and molecular mass standards (M) are shown. The sizes of the standard proteins, from the top down, are as follows: 55, 40, 35, 25, 15, and 10 kDa. The purified DnaT protein migrated between the 25 and 15 kDa standards on the SDS-PAGE.

Figure 4 Binding of DnaT to dT20–55. DnaT (0, 0.35, 0.7, 1.4, 2.8, 5.6, 11.3, 22.5, 45, and 90 μM; monomer) was incubated for 30 min at 25°C with 1.7 nM of (A) dT20, (B) dT25, (C) dT35, (D) dT50 or (E) dT55 in a total volume of 10 μl in 20 mM Tris-HCl pH 8.0 and 100 mM NaCl. Aliquots (5 μl) were removed from each reaction solution and added to 2 μl of gel-loading solution (0.25% bromophenol blue and 40% sucrose). The resulting samples were resolved on a native 8% polyacrylamide gel at 4°C in TBE buffer (89 mM Tris borate and 1 mM EDTA) for 1-1.5 h at 100 V and visualized by autoradiography. Complexed and free DNA bands were scanned and quantified.

Figure 5 Binding of DnaT26-179 to dT20–55. DnaT26-179 (0, 0.35, 0.7, 1.4, 2.8, 5.6, 11.3, 22.5, 45, and 90 μM; monomer) was incubated for 30 min at 25°C with 1.7 nM of (A) dT20, (B) dT25, (C) dT35, (D) dT50 or (E) dT55 in a total volume of 10 μl in 20 mM Tris-HCl pH 8.0 and 100 mM NaCl. Aliquots (5 μL) were removed from each reaction solution and added to 2 μl of gel-loading solution (0.25% bromophenol blue and 40% sucrose). The resulting samples were resolved on a native 8% polyacrylamide gel at 4°C in TBE buffer (89 mM Tris borate and 1 mM EDTA) for 1-1.5 h at 100 V and visualized by autoradiography. Complexed and free DNA bands were scanned and quantified.

Figure 6 Binding of DnaT42-179 to dT20–55. DnaT42-179 (0, 0.35, 0.7, 1.4, 2.8, 5.6, 11.3, 22.5, 45, and 90 μM; monomer) was incubated for 30 min at 25°C with 1.7 nM of (A) dT20, (B) dT25, (C) dT35, (D) dT50 or (E) dT55 in a total volume of 10 μl in 20 mM Tris-HCl pH 8.0 and 100 mM NaCl. Aliquots (5 μl) were removed from each reaction solution and added to 2 μl of gel-loading solution (0.25% bromophenol blue and 40% sucrose). The resulting samples were resolved on a native 8% polyacrylamide gel at 4°C in TBE buffer (89 mM Tris borate and 1 mM

EDTA) for 1-1.5 h at 100 V and visualized by autoradiography. Complexed and free DNA bands were scanned and quantified.

Figure 7 Oligomeric state of purified DnaT and DnaT42-179 in solution. (A) Gel-filtration chromatographic analysis of the purified DnaT variants. Purified protein in buffer (20 mM Tris-HCl and 100 mM NaCl at pH 8.0) was applied to a Superdex 200 HR 10/30 column equilibrated with the same buffer. The column was operated at a flow rate of 0.5 mL/min, and 0.5-mL fractions were collected. The protein was detected by measuring absorbance at 280 nm. The column was calibrated with proteins of known molecular masses (closed symbols): thyroglobulin (670 kDa), γ-globulin (158 kDa), ovalbumin (44 kDa), and myoglobin (17 kDa). The corresponding single peak shows the eluted DnaT and DnaT42-179, respectively. (B) A standard linear regression curve was generated by plotting the log of the molecular mass of the calibration proteins against their K_{av} values.

Figure 8 Structure modeling of DnaT. (A) Structure modeling of DnaT by the bioinformatic program $(PS)^2$. After searching and modeling, *Pyrococcus horikoshii* alpha-aminotransferase was suggested. The amino acid residue 14-165 in DnaT (pink) was matched in the alpha-aminotransferase of aa 143-314 (yellow), with 20% identity in amino acid sequence and 85% identity in the secondary structure. (B) Ribbon diagram of the modeled DnaT monomer (aa 14-165). The N-terminal region aa 14-41 is shown in marine color, and aa 42-165 in DnaT is in hot pink. (C) Ribbon diagram of a possible trimeric DnaT structure. The trimeric DnaT structure was manually built using 3-fold symmetry; each monomer (aa 14-165) is stabilized by two helices. The N-terminal region aa 14-41 is shown in marine color, and aa 42-165 in DnaT is in hot pink. (D) The putative ssDNA binding sites of DnaT. The highly conserved hydrophobic (green) and basic residues (blue) of DnaT, H136, H137, W140, K143, R146 and R151, located on the potential ssDNA binding surface, are indicated. (E) A model of the ssDNA-DnaT complex. The model was directly constructed by superimposing the modeled DnaT trimer with the crystal structure of the ssDNA-SSB complex (PDB code 1EYG). The ssDNA (25-mer) generated from the ssDNA-SSB complex is shown in gold.

Figure 9 Mutational analysis of DnaT. Binding of DnaT mutant protein, (A) DnaT42-179/W140A or (B) DnaT42-179/W140A,K143A to dT35. The mutant protein (0, 0.35, 0.7, 1.4, 2.8, 5.6, 11.3, 22.5, 45, and 90 μM; monomer) was incubated for 30 min at 25 °C with 1.7 nM of dT35 in a total volume of 10 μL in 20 mM Tris-HCl pH 8.0 and 100 mM NaCl. Aliquots (5 μL) were removed from each reaction solution and added to 2 μL of gel-loading solution (0.25% bromophenol blue and 40% sucrose). The resulting samples were resolved on a native 8% polyacrylamide gel at 4°C in TBE buffer (89 mM Tris borate and 1 mM EDTA) for 1-1.5 h at 100 V and visualized by autoradiography. Complexed and free DNA bands were scanned and quantified. (C) A proposed trimeric DnaT structure for DnaT42-179/W140A,K143A mutant. Because of a trimer, mutation in these two residues (W140 and K143) may lead to loss of six binding sites in the C-terminal region of DnaT.

Figure 10 An updated hand-off mechanism for the replication restart primosome assembly. In this study, we have identified DnaT as a kind of ssDNA-binding protein, and found that the ssDNA-binding activity of DnaT is ~2-fold higher than that of PriB. Thus, the hand-off mechanism for primosome assembly should be modified , such that (i) PriA recognizes and binds to a replication fork; (ii) PriB joins to PriA to form a PriA-PriB-DNA ternary complex; and (iii) DnaT interacts with ssDNA, PriA, and PriB, forces the release of ssDNA by PriB, and then the DnaB/C complex are loaded. This updated model explains the mechanism as to how DnaT binds to ssDNA and its partner proteins. However, the detailed action of DnaT in every key step for primosome assembly is still unclear.

Table 1. ssDNA binding properties of DnaT, DnaT26-179, and DnaT42-179 as analyzed by EMSA

	DnaT		DnaT26-179		DnaT42-179		PriB [1]	
DNA	$[Protein]_{50}$ [2]	N [3]	$[Protein]_{50}$	N	$[Protein]_{50}$	N	$[Protein]_{50}$	N
dT20	ND	1	ND	1	ND	1	ND	1
dT25	5.6 ± 0.3	1	6.5 ± 0.3	1	14 ± 2	1	18 ± 2	1
dT35	2.7 ± 0.2	1	6.1 ± 0.3	1	12 ± 2	1	8 ± 1	1
dT50	2.2 ± 0.2	1	2.8 ± 0.2	1	8.2 ± 1.2	1	4 ± 0.5	1
dT55	2.0 ± 0.2	2	2.9 ± 0.3	2	8.1 ± 1.5	2	4 ± 0.5	1

Errors are standard deviations determined by three independent titration experiments.

[1] EMSA results of *K. pneumoniae* PriB (Huang *et al.* 2012b).

[2] $[Protein]_{50}$ was calculated from the titration curves of EMSA by determining the concentration of the protein (μM) needed to achieve the midpoint value for input ssDNA binding. For dT55, input ssDNA binding were the sum of the intensities from the two separate ssDNA-protein complexes.

[3] N, complex number.

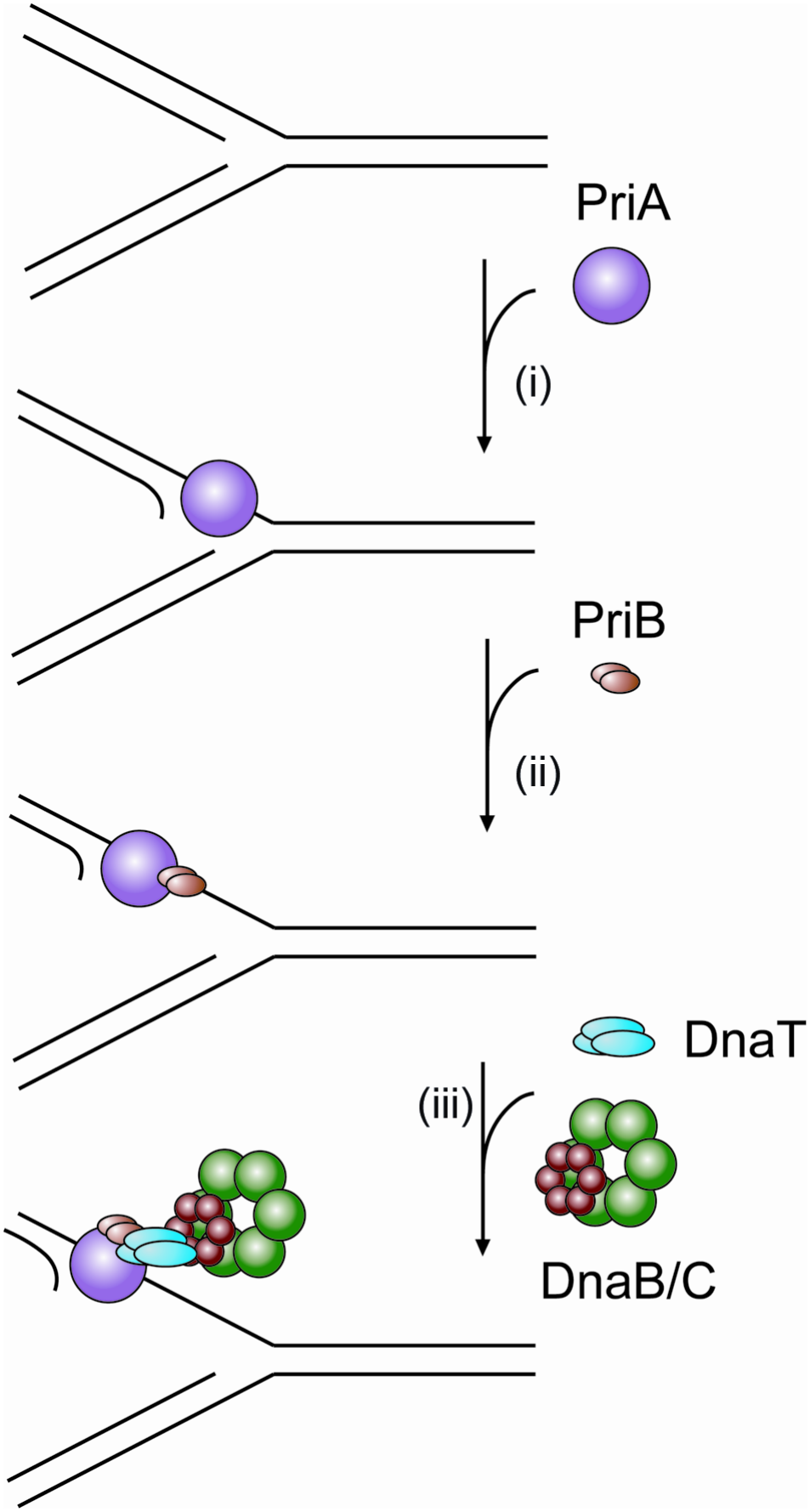

Figure 1

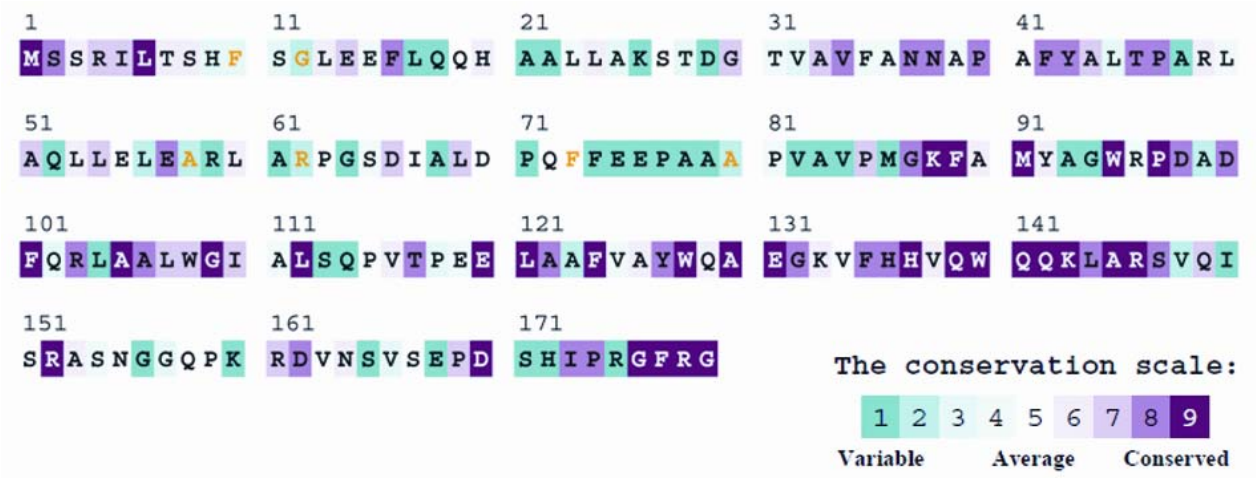
1 MSSRILTSHF
11 SGLEEFLQQH
21 AALLAKSTDG
31 TVAVFANNAP
41 AFYALTPARL
51 AQLLELEARL
61 ARPGSDIALD
71 PQFFEEPAAA
81 PVAVPMGKFA
91 MYAGWRPDAD
101 FQRLAALWGI
111 ALSQPVTPEE
121 LAAFVAYWQA
131 EGKVFHHVQW
141 QQKLARSVQI
151 SRASNGGQPK
161 RDVNSVSEPD
171 SHIPRGFRG
The conservation scale:
1 2 3 4 5 6 7 8 9
Variable
Average
Conserved

Figure 2

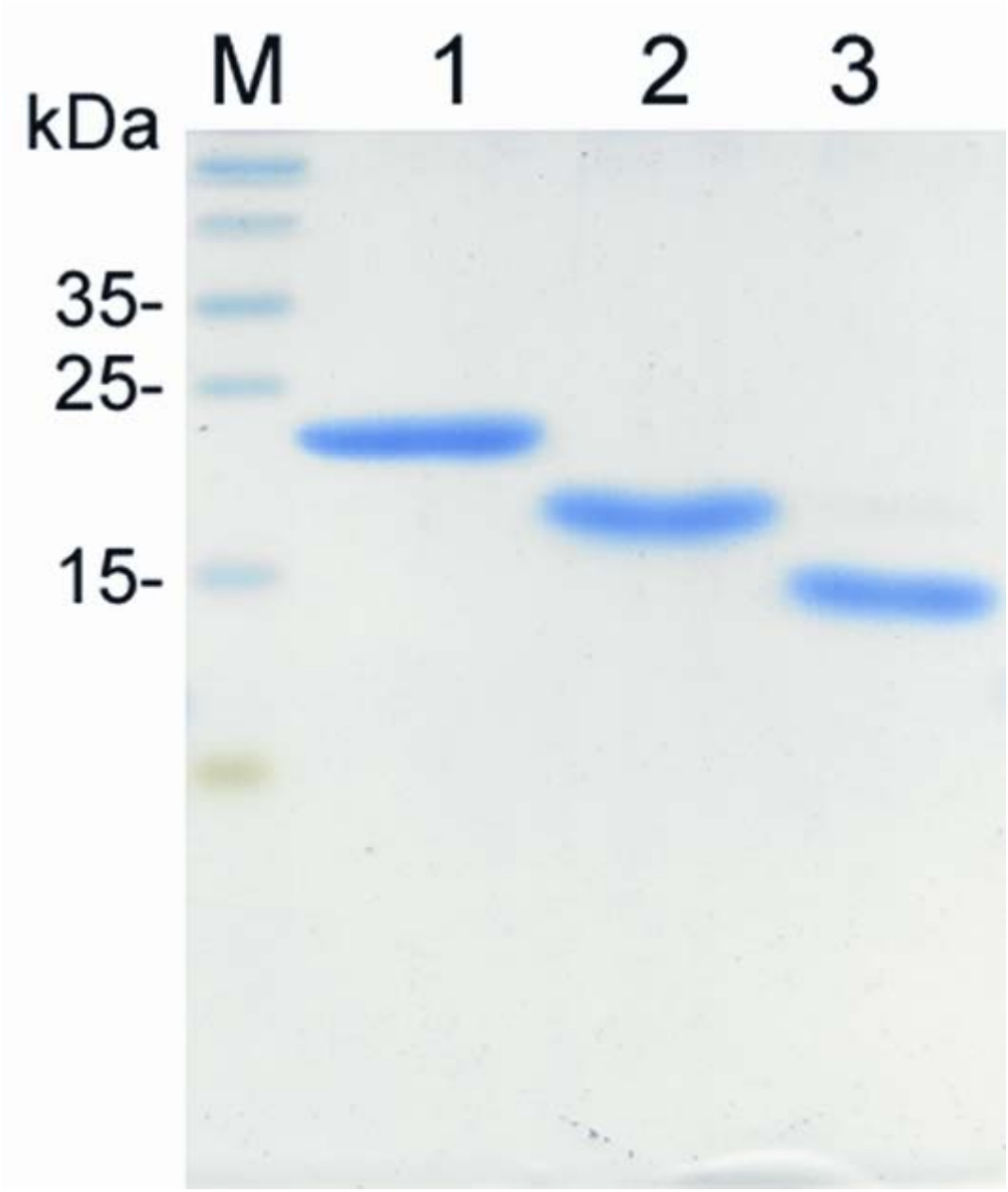

Figure 3

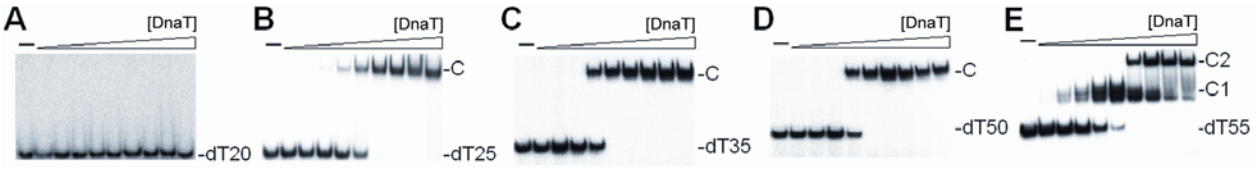

Figure 4

Figure 5

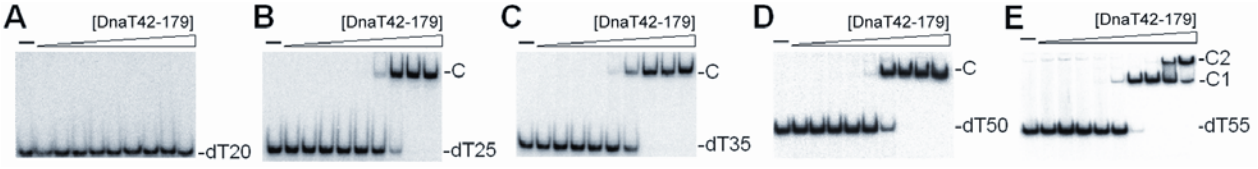

Figure 6

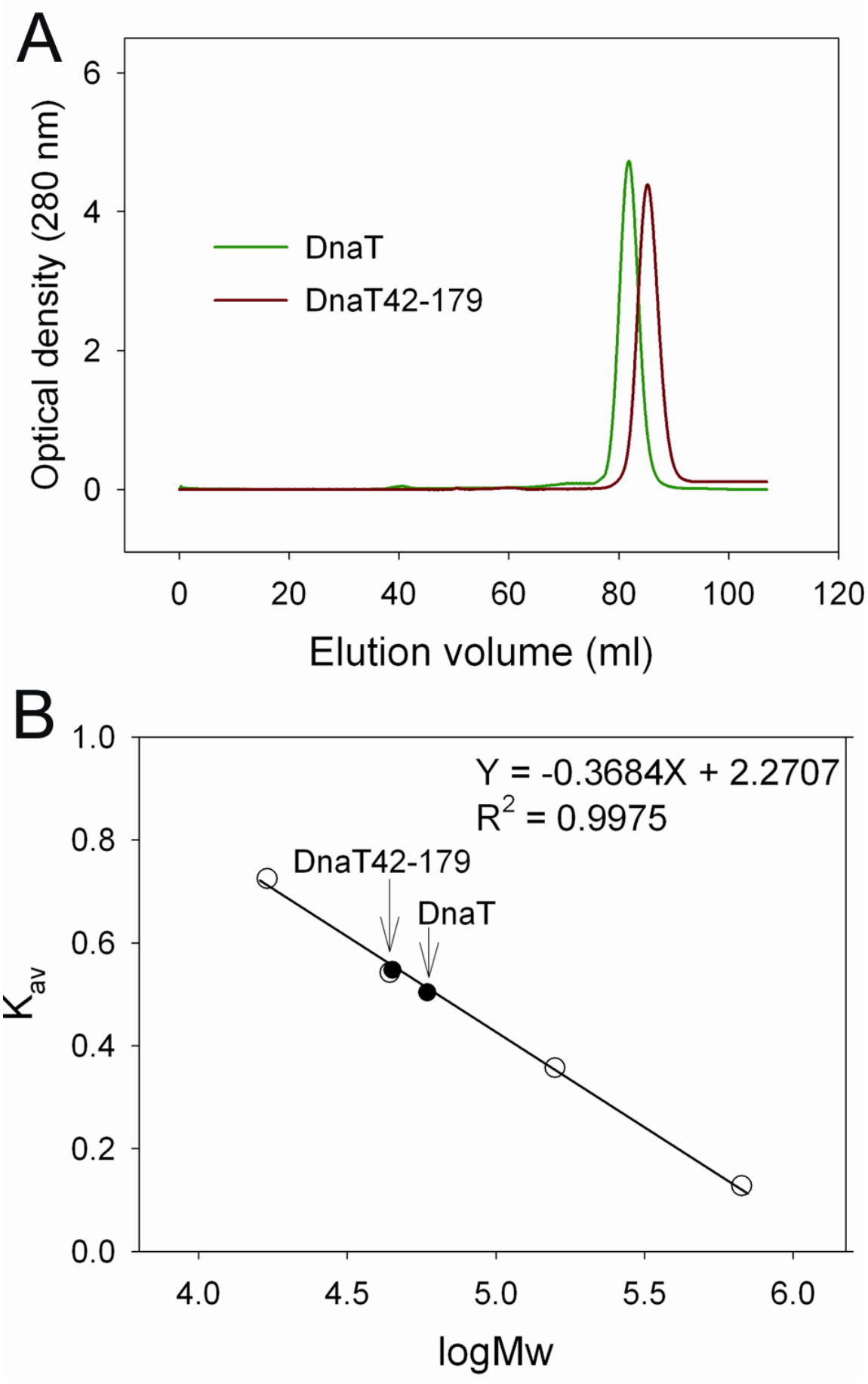
A
Optical density (280 nm)
6
4
2
0
DnaT
DnaT42-179
0
20
40
60
80
100
120
Elution volume (ml)
B
1.0
0.8
0.6
0.4
0.2
0.0
K_{av}
Y = -0.3684X + 2.2707
R^2 = 0.9975
DnaT42-179
DnaT
4.0
4.5
5.0
5.5
6.0
logMw

Figure 7

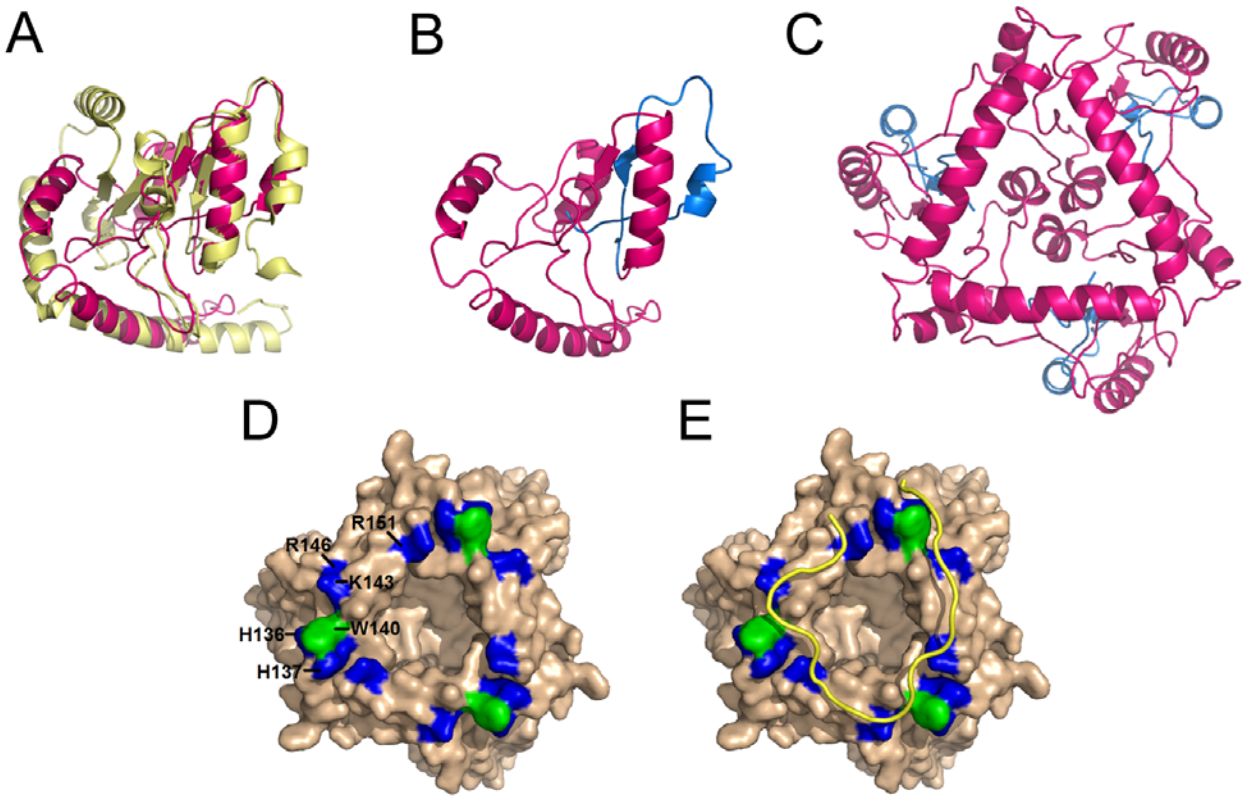

Figure 8

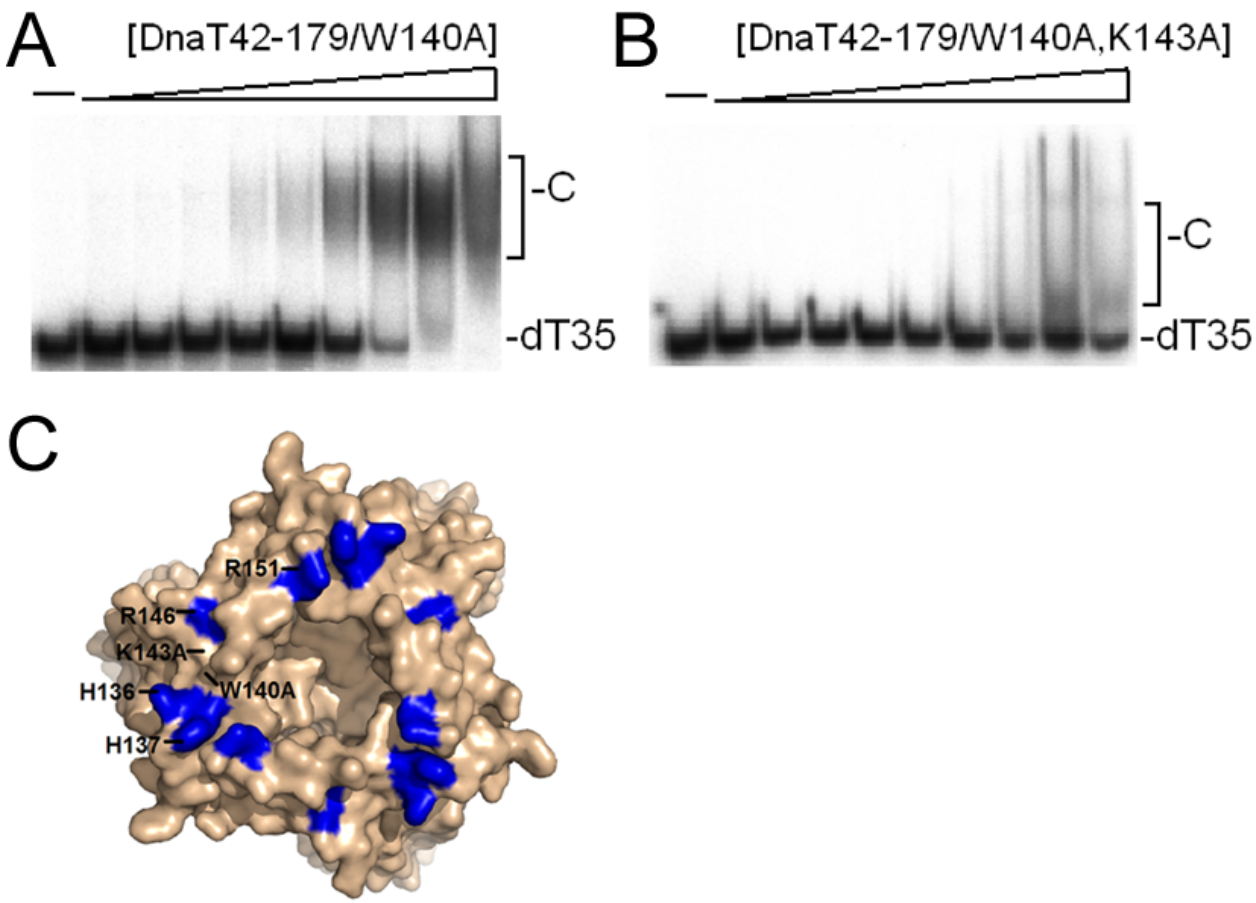
A
[DnaT42-179/W140A]
-C
-dT35
B
[DnaT42-179/W140A,K143A]
-C
-dT35
C
R151
R146
K143A
H136
W140A
H137

Figure 9

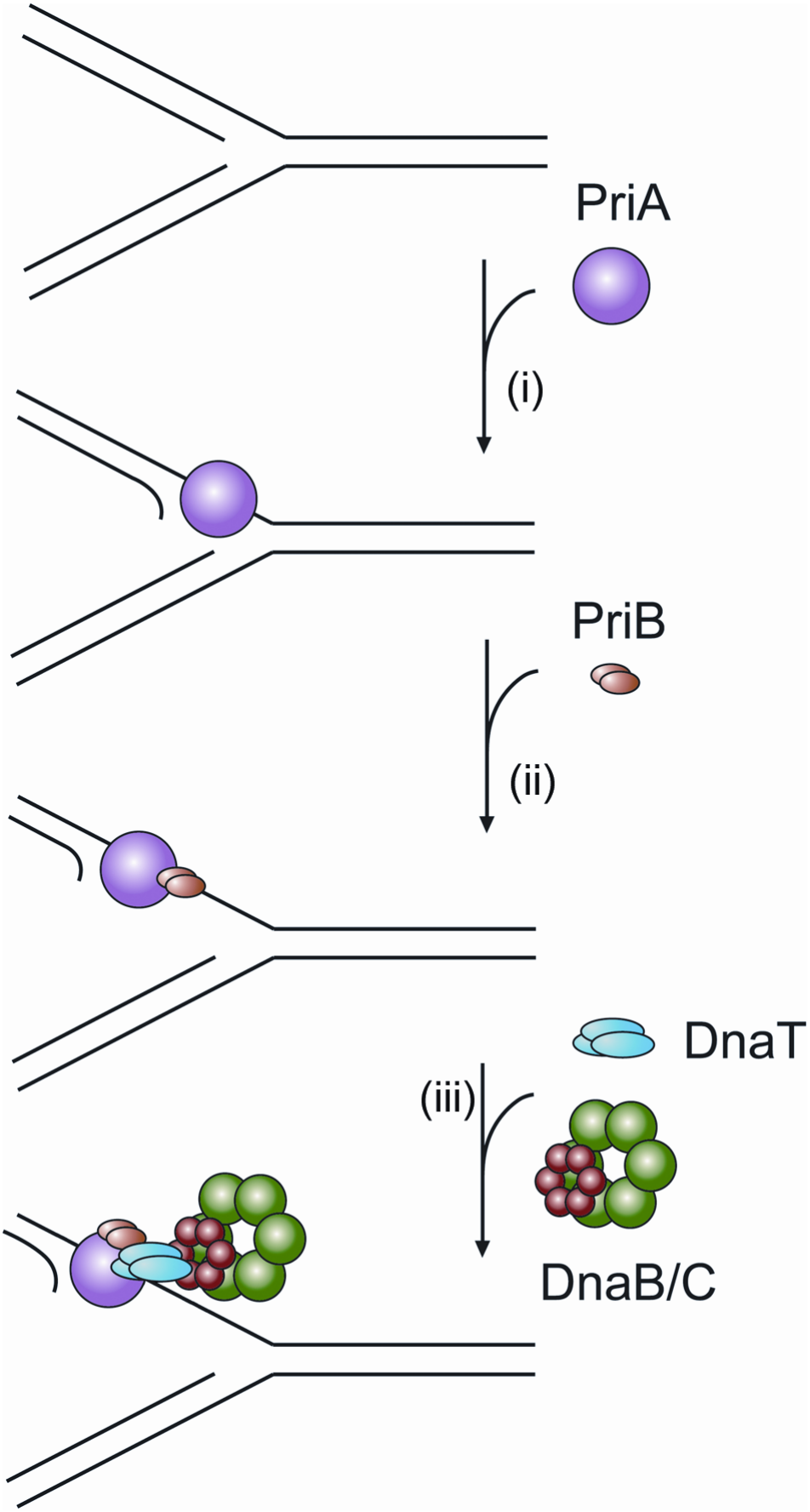

Figure 10

五、附件(學術論文)

5a Huang, Y.H., Lin, M.J., **Huang, C.Y.*** (2013) DnaT is a single-stranded DNA binding protein. ***Genes Cells***, 18, 1007-1019. (SCI)

5b Huang, Y.H., **Huang, C.Y.*** (2013) The N-terminal domain of DnaT, a primosomal DNA replication protein, is crucial for PriB binding and self-trimerization. ***Biochem. Biophys. Res. Commun.***, 442, 147-152. (SCI)

5c Peng, W.F., **Huang, C.Y.*** (2014) Allantoinase and dihydroorotase binding and inhibition by flavonols and the substrates of cyclic amidohydrolases. ***Biochimie***, 101, 113-122. (SCI)

5d Huang, Y.H., **Huang, C.Y.*** (2014) Structural insight into the DNA-binding mode of the primosomal proteins PriA, PriB, and DnaT. Review article. ***Biomed Res. Int.***, 2014, 195162. (SCI)

5e Huang, Y.H., **Huang, C.Y.*** (2014) C-terminal domain swapping of SSB changes the size of the ssDNA binding site. ***Biomed Res. Int.***, 2014, 573936. (SCI)

Genes to Cells

DnaT is a single-stranded DNA binding protein

Yen-Hua Huang[1], Min-Jon Lin[1,2] and Cheng-Yang Huang[1,2]*

[1]*School of Biomedical Sciences, Chung Shan Medical University, No. 110, Sec. 1, Chien-Kuo N. Rd, Taichung, Taiwan*
[2]*Department of Medical Research, Chung Shan Medical University Hospital, No. 110, Sec. 1, Chien-Kuo N. Rd, Taichung, Taiwan*

DnaT is one of the replication restart primosomal proteins required for reinitiating chromosomal DNA replication in bacteria. In this study, we identified and characterized the single-stranded DNA (ssDNA)-binding properties of DnaT using electrophoretic mobility shift analysis (EMSA), bioinformatic tools and two deletion mutant proteins, namely, DnaT26-179 and DnaT42-179. ConSurf analysis indicated that the N-terminal region of DnaT is highly variable. The analysis of purified DnaT and the deletion mutant protein DnaT42-179 by gel filtration chromatography showed a stable trimer in solution, indicating that the N-terminal region, amino acid 1–41, is not crucial for the oligomerization of DnaT. Contrary to PriB, which forms a single complex with a series of ssDNA homopolymers, DnaT, DnaT26-179 and DnaT42-179 form distinct complexes with ssDNA of different lengths and the size of binding site of 26 ± 2 nucleotides (nt). Using bioinformatic programs (PS)^2 and the analysis of the positively charged/hydrophobic residue distribution, as well as the biophysical results in this study, we propose a binding model for the DnaT trimer–ssDNA complex, in which 25-nt-long ssDNA is tethered on the surface groove located in the highly conserved C-terminal domain of DnaT. These results constitute the first study regarding ssDNA-binding activity of DnaT. Consequently, a hand-off mechanism for primosome assembly was modified.

Introduction

The ability to reinitiate chromosomal DNA replication to maintain genetic integrity after encountering DNA damage is essential for bacterial survival (Cox *et al.* 2000; Cox 2001; McGlynn & Lloyd 2002). Given that the DNA replication machinery of all organisms may stall anywhere on the chromosome, the collapsed DNA replication forks must be reactivated through origin-independent reloading of the replisome for genome duplication. The replication restart primosome (Schekman *et al.* 1974; Marians 2000; Sandler 2000), a formidable enzymatic machine, is a protein–DNA complex that reactivates stalled DNA replication at repaired replication forks after DNA damage (Masai *et al.* 2010). It travels along the lagging strand template, unwinds the duplex DNA and primes the Okazaki fragments that are required for replication fork progression (Patel *et al.* 2011; Zheng & Shen 2011). Contrary to the DnaA-directed primosome initiated at the unique *oriC* site (Mott & Berger 2007; Leonard & Grimwade 2011), the replication restart primosome preferentially recognizes three-way branched DNA structures possessing a leading strand (Tanaka *et al.* 2002, 2007; Mizukoshi *et al.* 2003; Sasaki *et al.* 2007). In *Escherichia coli*, the replication restart primosome includes seven essential proteins, namely PriA helicase, PriB, PriC, DnaB helicase, DnaC, DnaT and DnaG primase. At least two overlapping mechanisms are available for the reassembly of the replication forks, that is, initiation is induced by either the PriA helicase or PriC (Heller & Marians 2006a,b). In a PriA–PriB–DnaT-dependent reaction, PriB and DnaT are the second and third proteins to be assembled in the protein–DNA complex, respectively. In addition, the association of DnaT with PriA is facilitated by PriB (Liu *et al.* 1996). The binding site on PriB for the ssDNA overlaps the binding sites for PriA and DnaT, suggesting a dynamic primosome assembly process, in which single-stranded DNA (ssDNA) is handed off from one primosome protein to another as the repaired replication fork is reactivated (Lopper *et al.* 2007). The binding of DnaT to PriA and PriB induces the dissociation of PriB from the ssDNA

Communicated by: Hisao Masai
**Correspondence:* cyhuang@csmu.edu.tw

DOI: 10.1111/gtc.12095

(Fig. 1). However, the mechanism of PriA–PriB–DnaT in reloading the DnaC–DnaB complex and in the formation of the DnaB–DnaG complex at the forks remains unclear.

DnaT, formerly known as the 'protein i' (Arai *et al.* 1981; Masai *et al.* 1986; Masai & Arai 1988), has been initially described as a key component for phage φX174 (Marians 1992) and pBR322 plasmid replication, but not for R1 plasmid replication (Masai & Arai 1989). Genetic analysis for *E. coli* DnaT suggests an essential replication protein for bacterial cell growth because the *dnaT822* mutant shows colony size, cell morphology, inability to properly partition nucleoids, UV sensitivity and basal SOS expression similar to *priA2::kan* mutants (McCool *et al.* 2004). DnaT is a homotrimer of approximately 22 kDa subunits (Arai *et al.* 1981). However, recent studies have also indicated that the protein is in solution as a monomer–trimer equilibrium system (Szymanski *et al.* 2013). Although the role of DnaT in the recruitment of DnaB helicase has been proposed, little is known about the fundamental function of DnaT for the replication restart primosome assembly.

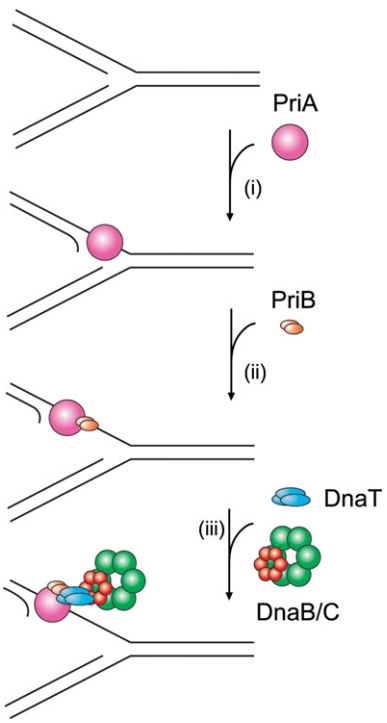

Figure 1 Hand-off mechanism for the replication restart primosome assembly. (i) PriA recognizes and binds to a replication fork; (ii) PriB joins to PriA to form a PriA–PriB–DNA ternary complex; and (iii) DnaT participates in this nucleocomplex to form a triprotein complex, in which, the recruitment of DnaT results in the release of ssDNA by PriB and then loads the DnaB/C complex. This figure is adapted from the published assembly mechanism presented earlier by Lopper *et al.* (2007).

Currently, infections occur that are resistant to all antibacterial options. Few therapies are effective against the six antibiotic-resistant ESKAPE pathogens (*Enterococcus faecium*, *Staphylococcus aureus*, *Klebsiella pneumoniae*, *Acinetobacter baumannii*, *Pseudomonas aeruginosa* and *Enterobacter* species; Bush 2010). *Klebsiella pneumoniae* is a ubiquitous opportunistic pathogen that causes severe diseases such as septicemia, pneumonia, urinary tract infections and soft tissue infections (Podschun & Ullmann 1998). As DnaT is required for reinitiating chromosomal DNA replication in bacteria, blocking the activity of DnaT would be detrimental to bacterial survival. In addition, because DnaT is not found in human, the *K. pneumoniae* DnaT protein may be a promising target in developing antibiotics.

The number of oligonucleotide/oligosaccharide-binding (OB)-fold proteins has grown rapidly over the past few years, and their mechanisms in interacting with ssDNA, including PriB and SSB, have been relatively understood (Flynn & Zou 2010). To date, little information on the ssDNA-binding mode of non-OB-fold proteins is available, especially for a trimeric protein. In this study, we identified a trimeric DnaT that could form stable complex(es) with dT homopolymers of 25 bases (dT25) or longer using electrophoretic mobility shift analysis (EMSA). EMSA is a very popular and well-established approach in molecular biology that facilitates the observation of the protein–DNA complex (Cadman *et al.* 2005; Huang 2012). In addition, we also found that the ssDNA-binding affinity of DnaT was approximately twofold higher than that of PriB, an OB-fold protein. Based on the bioinformatic analyses of DnaT using ConSurf (Landau *et al.* 2005) and $(PS)^2$ (Chen *et al.* 2006, 2009), as well as the results from the biophysical and mutational studies, we proposed a binding model for the DnaT trimer–ssDNA complex. A previously proposed hand-off mechanism for primosome assembly (Lopper *et al.* 2007) in replication restart was discussed and modified.

Results

Sequence analysis

Although DnaT has been identified as a component of the replication restart primosome, the fundamental

Figure 2 Amino acids sequence alignment of *Klebsiella pneumoniae* DnaT. An alignment consensus of 29 sequenced DnaT homologues by ConSurf (Landau *et al.* 2005) shows the degree of variability at each position along the primary sequence. Amino acid residues that are highly variable are colored teal, whereas highly conserved amino acid residues are colored burgundy. A consensus sequence was established by determining the amino acid residue that is most commonly found at each position relative to the primary sequence of *K. pneumoniae* DnaT. In general, amino acid residues in the C-terminal region of DnaT are highly conserved.

function of DnaT in the replication restart primosome assembly has yet to be properly presented. The gene *KPN04812*, encoding *K. pneumoniae* DnaT, was initially found using a database search through the National Center for Biotechnology Information (NCBI). Based on the known nucleotide sequence, the predicted DnaT monomer protein has a length of 179 amino acid residues and a molecular mass of approximately 20 kDa. Figure 2 shows that the alignment consensus of 29 sequenced DnaT homologues by ConSurf (Landau *et al.* 2005; Ho *et al.* 2013) revealed the degree of variability at each position along the primary sequence. Amino acid residues that are highly variable are colored teal, whereas highly conserved amino acid residues are colored burgundy. A consensus sequence was established by determining which amino acid residue that is most commonly found at each position relative to the primary sequence of *K. pneumoniae* DnaT. In general, amino acid residues in the C-terminal region of DnaT are highly conserved.

Purification of DnaT

The gene *KPN04812* encoding the putative DnaT was PCR-amplified using genomic DNA of *K. pneumoniae* subsp. *pneumoniae* MGH 78578 as template. This amplified gene was then ligated into the pET21b vector for protein expression. *Klebsiella pneumoniae* DnaT protein was hetero-overexpressed in *E. coli* and then purified from the soluble supernatant by Ni^{2+}-affinity chromatography (Fig. 3). Pure protein was obtained in this single chromatographic step with an elution of Buffer B (20 mM Tris–HCl, 250 mM imidazole and 0.5 M NaCl, pH 7.9) and then dialyzed against a dialysis buffer (20 mM Tris–HCl and 100 mM NaCl, pH 8.0; Buffer C). Approximately >60 mg of purified protein was obtained from 1 L of a culture of *E. coli* cells. The truncated and mutant DnaT proteins were also purified with the same protocol as that for the wild-type protein, and with very similar purification results.

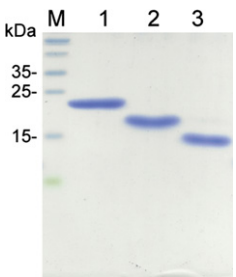

Figure 3 Protein purity. Coomassie Blue-stained SDS-PAGE (12%) of the purified DnaT (lane 1; 5.5 μg), DnaT26-179 (lane 2; 4.8 μg), DnaT42-179 (lane 3; 4.4 μg) and molecular mass standards (M) are shown. The sizes of the standard proteins, from the top down, are as follows: 55, 40, 35, 25, 15 and 10 kDa. The purified DnaT protein migrated between the 25 and 15 kDa standards on the SDS-PAGE.

DnaT has an ssDNA-binding activity

Aromatic stacking and electropositive interactions have an important role in ssDNA binding by proteins (Raghunathan *et al.* 2000; Huang *et al.* 2006). Given that DnaT contains 10 Arg, 5 Lys and 18 aromatic amino acid residues (11 Phe, 4 Trp and 3 Tyr), we attempted to test whether DnaT has ssDNA-binding activity. We studied the binding of DnaT to ssDNA of different lengths with different protein concentrations using EMSA (Fig. 4). EMSA is a well-established

approach in studies of molecular biology, allowing the detection of the distinct protein–DNA complex(es) (Huang 2012). When we incubated DnaT with dT20, no significant band shift was observed, indicating that DnaT could not form a stable complex with this homopolymer (Fig. 4A). To investigate the length of nucleotides sufficient for the formation of the DnaT–ssDNA complex, as well as the ssDNA-binding ability of DnaT, we furthermore tested dT25 (Fig. 4B), dT35 (Fig. 4C) and dT50 (Fig. 4D) to bind to DnaT. In contrast to dT20, longer dT homopolymers, dT25–50, produced a very significant band shift (C, complex). These findings confirm the ssDNA-binding activity of DnaT, which is strong enough to form a stable protein–DNA complex in solution. Furthermore, two different complexes for dT55 were formed by DnaT (Fig. 4E). At lower protein concentrations, DnaT formed a single complex (C1) with dT55, similar to that observed with dT50 (Fig. 4D). However, when the DnaT concentration was increased, another slower-migrating complex (C2) was observed. The appearance of the second complex resulted from the increased DnaT concentration, suggesting that two DnaT proteins may be contained per oligonucleotide. Although dT55 is only 5 nt longer than dT50, the presence of an extra 5 nt in dT55 compared with that of dT50 provides enough interaction space for the binding of two DnaT trimers. Therefore, one DnaT protein occupies 25 (50/2 = 25) nt to 27.5 (55/2 = 27.5) nt of the ssDNA. These results from EMSA suggest that the length of an ssDNA (or the binding site size; Huang 2012) required for DnaT binding is 26 ± 2 nt.

Design of the truncated DnaT proteins DnaT26-179 and DnaT42-179

The N-terminal region of the DnaT is shown by an alignment consensus of 29 sequenced DnaT homologues (Fig. 2), indicating that the function of DnaT can accommodate many different amino acids in the N-terminal region. Thus, the truncated DnaT proteins, DnaT26-179 (the N-terminal 25 amino acid (aa) was removed) and DnaT42-179 (the N-terminal 41 amino acid was removed), were constructed and purified (Fig. 3) to investigate whether the N-terminal region is essential for ssDNA binding and oligomerization of DnaT.

DnaT26-179 bound to ssDNA

The binding of DnaT26-179 to dT20 (Fig. 5A), dT25 (Fig. 5B), dT35 (Fig. 5C), dT50 (Fig. 5D) and dT55 (Fig. 5E) was examined using EMSA. As shown in Fig. 5A, no significant band shift was observed when DnaT26-179 was incubated with dT20. However, DnaT26-179 bound to dT25–50 and formed a single complex. For dT55, two different complexes of DnaT26-179 appeared at high protein concentrations. Regardless of the efficient concentrations for the ssDNA binding, the stoichiometry of DnaT26-179 was nearly identical to that of the wild-type DnaT.

DnaT42-179 bound to ssDNA

The binding of DnaT42-179 to dT20 (Fig. 6A), dT25 (Fig. 6B), dT35 (Fig. 6C), dT50 (Fig. 6D) and dT55 (Fig. 6E) was studied by EMSA. No significant band shift was observed when DnaT42-179 was incubated with dT20. DnaT42-179 could form a single complex with dT25–50 and form two distinct complexes with dT55, respectively. Although the efficient concentrations of DnaT42-179 for the complex(es) formation are higher than those of DnaT and DnaT26-179, their stoichiometries for ssDNA binding are very similar. These data indicate that deletion of the N-terminal 1–41 amino acid region does not influence the binding site size of DnaT.

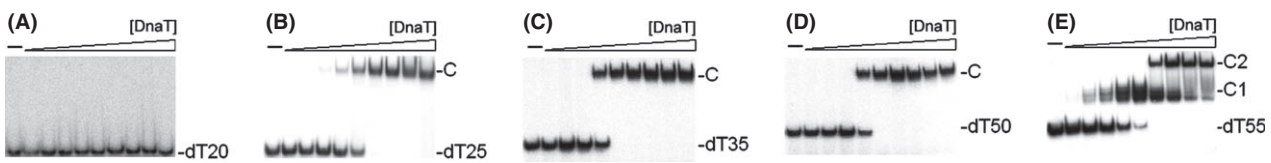

Figure 4 Binding of DnaT to dT20–55. DnaT (0, 0.35, 0.7, 1.4, 2.8, 5.6, 11.3, 22.5, 45 and 90 μM; monomer) was incubated for 30 min at 25 °C with 1.7 nM of (A) dT20, (B) dT25, (C) dT35, (D) dT50 or (E) dT55 in a total volume of 10 μL in 20 mM Tris–HCl pH 8.0 and 100 mM NaCl. Aliquots (5 μL) were removed from each reaction solution and added to 2 μL of gel-loading solution (0.25% bromophenol blue and 40% sucrose). The resulting samples were resolved on a native 8% polyacrylamide gel at 4 °C in TBE buffer (89 mM Tris borate and 1 mM EDTA) for 1–1.5 h at 100 V and visualized by autoradiography. Complexed and free DNA bands were scanned and quantified.

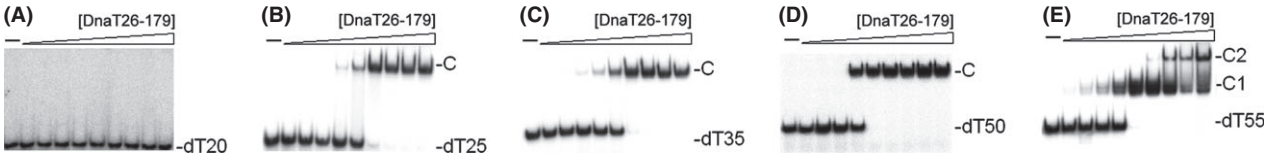

Figure 5 Binding of DnaT26-179 to dT20–55. DnaT26-179 (0, 0.35, 0.7, 1.4, 2.8, 5.6, 11.3, 22.5, 45 and 90 μM; monomer) was incubated for 30 min at 25 °C with 1.7 nM of (A) dT20, (B) dT25, (C) dT35, (D) dT50 or (E) dT55 in a total volume of 10 μL in 20 mM Tris–HCl pH 8.0 and 100 mM NaCl. Aliquots (5 μL) were removed from each reaction solution and added to 2 μL of gel-loading solution (0.25% bromophenol blue and 40% sucrose). The resulting samples were resolved on a native 8% polyacrylamide gel at 4 °C in TBE buffer (89 mM Tris borate and 1 mM EDTA) for 1–1.5 h at 100 V and visualized by autoradiography. Complexed and free DNA bands were scanned and quantified.

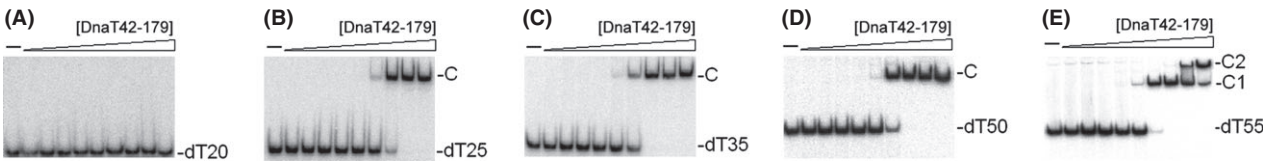

Figure 6 Binding of DnaT42-179 to dT20–55. DnaT42-179 (0, 0.35, 0.7, 1.4, 2.8, 5.6, 11.3, 22.5, 45 and 90 μM; monomer) was incubated for 30 min at 25 °C with 1.7 nM of (A) dT20, (B) dT25, (C) dT35, (D) dT50 or (E) dT55 in a total volume of 10 μL in 20 mM Tris–HCl pH 8.0 and 100 mM NaCl. Aliquots (5 μL) were removed from each reaction solution and added to 2 μL of gel-loading solution (0.25% bromophenol blue and 40% sucrose). The resulting samples were resolved on a native 8% polyacrylamide gel at 4 °C in TBE buffer (89 mM Tris borate and 1 mM EDTA) for 1–1.5 h at 100 V and visualized by autoradiography. Complexed and free DNA bands were scanned and quantified.

Table 1 ssDNA-binding properties of DnaT, DnaT26-179 and DnaT42-179 as analyzed by EMSA

	DnaT		DnaT26-179		DnaT42-179		PriB⋆	
DNA	$[Protein]_{50}$†	*N*	$[Protein]_{50}$	*N*	$[Protein]_{50}$	*N*	$[Protein]_{50}$	*N*
dT20	ND	1	ND	1	ND	1	ND	1
dT25	5.6 ± 0.3	1	6.5 ± 0.3	1	14 ± 2	1	18 ± 2	1
dT35	2.7 ± 0.2	1	6.1 ± 0.3	1	12 ± 2	1	8 ± 1	1
dT50	2.2 ± 0.2	1	2.8 ± 0.2	1	8.2 ± 1.2	1	4 ± 0.5	1
dT55	2.0 ± 0.2	2	2.9 ± 0.3	2	8.1 ± 1.5	2	4 ± 0.5	1

N, complex number; EMSA, electrophoretic mobility shift analysis.
Errors are standard deviations determined by three independent titration experiments.
⋆EMSA results of *Klebsiella pneumoniae* PriB (Huang *et al.* 2012b).
†$[Protein]_{50}$ was calculated from the titration curves of EMSA by determining the concentration of the protein (μM) needed to achieve the midpoint value for input ssDNA binding. For dT55, input ssDNA binding was the sum of the intensities from the two separate ssDNA–protein complexes.

Binding constants of the DnaT–ssDNA complexes determined from EMSA

To compare the ssDNA-binding abilities of DnaT, DnaT26-179 and DnaT42-179, the midpoint values for input ssDNA binding, calculated from the titration curves of EMSA and referred to as $[Protein]_{50}$, were quantified and are summarized in Table 1. Although the binding site size of these DnaT variants was very similar as previously discussed, their ssDNA-binding activities were different. The deletion of the N-terminal 1–25 amino acid region in the DnaT slightly affected the ssDNA binding (Table 1). DnaT42-179 had a 2.5- to 4-fold lesser affinity for binding to dT25–55 compared with those of DnaT.

The N-terminal region of DnaT was assumed to be not significant in the primosome assembly because

this region was quite variable (Fig. 2). Although the region amino acid 1–41 in DnaT does not contain highly conserved positively charged/aromatic residues for ssDNA interaction (except for F16), our EMSA results indicated that DnaT42-179 still had a defective ssDNA-binding ability compared with DnaT (Table 1). Thus, this region in DnaT may not be directly involved in ssDNA binding. Previous data have shown that the binding of SSB to long ssDNA results in a conformational change in the protein, making the glycine-rich region more easily accessible to the action of proteases (Curth *et al.* 1996). Although the flexible region in DnaT has not been identified yet, DnaT has been noted to contain 13 Pro and 11 Gly amino acid residues (Fig. 2), which are important components of the flexible region. We speculate that the phenomenon for SSB may be applied to DnaT. The N-terminal region amino acid 1–41 may be involved in some unknown conformational changes in DnaT, causing some ssDNA-binding sites to be more accessible to interact with ssDNA. Given the hand-off mechanism for the primosome assembly, we believe that some significant conformational changes in DnaT must occur during ssDNA binding (Lopper *et al.* 2007). Many bacteria do not contain a recognizable homologue of PriB (Dong *et al.* 2010) and other loading factors, such as PriC and DnaC. Thus, several regions that are important for protein–protein interaction and conformational change in DnaT are not necessarily conserved.

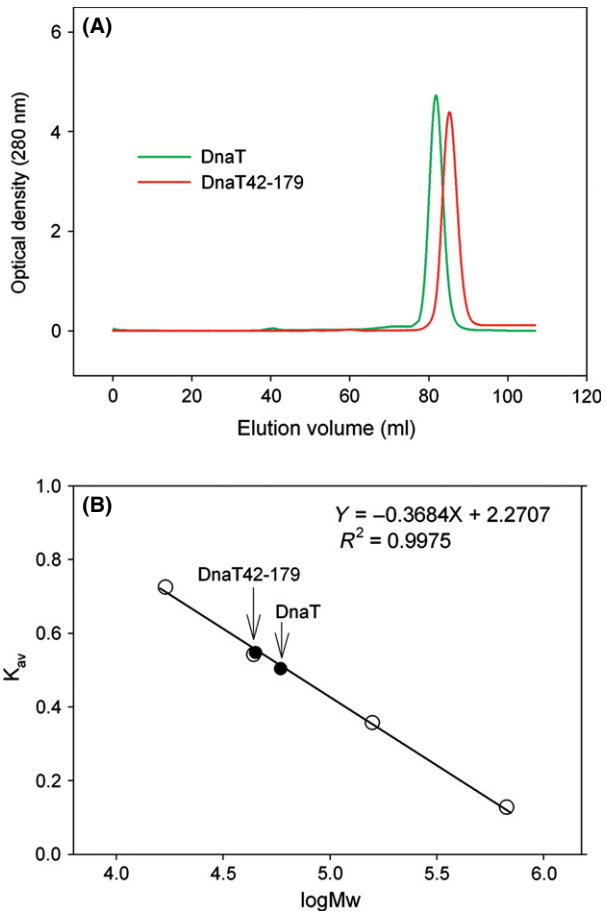

Figure 7 Oligomeric state of purified DnaT and DnaT42-179 in solution. (A) Gel filtration chromatographic analysis of the purified DnaT variants. Purified protein in buffer (20 mM Tris–HCl and 100 mM NaCl at pH 8.0) was applied to a Superdex 200 HR 10/30 column equilibrated with the same buffer. The column was operated at a flow rate of 0.5 mL/min, and 0.5 mL fractions were collected. The protein was detected by measuring absorbance at 280 nm. The column was calibrated with proteins of known molecular masses (closed symbols): thyroglobulin (670 kDa), γ-globulin (158 kDa), ovalbumin (44 kDa) and myoglobin (17 kDa). The corresponding single peak shows the eluted DnaT and DnaT42-179, respectively. (B) A standard linear regression curve was generated by plotting the log of the molecular mass of the calibration proteins against their K_{av} values.

Oligomeric state of DnaT in solution

The analysis of purified DnaT protein (4 mg/mL; 204 μM) by gel filtration chromatography showed a single peak with elution volume of 81.6 mL (Fig. 7A). Assuming that DnaT has a shape and partial specific volume similar to the standard proteins, the native molecular mass of DnaT was estimated to be 60 320 Da, calculated from a standard linear regression equation, $K_{av} = -0.3684$ (logMw) + 2.2707 (Fig. 7B). The native molecular mass for DnaT is approximately thrice as much as that of a DnaT monomer (approximately 20 kDa). In addition, a single peak with the same elution volume similar to that of 4 mg/mL was observed when 1 mg/mL (approximately 50 μM) DnaT concentration was used. Therefore, we believe that DnaT, under these conditions, is a stable trimer in solution. In addition, this concentration (50 μM) used in estimating the DnaT trimer was also used in EMSA (Fig. 4). Given the formation of a single complex with ssDNA (dT25–50), we speculate that only the trimeric form of DnaT, but not a mixture or other oligomeric form, is involved in the complex(es) formation.

Purified DnaT42-179 (4 mg/mL; 253 μM) was also analyzed by gel filtration chromatography to investigate the deletion effect in the oligomeric state

of DnaT. The chromatographic result also showed a single peak (Fig. 7A). The native molecular mass of DnaT42-179 was estimated to be 45 982 Da (Fig. 7B). Based on the molecular mass of the DnaT42-179 monomer (approximately 16 kDa), we concluded that DnaT42-179 in the solution is a stable trimer, similar to DnaT. Thus, deletion of the N-terminal 1–41 amino acid region does not cause any change in the oligomeric state of DnaT.

Structure modeling of DnaT

To obtain an in-depth understanding of the structure–function relationship of DnaT, we decided to model its three-dimensional structure by homology modeling. No protein with amino acid sequence similar to DnaT was found in the structure databank. Hence, homology modeling for the DnaT structure by several homology-based programs was not successful. For example, when we pasted the DnaT amino acid sequence to SWISS-MODEL (http://swissmodel.expasy.org/) for modeling, no result was provided (Arnold *et al.* 2006). Thus, DnaT may form a novel fold for ssDNA binding.

We subsequently used another type of the bioinformatic program $(PS)^2$ (Chen *et al.* 2006, 2009), for the structure modeling of DnaT. $(PS)^2$ (http://140.113.239.111/~ps2v2/docs.php) is an automatic homology modeling server that combines both sequence and secondary structure information to detect the homologous proteins with remote similarity and the target–template alignment. After pasting the amino acid sequence to the website of $(PS)^2$, one hit (Protein Data Bank entry: 1GD9), alpha-aminotransferase from *Pyrococcus horikoshii*, was suggested. The amino acid residue 14–165 in DnaT (pink) was matched in the alpha-aminotransferase (yellow) of amino acid 143–314, with 20% identity in amino acid sequence and 85% identity in the secondary structure (Fig. 8A). This model shows that the N-ter-

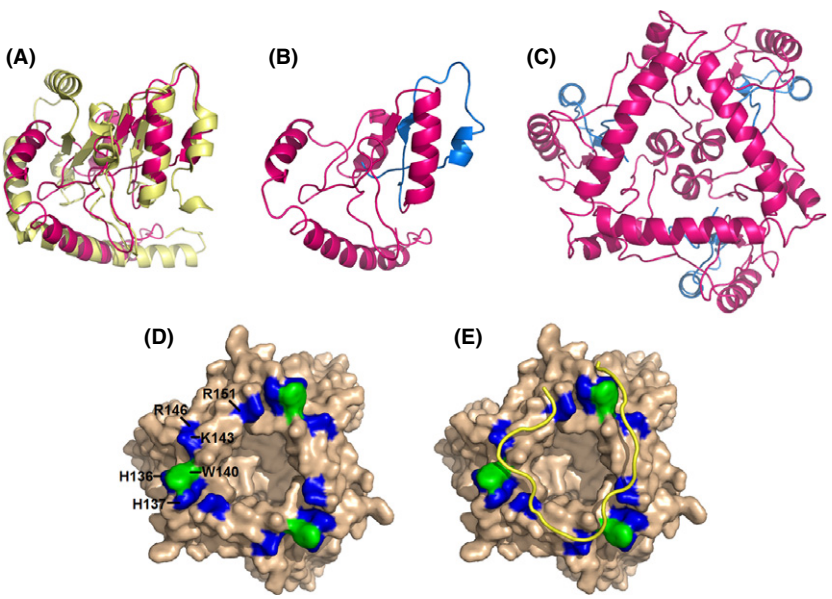

Figure 8 Structure modeling of DnaT. (A) Structure modeling of DnaT by the bioinformatic program $(PS)^2$. After searching and modeling, *Pyrococcus horikoshii* alpha-aminotransferase was suggested. The amino acid residue 14–165 in DnaT (pink) was matched in the alpha-aminotransferase of amino acid 143–314 (yellow), with 20% identity in amino acid sequence and 85% identity in the secondary structure. (B) Ribbon diagram of the modeled DnaT monomer (amino acid 14–165). The N-terminal region amino acid 14–41 is shown in marine color, and amino acid 42–165 in DnaT is in hot pink. (C) Ribbon diagram of a possible trimeric DnaT structure. The trimeric DnaT structure was manually built using threefold symmetry; each monomer (amino acid 14–165) is stabilized by two helices. The N-terminal region amino acid 14–41 is shown in marine color, and amino acid 42–165 in DnaT is in hot pink. (D) The putative ssDNA binding sites of DnaT. The highly conserved hydrophobic (green) and basic residues (blue) of DnaT, H136, H137, W140, K143, R146 and R151, located on the potential ssDNA binding surface, are indicated. (E) A model of the ssDNA–DnaT complex. The model was directly constructed by superimposing the modeled DnaT trimer with the crystal structure of the ssDNA–SSB complex (PDB code 1EYG). The ssDNA (25-mer) generated from the ssDNA–SSB complex is shown in gold.

minal region in the modeled structure of DnaT is flexible, and the C-terminal region contains helices with several loops (Fig. 8B). Given that the deletion in the N-terminal region did not cause any change in the oligomerization state of DnaT (Fig. 7), the C-terminal region of DnaT may serve as the oligomerization/ssDNA-binding domain, similar to the N-terminal oligomerization/ssDNA-binding domain in SSB (Raghunathan *et al.* 2000; Chan *et al.* 2009). However, the sequence and structure fold between DnaT and SSB are quite different.

Trimeric DnaT structure model

Although the ssDNA-binding ability of DnaT has been identified in this study, the ssDNA-binding mode remains ambiguous. Considering that the oligomerization state and ssDNA-binding properties of DnaT42-179 are similar to those of DnaT, the region amino acid 42–179 could be defined as the oligomerization/ssDNA-binding domain in DnaT. Accordingly, a possible trimeric DnaT structure was manually built using threefold symmetry; each monomer is stabilized by two helices (Fig. 8C). We found that the modeled DnaT trimer structure is ring-shaped. The ring-like structure of DnaT is slightly similar to that of the hexameric (consisted of three dimers) DnaC helicase from *Geobacillus kaustophilus*, a DnaB-like helicase (Lo *et al.* 2009). DnaT may bind to DnaB with a stoichiometry of 1 : 2, one DnaT monomer to a DnaB dimer. However, this DnaT structure is only a modeled structure, and these speculations must be furthermore confirmed by additional biophysical studies.

ssDNA-binding mode of DnaT

Based on the structural model of DnaT, the positively charged (blue) and aromatic residues (green) located in the C-terminus of DnaT have been suggested to be involved in ssDNA binding: H136, H137, W140, K143, R146 and R151 (Fig. 8D). In addition, these residues in DnaT are significantly conserved among the 29 sequenced DnaT proteins (Fig. 2). F73 and F74 are also potential binding sites for ssDNA, but they are not conserved in DnaT family. These residues in DnaT create a shallow groove on the surface that can potentially be wrapped around by ssDNA. According to the structure–function relationship of DnaT, we manually added and superimposed the ssDNA dC25 from the crystal structure of *E. coli* SSB (Raghunathan *et al.* 2000; Protein Data Bank entry: 1EYG) into the DnaT trimer structure (Fig. 8E). DnaT could form a stable complex with 25-mer ssDNA (Fig. 4B). In this modeled structure of DnaT–ssDNA complex, 25-mer ssDNA seems to suitably fit DnaT (Fig. 8E). However, this DnaT complex structure is only a modeled structure, and this binding mode must be furthermore confirmed by additional biophysical studies.

To test whether the proposed model is possible for forming the DnaT–ssDNA complex, alanine substitution mutant DnaT42-179/W140 and the double mutant DnaT42-179/W140, K143A were conducted and analyzed by EMSA. As shown in Fig. 9A, although the band shift was still observed when DnaT42-179/W140 was incubated with dT35, significant smears and decreased ability for ssDNA binding were found. The $[\text{Protein}]_{50}$ for the binding of DnaT42-179/W140 to dT35 is 16 ± 3 μM, a value

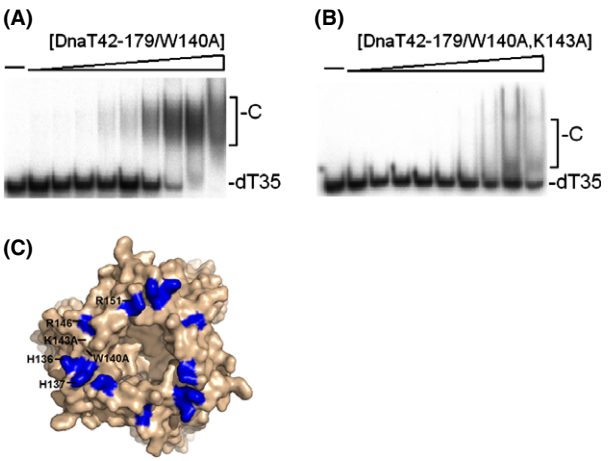

Figure 9 Mutational analysis of DnaT. Binding of DnaT mutant protein, (A) DnaT42-179/W140A or (B) DnaT42-179/W140A, K143A to dT35. The mutant protein (0, 0.35, 0.7, 1.4, 2.8, 5.6, 11.3, 22.5, 45 and 90 μM; monomer) was incubated for 30 min at 25 °C with 1.7 nM of dT35 in a total volume of 10 μL in 20 mM Tris–HCl pH 8.0 and 100 mM NaCl. Aliquots (5 μL) were removed from each reaction solution and added to 2 μL of gel-loading solution (0.25% bromophenol blue and 40% sucrose). The resulting samples were resolved on a native 8% polyacrylamide gel at 4 °C in TBE buffer (89 mM Tris borate and 1 mM EDTA) for 1–1.5 h at 100 V and visualized by autoradiography. Complexed and free DNA bands were scanned and quantified. (C) A proposed trimeric DnaT structure for DnaT42-179/W140A, K143A mutant. Because of a trimer, mutation in these two residues (W140 and K143) may lead to loss of six binding sites in the C-terminal region of DnaT.

lower than that for DnaT42-179 (12 ± 2 μM). For the double mutant DnaT42-179/W140, K143A, it could not form a stable complex, indicating a dramatically impaired ability for ssDNA binding of this mutant (Fig. 9B). Thus, residues suggested from the proposed model were involved in ssDNA binding of DnaT. Because of a trimer, mutation in these two residues (W140 and K143) may lead to loss of six binding sites in the C-terminal region of DnaT (Fig. 9C).

Discussion

DnaT is a novel ssDNA-binding protein

For the first time, the ssDNA-binding activity of DnaT was identified and assessed with a $K_{d,app}$ ($[Protein]_{50}$) of 5.6 ± 0.3 μM for dT25 binding and the binding site size of 26 ± 2 per DnaT trimer. To date, insufficient information on the ssDNA-binding mode for a trimeric protein is available. Although DnaT has been identified as a component of the replication restart primosome, the function of DnaT for DNA binding has yet to be properly presented. Although previous fluorescence anisotropy studies have indicated that DnaT has a very weak ssDNA-binding activity to determine its K_d (Lopper *et al.* 2007), with the use of EMSA, we showed in our study that the ssDNA-binding activity of DnaT is strong enough for forming a stable complex with ssDNA. This activity for ssDNA binding by DnaT, assayed in the same manner, is even higher than that of an OB-fold protein PriB (Table 1), another loading factor for primosome assembly (Huang *et al.* 2012b). EMSA is a useful technology in molecular biology, and the use of radioactive DNA makes it highly sensitive and allows for the observation of the distinct complexes (Huang 2012). For 25-mer ssDNA or longer, stable DnaT–ssDNA complex(es) is clearly shown from EMSA (Fig. 4). However, whether this significant disparity is due to inherent differences among the species, the use of different assay methods, or the effect of different investigators, remains unknown. We also noted that these seemingly contradictory data may reconcile. In a previous study that used fluorescence anisotropy (Lopper *et al.* 2007), the ssDNA-binding ability of DnaT was assayed with 18-mer ssDNA, and a very weak activity of DnaT for ssDNA-binding was then observed and concluded. Similarly, DnaT could not bind to short ssDNA from our EMSA result (Fig. 4A).

Comparison with PriB

Various single-stranded DNA binding proteins bind to ssDNA with some degree of positive cooperativity (Lohman & Ferrari 1994; Wold 1997; Huang *et al.* 2006). In this study, we found different EMSA behaviors between PriB and DnaT proteins. DnaT variants form multiple distinct complexes with ssDNA of different lengths (Figs 4–6), whereas binding of PriB to ssDNA dT20–dT60 forms a single complex only (Huang *et al.* 2012b). Considering their binding activities (Table 1), these findings suggest that DnaT binds to ssDNA with higher binding affinity but lower cooperativity than PriB. Although DnaT is not an OB-fold protein predicted from sequence analysis and structure modeling, DnaT has a higher ssDNA-binding activity than that of PriB, an OB-fold protein.

Insight into the hand-off mechanism: a modified version

A hand-off mechanism for primosome assembly (Lopper *et al.* 2007) has been proposed (Fig. 1), where (i) PriA recognizes and binds to a replication fork; (ii) PriB joins to PriA to form a PriA–PriB–DNA ternary complex; and (iii) DnaT participates in this nucleocomplex to form a triprotein complex, in which, the recruitment of DnaT results in the release of ssDNA by PriB and then loads the DnaB/C complex. In this study, we have identified DnaT as a kind of ssDNA-binding protein and found that the ssDNA-binding activity of DnaT is approximately twofold higher than that of PriB. Thus, the hand-off mechanism for primosome assembly should be modified (Fig. 10), such that (i) PriA recognizes and binds to a replication fork; (ii) PriB joins to PriA to form a PriA–PriB–DNA ternary complex; and (iii) DnaT interacts with ssDNA, PriA and PriB, forces the release of ssDNA by PriB and then the DnaB/C complex is loaded. This updated model explains the mechanism as to how DnaT binds to ssDNA and its partner proteins. However, the detailed action of DnaT in every key step for primosome assembly is still unclear. In addition, whether DnaT is a necessary factor for primosome assembly because many bacteria do not have a recognizable homologue of DnaT still remains to be explored. Furthermore, given that only one monomer of the PriB dimer can engage in interactions with the DNA and the partner protein(s) (Huang *et al.* 2006; Szymanski *et al.* 2010), whether the binding site on PriB for ssDNA is necessary to overlap the binding sites for PriA and DnaT should

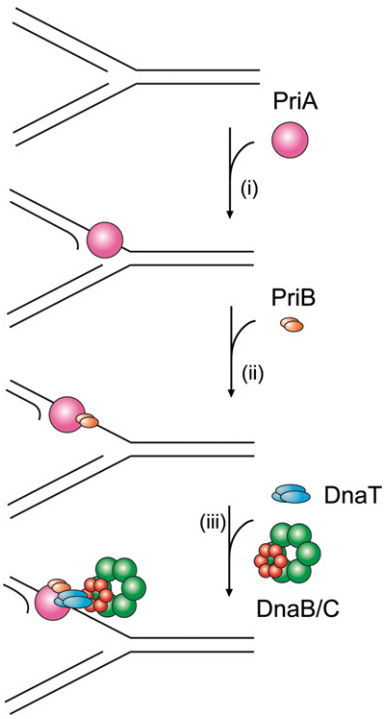

Figure 10 An updated hand-off mechanism for the replication restart primosome assembly. In this study, we have identified DnaT as a kind of ssDNA-binding protein and found that the ssDNA-binding activity of DnaT is approximately twofold higher than that of PriB. Thus, the hand-off mechanism for primosome assembly should be modified, such that (i) PriA recognizes and binds to a replication fork; (ii) PriB joins to PriA to form a PriA–PriB–DNA ternary complex; and (iii) DnaT interacts with ssDNA, PriA and PriB, forces the release of ssDNA by PriB and then the DnaB/C complex are loaded. This updated model explains the mechanism as to how DnaT binds to ssDNA and its partner proteins. However, the detailed action of DnaT in every key step for primosome assembly is still unclear.

be determined. The more complex structures of PriB and DnaT are useful in helping our understanding of the primosome assembly mechanism(s).

Experimental procedures

Materials

All restriction enzymes and DNA-modifying enzymes were purchased from New England Biolabs (Ipswich, MA) unless explicitly stated otherwise. All chemicals were purchased from Sigma-Aldrich (St. Louis, MO) unless explicitly stated otherwise. The *E. coli* strains TOP10F' (Invitrogen) and BL21 (DE3)pLysS (Novagen, UK) were used for genetic construction and protein expression, respectively.

Construction of the DnaT, DnaT26-179 and DnaT42-179 expression plasmids

The gene *KPN04812* encoding the putative DnaT was PCR-amplified using genomic DNA of *K. pneumoniae* subsp. *pneumoniae* MGH 78578 as template. The forward (5′-GAAGGGGCATATGTCTTCGCGAATTTTAACCTC-3′) and the reverse (5′-GGGGCTCGAGTCCTCGGAAACCTCGCGGAAT-3′) primers were designed to introduce unique *Nde*I and *Xho*I restriction sites (underlined) into DnaT, permitting insertion of the amplified gene into the pET21b vector (Novagen Inc., Madison, WI) for protein expression in *E. coli*. The DnaT26-179 and DnaT42-179 expression plasmids were constructed using the same protocol for DnaT. The oligonucleotide primers for preparation of the DnaT26-179 and DnaT42-179 expression plasmids were as follows: 5′-GGGCATATGAAATCGACTGACGGCACC-3′ and 5′-GGGCTCGAGTCCTCGGAAACCTCGCGG-3′ for DnaT26-179 and 5′-GGGCATATGTTCTATGCGCTGACGCCA-3′ and 5′-GGGCTCGAGTCCTCGGAAACCTCGCGG-3′ for DnaT42-179. The expected gene product expressed by these plasmids has a His tag, which is useful for purifying the recombinant protein.

Protein expression and purification

The recombinant DnaT proteins were expressed and purified using the protocol described previously for allantoinase (Ho *et al.* 2013), hydantoinase (Huang *et al.* 2009), dihydroorotase (Wang *et al.* 2010), PriB (Huang *et al.* 2012b), DnaB (Lin & Huang 2012) and SSB (Huang & Huang 2012). Briefly, *E. coli* BL21(DE3) cells were individually transformed with the expression vector and grown to OD_{600} of 0.9 at 37 °C in Luria-Bertani medium containing 250 μg/mL ampicillin with rapid shaking. Over-expression of the expression plasmids was induced by incubating with 1 mM isopropyl thiogalactoside for 3 h at 37 °C. The cells overexpressing the protein were chilled on ice, harvested by centrifugation, resuspended in Buffer A (20 mM Tris–HCl, 5 mM imidazole and 0.5 M NaCl, pH 7.9) and disrupted by sonication with ice cooling. The protein purified from the soluble supernatant by Ni^{2+}-affinity chromatography (HiTrap HP; GE Healthcare Bio-Sciences, Piscataway, NJ) was eluted with Buffer B (20 mM Tris–HCl, 250 mM imidazole and 0.5 M NaCl, pH 7.9) and dialyzed against a dialysis buffer (20 mM Tris–HCl and 100 mM NaCl, pH 8.0; Buffer C). Protein purity remained >97% as determined by Coomassie-stained SDS-PAGE (Mini-PROTEAN Tetra System; Bio-Rad, CA).

Protein concentration

The protein concentration of the solutions was determined by the Bio-Rad Protein Assay using bovine serum albumin as a standard (Bio-Rad). The Bio-Rad Protein Assay is a dye-binding assay in which a differential color change of a dye occurs in response to various concentrations of protein.

Gel filtration chromatography

Gel filtration chromatography was carried out by the AKTA-FPLC system (GE Healthcare Bio-Sciences). Briefly, purified protein (4 mg/mL) in Buffer C was applied to a Superdex 200 HR 10/30 column (GE Healthcare Bio-Sciences) equilibrated with the same buffer. The column was operated at a flow rate of 0.5 mL/min, and 0.5 mL fractions were collected. The proteins were detected by measuring the absorbance at 280 nm. The column was calibrated with proteins of known molecular weight: thyroglobulin (670 kDa), γ-globulin (158 kDa), ovalbumin (44 kDa) and myoglobin (17 kDa). The K_{av} values for the standard proteins and the DnaT variants were calculated from the equation: $K_{av} = (V_e - V_o)/(V_c - V_o)$, where V_o is column void volume, V_e is elution volume and V_c is geometric column volume.

Electrophoretic mobility shift assay

Electrophoretic mobility shift analysis for the DnaT variants was carried out by the protocol described previously for DnaB (Lin & Huang 2012), PriB (Hsieh & Huang 2011; Huang *et al.* 2012a,b) and SSB proteins (Huang *et al.* 2011; Jan *et al.* 2011; Huang & Huang 2012). Briefly, radiolabeling of various lengths of ssDNA oligonucleotides was carried out with [γ^{32}P] ATP (6000 Ci/mmol; PerkinElmer Life Sciences, Waltham, MA) and T4 polynucleotide kinase (Promega, Madison, WI). DnaT, DnaT26-179 and DnaT42-179 (0, 0.35, 0.7, 1.4, 2.8, 5.6, 11.3, 22.5, 45 and 90 μM) were individually incubated for 30 min at 25 °C with 1.7 nM DNA substrates (dT20–55) in a total volume of 10 μL in 20 mM Tris–HCl pH 8.0 and 100 mM NaCl. Aliquots (5 μL) were removed from each of the reaction solutions and added to 2 μL of gel-loading solution (0.25% bromophenol blue and 40% sucrose). The resulting samples were resolved on a native 8% polyacrylamide gel at 4 °C in TBE buffer (89 mM Tris borate and 1 mM EDTA) for 1–1.5 h at 100 V and were visualized by autoradiography. Complexed and free DNA bands were scanned and quantified.

ssDNA-binding ability

The ssDNA-binding ability ($[Protein]_{50}$; $K_{d,app}$) for the protein was estimated from the protein concentration that binds 50% of the input ssDNA (Huang 2012). Each $[Protein]_{50}$ is calculated as the average of at least three measurements ± SD.

Site-directed mutagenesis

Two DnaT mutants, DnaT42-179/W140A and DnaT42-179/W140A, K143A, were generated using a QuikChange Site-Directed Mutagenesis kit according to the manufacturer's protocol (Stratagene, LaJolla, CA). The presence of the mutation was verified by DNA sequencing in each construct. The oligonucleotide primers for the preparation of mutants were as follows: 5′-TTTCACCACGTGCAGGCGCAGCAGAAG-3′ and 5′-CAGCTTCTGCTGCGCCTGCACGTGGTG-3′ for DnaT42-179/W140A (the pET21b-DnaT42-179 as template); 5′-GTGCAGGCGCAGCAGGCGCTGGCACGTAGC-3′ and 5′-GCTACGTGCCAGCGCCTGCTGCGCCTGCAC-3′ for DnaT42-179/W140A, K143A (the pET21b-DnaT42-179/W140A as template). The underlined sequences denote the mutated amino acid(s).

Bioinformatics

The amino acid sequences of 29 sequenced DnaT homologues were aligned using ConSurf (Landau *et al.* 2005). The model of DnaT was built from the coordinate of 1GD9 (crystal structure of *P. horikoshii* alpha-aminotransferase) using $(PS)^2$ (Chen *et al.* 2006, 2009). The 25-mer ssDNA in the model of the ssDNA–DnaT complex was generated from the coordinate of 1EYG (crystal structure of the ssDNA–SSB complex; Raghunathan *et al.* 2000), in which dC3-27 (25-mer ssDNA) was used. The structures were visualized using the program PyMol.

Acknowledgements

We would like to thank two anonymous reviewers and the editor for their comments. We also thank Mr. Jiun-De Huang for preparing the Figs 1 and 10. This research was supported by a grant from the National Science Council, Taiwan (NSC 102-2320-B-040-019 to C.Y. Huang).

References

Arai, K., McMacken, R., Yasuda, S. & Kornberg, A. (1981) Purification and properties of *Escherichia coli* protein i, a prepriming protein in phi X174 DNA replication. *J. Biol. Chem.* **256**, 5281–5286.

Arnold, K., Bordoli, L., Kopp, J. & Schwede, T. (2006) The SWISS-MODEL workspace: a web-based environment for protein structure homology modelling. *Bioinformatics* **22**, 195–201.

Bush, K. (2010) Alarming beta-lactamase-mediated resistance in multidrug-resistant *Enterobacteriaceae*. *Curr. Opin. Microbiol.* **13**, 558–564.

Cadman, C.J., Lopper, M., Moon, P.B., Keck, J.L. & McGlynn, P. (2005) PriB stimulates PriA helicase via an interaction with single-stranded DNA. *J. Biol. Chem.* **280**, 39693–39700.

Chan, K.W., Lee, Y.J., Wang, C.H., Huang, H. & Sun, Y.J. (2009) Single-stranded DNA-binding protein complex from *Helicobacter pylori* suggests an ssDNA-binding surface. *J. Mol. Biol.* **388**, 508–519.

Chen, C.C., Hwang, J.K. & Yang, J.M. (2006) $(PS)^2$: protein structure prediction server. *Nucleic Acids Res.* **34**, W152–W157.

Chen, C.C., Hwang, J.K. & Yang, J.M. (2009) $(PS)^2$-v2: template-based protein structure prediction server. *BMC Bioinformatics* **10**, 366.

Cox, M.M. (2001) Recombinational DNA repair of damaged replication forks in *Escherichia coli*: questions. *Annu. Rev. Genet.* **35**, 53–82.

Cox, M.M., Goodman, M.F., Kreuzer, K.N., Sherratt, D.J., Sandler, S.J. & Marians, K.J. (2000) The importance of repairing stalled replication forks. *Nature* **404**, 37–41.

Curth, U., Genschel, J., Urbanke, C. & Greipel, J. (1996) In vitro and in vivo function of the C-terminus of *Escherichia coli* single-stranded DNA binding protein. *Nucleic Acids Res.* **24**, 2706–2711.

Dong, J., George, N.P., Duckett, K.L., DeBeer, M.A. & Lopper, M.E. (2010) The crystal structure of *Neisseria gonorrhoeae* PriB reveals mechanistic differences among bacterial DNA replication restart pathways. *Nucleic Acids Res.* **38**, 499–509.

Flynn, R.L. & Zou, L. (2010) Oligonucleotide/oligosaccharide-binding fold proteins: a growing family of genome guardians. *Crit. Rev. Biochem. Mol. Biol.* **45**, 266–275.

Heller, R.C. & Marians, K.J. (2006a) Replication fork reactivation downstream of a blocked nascent leading strand. *Nature* **439**, 557–562.

Heller, R.C. & Marians, K.J. (2006b) Replisome assembly and the direct restart of stalled replication forks. *Nat. Rev. Mol. Cell Biol.* **7**, 932–943.

Ho, Y.Y., Huang, Y.H. & Huang, C.Y. (2013) Chemical rescue of the post-translationally carboxylated lysine mutant of allantoinase and dihydroorotase by metal ions and short-chain carboxylic acids. *Amino Acids* **44**, 1181–1191.

Hsieh, H.C. & Huang, C.Y. (2011) Identification of a novel protein, PriB, in *Klebsiella pneumoniae*. *Biochem. Biophys. Res. Commun.* **404**, 546–551.

Huang, C.Y. (2012) Determination of the binding site-size of the protein-DNA complex by use of the electrophoretic mobility shift assay. In: *Stoichiometry and Research—The Importance of Quantity in Biomedicine* (ed. A. Innocenti), pp. 235–242. Rijeka, Croatia: InTech Press.

Huang, C.Y., Hsu, C.C., Chen, M.C. & Yang, Y.S. (2009) Effect of metal binding and posttranslational lysine carboxylation on the activity of recombinant hydantoinase. *J. Biol. Inorg. Chem.* **14**, 111–121.

Huang, C.Y., Hsu, C.H., Sun, Y.J., Wu, H.N. & Hsiao, C.D. (2006) Complexed crystal structure of replication restart primosome protein PriB reveals a novel single-stranded DNA-binding mode. *Nucleic Acids Res.* **34**, 3878–3886.

Huang, Y.H. & Huang, C.Y. (2012) Characterization of a single-stranded DNA-binding protein from *Klebsiella pneumoniae*: mutation at either Arg73 or Ser76 causes a less cooperative complex on DNA. *Genes Cells* **17**, 146–157.

Huang, Y.H., Lee, Y.L. & Huang, C.Y. (2011) Characterization of a single-stranded DNA binding protein from *Salmonella enterica* serovar Typhimurium LT2. *Protein J.* **30**, 102–108.

Huang, Y.H., Lin, H.H. & Huang, C.Y. (2012a) A single residue determines the cooperative binding property of a primosomal DNA replication protein, PriB, to single-stranded DNA. *Biosci. Biotechnol. Biochem.* **76**, 1110–1115.

Huang, Y.H., Lo, Y.H., Huang, W. & Huang, C.Y. (2012b) Crystal structure and DNA-binding mode of *Klebsiella pneumoniae* primosomal PriB protein. *Genes Cells* **17**, 837–849.

Jan, H.C., Lee, Y.L. & Huang, C.Y. (2011) Characterization of a single-stranded DNA-binding protein from *Pseudomonas aeruginosa* PAO1. *Protein J.* **30**, 20–26.

Landau, M., Mayrose, I., Rosenberg, Y., Glaser, F., Martz, E., Pupko, T. & Ben-Tal, N. (2005) ConSurf 2005: the projection of evolutionary conservation scores of residues on protein structures. *Nucleic Acids Res.* **33**, W299–W302.

Leonard, A.C. & Grimwade, J.E. (2011) Regulation of DnaA assembly and activity: taking directions from the genome. *Annu. Rev. Microbiol.* **65**, 19–35.

Lin, H.H. & Huang, C.Y. (2012) Characterization of flavonol inhibition of DnaB helicase: real-time monitoring, structural modeling, and proposed mechanism. *J. Biomed. Biotechnol.* **2012**, 735368.

Liu, J., Nurse, P. & Marians, K.J. (1996) The ordered assembly of the phiX174-type primosome. III. PriB facilitates complex formation between PriA and DnaT. *J. Biol. Chem.* **271**, 15656–15661.

Lo, Y.H., Tsai, K.L., Sun, Y.J., Chen, W.T., Huang, C.Y. & Hsiao, C.D. (2009) The crystal structure of a replicative hexameric helicase DnaC and its complex with single-stranded DNA. *Nucleic Acids Res.* **37**, 804–814.

Lohman, T.M. & Ferrari, M.E. (1994) *Escherichia coli* single-stranded DNA-binding protein: multiple DNA-binding modes and cooperativities. *Annu. Rev. Biochem.* **63**, 527–570.

Lopper, M., Boonsombat, R., Sandler, S.J. & Keck, J.L. (2007) A hand-off mechanism for primosome assembly in replication restart. *Mol. Cell* **26**, 781–793.

Marians, K.J. (1992) Prokaryotic DNA replication. *Annu. Rev. Biochem.* **61**, 673–719.

Marians, K.J. (2000) PriA-directed replication fork restart in *Escherichia coli*. *Trends Biochem. Sci.* **25**, 185–189.

Masai, H. & Arai, K. (1988) Initiation of lagging-strand synthesis for pBR322 plasmid DNA replication in vitro is dependent on primosomal protein i encoded by dnaT. *J. Biol. Chem.* **263**, 15016–15023.

Masai, H. & Arai, K. (1989) *Escherichia coli* dnaT gene function is required for pBR322 plasmid replication but not for R1 plasmid replication. *J. Bacteriol.* **171**, 2975–2980.

Masai, H., Bond, M.W. & Arai, K. (1986) Cloning of the *Escherichia coli* gene for primosomal protein i: the relationship to dnaT, essential for chromosomal DNA replication. *Proc. Natl Acad. Sci. USA* **83**, 1256–1260.

Masai, H., Tanaka, T. & Kohda, D. (2010) Stalled replication forks: making ends meet for recognition and stabilization. *BioEssays* **32**, 687–697.

McCool, J.D., Ford, C.C. & Sandler, S.J. (2004) A dnaT mutant with phenotypes similar to those of a priA2:kan mutant in *Escherichia coli* K-12. *Genetics* **167**, 569–578.

McGlynn, P. & Lloyd, R.G. (2002) Recombinational repair and restart of damaged replication forks. *Nat. Rev. Mol. Cell Biol.* **3**, 859–870.

Mizukoshi, T., Tanaka, T., Arai, K., Kohda, D. & Masai, H. (2003) A critical role of the 3′ terminus of nascent DNA chains in recognition of stalled replication forks. *J. Biol. Chem.* **278**, 42234–42239.

Mott, M.L. & Berger, J.M. (2007) DNA replication initiation: mechanisms and regulation in bacteria. *Nat. Rev. Microbiol.* **5**, 343–354.

Patel, S.S., Pandey, M. & Nandakumar, D. (2011) Dynamic coupling between the motors of DNA replication: hexameric helicase, DNA polymerase, and primase. *Curr. Opin. Chem. Biol.* **15**, 595–605.

Podschun, R. & Ullmann, U. (1998) *Klebsiella* spp. as nosocomial pathogens: epidemiology, taxonomy, typing methods, and pathogenicity factors. *Clin. Microbiol. Rev.* **11**, 589–603.

Raghunathan, S., Kozlov, A.G., Lohman, T.M. & Waksman, G. (2000) Structure of the DNA binding domain of *E. coli* SSB bound to ssDNA. *Nat. Struct. Biol.* **7**, 648–652.

Sandler, S.J. (2000) Multiple genetic pathways for restarting DNA replication forks in *Escherichia coli* K-12. *Genetics* **155**, 487–497.

Sasaki, K., Ose, T., Okamoto, N., Maenaka, K., Tanaka, T., Masai, H., Saito, M., Shirai, T. & Kohda, D. (2007) Structural basis of the 3′-end recognition of a leading strand in stalled replication forks by PriA. *EMBO J.* **26**, 2584–2593.

Schekman, R., Weiner, A. & Kornberg, A. (1974) Multienzyme systems of DNA replication. *Science* **186**, 987–993.

Szymanski, M.R., Jezewska, M.J. & Bujalowski, W. (2010) Interactions of the *Escherichia coli* primosomal PriB protein with the single-stranded DNA. Stoichiometries, intrinsic affinities, cooperativities, and base specificities. *J. Mol. Biol.* **398**, 8–25.

Szymanski, M.R., Jezewska, M.J. & Bujalowski, W. (2013) The *Escherichia coli* primosomal dnat protein exists in solution as a monomer-trimer equilibrium system. *Biochemistry* **52**, 1845–1857.

Tanaka, T., Mizukoshi, T., Sasaki, K., Kohda, D. & Masai, H. (2007) *Escherichia coli* PriA protein, two modes of DNA binding and activation of ATP hydrolysis. *J. Biol. Chem.* **282**, 19917–19927.

Tanaka, T., Mizukoshi, T., Taniyama, C., Kohda, D., Arai, K. & Masai, H. (2002) DNA binding of PriA protein requires cooperation of the N-terminal D-loop/arrested-fork binding and C-terminal helicase domains. *J. Biol. Chem.* **277**, 38062–38071.

Wang, C.C., Tsau, H.W., Chen, W.T. & Huang, C.Y. (2010) Identification and characterization of a putative dihydroorotase, KPN01074, from *Klebsiella pneumoniae*. *Protein J.* **29**, 445–452.

Wold, M.S. (1997) Replication protein A: a heterotrimeric, single-stranded DNA-binding protein required for eukaryotic DNA metabolism. *Annu. Rev. Biochem.* **66**, 61–92.

Zheng, L. & Shen, B. (2011) Okazaki fragment maturation: nucleases take centre stage. *J. Mol. Cell Biol.* **3**, 23–30.

Received: 17 April 2013
Accepted: 11 August 2013

Biochemical and Biophysical Research Communications 442 (2013) 147–152

Contents lists available at ScienceDirect

Biochemical and Biophysical Research Communications

journal homepage: www.elsevier.com/locate/ybbrc

The N-terminal domain of DnaT, a primosomal DNA replication protein, is crucial for PriB binding and self-trimerization

Yen-Hua Huang [a], Cheng-Yang Huang [a,b,*]

[a] School of Biomedical Sciences, Chung Shan Medical University, No. 110, Sec. 1, Chien-Kuo N. Rd., Taichung City, Taiwan
[b] Department of Medical Research, Chung Shan Medical University Hospital, No. 110, Sec. 1, Chien-Kuo N. Rd., Taichung City, Taiwan

ARTICLE INFO

Article history:
Received 14 November 2013
Available online 23 November 2013

Keywords:
DnaT
PriB
DNA replication restart
Single-stranded DNA
Primosome

ABSTRACT

DnaT and PriB are replication restart primosomal proteins required for re-initiating chromosomal DNA replication in bacteria. Although the interaction of DnaT with PriB has been proposed, which region of DnaT is involved in PriB binding and self-trimerization remains unknown. In this study, we identified the N-terminal domain in DnaT (aa 1–83) that is important in PriB binding and self-trimerization but not in single-stranded DNA (ssDNA) binding. DnaT and the deletion mutant DnaT42-179 protein can bind to PriB according to native polyacrylamide gel electrophoresis, Western blot analysis, and pull-down assay, whereas DnaT84-179 cannot bind to PriB. In contrast to DnaT, DnaT26-179, and DnaT42-179 proteins, which form distinct complexes with ssDNA of different lengths, DnaT84-179 forms only a single complex with ssDNA. Analysis of DnaT84-179 protein by gel filtration chromatography showed a stable monomer in solution rather than a trimer, such as DnaT, DnaT26-179, and DnaT42-179 proteins. These results constitute a pioneering study of the domain definition of DnaT. Further research can directly focus on determining how DnaT binds to the PriA–PriB–DNA tricomplex in replication restart by the hand-off mechanism.

1. Introduction

Genetic integrity should be maintained from generation to generation for bacteria to survive [1]. When DNA is damaged, the DNA replication machinery may be arrested anywhere in the chromosome [2]. Collapsed DNA replication forks must be reactivated by the replication restart primosome by the origin-independent reloading of the polymerase to duplicate genomes [2,3]. After DNA repair, the replication restart primosome [4–6], a formidable enzymatic machine, travels along the lagging strand template, unwinds the duplex DNA, and primes the Okazaki fragments required for the progression of replication forks [7,8]. The replication restart primosome preferentially recognizes three-way branched DNA structures with a leading strand [9–12]. In *Escherichia coli*, the PriA-directed primosome includes six essential proteins, namely, PriA, PriB, DnaB, DnaC, DnaT, and DnaG [5]. PriA, an initiator protein, first binds to the forked DNA. PriB and DnaT are the second and third proteins, respectively, to be assembled in the protein–DNA complex. The association of DnaT with PriA is facilitated by PriB [13]. The binding of DnaT to PriA and PriB dissociates PriB from single-stranded DNA (ssDNA) [14]. However, which region of DnaT interacts with PriB remains unclear.

DnaT, formerly known as protein i [15–17], is a key component for the replication of phage ϕX174 [18] and pBR322 plasmid but not for that of R1 plasmid [19]. Genetic analysis of *E. coli* DnaT suggests an essential replication protein for the growth of bacterial cells because the *dnaT822* mutant shows colony size, cell morphology, inability to properly partition nucleoids, UV sensitivity, and basal SOS expression similar to those of *priA2::kan* mutants [20]. DnaT is also required for *E. coli* growth at elevated pressure [21] and for the lytic cycle of Mu growth [22].

DnaT is a homotrimer of approximately 22 kDa subunits [17,23]. The N-terminal region, aa 1–41, is not crucial for the oligomerization of DnaT [23]. However, DnaT also exists in solution as a monomer–trimer equilibrium system [24]. The ssDNA-binding site of DnaT may primarily be located in the C-terminal region (aa 42–179) with a size of 26 ± 2 nt [23]. Yeast two-hybrid analyses revealed that DnaT can interact with PriB alone [25]. Although the role of DnaT in the recruitment of DnaB helicase has been proposed, little is known about the fundamental function of DnaT for the assembly of the replication restart primosome.

Abbreviations: ssDNA, single-stranded DNA; aa, amino acid residues; SDS–PAGE, sodium dodecyl sulfate–polyacrylamide gel electrophoresis; EDTA, ethylenediamine tetraacetic acid; IPTG, isopropyl thiogalactoside; nt, nucleotides; EMSA, electrophoretic mobility shift analysis.

* Corresponding author at: School of Biomedical Sciences, Chung Shan Medical University, No. 110, Sec. 1, Chien-Kuo N. Rd., Taichung City, Taiwan.
E-mail address: cyhuang@csmu.edu.tw (C.-Y. Huang).

0006-291X/$ - see front matter © 2013 Elsevier Inc. All rights reserved.
http://dx.doi.org/10.1016/j.bbrc.2013.11.069

In this study, we defined a two-domain structure for DnaT and thus identified the involvement of the N-terminal domain (aa 1–83) in PriB binding and of the C-terminal domain (aa 84–179) in ssDNA binding. The lack of the N-terminal domain in DnaT resulted in the failure to trimerize. Further research can focus on determining how PriB and DnaT bind to the PriA–DNA complex in replication restart.

2. Materials and methods

2.1. Construction of expression plasmids of DnaT, DnaT1-83, DnaT1-120, DnaT1-139, DnaT42-179, DnaT84-179, and PriB(dHis)

A fragment containing the coding sequence of DnaT variants was amplified by PCR with the genomic DNA of *Klebsiella pneumoniae* subsp. *pneumoniae* MGH 78578 as template. The PCR products with unique NdeI and XhoI restriction sites were then cloned into the pET21b vector (Novagen, Madison, WI, USA) for protein expression in *E. coli*. The primers used to construct these plasmids are summarized in Supplementary Table 1. These plasmids were verified by DNA sequencing. The expected gene product expressed by these plasmids had a His tag, which is useful for purifying the recombinant protein and Western blot by the anti-His antibody. To distinguish proteins in the Western blot, we also constructed plasmid pET21b-PriB(dHis) to express PriB without a His tag.

2.2. Protein expression and purification

The recombinant DnaT variants were expressed and purified using the protocol described previously for DnaT [23]. Briefly, *E. coli* BL21(DE3) cells were individually transformed with the expression vector and grown to OD_{600} of 0.9 at 37 °C in Luria–Bertani medium containing 250 μg/mL ampicillin with rapid shaking. Overexpression of the expression plasmids was induced by incubating with 1 mM isopropyl thiogalactoside for 3 h at 37 °C. The cells overexpressing the protein were chilled on ice, harvested by centrifugation, resuspended in Buffer A (20 mM Tris–HCl, 5 mM imidazole, and 0.5 M NaCl, pH 7.9) and disrupted by sonication with ice cooling. The protein purified from the soluble supernatant by Ni^{2+}-affinity chromatography (HiTrap HP; GE Healthcare Bio-Sciences, Piscataway, NJ, USA) was eluted with Buffer B (20 mM Tris–HCl, 250 mM imidazole, and 0.5 M NaCl, pH 7.9) and dialyzed against a dialysis buffer (20 mM Tris–HCl and 100 mM NaCl, pH 8.0; Buffer C). PriB(dHis) was expressed using the same protocol, but was purified in different way. The soluble supernatant (20 mM Tris–HCl and 100 mM NaCl, pH 5.9; Buffer D) containing PriB(dHis) was applied to the SP column (GE Healthcare Bio-Sciences, Piscataway, NJ, USA). PriB(dHis) was eluted with a linear NaCl gradient from 0.1 to 1 M with Buffer D using the AKTA–FPLC system (GE Healthcare Bio-Sciences, Piscataway, NJ, USA). Purity of these proteins remained greater than 97% as determined by Coomassie-stained SDS–PAGE (Mini-PROTEAN Tetra System; Bio-Rad, CA, USA).

2.3. Gel-filtration chromatography

Gel-filtration chromatography was carried out by the AKTA–FPLC system. Briefly, purified protein (25 mg/mL) in Buffer C was applied to a Superdex 200 HR 10/30 column (GE Healthcare Bio-Sciences, Piscataway, NJ, USA) equilibrated with the same buffer. The column was operated at a flow rate of 0.5 mL/min, and 0.5-mL fractions were collected. The proteins were detected by measuring the absorbance at 280 nm. The column was calibrated with proteins of known molecular weight: γ-globulin (158 kDa), ovalbumin (44 kDa), myoglobin (17 kDa), and vitamin B_{12} (1.35 kDa). The K_{av} values for the standard proteins and the DnaT variant were calculated from the equation: $K_{av} = (V_e - V_o)/(V_c - V_o)$, where V_o is column void volume, V_e is elution volume, and V_c is geometric column volume.

2.4. Electrophoretic mobility shift assay (EMSA)

EMSA for DnaT84-179 was conducted according to the protocol previously described for DnaT [23]. ssDNA oligonucleotides of various lengths were radiolabeled with [γ^{32}P]ATP (6000 Ci/mmol; PerkinElmer Life Sciences, Waltham, MA) and T4 polynucleotide kinase (Promega, Madison, WI, USA). DnaT84-179 (0, 1.3, 2.5, 5.0, and 10.0 μM) was individually incubated at 25 °C for 30 min with 1.7 nM DNA substrates (dT10–70) at a total volume of 10 μL in 20 mM Tris–HCl (pH 8.0) and 100 mM NaCl. Aliquots (5 μL) were removed from each reaction solution and were added to 2 μL of gel-loading solution (0.25% bromophenol blue and 40% sucrose). The resulting samples were resolved on a native 8% polyacrylamide gel at 4 °C in TBE buffer (89 mM Tris borate and 1 mM EDTA) at 100 V for 60 min to 90 min and were visualized by autoradiography. Complexed and free DNA bands were scanned and quantified.

2.5. Native PAGE for analyzing protein–protein interaction

DnaT, DnaT42-179, or DnaT84-179 (0–60 μM) was incubated at 25 °C for 20 min with PriB(dHis) (60 μM) at a total volume of 100 μL in Buffer C. Aliquots (10 μL) were removed from each reaction solution and were added to 3 μL of gel-loading solution (0.25% bromophenol blue and 40% sucrose). The resulting samples were resolved on a native 9% polyacrylamide gel at 4 °C in TBE buffer (89 mM Tris borate and 1 mM EDTA) at 150 V for 2 h and were visualized by Coomassie staining.

2.6. Western blot analysis

After native PAGE, the proteins were transferred onto a nitrocellulose membrane (Whattman). After overnight blocking with 1% (w/v) bovine serum albumin, the membrane was sequentially incubated with a mouse anti-6xHis-tag IgG1 monoclonal antibody conjugated to horseradish peroxidase (1:1000) (Serotec). Between these successive 2 h incubations, the membrane was washed with PBS-0.1% Tween 20. A chemiluminescent HRP substrate (Millipore) was used for detection.

2.7. Pull-down assay

DnaT, DnaT42-179, or DnaT84-179 (20 μM) was incubated at 25 °C for 20 min with PriB(dHis) (20 μM) in Buffer C. Nickel-NTA agarose beads (GE Healthsciences) were added to each sample, incubated for 2 min, and centrifuged for 1 min at 6000*g*. The beads were washed several times with Buffer C. Proteins were eluted with Buffer B and visualized by Coomassie stained SDS–PAGE.

2.8. ssDNA-binding ability

The ssDNA binding ability ($[Protein]_{50}$; $K_{d,app}$) for the protein was estimated from the protein concentration that binds 50% of the input ssDNA. Each $[Protein]_{50}$ is calculated as the average of at least three measurements ± SD.

3. Results and discussion

3.1. Purifying DnaT, DnaT1-83, DnaT1-120, DnaT1-139, DnaT42-179, DnaT84-179, and PriB(dHis)

The *K. pneumoniae* proteins were hetero-overexpressed in *E. coli* and were then purified from the soluble supernatant by Ni^{2+}-affinity chromatography and the SP column (Fig. 1A). However, DnaT1-83, DnaT1-120, and DnaT1-139 were all expressed as protein pellets, suggesting that the C-terminal region was important for the solubility of DnaT.

3.2. DnaT84-179 is a monomer

DnaT is a trimeric protein whose N-terminal region (aa 1–41) is unimportant for oligomerization [23]. To determine whether the length of DnaT affects its oligomerization state, we analyzed DnaT84-179 by gel filtration chromatography and found a single peak with an elution volume of 98.08 mL (Fig. 1B). Assuming that DnaT84-179 has a shape and partial specific volume similar to those of standard proteins, the native molecular mass of DnaT84-179 was estimated to be 10816 Da, calculated from a standard linear regression equation, $K_{av} = -0.2921\ (\log Mw) + 1.8984$ (Fig. 1C). The native molecular mass of DnaT84-179 is approximately equal to that of a DnaT84-179 monomer (~11 kDa). Thus, the deletion of the N-terminal 1–83 aa region significantly changed the oligomeric state of DnaT (i.e., from a trimer to a monomer) in contrast to that of DnaT42-179, which remains a trimer [23]. The N-terminal aa 43–83 region was critical for DnaT self-trimerization. The properties of the deletion mutant of DnaT are summarized in Table 1.

3.3. DnaT84-179 bound to ssDNA

In contrast to DnaT, which forms a trimer, DnaT84-179 was a monomeric protein. To confirm whether small protein DnaT84-179 can still bind to ssDNA, we assessed the binding of DnaT84-179 to dT10, dT20, dT30, dT40, dT50, dT60, and dT70 (Fig. 2) at different protein concentrations by EMSA. EMSA, a popular and well-established approach in studies of molecular biology, detects distinct protein–DNA complexes [26]. No significant band shift was observed when DnaT84-179 was incubated with dT10 (Fig. 2A), indicating that DnaT84-179 cannot form a stable complex with dT10 during electrophoresis. In contrast to dT10, long dT homopolymers bound to DnaT84-179 and formed a single complex (Fig. 2B–G). DnaT84-179 can bind to dT20, but DnaT, DnaT26-179, and DnaT42-179 cannot [23]. Surprisingly, in contrast to DnaT, DnaT26-179, and DnaT42-179, which form distinct complexes with ssDNA of varying lengths [23], DnaT84-179 complexed with ssDNA formed a single complex. Because only one complex of DnaT84-179 molecules bound per ssDNA was visible when the length of the dT homopolymers was increased to 70 nt, these interactions were more highly cooperative than those of DnaT, DnaT26-179, and DnaT42-179. No other distinctive complex or intermediate form was observed. Thus, small monomeric protein DnaT84-179 can still bind to ssDNA with unexpected positive cooperativity.

Table 1
The properties of the deletion mutant of DnaT.

	Oliomerization	PriB binding	ssDNA binding
DnaT	Trimer	+	+
DnaT42-179	Trimer	+	+
DnaT84-179	Monomer	–	+
DnaT1-83	Expressed as protein pellets		
DnaT1-120	Expressed as protein pellets		
DnaT1-139	Expressed as protein pellets		

To compare the ssDNA-binding abilities of DnaT, DnaT26-179, DnaT42-179, and DnaT84-179, the midpoint value for the input ssDNA binding of DnaT84-179, calculated from the titration curves of EMSA and referred to as $[Protein]_{50}$, was quantified (Table 2). $[DnaT84\text{-}179]_{50}$ values ranged from 2.7 μM to 5.2 μM, similar to those of DnaT and DnaT26-179 but different from those of DnaT42-179. The reason for such discrepancy remains unknown. Thus, the deletion of the N-terminal 1–83 aa region in DnaT changed the oligomerization state and DNA binding behavior (complex number) but did not decrease ssDNA binding ability (Table 2).

3.4. Native PAGE analysis for identifying regions of interaction of DnaT with PriB

Yeast two-hybrid analyses show the interaction of DnaT with PriB in vivo [25]. To assess such interaction in vitro, native PAGE analysis using purified proteins was conducted together with Western blot. DnaT, DnaT42-179, and DnaT84-179 have a His tag and therefore can be detected by the anti-His antibody. Native PAGE analysis expects that the interaction of a protein with another forms a protein complex(es), whose electrophoretic mobility differs from that of the uncomplexed form(s) of the protein. DnaT and DnaT42-179 (Fig. 3A and B), but not DnaT84-179 (Fig. 3C), incubated with PriB(dHis) caused a significant band shift, indicating different mobilities because of the addition of PriB(dHis). Thus, DnaT can use its N-terminal region (aa 1–83) to interact with PriB in the absence of DNA. Although we wanted to investigate several deletion mutants in the C-terminal region, namely, DnaT1-83,

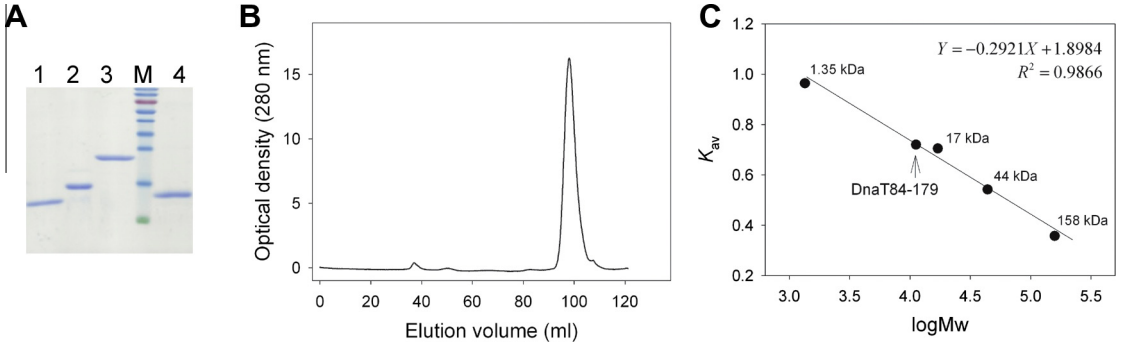

Fig. 1. (A) Protein purity. Coomassie Blue-stained SDS–PAGE (14%) of the purified DnaT84-179 (lane 1), DnaT42-179 (lane 2), DnaT (lane 3), PriB(dHis) (lane 4), and molecular mass standards (M) are shown. (B) Gel-filtration chromatographic analysis of the purified DnaT84-179 protein. The column (Superdex 200 HR 10/30) was calibrated with proteins of known molecular masses: γ-globulin (158 kDa), ovalbumin (44 kDa), myoglobin (17 kDa), and vitamin B_{12} (1.35 kDa). The single peak shows the eluted DnaT84-179 protein. (C) A standard linear regression curve was generated by plotting the log of the molecular mass of the calibration proteins against their K_{av} values.

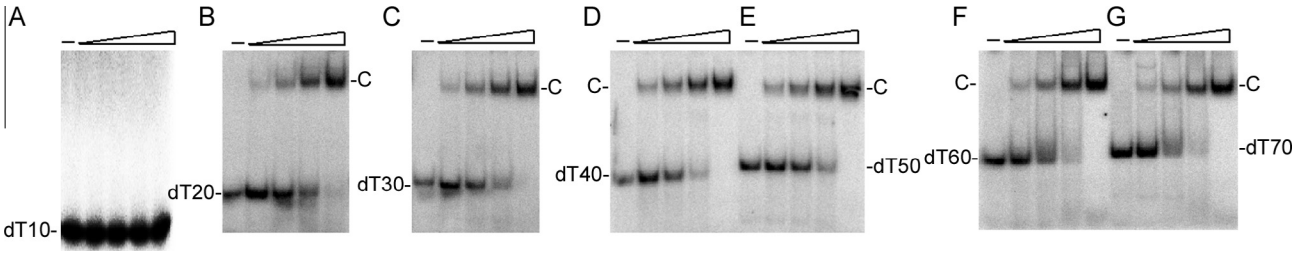

Fig. 2. Binding of DnaT84-179 to (A) dT10, (B) dT20, (C) dT30, (D) dT40, (E) dT50, (F) dT60, and (G) dT70. The reaction solutions contain 1.7 nM of the oligonucleotide and the purified DnaT84-179 protein (0–10 μM).

Table 2
ssDNA binding properties of DnaT84-179 as analyzed by EMSA.

DNA	$[Protein]_{50}$	N
dT10	ND	0
dT20	5.2 ± 0.4	1
dT30	3.1 ± 0.5	1
dT40	2.9 ± 0.2	1
dT50	2.9 ± 0.4	1
dT60	2.7 ± 0.3	1
dT70	2.7 ± 0.4	1

Errors are standard deviations determined by three independent titration experiments.
N, complex number.

DnaT1-120, and DnaT1-139, they were expressed as protein pellets, which cannot be characterized.

3.5. Pull-down assay

To verify direct interaction of DnaT with PriB, we performed pull-down experiments using DnaT variants and PriB(dHis). If there is physical interaction between DnaT and PriB(dHis), untagged PriB(dHis) will be eluted with His-tagged DnaT in this assay. As shown in Fig. 3D–F, DnaT and DnaT42-179, but not DnaT84-179, eluted with PriB(dHis). PriB(dHis) was found in washing solution when DnaT84-179 was used in this experiment (Fig. 3F). Taken together, DnaT and DnaT42-179 can bind to PriB according to native polyacrylamide gel electrophoresis, Western blot analysis, and pull-down assay, whereas DnaT84-179 cannot bind to PriB. In addition, these interactions did not require addition of DNA. These results constitute a pioneering study of the sites of interaction of DnaT with PriB.

3.6. Functional domains of DnaT

Previously we have modeled the DnaT structure by $(PS)^2$ [23]. The C-terminal region of DnaT contains highly conserved positively charged or aromatic residues for ssDNA interaction [23]. In the current study, we found that DnaT84-179, although a monomer, can bind to ssDNA with similar affinity to that of DnaT. The N-terminal region of DnaT was assumed to be insignificant in primosome assembly because this region is variable [23]. However, we found that the N-terminal domain (aa 1–83), especially region aa 43–83, of DnaT, is essential for PriB binding (Table 1). Many bacteria have no recognizable homolog of DnaT and other loading factors, such as PriB, PriC, and DnaC. These Gram-positive bacteria still employ replication restart [27]. We proposed that DnaT serves as an accessory protein for regulating the translocase or helicase activity of replicative DnaB helicase. Thus, several regions that are important for protein–protein interaction and conformational change in DnaT, even those that are important for the interaction of PriB or other primosomal proteins, are not necessarily conserved.

3.7. Domain mapping of DnaT: insight into hand-off mechanism

A hand-off mechanism for primosome assembly [14] has been proposed whereby (i) PriA recognizes and binds to a replication fork, (ii) PriB joins to PriA to form a PriA–PriB–DNA ternary complex, and (iii) DnaT participates in this nucleocomplex to form a triprotein complex, in which the recruitment of DnaT results in the

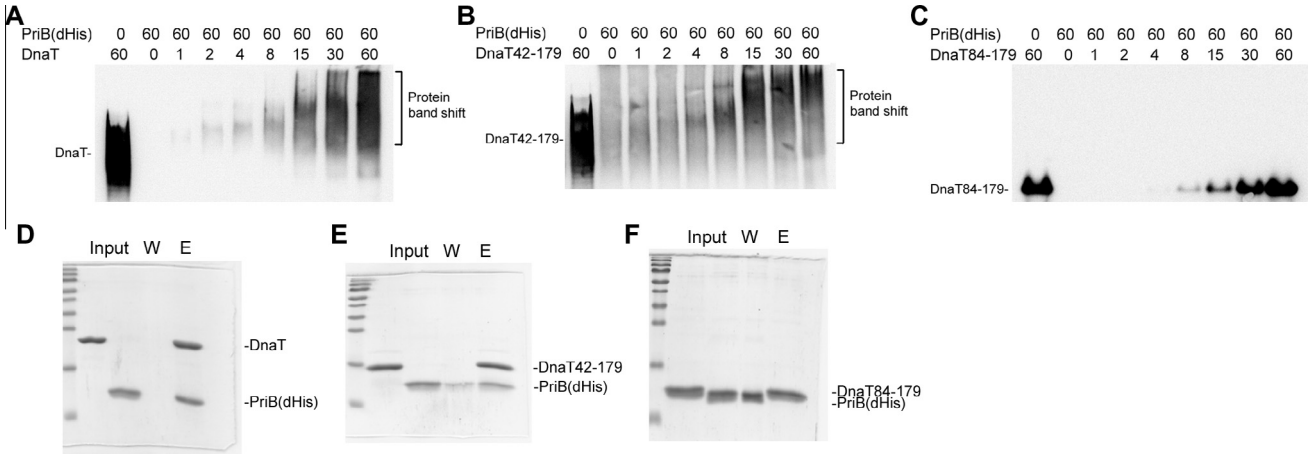

Fig. 3. (A–C) Native PAGE with Western blot analysis. (A) DnaT, (B) DnaT42-179, and (C) DnaT84-179 (0–60 μM) was incubated with PriB(dHis) (60 μM). The reaction solution was analyzed by native PAGE with Western blot. (D–F) Pull-down assay. (D) DnaT, (E) DnaT42-179, and (F) DnaT84-179 was incubated with PriB(dHis) and then the pull-down experiments were performed. W, washing solution; E, elution solution.

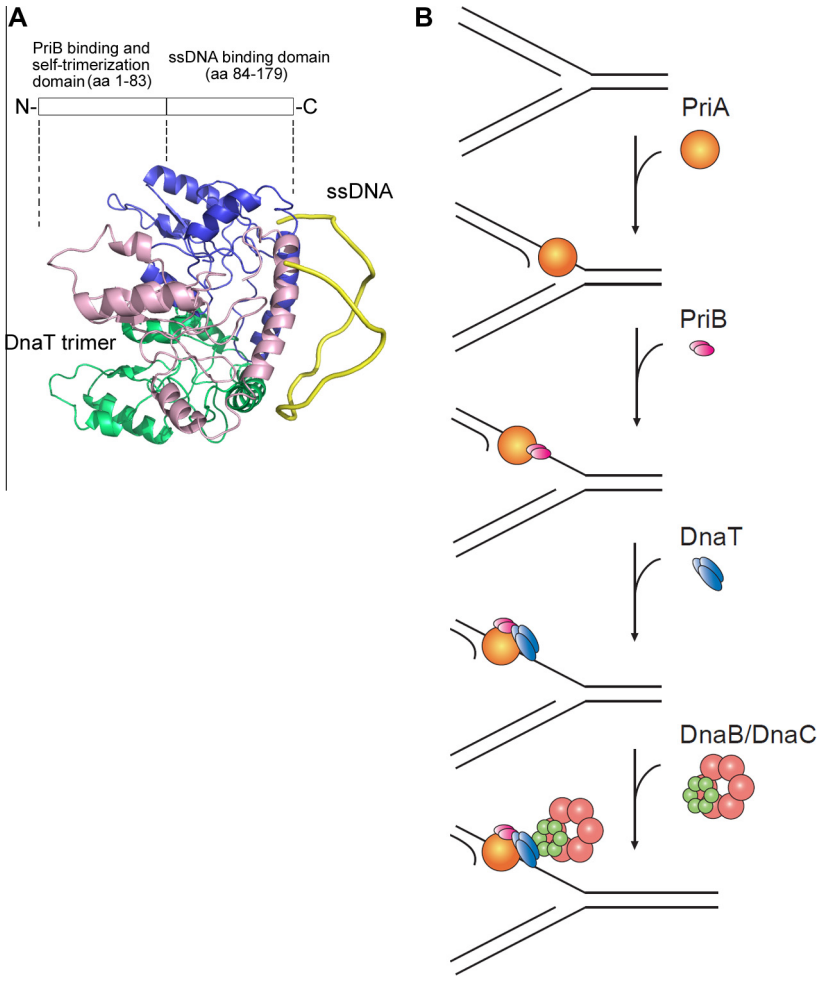

Fig. 4. (A) Domain definition of DnaT. This trimeric DnaT structure (aa 14–165) with ssDNA (25 mer; shown in gold) modeled by $(PS)^2$ was adapted from [23]. (B) On the basis of results in this study, the hand-off mechanism for primosome assembly is updated such that (i) PriA recognizes and binds to a replication fork, (ii) PriB joins to PriA to form a PriA–PriB–DNA ternary complex, and (iii) DnaT interacts with PriA, ssDNA (via the C-terminal domain), and PriB (via the N-terminal domain) and the DnaB/C complex is loaded. This modified model explains the mechanism as to how DnaT simultaneously binds to ssDNA and its partner protein, PriB.

release of ssDNA by PriB and then loads the DnaB/C complex. Very recently, we have identified DnaT as a kind of ssDNA binding protein and then modified the hand-off mechanism for primosome assembly [23]. In the current study, we identified that the N-terminal domain of DnaT is responsible for PriB binding and that its C-terminal domain is involved in ssDNA binding (Fig. 4A). Thus, the hand-off mechanism for primosome assembly is updated (Fig. 4B) such that (i) PriA recognizes and binds to a replication fork, (ii) PriB joins to PriA to form a PriA–PriB–DNA ternary complex, and (iii) DnaT interacts with PriA, ssDNA (via the C-terminal domain), and PriB (via the N-terminal domain) and the DnaB/C complex is loaded. This modified model explains the mechanism as to how DnaT binds to ssDNA and its partner protein, PriB. To further elucidate the function and structure of DnaT, our laboratory is obtaining several crystals of DnaT84-179 in complex with ssDNA for crystallographic analysis. A large number of complex structures of DnaT will enhance our understanding of the mechanism for primosome assembly.

In this study, we constructed and analyzed several deletion mutants of DnaT, in which DnaT84-179 can bind to ssDNA but cannot interact with PriB and cannot form an oligomer. On the basis of this biophysical characterization and extensive evidence from other literature, we mapped the domain functions of DnaT. The N-terminal domain (aa 1–83), especially aa 43–83, is important in PriB binding and self-trimerization, and the C-terminal domain (aa 84–179) is crucial for ssDNA binding. Further research can directly focus on determining how DnaT binds to the PriA–PriB–DNA tricomplex in replication restart by the hand-off mechanism.

Acknowledgments

This research was supported by a grant from the National Science Council, Taiwan (NSC 102-2320-B-040-019 to C.-Y. Huang).

Appendix A. Supplementary data

Supplementary data associated with this article can be found, in the online version, at http://dx.doi.org/10.1016/j.bbrc.2013.11.069.

References

[1] P. McGlynn, R.G. Lloyd, Recombinational repair and restart of damaged replication forks, Nat. Rev. Mol. Cell Biol. 3 (2002) 859–870.
[2] H. Masai, T. Tanaka, D. Kohda, Stalled replication forks: making ends meet for recognition and stabilization, Bioessays 32 (2010) 687–697.
[3] M.M. Cox, M.F. Goodman, K.N. Kreuzer, D.J. Sherratt, S.J. Sandler, K.J. Marians, The importance of repairing stalled replication forks, Nature 404 (2000) 37–41.
[4] S.J. Sandler, Multiple genetic pathways for restarting DNA replication forks in *Escherichia coli* K-12, Genetics 155 (2000) 487–497.
[5] K.J. Marians, PriA-directed replication fork restart in *Escherichia coli*, Trends Biochem. Sci. 25 (2000) 185–189.
[6] R. Schekman, A. Weiner, A. Kornberg, Multienzyme systems of DNA replication, Science 186 (1974) 987–993.

[7] L. Zheng, B. Shen, Okazaki fragment maturation: nucleases take centre stage, J. Mol. Cell Biol. 3 (2011) 23–30.
[8] S.S. Patel, M. Pandey, D. Nandakumar, Dynamic coupling between the motors of DNA replication: hexameric helicase, DNA polymerase, and primase, Curr. Opin. Chem. Biol. 15 (2011) 595–605.
[9] T. Tanaka, T. Mizukoshi, K. Sasaki, D. Kohda, H. Masai, *Escherichia coli* PriA protein, two modes of DNA binding and activation of ATP hydrolysis, J. Biol. Chem. 282 (2007) 19917–19927.
[10] K. Sasaki, T. Ose, N. Okamoto, K. Maenaka, T. Tanaka, H. Masai, M. Saito, T. Shirai, D. Kohda, Structural basis of the 3′-end recognition of a leading strand in stalled replication forks by PriA, EMBO J. 26 (2007) 2584–2593.
[11] T. Mizukoshi, T. Tanaka, K. Arai, D. Kohda, H. Masai, A critical role of the 3′ terminus of nascent DNA chains in recognition of stalled replication forks, J. Biol. Chem. 278 (2003) 42234–42239.
[12] T. Tanaka, T. Mizukoshi, C. Taniyama, D. Kohda, K. Arai, H. Masai, DNA binding of PriA protein requires cooperation of the N-terminal D-loop/arrested-fork binding and C-terminal helicase domains, J. Biol. Chem. 277 (2002) 38062–38071.
[13] J. Liu, P. Nurse, K.J. Marians, The ordered assembly of the phiX174-type primosome. III. PriB facilitates complex formation between PriA and DnaT, J. Biol. Chem. 271 (1996) 15656–15661.
[14] M. Lopper, R. Boonsombat, S.J. Sandler, J.L. Keck, A hand-off mechanism for primosome assembly in replication restart, Mol. Cell 26 (2007) 781–793.
[15] H. Masai, K. Arai, Initiation of lagging-strand synthesis for pBR322 plasmid DNA replication in vitro is dependent on primosomal protein i encoded by dnaT, J. Biol. Chem. 263 (1988) 15016–15023.
[16] H. Masai, M.W. Bond, K. Arai, Cloning of the *Escherichia coli* gene for primosomal protein i: the relationship to dnaT, essential for chromosomal DNA replication, Proc. Natl. Acad. Sci. USA 83 (1986) 1256–1260.
[17] K. Arai, R. McMacken, S. Yasuda, A. Kornberg, Purification and properties of *Escherichia coli* protein i, a prepriming protein in phi X174 DNA replication, J. Biol. Chem. 256 (1981) 5281–5286.
[18] K.J. Marians, Prokaryotic DNA replication, Annu. Rev. Biochem. 61 (1992) 673–719.
[19] H. Masai, K. Arai, *Escherichia coli* dnaT gene function is required for pBR322 plasmid replication but not for R1 plasmid replication, J. Bacteriol. 171 (1989) 2975–2980.
[20] J.D. McCool, C.C. Ford, S.J. Sandler, A dnaT mutant with phenotypes similar to those of a priA2::kan mutant in *Escherichia coli* K-12, Genetics 167 (2004) 569–578.
[21] S.L. Black, A. Dawson, F.B. Ward, R.J. Allen, Genes required for growth at high hydrostatic pressure in *Escherichia coli* K-12 identified by genome-wide screening, PLoS One 8 (2013) e73995.
[22] S. Jang, S.J. Sandler, R.M. Harshey, Mu insertions are repaired by the double-strand break repair pathway of *Escherichia coli*, PLoS Genet. 8 (2012) e1002642.
[23] Y.H. Huang, M.J. Lin, C.Y. Huang, DnaT is a single-stranded DNA binding protein, Genes Cells 18 (2013) 1007–1019.
[24] M.R. Szymanski, M.J. Jezewska, W. Bujalowski, The *Escherichia coli* primosomal DnaT protein exists in solution as a monomer-trimer equilibrium system, Biochemistry 52 (2013) 1845–1857.
[25] Y.H. Huang, M.J. Lin, C.Y. Huang, Yeast two-hybrid analysis of PriB-interacting proteins in replication restart primosome: a proposed PriB–SSB interaction model, Protein J. 32 (2013) 477–483.
[26] C.Y. Huang, Determination of the Binding Site-Size of the Protein–Dna Complex by Use of the Electrophoretic Mobility Shift Assay, InTech Press, Rijeka, Croatia, 2012.
[27] H. Merrikh, C. Machon, W.H. Grainger, A.D. Grossman, P. Soultanas, Co-directional replication-transcription conflicts lead to replication restart, Nature 470 (2011) 554–557.

Biochimie 101 (2014) 113–122

Contents lists available at ScienceDirect

Biochimie

journal homepage: www.elsevier.com/locate/biochi

Research paper

Allantoinase and dihydroorotase binding and inhibition by flavonols and the substrates of cyclic amidohydrolases

Wei-Feng Peng [a,b], Cheng-Yang Huang [a,c,*]

[a] School of Biomedical Sciences, Chung Shan Medical University, No. 110, Sec. 1, Chien-Kuo N. Rd., Taichung City, Taiwan
[b] School of Medicine, College of Medicine, Chung Shan Medical University, No. 110, Sec. 1, Chien-Kuo N. Rd., Taichung City, Taiwan
[c] Department of Medical Research, Chung Shan Medical University Hospital, No. 110, Sec. 1, Chien-Kuo N. Rd., Taichung City, Taiwan

ARTICLE INFO

Article history:
Received 14 October 2013
Accepted 2 January 2014
Available online 10 January 2014

Keywords:
Allantoinase
Dihydroorotase
Hydantoinase
Imidase
Amidohydrolase

ABSTRACT

Allantoinase and dihydroorotase are members of the cyclic amidohydrolases family. Allantoinase and dihydroorotase possess very similar binuclear metal centers in the active site and may use a similar mechanism for catalysis. However, whether the substrate specificities of allantoinase and dihydroorotase overlap and whether the substrates of other cyclic amidohydrolases inhibit allantoinase and dihydroorotase remain unknown. In this study, the binding and inhibition of allantoinase (*Salmonella enterica* serovar Typhimurium LT2) and dihydroorotase (*Klebsiella pneumoniae*) by flavonols and the substrates of other cyclic amidohydrolases were investigated. Hydantoin and phthalimide, substrates of hydantoinase and imidase, were not hydrolyzed by allantoinase and dihydroorotase. Hydantoin and dihydroorotate competitively inhibited allantoinase, whereas hydantoin and allantoin bind to dihydroorotase, but do not affect its activity. We further investigated the effects of the flavonols myricetin, quercetin, kaempferol, and galangin, on the inhibition of allantoinase and dihydroorotase. Allantoinase and dihydroorotase were both significantly inhibited by kaempferol, with IC_{50} values of 35 ± 3 μM and 31 ± 2 μM, respectively. Myricetin strongly inhibited dihydroorotase, with an IC_{50} of 40 ± 1 μM. The double reciprocal of the Lineweaver–Burk plot indicated that kaempferol was a competitive inhibitor for allantoinase but an uncompetitive inhibitor for dihydroorotase. A structural study using PatchDock showed that kaempferol was docked in the active site pocket of allantoinase but outside the active site pocket of dihydroorotase. These results constituted a first study that naturally occurring product flavonols inhibit the cyclic amidohydrolases, allantoinase, and dihydroorotase, even more than the substrate analogs (>3 orders of magnitude). Thus, flavonols may serve as drug leads for designing compounds that target several cyclic amidohydrolases.

1. Introduction

The amidohydrolase superfamily comprises a remarkable set of enzymes that catalyze the hydrolysis of a wide range of substrates with amide or ester functional groups at their carbon and phosphorus centers [1–3]. Based on their functional and structural similarities to related enzymes, hydantoinase, allantoinase, dihydropyrimidinase, and dihydroorotase belong to the cyclic amidohydrolase family [4,5]. Hydantoinase is also known as dihydro pyrimidinase because of an overlap in substrate specificity [6]. Enzymes in this family [7–11], including imidase, are imide-hydrolyzing enzymes. Even though they are functionally similar, these enzymes have a relatively low amino acid sequence identity. These metal-dependent enzymes catalyze the ring-opening hydrolysis of the cyclic amide bond of each substrate in either five- or six-member rings in the metabolism of purines, pyrimidines, and many xenobiotics (Fig. 1A).

Allantoinase occurs in a wide variety of organisms, including bacteria, fungi, and plants, and a few animals. Allantoinase catalyzes the reversible hydrolysis of allantoin to allantoic acid, which is a key reaction in the biosynthesis and degradation of ureide required for the utilization of nitrogen in purine-derived compounds [12]. Allantoinase is a homotetrameric dinuclear metalloenzyme [13,14], but some allantoinases initially annotated as polysaccharide deacetylases [15] are metal independent. Thus, even without the allantoinase gene, some bacteria use allantoin to utilize nitrogen.

* Corresponding author. School of Biomedical Sciences, Chung Shan Medical University, No. 110, Sec. 1, Chien-Kuo N. Rd., Taichung City, Taiwan. Tel.: +886 4 24730022x11472; fax: +886 4 23248187.
E-mail address: cyhuang@csmu.edu.tw (C.-Y. Huang).

0300-9084/$ – see front matter © 2014 Elsevier Masson SAS. All rights reserved.
http://dx.doi.org/10.1016/j.biochi.2014.01.001

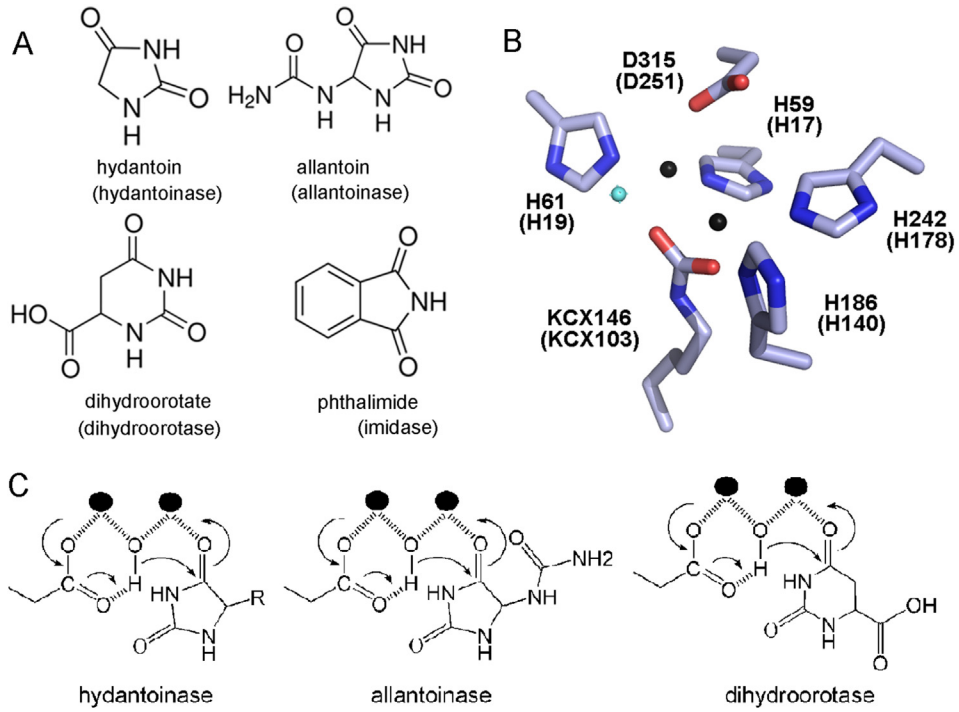

Fig. 1. Properties of the cyclic amidohydrolase family. (A) Substrate of hydantoinase/dihydropyrimidinase, allantoinase, dihydroorotase, and imidase. (B) The binuclear metal center within the active site of allantoinase and dihydroorotase (in parentheses). Allantoinase and dihydroorotase contains four histidine, one aspartate, and one post-carboxylated lysine residue, which are required for metal binding and catalytic activity, as revealed by their crystal structures. The coordinate was obtained from the Protein Data Bank (entry 3E74). KCX, a post-carboxylated lysine. The metal ions (in black) and a metal-bound water molecule (in light blue) are also shown. (C) The chemical mechanisms of hydantoinase, allantoinase and dihydroorotase. The hydrolysis of the substrates likely undergoes three steps: the hydrolytic water molecule must be activated for nucleophilic attack, and then the amide bond of the substrate must be made more electrophilic by polarization of the carbonyl-oxygen bond, and the leaving-group nitrogen must be protonated as the carbon–nitrogen bond is cleaved. The metal ions are shown as black circles.

Dihydroorotase catalyzes the reversible cyclization of carbamoyl aspartate into dihydroorotate in the third step of the de novo pyrimidine nucleotide biosynthetic pathway [16]. In mammals, this enzyme is part of the large multifunctional protein carbamoyl phosphate synthetase/aspartate transcarbamoylase/dihydroorotase (CAD) [16–19]. However, in prokaryotic organisms, CADs are usually expressed separately and function independently [20] or form multifunctional complexes [17,21,22]. Similar to allantoinase, dihydroorotase is a metalloenzyme [21,23]. The active site of allantoinase [14] and dihydroorotase [23] contains four histidine, one aspartate, and one post-carboxylated lysine residue or a second aspartate residue, which are required for metal binding and catalytic activity, as revealed by their crystal structures (Fig. 1B) [13,24]. The presence of a post-carboxylated lysine in hydantoinase is also involved in binuclear metal center self-assembly [25] and increases the nucleophilicity of the hydroxide for catalysis [26]. Nevertheless, the substrate specificities of allantoinase, hydantoinase, and dihydroorotase may differ. However, whether the substrate of each enzyme competitively inhibits other enzymes in this family remains unclear.

Infections that are resistant to all antibacterial options have recently developed. Few therapies are effective against the six antibiotic-resistant ESKAPE pathogens (*Enterococcus faecium*, *Staphylococcus aureus*, *Klebsiella pneumoniae*, *Acinetobacter baumannii*, *Pseudomonas aeruginosa*, and *Enterobacter species*) [27]. Considering allantoinase and dihydroorotase are required for metabolizing purines and pyrimidines, blocking their activities would be detrimental to bacterial survival. In addition, allantoinase is not found in humans, and mammalian and prokaryotic dihydroorotases exhibit distinct differences. Thus, these enzymes may be promising therapeutic targets for developing antibiotics. Although some chelators inhibit allantoinase and dihydroorotase, they may be harmful to human health.

Flavonoids are the most common group of plant polyphenols and are responsible for much of the flavor and color of fruits and vegetables [28]. Over 5000 different flavonoids have been described, many which display structure-dependent biological and pharmacologic activities [29]. The six major subclasses of flavonoids are flavonols, flavones, flavanones, flavanols, anthocyanidins, and isoflavones [28]. Flavonols, which are composed of two aromatic rings linked by a heterocyclic pyran-4-one ring, are known to have antioxidant [30], antiradical [31], antiviral [32,33], and antibacterial activities [34,35]. In this study, we investigated the effects of the substrates of cyclic amidohydrolase and the flavonols myricetin, quercetin, kaempferol, and galangin on inhibiting the catalytic activity of allantoinase and dihydroorotase.

2. Materials and methods

2.1. Materials

All restriction enzymes and DNA-modifying enzymes were purchased from New England Biolabs (Ipswich, MA, USA), unless otherwise stated. All custom oligonucleotide primers were obtained from Invitrogen Corporation (Carlsbad, CA, USA). All chemicals were purchased from Sigma–Aldrich (St. Louis, MO, USA) unless otherwise stated.

2.2. Protein expression and purification

The construction of pET21e-*Kp*DHO expression vector for *Klebsiella pneumoniae* dihydroorotase expression has been previously

described [36]. The construction of pET21b-*St*ALL expression vector for *Salmonella enterica* serovar Typhimurium LT2 allantoinase expression has been previously described [13]. Recombinant proteins were expressed and purified using a previously described protocol [13,25,37–40]. In a typical procedure, *Escherichia coli* BL21(DE3) cells were individually transformed with the plasmid by the heat shock method, and then grown to 0.9 OD_{600} at 37 °C in Luria–Bertani medium containing 250 μg/mL ampicillin and 1 mM $MnCl_2$ with rapid shaking. Overexpression of the construct was induced by incubating with 1 mM isopropyl thiogalactoside (IPTG) for 3 h at 37 °C. The cells overexpressing the protein were chilled on ice, harvested by centrifugation, resuspended in buffer A (20 mM Tris–HCl, 5 mM imidazole, and 0.5 M NaCl, pH 7.9) and disrupted by sonication with ice cooling. The protein purified from the soluble supernatant by Ni^{2+}-affinity chromatography (HiTrap HP; GE Healthcare Bio-Sciences, Piscataway, NJ, USA) was eluted with buffer B (20 mM Tris–HCl, 250 mM imidazole, and 0.5 M NaCl, pH 7.9) and dialyzed against a dialysis buffer (50 mM HEPES and 50 mM NaCl, pH 7.0). Protein purity remained greater than 95% as determined by Coomassie-stained SDS-PAGE (Mini-PROTEAN Tetra System; Bio-Rad, CA, USA).

2.3. Protein concentration

The protein concentrations of enzyme solution were determined by the bicinchoninic acid protein assay using bovine serum albumin as a standard [41].

2.4. Enzyme assay

A rapid spectrophotometric assay was used to determine the enzymatic activity according to a previously described protocol for allantoinase [42], dihydroorotase [36], imidase [8,9], and hydantoinase [25]. In a typical procedure, the hydrolysis of allantoin and dihydroorotate was measured at 25 °C as the decrease in absorbance at 258 and 230 nm, respectively. To start the reaction, the protein solution (1–30 μg) was added to a 2 mL solution containing the substrate and 100 mM Tris–HCl (pH 8.0). The extinction coefficients of allantoin and dihydroorotate were 0.0261 mM^{-1} cm^{-1} at 258 nm and 0.92 mM^{-1} cm^{-1} at 230 nm, respectively. Substrate hydrolysis was monitored with a UV/vis spectrophotometer (Hitachi U 3300, Hitachi High-Technologies, Tokyo, Japan). The initial rates of change were a function of enzyme concentration within the absorbance range of 0.01–0.3 min^{-1}. A unit of activity was defined as the amount of enzyme catalyzing the hydrolysis of 1 μmol substrate/min, and the specific activity was expressed in terms of units of activity per milligram of enzyme. The kinetic parameters K_m and V_{max} were determined by fitting the hydrolyzing rate from individual experiments to the Michaelis–Menten equation.

2.5. Dissociation constants determined by fluorescence spectrophotometer

Determination of the dissociation constants (K_d) for allantoinase and dihydroorotase was using the fluorescence quenching method as previously described for DnaB helicase [34,37]. An aliquot of each compound was added into the solution containing allantoinase or dihydroorotase (0.8 μM), 50 mM HEPES at pH 7.0 with a final volume of 2 mL in a quartz cuvettes of 1 cm square cross-section. The decrease in intrinsic fluorescence of protein was measured at 330 nm upon excitation at 280 nm and 25 °C with a spectrofluorimeter (Hitachi F-2700; Hitachi High-Technologies, Tokyo, Japan). At least seven data points were used to calculate each K_d. Each data point was an average of 2–3 determinants, and the difference of the determinants was within 10%. The K_d was obtained by the equation: $\Delta F = \Delta F_{max} - K_d(\Delta F/[\text{compound}])$ (Enzyme Kinetics module of Sigma-Plot; Systat Software, Chicago, IL, USA).

2.6. Determination of IC_{50}

Dose-response curves were generated by titrating compound into the enzyme assay solution. The concentration of the compound required for 50% inhibition (IC_{50}) was determined directly from the graphic analysis. Due to solubility, IC_{50} of some compounds for allantoinase and dihydroorotase were not determined.

2.7. Bioinformatics

The model of *S. enterica* allantoinase was built from the coordinates of *Bacillus halodurans* allantoinase (3HM7; 42% identity) using SWISS-MODEL, (http://swissmodel.expasy.org) [43]. Similarly, the model of *K. pneumoniae* dihydroorotase was built from the coordinates of *S. enterica* dihydroorotase (3JZE; 93% identity). The coordinate and topology file of the flavonols, myricetin, quercetin, kaempferol, and galangin, was found in DrugBank, http://www.drugbank.ca/ [44]. Kaempferol was computationally docked into the three-dimensional models of allantoinase and dihydroorotase by using PatchDock, http://bioinfo3d.cs.tau.ac.il/PatchDock/ [45]. The hydantoin-complexed structure models of allantoinase and dihydroorotase were directly constructed by superimposing the structure of the apo form with the crystal structure of the hydantoin-dihydropyrimidinase complex (the coordinate of 4LCS). The structures were visualized by using the program PyMol.

3. Results

3.1. Hydantoin is not a substrate for allantoinase and dihydroorotase

Bacterial allantoinase and dihydroorotase are members of the cyclic amidohydrolase family. This family includes hydantoinase/dihydropyrimidinase, dihydroorotase, allantoinase, and imidase, which use hydantoin, dihydroorotate, allantoin, and phthalimide as a substrate, respectively (Fig. 1A). Members of this family have very similar active sites (Fig. 1B) and may use the same catalytic mechanism for substrate hydrolysis (Fig. 1C). This condition raises an interesting question as to whether the substrate specificities of allantoinase and dihydroorotase partially overlap with those of the other cyclic amidohydrolases. Hydantoinase/dihydropyrimidinase [6,46,47] and imidase [7,8,11] have broad and overlapping substrate specificities. However, the standard assays showed no reaction over 2 h when allantoinase was incubated with hydantoin (10 and 100 mM), dihydroorotate (1 and 10 mM), or pthalimide (0.1 and 1 mM) (data not shown). Similarly, dihydroorotase showed no reaction when tested with allantoin (4 and 40 mM), hydantoin (10 and 100 mM), or pthalimide (0.1 and 1 mM) (data not shown). The maximal concentration of phthalimide was limited to 1 mM due to its minimal solubility. Thus, unlike hydantoinase and imidase, allantoinase and dihydroorotase have absolute substrate specificities toward their own substrates, namely, allantoin and dihydroorotate, respectively. Although these cyclic amidohydrolases may use a similar active site and mechanism for catalysis, no substrate overlapping was observed for allantoinase and dihydroorotase.

3.2. Hydantoin and dihydroorotate are potential competitive inhibitors of allantoinase

Based on the catalytic mechanism of the cyclic amidohydrolases (Fig. 1C), hydantoin should be, but is actually not, a substrate of

Table 1
Apparent Michaelis–Menten constants for allantoinase in the presence of kaempferol and the substrate of other cyclic amidohydrolases.

Compound	Allantoinase			
	V_{max}	K_m	V_{max}/K_m	Fold
Non	130.5 ± 21.5	85.9 ± 20.0	1.52	1.00
Dihydroorotate	125.2 ± 21.9	129.6 ± 27.1	0.97	0.64
Phthalimide	130.0 ± 22.0	86.0 ± 20.4	1.51	0.99
Hydantoin	120.9 ± 18.4	108.3 ± 20.7	1.12	0.74
Kaempferol	118.8 ± 18.3	231.6 ± 29.2	0.51	0.34

At least seven data points were used to calculate each V_{max} and K_m. Each data point was an average of 2–3 determinants, and the difference of the determinants was within 10%. The kinetic parameters *K*m and *V*max were determined by fitting the hydrolyzing rate from individual experiments to the Michaelis–Menten equation, and then the standard errors were given.

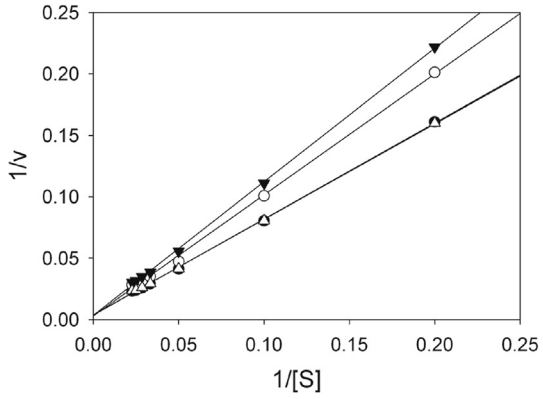

Fig. 2. Inhibition of allantoinase by substrate analogs. Inhibition of allantoinase by some substrates of other cyclic amidohydrolase. To determine which type of inhibitor is, the double reciprocal of the Lineweaver–Burk plots was used. The standard assay solution was conducted with hydantoin (open circle), dihydroorotate (inverted filled triangle), phthalimide (open triangle), or without any supplement (filled circle). The inhibitions of allantoinase by these compounds resulted in the Lineweaver–Burk plots where the lines are cross the *y*-axis at the very similar point, indicating that these compounds are competitive inhibitors for allantoinase. Data points are an average of 2–3 determinations within 10% error.

allantoinase and dihydroorotase. Hydantoin has a structure similar to that of allantoin, except for the 5′ side chain (Fig. 1A). Thus, hydantoin may be a potential allantoinase inhibitor. To assess whether hydantoin inhibits the activity of allantoinase, hydantoin (50 mM) was included in the standard allantoinase assay. In addition, dihydroorotate (2 mM) and phthalimide (1 mM) were also individually used for allantoinase inhibition studies (Table 1). The kinetic parameters of allantoinase were calculated from the double reciprocal of the Lineweaver–Burk plot with and without the substrate analog as a potential inhibitor. As shown in Fig. 2, inhibition of allantoinase by hydantoin and dihydroorotate resulted in Lineweaver–Burk plots where the lines intersect the *y*-axis at a similar point, which indicates that these compounds are competitive inhibitors of allantoinase. The inclusion of phthalimide into the assay at 1 mM did not affect the allantoinase activity. Thus, substrates of the cyclic amidohydrolase, at least hydantoin and dihydroorotate competed with allantoin for allantoinase active sites.

3.3. IC_{50} of dihydroorotate, phthalimide, and hydantoin for allantoinase

To compare the inhibitory capability of dihydroorotate, phthalimide, and hydantoin on allantoinase, their IC_{50} values, that is, the inhibitor concentration required to reduce the activity of the enzyme by 50%, were determined and compared. As shown in Fig. 3, dihydroorotate, phthalimide, and hydantoin at different concentrations were used to determine the IC_{50} for allantoinase. The activity of allantoinase continued to decrease as the concentrations of dihydroorotate (Fig. 3A) and hydantoin (Fig. 3B) increased. Only 1 mM of phthalimide was used as the maximal concentration for IC_{50} determination because of its poor solubility (data not shown). Phthalimide did not inhibit the activity of allantoinase. The IC50 for allantoinase of dihydroorotate was 18.6 ± 1.1 mM and that of hydantoin was 230 ± 10 mM. Thus, the inhibitory capability of dihydroorotate toward allantoinase was 12-fold higher than that of hydantoin, based on their IC_{50} (Table 2).

3.4. K_d of allantoinase bound to dihydroorotate, phthalimide, and hydantoin

From our initial inhibition study, some substrate analogs were identified as competitive inhibitors of allantoinase (Table 1 and Fig. 2). To determine whether their inhibitory capabilities are correlated with their binding abilities, the dissociation constants (K_d) of allantoinase for dihydroorotate, phthalimide, and hydantoin were determined through fluorescence quenching. The fluorescence emission spectra of allantoinase significantly quenched with hydantoin are shown in Fig. 4A. The fluorescence intensity of allantoinase also decreased remarkably with increasing dihydroorotate concentration, but not phthalimide (data not shown). Adding hydantoin and dihydroorotate resulted in a blue shift (~5 nm) of the allantoinase emission wavelength (λ_{em}), which indicates that dihydroorotate and hydantoin interact with allantoinase and suggest that dihydroorotate and hydantoin can form stable complexes with allantoinase. The K_d values of allantoinase bound to dihydroorotate and hydantoin, as determined through

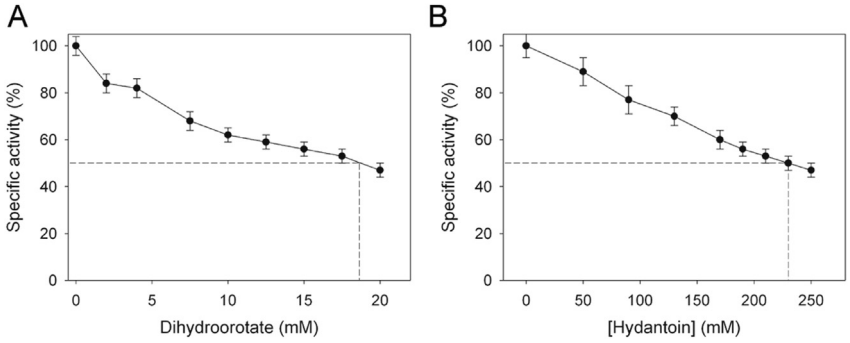

Fig. 3. IC_{50} determinations for allantoinase (A) The concentration of dihydroorotate required for 50% inhibition of the activity of allantoinase was directly determined using graphic analysis. (B) IC_{50} determination of hydantoin for allantoinase. The errors are standard deviation determined at 3 measurements.

Table 2
Effect of the flavonols and the substrate of other cyclic amidohydrolases on the activity of allantoinase and dihydroorotase.

Compound	IC_{50} (mM)	
	Allantoinase	Dihydroorotase
Dihydroorotate	18.6 ± 1.1	–
Phthalimide	–	–
Hydantoin	230 ± 10	–
Myricetin	ND	0.040 ± 0.001
Quercetin	ND	ND
Kaempferol	0.035 ± 0.003	0.031 ± 0.002
Galangin	ND	ND

–: No effect under the concentration range of the compound.
ND: due to solubility, the IC_{50} value was not determined.

Table 3
Binding of allantoinase and dihydroorotase to the substrate of other cyclic amidohydrolases and kaempferol.

Compound	K_d (mM)	
	Allantoinase	Dihydroorotase
Dihydroorotate	3.89 ± 1.15	ND
Hydantoin	6.06 ± 1.18	39.5 ± 6.8
Allantoin	ND	57.7 ± 2.3
Kaempferol	0.028 ± 0.004	0.021 ± 0.004

The decrease in intrinsic fluorescence of protein was measured at 330 nm upon excitation at 280 nm and 25 °C with a spectrofluorimeter. At least seven data points were used to calculate each K_d. Each data point was an average of 2–3 determinants, and the difference of the determinants was within 10%. The K_d was obtained by the equation: $\Delta F = \Delta F_{max} - K_d(\Delta F/[\text{compound}])$, and then the standard error was given.
ND, not determined.

their titration curves (Fig. 4B), were 3.89 ± 1.15 and 6.06 ± 1.18 mM, respectively (Table 3). Therefore, dihydroorotate exhibits the strongest binding and inhibitory capabilities toward allantoinase.

3.5. Allantoin and hydantoin bind to dihydroorotase, but does not inhibit its activity

Dihydroorotase cannot use hydantoin, phthalimide, and allantoin as a substrate. To test the dihydroorotase inhibitory capability of these compounds, allantoin (10 mM), phthalimide (1 mM), and hydantoin (50 mM) were individually included in the standard assay for dihydroorotase. However, unlike allantoinase, hydantoin, phthalimide, and allantoin did not affect dihydroorotase activity. Allantoin at 1 mM–40 mM and hydantoin at 1 mM–100 mM did not affect dihydroorotase activity. Thus, hydantoin, phthalimide, and allantoin were not inhibitors of dihydroorotase.

Fluorescence quenching was used to determine the K_d of dihydroorotase for hydantoin and allantoin. The fluorescence emission spectra of dihydroorotase significantly quenched with hydantoin are shown in Fig. 5A. The fluorescence intensity of dihydroorotase also decreased remarkably with increasing allantoin concentration (data not shown). Adding hydantoin and allantoin resulted in a blue shift (~10 nm) of the emission wavelength (λ_{em}) of dihydroorotase, which indicates that dihydroorotase interacts with allantoin and hydantoin. The K_d values of dihydroorotase bound to allantoin and hydantoin determined using titration curves (Fig. 5B) were 57.7 ± 2.3 and 39.5 ± 6.8 mM, respectively (Table 3). Thus, dihydroorotase can bind to allantoin and hydantoin, but cannot hydrolyze these compounds. Given that the V_{max} and K_m of dihydroorotase, determined from the titration curves (Fig. 5C), were 11.8 ± 0.4 μmol/mg/min and 0.13 ± 0.02 mM, respectively, the binding of allantoin and hydantoin to dihydroorotase is possibly too weak (<100 folds) to compete with dihydroorotate for the dihydroorotase active site.

3.6. Use of flavonols in allantoinase and dihydroorotase inhibition

Substrate analogs for any enzyme are usually potential inhibitors. Although we found that substrate analogs such as dihydroorotate and hydantoin inhibit allantoinase activity, their IC_{50} values were at the mM range, which is not significant for designing inhibitors. To determine whether a natural product is an inhibitor for allantoinase and dihydroorotase, the inhibitory capability of the flavonols myricetin, quercetin, kaempferol, and galangin toward allantoinase and dihydroorotase were tested (Fig. 6A).

3.7. Identification of the flavonol inhibition of allantoinase and dihydroorotase

Flavonols are known to have antioxidant [30], antiradical [31], and antibacterial activities [35]. To determine whether flavonols inhibit allantoinase and dihydroorotase, myricetin, quercetin, kaempferol, and galangin at different concentrations were included in the standard assay. The titration curves shown in Fig. 6B suggest that kaempferol most strongly inhibited allantoinase. The order of the inhibitory capability of the flavonols is as follows: kaempferol > galangin > quercetin > myricetin. For dihydroorotase, kaempferol also exhibited the strongest inhibition of enzyme activity. The order of inhibitory capability of the flavonols is as follows: kaempferol > myricetin > galangin > quercetin (Fig. 6C). Thus, flavonols, especially kaempferol, are novel inhibitors of allantoinase and dihydroorotase. In addition, the inhibitory capability of these flavonols (at the μM range) was significantly higher

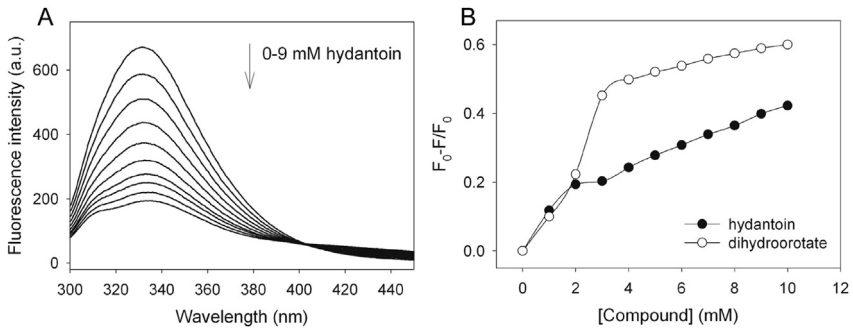

Fig. 4. Binding of allantoinase to the substrate of other cyclic amidohydrolases. (A) The fluorescence emission spectra of allantoinase with hydantoin of different concentrations (0–9 mM). The decrease in intrinsic fluorescence of protein was measured at 330 nm upon excitation at 280 nm and 25 °C with a spectrofluorimeter. The fluorescence intensity emission spectra of allantoinase significantly quenched with hydantoin. (B) An aliquot amount of hydantoin and dihydroorotate was individually added to the enzyme solution for each K_d. The K_d was obtained by the equation: $\Delta F = \Delta F_{max} - K_d(\Delta F/[\text{compound}])$. Data points are an average of 2–3 determinations within 10% error.

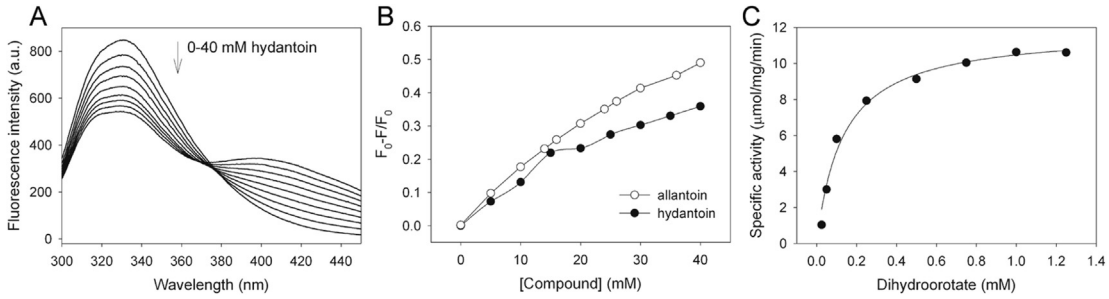

Fig. 5. Allantoin and hydantoin can bind, but cannot inhibit the activity of dihydroorotase. (A) The fluorescence emission spectra of dihydroorotase with hydantoin of different concentrations (0–40 mM). The decrease in intrinsic fluorescence of protein was measured at 330 nm upon excitation at 280 nm and 25 °C with a spectrofluorimeter. The fluorescence intensity emission spectra of dihydroorotase significantly quenched with hydantoin. (B) An aliquot amount of hydantoin and allantoin was individually added to the enzyme solution for each K_d. The K_d was obtained by the equation: $\Delta F = \Delta F_{max} - K_d(\Delta F/[\text{compound}])$. (C) Kinetic analysis of dihydroorotase using dihydroorotate of different concentrations (0–1.25 mM) with the V_{max} value of 11.8 ± 0.4 μmol/mg/min and the K_m value of 0.13 ± 0.02 mM. Data points are an average of 2–3 determinations within 10% error.

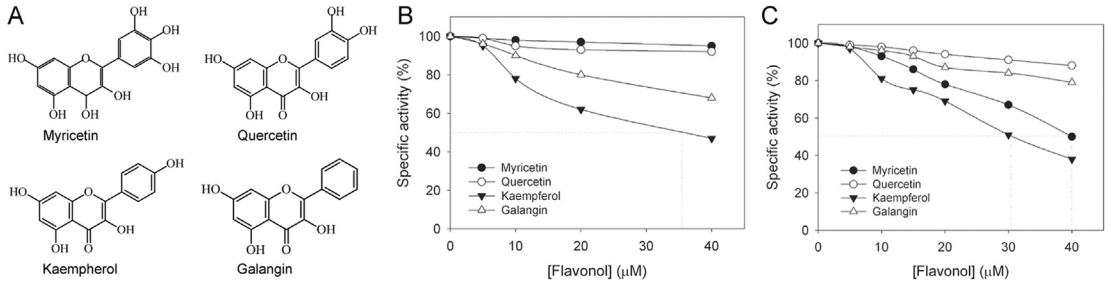

Fig. 6. The flavonol inhibitions of allantoinase and dihydroorotase. (A) Molecular structure of the flavonols, myricetin, quercetin, kaempferol, and galangin. They have a similar structure but contain different numbers of hydroxyl substituents on the aromatic rings. (B) IC_{50} determination of flavonols for allantoinase. Due to solubility, IC_{50} of some flavonols was not determined from the graphic analysis. (C) IC_{50} determination of flavonols for dihydroorotase. Data points are an average of 2–3 determinations within 10% error.

than that of the substrate analogs (at the mM range) of allantoinase and dihydroorotase. However, because of the poor solubility of these flavonols, only some IC_{50} values for allantoinase and dihydroorotase were determined (Table 2). Based on our knowledge, kaempferol remains the best inhibitor for allantoinase, with an IC_{50} of 35 ± 3 μM, and for dihydroorotase, with IC_{50} of 31 ± 2 μM.

3.8. K_d of allantoinase and dihydroorotase bound to kaempferol

The initial inhibition study of flavonols indicated that allantoinase and dihydroorotase were both significantly inhibited by kaempferol. To determine whether the inhibitory capabilities are correlated with their binding abilities, the K_d values of allantoinase and dihydroorotase for kaempferol were determined through fluorescence quenching. The K_d values of allantoinase and dihydroorotase bound to kaempferol determined using titration curve (Fig. 7) were 28.3 ± 3.8 and 20.9 ± 3.9 μM, respectively (Table 3). Thus, kaempferol can inhibit and bind to allantoinase and dihydroorotase with IC_{50} and K_d values at the μM range, significantly higher than those of the substrate analogs of allantoinase and dihydroorotase (at the mM range).

3.9. Kaempferol is a competitive inhibitor of allantoinase

From our initial inhibition screening, the flavonol kaempferol was identified as an inhibitor of allantoinase for the first time. To determine which type of inhibitor kaempferol is, this flavonol (40 μM) was included in the standard assay for allantoinase with different concentrations of allantoin, and the kinetic parameters of allantoinase were calculated from the double reciprocal of the Lineweaver–Burk plot. As shown in Fig. 8, inhibition of allantoinase by kaempferol resulted in Lineweaver–Burk plots with lines that cross the y-axis at a similar point, which indicates that kaempferol is a competitive inhibitor for allantoinase. Thus, similar to hydantoin and dihydroorotate, kaempferol can compete with allantoin for the active site of allantoinase, but with significantly stronger activity.

3.10. Kaempferol is an uncompetitive inhibitor for dihydroorotase

In this study, the flavonol kaempferol was identified as an inhibitor of dihydroorotase for the first time. To determine whether kaempferol competitively inhibits dihydroorotase, as with allantoinase, kaempferol (40 μM) was included in the standard assay for

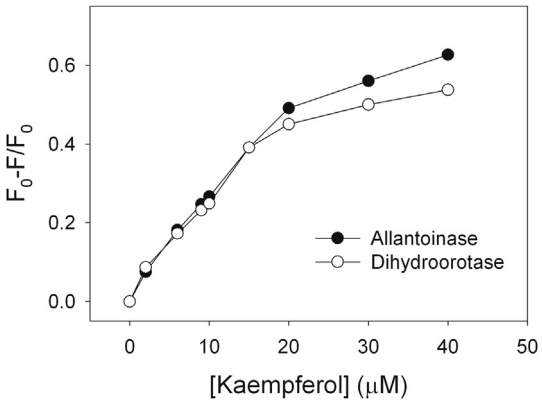

Fig. 7. Fluorescence titrations of kaempferol with allantoinase and dihydroorotase. An aliquot amount of kaempferol was added to the enzyme solution for each K_d. The K_d was obtained by the equation: $\Delta F = \Delta F_{max} - K_d(\Delta F/[\text{kaempferol}])$. Data points are an average of 2–3 determinations within 10% error.

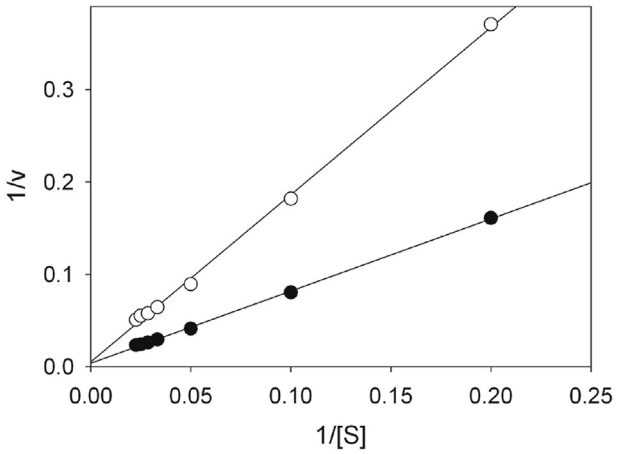

Fig. 8. Kaempferol is a competitive inhibitor for allantoinase. Inhibition of allantoinase by kaempferol resulted in Lineweaver–Burk plots where the lines are cross the *y*-axis at the similar point, indicating that kaempferol is a competitive inhibitor for allantoinase. Data points are an average of 2–3 determinations within 10% error.

dihydroorotase with different dihydroorotate concentrations. Unexpectedly, the inhibition of dihydroorotase by kaempferol resulted in Lineweaver–Burk plots with lines parallel that intersect the *y*-axis at different points, which indicates that kaempferol is an uncompetitive inhibitor (Fig. 9). Dihydroorotase in the presence of 40 μM kaempferol had a V_{max} of 4.24 ± 0.06 μmol/mg/min and a K_m of 0.048 ± 0.004 mM. Based on these kinetic results, kaempferol binds to the dihydroorotase–dihydroorotate complex rather than acts to a free enzyme, and then allosterically inhibits dihydroorotase. Taken together, kaempferol is a competitive inhibitor of allantoinase and an uncompetitive inhibitor of dihydroorotase.

3.11. Binding mode of allantoinase to kaempferol

To understand the inhibitory mechanism of kaempferol on allantoinase, the structure of allantoinase was built through homology modeling. Kaempferol, which is found in the DrugBank, was then computationally docked into the three-dimensional model of allantoinase using PatchDock (http://bioinfo3d.cs.tau.ac.il/PatchDock/) [45]. Docking was automatically performed after uploading the coordinate and topology file of flavonol and allantoinase. The three docking models (Supplementary materials) with the highest score for allantoinase interacting with kaempferol are shown in Fig. 10A. Kaempferol with different binding poses was docked into the active site pocket of allantoinase. For solution 1 with the highest docking score, the hydroxyl groups of kaempferol on the ring interact with Ser286 and Ser317 (Fig. 10B). Ser317 is a critical substrate binding site for allantoinase [14]. Thus, the docking study shows that kaempferol partially occupies the allantoinase active site. Consistent with the kinetic evidence, the docking study also shows that kaempferol competitively inhibits allantoinase.

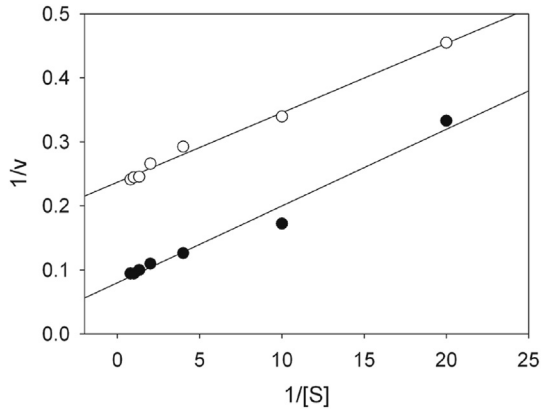

Fig. 9. Kaempferol is an uncompetitive inhibitor for dihydroorotase. Inhibition of dihydroorotase by kaempferol resulted in Lineweaver–Burk plots where the lines are parallel and cross the *y*-axis at different points, revealing an uncompetitive inhibitor. Data points are an average of 2–3 determinations within 10% error.

3.12. Binding mode of dihydroorotase to kaempferol

To study the inhibitory effect of kaempferol on dihydroorotase and the dihydroorotase–kaempferol complex, the model of *K. pneumoniae* dihydroorotase was computationally docked with kaempferol using PatchDock, as was done for allantoinase. The three dihydroorotase docking models (Supplementary materials) with the highest score for interacting with kaempferol are shown in Fig. 11A. Unlike allantoinase, the binding poses of kaempferol were all found to be docked outside the active site pocket of dihydroorotase. For solution 1 with the highest docking score, the hydroxyl groups of kaempferol on the ring interacted with E35, G277, and V346 (Fig. 11B). The docking study shows that kaempferol does not interact with the active site of dihydroorotase, a result consistent with the kinetic study (see Discussion).

4. Discussion

The development of clinically useful small-molecule antibiotics has been a seminal event in the field of infectious diseases [48]. DNA metabolism is one of the most basic biological functions and should be a prime target in antibiotic development. Considering allantoinase and dihydroorotase are required for metabolizing purines and pyrimidines, blocking their activities would be detrimental to bacterial survival. In addition, allantoinase is not found in humans; hence, these inhibitors are potentially safe for human use. The distinct differences between mammalian and prokaryotic dihydroorotases make bacterial dihydroorotases suitable targets for antibiotic development [16]. Although some chelators, such as 8-HQSA [42], inhibit allantoinase, such chelators are harmful to humans. In this study, we have shown that some flavonol compounds inhibit the catalytic activities of allantoinase (Fig. 6B) and dihydroorotase (Fig. 6C). Furthermore, the metabolic effects and safety of the flavonols are well established, making such flavonols beneficial for humans [28]. Thus, flavonols inhibit allantoinase and dihydroorotase, as well as potential antibiotics for further development.

We found that the flavonols myricetin, quercetin, kaempferol, and galangin, which contain different numbers of hydroxyl substituents on their aromatic rings (Fig. 6A), have different inhibitory effects on allantoinase and dihydroorotase (Fig. 6B and C). The catalytic activities of allantoinase and dihydroorotase were inhibited by flavonols in the following order: kaempferol > galangin > quercetin > myricetin for allantoinase, and kaempferol > myricetin > galangin > quercetin for dihydroorotase, respectively. Kaempferol, which contains one hydroxyl substituent on the flavonol aromatic ring, was the best inhibitor for allantoinase, with an IC_{50} of 35 ± 3 μM, and for dihydroorotase, with an IC_{50} of 31 ± 2 μM (Fig. 5A). Although flavonols are known to have several hydroxyl groups, thus, they have remarkable potential for binding any protein, the strength of the inhibitory effect (IC_{50}) on allantoinase and dihydroorotase did not correlate with the number of hydroxyl substituents on the flavonol aromatic rings.

The docking experiments of allantoinase and dihydroorotase suggested that kaempferol docks into the active site pocket of

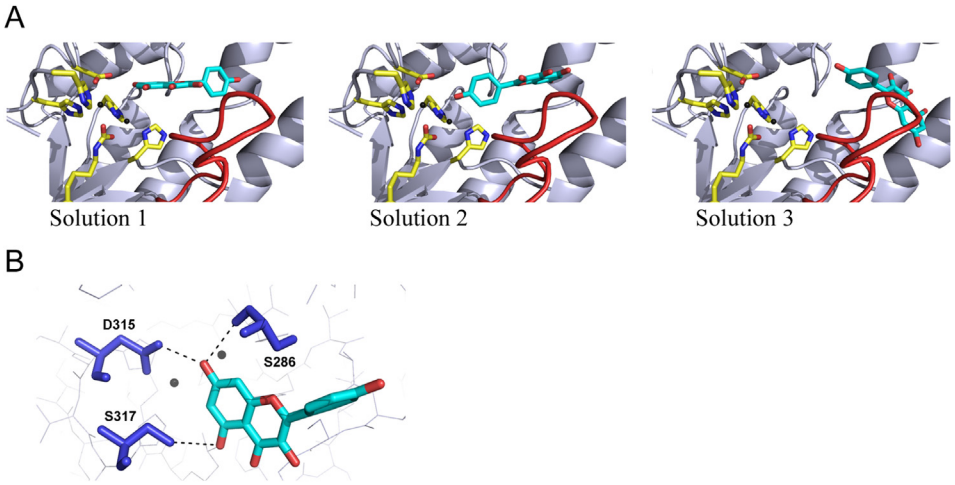

Fig. 10. Representation of the docking models of allantoinase–kaempferol complex from PatchDock. (A) The three docking models with the highest score for allantoinase interacting with kaempferol are shown. The active site residues of allantoinase are colored in yellow, and the substrate binding loop is colored in red. Kaempferol is colored in cyan. (B) Binding environment of kaempferol to allantoinase for Solution 1. The hydroxyl groups of kaempferol on the ring interact with S286, D315, and S317 of allantoinase.

allantoinase, but outside the active site pocket of dihydroorotase. Consistent with the docking results, the kinetic studies further identified kaempferol as a competitive inhibitor of allantoinase, but an uncompetitive inhibitor of dihydroorotase. Three docking solutions with the highest scores all show that kaempferol partially occupies the active site of allantoinase by interacting with the putative substrate-binding loop (Fig. 10). For dihydroorotase, kaempferol was bound to the loop with an unknown function. However, the corresponding positions of dihydroorotase for dihydropyrimidinase are structurally near the place for the conformational change of dihydropyrimidinase [49]. Thus, kaempferol may inhibit dihydroorotase allosterically. No potent inhibitor has been identified for these cyclic amidohydrolases. Thus, inhibitors designed to target the loop(s) to lock the conformation of the cyclic amidohydrolases may be worth to test in the future.

The cyclic amidohydrolases, at least hydantoinase [25,46,47], dihydropyrimidinase [50,51], and imidase [7,8,10,11], are known to catalyze the hydrolysis of a wide range of substrates and exhibit some overlapping substrate specificities. Our study clearly indicates that hydantoin, dihydroorotate, and phthalimide are not substrates, but are competitive inhibitors of allantoinase (Fig. 2). Unlike allantoinase, although hydantoin, allantoin, and phthalimide are not dihydroorotase substrates, they did not affect dihydroorotase activity. Nevertheless, dihydroorotase still binds to hydantoin and allantoin (Fig. 5A and Table 3).

The chemical mechanism of the binuclear metal center–containing amidohydrolase [2] likely has three steps (Fig. 1C): (1) the hydrolytic water molecule must be activated for nucleophilic attack, (2) the amide bond of the substrate must be made more electrophilic by the polarization of the carbonyl–oxygen bond, and (3) the leaving group nitrogen must be protonated as the carbon–nitrogen bond is cleaved. Thus, a single group must be unprotonated for the catalytic activity [52]. Based on the crystal structures of hydantoinase [53], dihydropyrimidinase [51], dihydroorotase [23], and allantoinase [14], the bimetal ion likely functions as a Lewis acid for polarizing the carbonyl group of the substrate of the imide group [13,24,25]. The carbonyl oxygen of the substrate that directly interacts with the metal center will diminish the electron density and facilitate nucleophilic attacks by the bridging the hydroxide. In the final step, the amide nitrogen of the substrate must be protonated. The conserved Asp in the active site of these cyclic amidohydrolases is responsible for proton transfer (Fig. 1B and C).

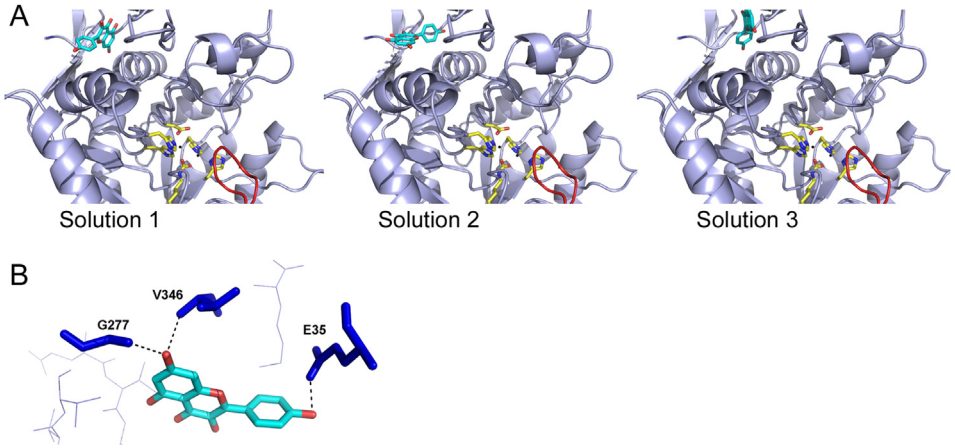

Fig. 11. Representation of the docking models of dihydroorotase–kaempferol complex from PatchDock. The three docking models with the highest score for dihydroorotase interacting with kaempferol are shown. The active site residues of dihydroorotase are colored in yellow, and the substrate binding loop is colored in red. Kaempferol is colored in cyan. (B) Binding environment of kaempferol to dihydroorotase for Solution 1. The hydroxyl groups of kaempferol on the ring interact with E35, G277, and V346 of dihydroorotase.

This residue has been proposed as the group that shuttles the proton from the bridging hydroxide to and from the substrate and product during catalysis. However, an important question remains as to why even at more than 100 mM, hydantoin can bind to, but absolutely cannot be hydrolyzed by, allantoinase and dihydroorotase. In addition, hydantoin can be docked into the active site of allantoinase (data not shown). Does the 5′ side chain of allantoin play an important role not only in interacting with the substrate binding loop of allantoinase but also involve in electron/proton delocalization as the driving force for imide hydrolysis? Further studies are needed to investigate the substrate specificity, selectivity, and the catalytic mechanism of allantoinase and dihydroorotase.

In conclusion, we identified a novel inhibitor, the flavonol kaempferol, and demonstrated its inhibitory mechanism on allantoinase and dihydroorotase using kinetic and docking experiments. We also found that allantoinase and dihydroorotase cannot use the substrates of other cyclic amidohydrolases as substrate. The significant inhibitory effect of kaempferol on allantoinase and dihydroorotase (>3 orders of magnitude than hydantoin) make it a promising drug lead for developing antibiotics targeting bacteria.

Disclosure statement

The authors have no conflicts of interest.

Acknowledgments

We would like to thank four anonymous reviewers and the editor for their comments. This research was supported by a grant from the National Science Council, Taiwan (NSC 102-2320-B-040-019 to C.Y. Huang).

Appendix A. Supplementary data

Supplementary data related to this article can be found at http://dx.doi.org/10.1016/j.biochi.2014.01.001.

References

[1] J.A. Gerlt, K.N. Allen, S.C. Almo, R.N. Armstrong, P.C. Babbitt, J.E. Cronan, D. Dunaway-Mariano, H.J. Imker, M.P. Jacobson, W. Minor, C.D. Poulter, F.M. Raushel, A. Sali, B.K. Shoichet, J.V. Sweedler, The enzyme function initiative, Biochemistry 50 (2011) 9950–9962.
[2] C.M. Seibert, F.M. Raushel, Structural and catalytic diversity within the amidohydrolase superfamily, Biochemistry 44 (2005) 6383–6391.
[3] J.A. Gerlt, P.C. Babbitt, Divergent evolution of enzymatic function: mechanistically diverse superfamilies and functionally distinct suprafamilies, Annu. Rev. Biochem. 70 (2001) 209–246.
[4] G.J. Kim, H.S. Kim, Identification of the structural similarity in the functionally related amidohydrolases acting on the cyclic amide ring, Biochem. J. 330 (1998) 295–302.
[5] L. Holm, C. Sander, An evolutionary treasure: unification of a broad set of amidohydrolases related to urease, Proteins 28 (1997) 72–82.
[6] J. Altenbuchner, M. Siemann-Herzberg, C. Syldatk, Hydantoinases and related enzymes as biocatalysts for the synthesis of unnatural chiral amino acids, Curr. Opin. Biotechnol. 12 (2001) 559–563.
[7] Y.W. Shi, X.Q. Liu, P. Shi, X.Y. Zhang, Characterization of zinc-binding properties of a novel imidase from *Pseudomonas putida* YZ-26, Arch. Biochem. Biophys. 494 (2009) 1–6.
[8] C.Y. Huang, Y.S. Yang, A novel cold-adapted imidase from fish *Oreochromis niloticus* that catalyzes hydrolysis of maleimide, Biochem. Biophys. Res. Commun. 312 (2003) 467–472.
[9] C.Y. Huang, Y.S. Yang, The role of metal on imide hydrolysis: metal content and pH profiles of metal ion-replaced mammalian imidase, Biochem. Biophys. Res. Commun. 297 (2002) 1027–1032.
[10] J. Ogawa, C.L. Soong, M. Honda, S. Shimizu, Imidase, a dihydropyrimidinase-like enzyme involved in the metabolism of cyclic imides, Eur. J. Biochem. 243 (1997) 322–327.
[11] Y.S. Yang, S. Ramaswamy, W.B. Jakoby, Rat liver imidase, J. Biol. Chem. 268 (1993) 10870–10875.
[12] S. Hayashi, S. Fujiwara, T. Noguchi, Evolution of urate-degrading enzymes in animal peroxisomes, Cell. Biochem. Biophys. 32 (2000) 123–129.
[13] Y.Y. Ho, Y.H. Huang, C.Y. Huang, Chemical rescue of the post-translationally carboxylated lysine mutant of allantoinase and dihydroorotase by metal ions and short-chain carboxylic acids, Amino Acids 44 (2013) 1181–1191.
[14] K. Kim, M.I. Kim, J. Chung, J.H. Ahn, S. Rhee, Crystal structure of metal-dependent allantoinase from *Escherichia coli*, J. Mol. Biol. 387 (2009) 1067–1074.
[15] I. Ramazzina, L. Cendron, C. Folli, R. Berni, D. Monteverdi, G. Zanotti, R. Percudani, Logical identification of an allantoinase analog (puuE) recruited from polysaccharide deacetylases, J. Biol. Chem. 283 (2008) 23295–23304.
[16] D.R. Evans, H.I. Guy, Mammalian pyrimidine biosynthesis: fresh insights into an ancient pathway, J. Biol. Chem. 279 (2004) 33035–33038.
[17] T. Nara, M. Hashimoto, H. Hirawake, C.W. Liao, Y. Fukai, S. Suzuki, A. Tsubouchi, J. Morales, S. Takamiya, T. Fujimura, H. Taka, R. Mineki, C.K. Fan, D.K. Inaoka, M. Inoue, A. Tanaka, S. Harada, K. Kita, T. Aoki, Molecular interaction of the first 3 enzymes of the de novo pyrimidine biosynthetic pathway of *Trypanosoma cruzi*, Biochem. Biophys. Res. Commun. 418 (2012) 140–143.
[18] M.I. Mally, D.R. Grayson, D.R. Evans, Catalytic synergy in the multifunctional protein that initiates pyrimidine biosynthesis in Syrian hamster cells, J. Biol. Chem. 255 (1980) 11372–11380.
[19] R.I. Christopherson, M.E. Jones, The overall synthesis of L-5,6-dihydroorotate by multienzymatic protein pyr1-3 from hamster cells. Kinetic studies, substrate channeling, and the effects of inhibitors, J. Biol. Chem. 255 (1980) 11381–11395.
[20] M.W. Washabaugh, K.D. Collins, Dihydroorotase from *Escherichia coli*. Purification and characterization, J. Biol. Chem. 259 (1984) 3293–3298.
[21] P. Zhang, P.D. Martin, C. Purcarea, A. Vaishnav, J.S. Brunzelle, R. Fernando, H.I. Guy-Evans, D.R. Evans, B.F. Edwards, Dihydroorotase from the hyperthermophile *Aquifex aeolicus* is activated by stoichiometric association with aspartate transcarbamoylase and forms a one-pot reactor for pyrimidine biosynthesis, Biochemistry 48 (2009) 766–778.
[22] D. McPhail, M. Shepherdson, The aspartate transcarbamoylase-dihydroorotase complex in *Deinococcus radiophilus* has an active dihydroorotase, Arch. Microbiol. 185 (2006) 78–81.
[23] J.B. Thoden, G.N. Phillips Jr., T.M. Neal, F.M. Raushel, H.M. Holden, Molecular structure of dihydroorotase: a paradigm for catalysis through the use of a binuclear metal center, Biochemistry 40 (2001) 6989–6997.
[24] T.N. Porter, Y. Li, F.M. Raushel, Mechanism of the dihydroorotase reaction, Biochemistry 43 (2004) 16285–16292.
[25] C.Y. Huang, C.C. Hsu, M.C. Chen, Y.S. Yang, Effect of metal binding and post-translational lysine carboxylation on the activity of recombinant hydantoinase, J. Biol. Inorg. Chem. 14 (2009) 111–121.
[26] V. Kumar, N. Saxena, M. Sarma, K.V. Radha Kishan, Carboxylated lysine is required for higher activities in hydantoinases, Protein Pept. Lett. 18 (2011) 663–669.
[27] K. Bush, Alarming beta-lactamase-mediated resistance in multidrug-resistant *Enterobacteriaceae*, Curr. Opin. Microbiol. 13 (2010) 558–564.
[28] J.A. Ross, C.M. Kasum, Dietary flavonoids: bioavailability, metabolic effects, and safety, Annu. Rev. Nutr. 22 (2002) 19–34.
[29] F. Teillet, A. Boumendjel, J. Boutonnat, X. Ronot, Flavonoids as RTK inhibitors and potential anticancer agents, Med. Res. Rev. 28 (2008) 715–745.
[30] K.L. Wolfe, R.H. Liu, Structure-activity relationships of flavonoids in the cellular antioxidant activity assay, J. Agric. Food. Chem. 56 (2008) 8404–8411.
[31] S. Burda, W. Oleszek, Antioxidant and antiradical activities of flavonoids, J. Agric. Food Chem. 49 (2001) 2774–2779.
[32] M.S. Yu, J. Lee, J.M. Lee, Y. Kim, Y.W. Chin, J.G. Jee, Y.S. Keum, Y.J. Jeong, Identification of myricetin and scutellarein as novel chemical inhibitors of the SARS coronavirus helicase, nsP13, Bioorg. Med. Chem. Lett. 22 (2012) 4049–4054.
[33] Y.S. Keum, Y.J. Jeong, Development of chemical inhibitors of the SARS coronavirus: viral helicase as a potential target, Biochem. Pharmacol. 84 (2012) 1351–1358.
[34] C.C. Chen, C.Y. Huang, Inhibition of *Klebsiella pneumoniae* DnaB helicase by the flavonol galangin, Protein J. 30 (2011) 59–65.
[35] T.P. Cushnie, A.J. Lamb, Antimicrobial activity of flavonoids, Int. J. Antimicrob. Agents 26 (2005) 343–356.
[36] C.C. Wang, H.W. Tsau, W.T. Chen, C.Y. Huang, Identification and characterization of a putative dihydroorotase, KPN01074, from *Klebsiella pneumoniae*, Protein J. 29 (2010) 445–452.
[37] H.H. Lin, C.Y. Huang, Characterization of flavonol inhibition of DnaB helicase: real-time monitoring, structural modeling, and proposed mechanism, J. Biomed. Biotechnol. 2012 (2012) 735368.
[38] Y.H. Huang, Y.H. Lo, W. Huang, C.Y. Huang, Crystal structure and DNA-binding mode of *Klebsiella pneumoniae* primosomal PriB protein, Genes Cells 17 (2012) 837–849.
[39] Y.H. Huang, C.Y. Huang, Characterization of a single-stranded DNA-binding protein from *Klebsiella pneumoniae*: mutation at either Arg73 or Ser76 causes a less cooperative complex on DNA, Genes Cells 17 (2012) 146–157.
[40] C.Y. Huang, C.H. Hsu, Y.J. Sun, H.N. Wu, C.D. Hsiao, Complexed crystal structure of replication restart primosome protein PriB reveals a novel single-stranded DNA-binding mode, Nucleic Acids Res. 34 (2006) 3878–3886.
[41] P.K. Smith, R.I. Krohn, G.T. Hermanson, A.K. Mallia, F.H. Gartner, M.D. Provenzano, E.K. Fujimoto, N.M. Goeke, B.J. Olson, D.C. Klenk, Measurement of protein using bicinchoninic acid, Anal. Biochem. 150 (1985) 76–85.

[42] Y.Y. Ho, H.C. Hsieh, C.Y. Huang, Biochemical characterization of allantoinase from *Escherichia coli* BL21, Protein J. 30 (2011) 384–394.
[43] K. Arnold, L. Bordoli, J. Kopp, T. Schwede, The SWISS-MODEL workspace: a web-based environment for protein structure homology modelling, Bioinformatics 22 (2006) 195–201.
[44] C. Knox, V. Law, T. Jewison, P. Liu, S. Ly, A. Frolkis, A. Pon, K. Banco, C. Mak, V. Neveu, Y. Djoumbou, R. Eisner, A.C. Guo, D.S. Wishart, DrugBank 3.0: a comprehensive resource for 'omics' research on drugs, Nucleic Acids Res. 39 (2011) D1035–D1041.
[45] D. Schneidman-Duhovny, Y. Inbar, R. Nussinov, H.J. Wolfson, PatchDock and SymmDock: servers for rigid and symmetric docking, Nucleic Acids Res. 33 (2005) W363–W367.
[46] U. Engel, C. Syldatk, J. Rudat, Stereoselective hydrolysis of aryl-substituted dihydropyrimidines by hydantoinases, Appl. Microbiol. Biotechnol. 94 (2012) 1221–1231.
[47] J.M. Clemente-Jimenez, S. Martinez-Rodriguez, F. Rodriguez-Vico, F.J. Heras-Vazquez, Optically pure alpha-amino acids production by the "Hydantoinase Process", Recent Pat. Biotechnol. 2 (2008) 35–46.
[48] A. Koul, E. Arnoult, N. Lounis, J. Guillemont, K. Andries, The challenge of new drug discovery for tuberculosis, Nature 469 (2011) 483–490.
[49] Y.C. Hsieh, M.C. Chen, C.C. Hsu, S.I. Chan, Y.S. Yang, C.J. Chen, Crystal structures of vertebrate dihydropyrimidinase and complexes from *Tetraodon nigroviridis* with lysine carbamylation: metal and structural requirements for post-translational modification and function, J. Biol. Chem. 288 (2013) 30645–30658.
[50] S. Martinez-Rodriguez, A.I. Martinez-Gomez, J.M. Clemente-Jimenez, F. Rodriguez-Vico, J.M. Garcia-Ruiz, F.J. Las Heras-Vazquez, J.A. Gavira, Structure of dihydropyrimidinase from *Sinorhizobium meliloti* CECT4114: new features in an amidohydrolase family member, J. Struct. Biol. 169 (2010) 200–208.
[51] B. Lohkamp, B. Andersen, J. Piskur, D. Dobritzsch, The crystal structures of dihydropyrimidinases reaffirm the close relationship between cyclic amidohydrolases and explain their substrate specificity, J. Biol. Chem. 281 (2006) 13762–13776.
[52] D.W. Christianson, J.D. Cox, Catalysis by metal-activated hydroxide in zinc and manganese metalloenzymes, Annu. Rev. Biochem. 68 (1999) 33–57.
[53] Y.H. Cheon, H.S. Kim, K.H. Han, J. Abendroth, K. Niefind, D. Schomburg, J. Wang, Y. Kim, Crystal structure of D-hydantoinase from *Bacillus stearothermophilus*: insight into the stereochemistry of enantioselectivity, Biochemistry 41 (2002) 9410–9417.

Hindawi Publishing Corporation
BioMed Research International
Volume 2014, Article ID 195162, 14 pages
http://dx.doi.org/10.1155/2014/195162

Review Article

Structural Insight into the DNA-Binding Mode of the Primosomal Proteins PriA, PriB, and DnaT

Yen-Hua Huang[1] and Cheng-Yang Huang[1,2]

[1] *School of Biomedical Sciences, Chung Shan Medical University, No. 110, Section 1, Chien-Kuo N. Road, Taichung City 40201, Taiwan*
[2] *Department of Medical Research, Chung Shan Medical University Hospital, No. 110 Section 1, Chien-Kuo N. Road, Taichung City 40201, Taiwan*

Correspondence should be addressed to Cheng-Yang Huang; cyhuang@csmu.edu.tw

Received 18 April 2014; Revised 20 June 2014; Accepted 1 July 2014; Published 21 July 2014

Academic Editor: Yoshito Abe

Replication restart primosome is a complex dynamic system that is essential for bacterial survival. This system uses various proteins to reinitiate chromosomal DNA replication to maintain genetic integrity after DNA damage. The replication restart primosome in *Escherichia coli* is composed of PriA helicase, PriB, PriC, DnaT, DnaC, DnaB helicase, and DnaG primase. The assembly of the protein complexes within the forked DNA responsible for reloading the replicative DnaB helicase anywhere on the chromosome for genome duplication requires the coordination of transient biomolecular interactions. Over the last decade, investigations on the structure and mechanism of these nucleoproteins have provided considerable insight into primosome assembly. In this review, we summarize and discuss our current knowledge and recent advances on the DNA-binding mode of the primosomal proteins PriA, PriB, and DnaT.

1. Introduction

Genome integrity should be maintained from generation to generation to ensure proper cell function and survival [1–3]. In bacteria, some exogenous and endogenous sources of DNA damage can inactivate a large proportion of replication forks [4, 5]. When DNA is damaged, the replication machinery, originally initiated at *oriC*, can be arrested and disassembled anywhere along the DNA, leading to replication failure [5, 6]. To reload DnaB helicase for *oriC*-independent DNA replication, collapsed DNA replication forks must be reactivated by the replication restart primosome [7, 8]. Primosome is the protein complex responsible for the conversion of single-stranded circular DNA to the replicative-form DNA in the replication cycle of ϕX174 phage [9, 10]. After DNA repair, the replication restart primosome [11–13], a formidable enzymatic machine, can translocate along the single-stranded DNA-binding protein (SSB), unwind the duplex DNA, and prime the Okazaki fragments required for the progression of replication forks [14]. In *Escherichia coli*, the replication restart primosome is composed of PriA helicase, PriB, PriC, DnaB helicase, DnaC, DnaT, and DnaG primase [3]. To date, two DnaB helicase-recruiting pathways are known: PriA-PriB-DnaT-DnaC-dependent and PriC-DnaC-dependent systems; the former system uses fork structures without gaps in the leading strand, whereas the latter system preferentially uses fork structures with large gaps (>5 nucleotides) in the leading strand [3]. As shown in Figure 1, PriA can bind directly and assemble a primosome on the template without gaps in the leading strand, and PriC initiates the assembly of a primosome on a fork containing gaps in the leading strand.

A hand-off mechanism for PriA-directed primosome assembly [15] has been proposed (Figure 2), whereby (i) PriA recognizes and binds to a replication fork; (ii) PriB joins PriA to form a PriA-PriB-DNA ternary complex; (iii) DnaT participates in this nucleocomplex to form a triprotein complex, in which PriB is released from ssDNA due to recruitment of DnaT; (iv) the PriA-PriB-DnaT-DNA quaternary complex

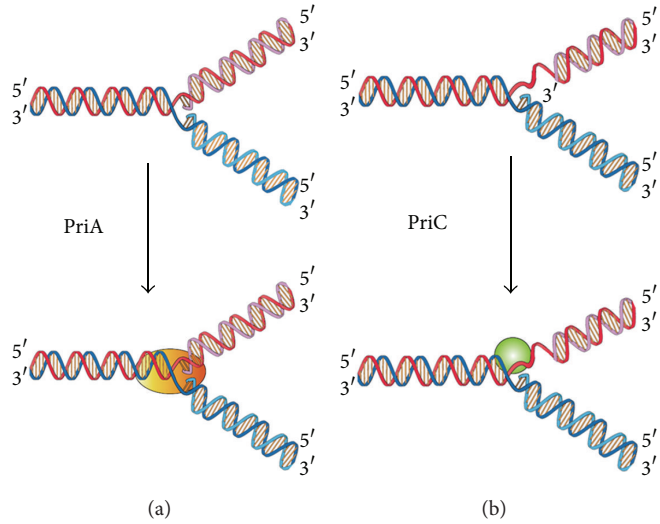

Figure 1: Two DnaB helicase-recruiting pathways for DNA replication restart at the stalled replication fork in vitro. The PriA-directed pathway (i.e., PriA-PriB-DnaT-DnaC-dependent reaction) preferentially uses fork structures without gaps in the leading strand, whereas the PriC-directed pathway (i.e., PriC-DnaC-dependent system) preferentially uses fork structures containing large gaps (>5 nucleotides) in the leading strand.

loads the DnaB/C complex; (v) DnaB is loaded on the lagging strand template. Genetic analyses suggest that these primosomal proteins are essential replication proteins for bacterial cell growth [12, 16–21]. These proteins are required for reinitiating chromosomal DNA replication in bacteria; thus, blocking their activities would be detrimental to bacterial survival [22, 23]. Several primosomal proteins, such as PriA, PriB, PriC, and DnaT, are not found in humans; thus, these proteins may be potential targets in developing antibiotics for the six antibiotic-resistant pathogens (*Enterococcus faecium*, *Staphylococcus aureus*, *Klebsiella pneumoniae*, *Acinetobacter baumannii*, *Pseudomonas aeruginosa*, and *Enterobacter* sp.) [24, 25]. The recently discovered inhibitor CGS 15943 targets *Neisseria gonorrhoeae* PriA helicase with an IC_{50} of 114 ± 24 μM [26].

Over the past 10 years, considerable progress has been made in the structural mechanisms of the replication restart primosome assembly. The structural information is a prerequisite for formulating any model of the assembly mechanism of the primosome (Table 1). In the following sections, we summarize and discuss our current knowledge and recent advances on the DNA-binding mode of the primosomal proteins PriA, PriB, and DnaT.

2. Structural Insights into the DNA-Binding Mode

2.1. PriA Helicase. PriA functions as a scaffold that recruits other primosomal proteins. It was originally discovered as an essential factor for the conversion of single-stranded circular DNA to the replicative-form DNA of ϕX174 single-stranded phage in vitro [27]. The *priA* mutant of *E. coli* exhibits complex phenotypes that include reduced viability, chronic induction of SOS response, rich media sensitivity, decreased homologous recombination, sensitivity to UV irradiation, defective double-stranded break repair, and both induced and constitutive stable DNA replication [6, 12, 28–30]. The native PriA is a monomer with a molecular mass of ~82 kDa. The tertiary structure of the monomer contains two functional domains, namely, the helicase domain (HD), which encompasses ~540 amino acid residues from the C-terminus, and the DNA-binding domain, which comprises ~181 amino acid residues from the N-terminus [31–33]. PriA is a DEXH-type helicase that unwinds DNA with a 3′ to 5′ polarity [34]. Fuelled by the binding and hydrolysis of ATP, PriA moves along the nucleic acid filaments with other primosomal proteins and separates double-stranded DNA into their complementary single strands [35]. PriA preferentially binds to a D-loop-like structure by recognizing a bend at the three-way branched DNA structures and duplex DNA with a protruding 3′ single strand [32, 36, 37]. PriA interacts with SSB [38], PriB [15, 39, 40], and DnaT [15]. PriA can unwind the nascent lagging strand DNA to create a suitable binding site to help PriC load the DnaB helicase onto stalled replication forks where a gap exists in the nascent leading strand [41, 42]. The crystal structures of the N-terminal 105 amino acid residue segment of *E. coli* PriA (EcPriA) in complex with different deoxydinucleotides show a feasible interaction model for the base-non-selective recognition of the 3′-terminus of DNA between the nucleobase and the DNA-binding sites of EcPriA [43].

Figure 3(a) shows that the alignment consensus of 150 sequenced PriA homologs by ConSurf [44] reveals the degree of variability at each position along the primary sequence. The highly variable amino acid residues are colored teal, whereas the highly conserved are colored burgundy. A consensus sequence was established by determining the most commonly found amino acid residue at each position relative to the primary sequence of *K. pneumoniae* PriA (KpPriA).

Table 1: List of the structures of the primosomal proteins available in Protein Data Bank.

	PDB ID	X-ray	NMR	Length
PriA	2D7E	The N-terminal domain of *Escherichia coli* PriA		105
	2DwN	The N-terminal domain of *Escherichia coli* PriA bound to AG		105
	2D7G	The N-terminal domain of *Escherichia coli* PriA bound to AA		105
	2D7H	The N-terminal domain of *Escherichia coli* PriA bound to CCC		105
	2Dwl	The N-terminal domain of *Escherichia coli* PriA bound to AC		105
	2Dwm	The N-terminal domain of *Escherichia coli* PriA bound to AT		105
	4NL4	*Klebsiella pneumoniae* PriA bound to ADP		731
	4NL8	*Klebsiella pneumoniae* PriA bound to SSB C-terminal tail peptide		731
PriB	2CCZ	*Escherichia coli* PriB bound to ssDNA (15 mer)		104
	1V1Q	*Escherichia coli* PriB		104
	1WOC	*Escherichia coli* PriB		100
	1TXY	*Escherichia coli* PriB		100
	2PNH	*Escherichia coli* PriB E39A		100
	4APV	*Klebsiella pneumoniae* PriB		102
	3K8A	*Neisseria gonorrhoeae* PriB		100
	4FDB	*Ralstonia solanacearum* PriB		99
	3EN2	*Ralstonia solanacearum* PriB		95
	3FHW	*Bordetella parapertussis* PriB		102
	3KLW	*Bordetella pertussis* PriB		98
	4GS3	The N-terminal domain of *Thermoanaerobacter tengcongensis* PriB		104
DnaT		None		
DnaB	4ESV	*Geobacillus stearothermophilus* DnaB bound to DNA (14 mer)		441
	2R6E	*Geobacillus stearothermophilus* DnaB		441
	2R6D	*Geobacillus stearothermophilus* DnaB		441
	2R6A	*Geobacillus stearothermophilus* DnaB bound to DnaG		441
	2R6C	*Geobacillus stearothermophilus* DnaB bound to DnaG		441
	4M4W	*Geobacillus stearothermophilus* DnaB bound to DnaG and DnaI		454
	2R5U	The N-terminal domain of *Mycobacterium tuberculosis* DnaB		167
	2Q6T	*Thermus aquaticus* DnaB		440
	3GXV	The N-terminal domain of *Helicobacter pylori* DnaB		121
	4A1F	The C-terminal domain of *Helicobacter pylori* DnaB		323
	4NMN	*Aquifex aeolicus* DnaB bound to ADP		434
	2VYF	*Geobacillus kaustophilus* DnaC		441
	2VYE	*Geobacillus kaustophilus* DnaC bound to ssDNA (9 mer)		441
	1B79	The N-terminal domain of *Escherichia coli* DnaB		128
	1JWE		The N-terminal domain of *Escherichia coli* DnaB	114
DnaC	3EC2	*Aquifex aeolicus* DnaC 42–221		180
	3ECC	*Aquifex aeolicus* DnaC bound to ADP	The N-terminal domain of *Bacillus subtilis* DnaI	185
	2W58	*Geobacillus kaustophilus* DnaI		199
	4M4W	*Geobacillus stearothermophilus* DnaB bound to DnaG and DnaI		278

Table 1: Continued.

	PDB ID	X-ray	NMR	Length
	2QGZ	*Streptococcus pyogenes* DnaI		308
	2K7R			106
DnaG	3B39	*Escherichia coli* DnaG 109–427 bound to ssDNA (15 mer)		321
	1DD9	*Escherichia coli* DnaG 115–428		338
	1DDE	*Escherichia coli* DnaG 115–428		338
	1T3W	The C-terminal domain of *Escherichia coli* DnaG		148
	2HAJ		*Escherichia coli* DnaG 447–581	135
	4E2K	*Staphylococcus aureus* DnaG 108–428		321
	4EDG	*Staphylococcus aureus* DnaG 108–428 bound to ATP		321
	4EDK	*Staphylococcus aureus* DnaG 108–428 bound to GTP		319
	4EDT	*Staphylococcus aureus* DnaG 108–428 bound to ppGpp		321
	4EDV	*Staphylococcus aureus* DnaG 108–428 bound to ppGpp		321
	4EE1	*Staphylococcus aureus* DnaG 108–428 bound to CTP		321
	4EDR	*Staphylococcus aureus* DnaG 108–428 bound to UTP		321
	2LZN		*Staphylococcus aureus* DnaG 462-605	143
	1Z8S		*Bacillus stearothermophilus* DnaG 452–597	146
	4EHS	The C-terminal domain of *Helicobacter pylori* DnaG 438–559		122
	4M4W	*Geobacillus stearothermophilus* DnaB bound to DnaI and DnaG		143
	2R6A	*Geobacillus stearothermophilus* DnaB bound to DnaG		143
	2R6C	*Geobacillus stearothermophilus* DnaB bound to DnaG		143
	2AU3	*Aquifex aeolicus* DnaG 1–403		403
PriC	2RT6		The N-terminal domain of *Escherichia coli* PriC	98

Length and amino acid residues.

The amino acid sequences of KpPriA and EcPriA share 88% identity [45]. The N-terminal 19–219 amino acid residues in PriA are not highly conserved. The crystal structure of KpPriA has been recently determined [45]. KpPriA has six subdomains (Figure 3(b)), namely, a 3′ DNA-binding domain (3′BD; orange), a winged-helix domain (WH; green), two lobes of the helicase core (colored hot pink and blue, resp.), a Cys-rich region (CRR; dark blue), and a C-terminal domain (CTD; red). The 3′BD and WH comprise the N-terminal DNA-binding domain (DBD), and the other four subdomains (two lobes of the helicase core, CRR, and CTD) comprise the HD. Asp17, located in the 3′BD of EcPriA, is crucial for the 3′ base-non-selective recognition of DNA [43], and Arg697, located in the CTD of KpPriA, is crucial for the C-terminal tail of SSB (SSB-Ct) binding and induction of structural changes in the SSB-DNA complex [45]; both are significantly invariable. Many biochemical and genetic studies have been performed on the DNA-binding mode of PriA [7, 8], but the structural basis for the full length PriA-DNA complex is still lacking.

To elucidate the structural mechanism of DNA binding and unwinding by PriA, Bhattacharyya et al. [45] compared the structure of the full length KpPriA with those of other DNA helicases of superfamily II, namely, RecQ1 (Protein Data Bank entry: 2WWY) [46, 47] and Hel308 (Protein Data Bank entry: 2P6R) [48]. The structures of these helicases have been solved in complex with substrate DNA. RecQ1 and Hel308 bind to single-stranded DNA tailed duplex and unwind via the DNA unwinding wedge element, a prominent β-hairpin for strand separation [47, 49]. PriA also shares sequence similarity with other helicases, such as PcrA (Protein Data Bank entry: 3PJR) [50], a DNA helicase of superfamily I, and RecG (Protein Data Bank entry: 1GM5) [51], a DNA helicase of superfamily II. The structures of

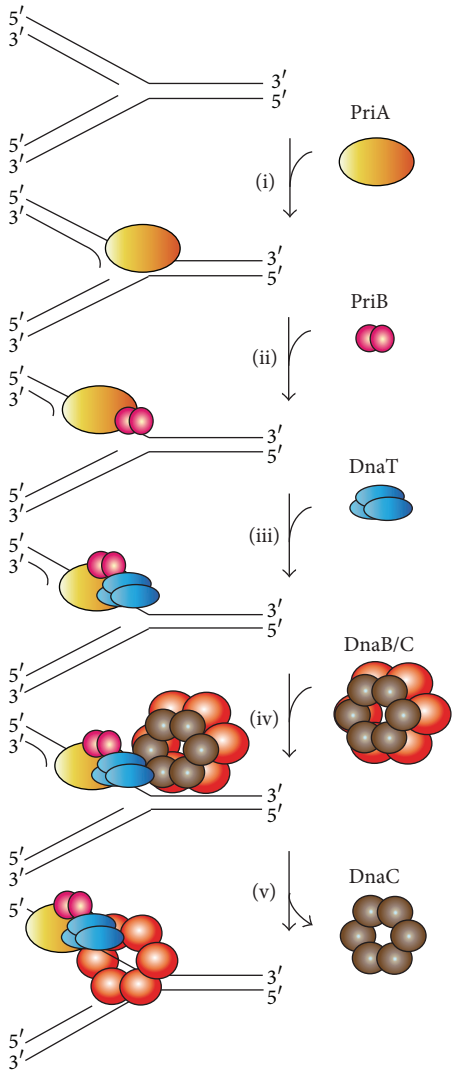

FIGURE 2: A hand-off mechanism for the replication restart primosome assembly. The proposed assembly mechanism is as follows. (i) PriA recognizes and binds to a replication fork, (ii) PriB joins PriA to form a PriA-PriB-DNA ternary complex, (iii) DnaT participates in this nucleocomplex to form a triprotein complex, in which PriB is released from ssDNA due to recruitment of DnaT, (iv) the PriA-PriB-DnaT-DNA quaternary complex loads the DnaB/C complex, and (v) DnaB is loaded on the lagging strand template.

these helicases bound to DNA, along with KpPriA, are shown in Figure 3(c) for comparison. According to the crystal structures of the helicase-DNA complex, the two lobes of the helicase core of KpPriA (colored hot pink and blue, resp.) are aligned and manually superimpose the location of the dsDNA from the complex structure with KpPriA structure. These modeled structures of KpPriA show that the DNA-binding modes and thus the DNA-unwinding modes are different. Considering the known ssDNA-binding site at DBD and the putative wedge element in KpPriA located at CRR, KpPriA may use the Hel308-based model to bind DNA. The DNA-binding mode, fork DNA recognition site(s), and the helicase translocation using either the inchworm stepping or Brownian motor mechanism [52] must be further confirmed by additional biophysical and structural studies.

2.2. PriB Protein. PriB is a basic accessory protein in PriA-directed DNA replication restart primosome [11, 13]. It was originally discovered as an essential factor for the conversion of single-stranded circular DNA to the replicative-form DNA of ϕX174 single-stranded phage in vitro. In contrast to the ϕX174 model, *del(priB)302* mutant has almost wild-type phenotypes [53], suggesting that PriB is not absolutely required for bacterial DNA replication. PriB was formerly known as the "n protein" because it can be inactivated by treatment with *N*-ethylmaleimide [54]. In a PriA-PriB-DnaT-dependent reaction, PriB is the second protein to be assembled in the protein-DNA complex. It stabilizes the binding of PriA to DNA hairpin [35, 55] and then stimulates PriA helicase activity [40, 56]. The PriA stimulation by PriB correlates with the ability of PriB to form a stable PriA-PriB-DNA complex [40]. PriB also facilitates the association of DnaT with PriA [57]. More than one PriA-PriB complex is possibly involved in the initiation of primosome formation, and the effect of PriB on the PriA-DNA association is dependent on the DNA structure [58]. PriB interacts with PriA [15, 39], DnaT [15, 59, 60], SSB [54, 61], and itself [61, 62] and does not interact with DnaA, DnaB, DnaC, or DnaG [61]. The mechanisms of DnaC-DnaB complex loading by PriA-PriB-DnaT complex at the forks and then DnaB-DnaG complex formation remain unclear.

PriB is a homodimer with polypeptide chains of 104 amino acid residues [63–65] (Figure 4(a)). Each PriB monomer has an oligonucleotide/oligosaccharide-binding (OB) fold structure [66–69] with three flexible β-hairpin loops: L_{12} (residues 20–24), L_{23} (residues 37–44), and L_{45} (residues 81–88) (Figure 4(b)). PriB can bind to ssDNA [15, 39, 40, 54, 56, 62–65, 70–73], ssRNA [65], double-stranded DNA [56, 70], and circular ϕX viral DNA [73]. Although PriB is a dimer, it has only one DNA-binding site [73], which is located in loop L_{45} centrally within the dimer, and this site occupies a total site size of 12 ± 1 nucleotides [72]. The N-terminal 1–49 amino acid residue region of PriB is crucial for dimerization, whereas the C-terminal 50–104 amino acid residue region is crucial for ssDNA binding [71]. PriB shares structural similarity with the N-terminal DNA-binding domain of the *E. coli* SSB (EcSSB) [63–65, 74, 75]. Sequence comparisons and operon organization analyses also show that PriB evolves from the duplication of the SSB gene [76], but they differ in their ssDNA-binding properties and strategies [70, 73]. For example, EcSSB possesses three conserved aromatic residues (Trp40, Trp54, and Phe60) in the L_{45} loop of the OB fold. These residues serve important functions in ssDNA binding. Two of these residues (Trp40 and Phe60 in EcSSB) are replaced with nonconserved amino acids in the PriB family. In contrast to the EcSSB-DNA complex, the L_{23} loop from each subunit of PriB makes a close contact with the β-barrel core. The longer and extended L_{23} loops in EcSSB greatly increase the interactions between EcSSB and ssDNA [73, 75].

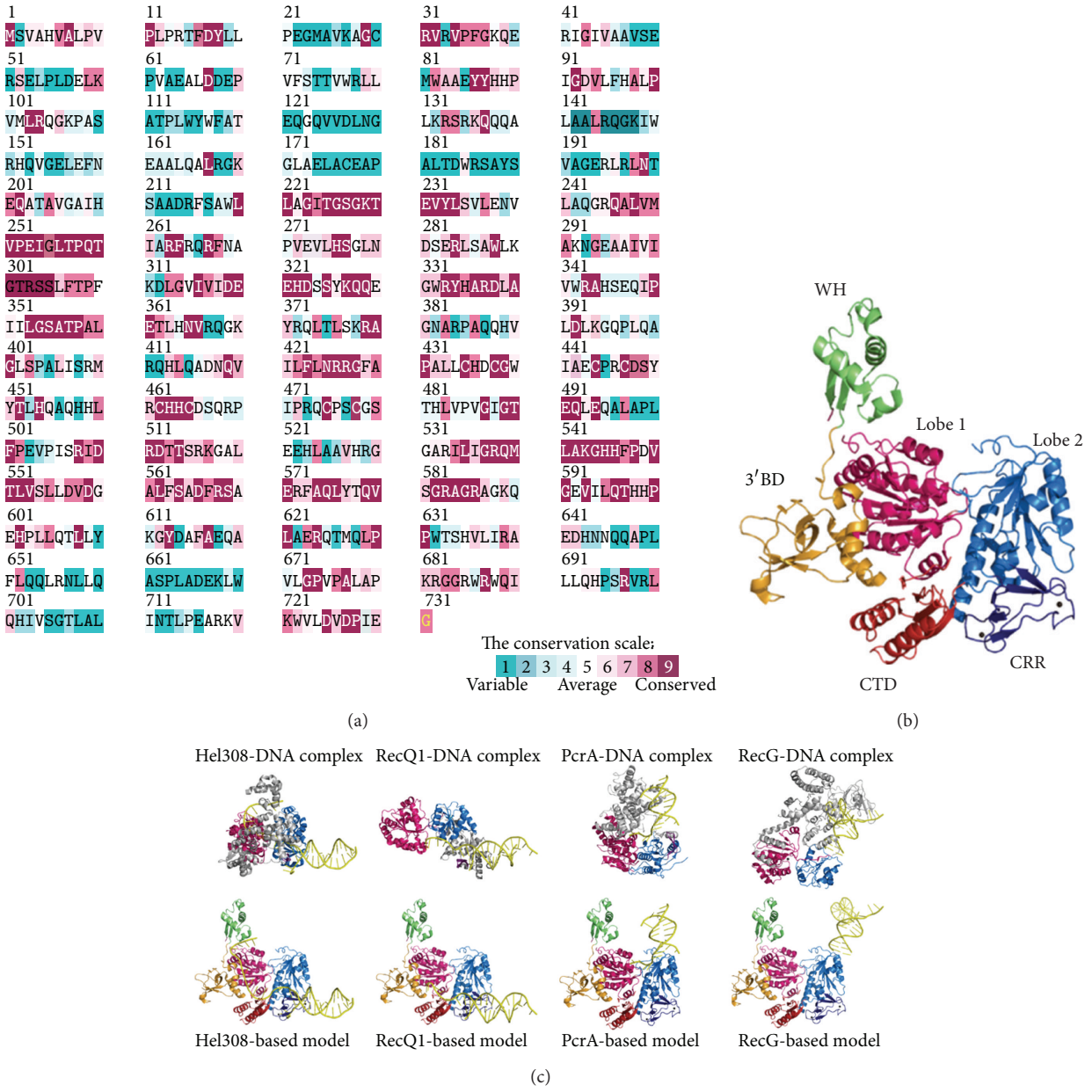

Figure 3: (a) Amino acid sequence alignment of KpPriA. An alignment consensus of 150 sequenced PriA homologs by the program ConSurf reveals the degree of variability at each position along the primary sequence. Highly variable amino acids are colored teal, whereas those highly conserved are colored burgundy. A consensus sequence was established by determining the most commonly found amino acid residue at each position relative to the primary sequence of KpPriA. The N-terminal 19–219 amino acid residues in PriA are not highly conserved. Asp17, located in the 3′BD of EcPriA, is crucial for the 3′ base-non-selective recognition of DNA, and Arg697, located in the CTD of KpPriA, is crucial for the SSB-Ct binding and induction of structural changes in the SSB-DNA complex; both are significantly invariable. (b) Crystal structure of KpPriA. KpPriA has six subdomains (Protein Data Bank entry: 4NL4), namely, a 3′ DNA-binding domain (3′BD; orange), a winged-helix domain (WH; green), two lobes of the helicase core (colored hot pink and blue, resp.), a Cys-rich region (CRR; dark blue), and a C-terminal domain (CTD; red). 3′BD and WH comprise the N-terminal DNA-binding domain (DBD), and the other four subdomains (two lobes of the helicase core, CRR, and CTD) comprise the helicase domain (HD). (c) Putative DNA-binding mode of KpPriA. The DNA-binding models of KpPriA are directly constructed by manually superimposing the KpPriA with DNA-bound crystal structure of Hel308 (Protein Data Bank entry: 2P6R), RecQ1 (Protein Data Bank entry: 2WWY), PcrA (Protein Data Bank entry: 3PJR), and RecG (Protein Data Bank entry: 1GM5). Considering the known ssDNA-binding site at DBD and the putative wedge element in KpPriA located at CRR, KpPriA may use the Hel308-based model to bind DNA. The β-hairpin, an important motif for DNA strand separation by helicase, is colored in magenta.

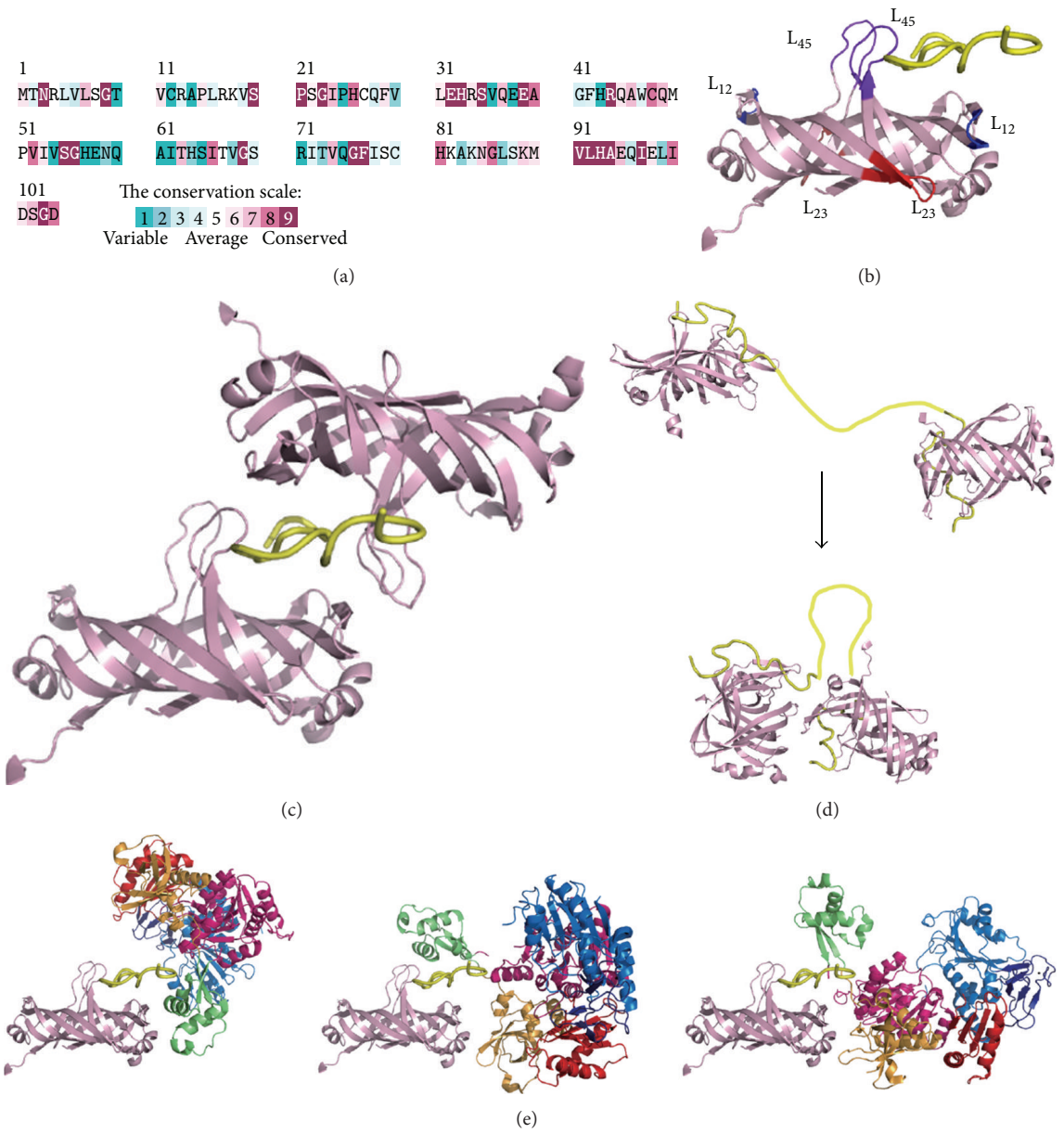

FIGURE 4: (a) Amino acid sequence alignment of EcPriB. An alignment consensus of 111 sequenced PriB homologs by the program ConSurf reveals the degree of variability at each position along the primary sequence. In general, the overall amino acid sequences among PriB proteins are not highly conserved, including many residues found important for ssDNA binding by EcPriB, such as Phe42, Trp47, Lys82, Lys84, and Lys89. (b) EcPriB is a homodimer with polypeptide chains of 104 amino acid residues. Each PriB monomer has an OB-fold structure with three flexible β-hairpin loops: L_{12} (residues 20–24; colored in blue), L_{23} (residues 37–44; colored in red), and L_{45} (residues 81–88; colored in purple blue). The ssDNA in the complex is shown in gold. (c) Crystal structure of EcPriB in complex with DNA. The complex structure of EcPriB (Protein Data Bank entry: 2CCZ) shows that a single dT15 ssDNA periodically interacts with two OB folds from two symmetrically related EcPriB dimers in the crystal and that the DNA is sandwiched by PriB dimers via their L_{45} loops. (d) Possible working model of interaction between two PriB proteins on ssDNA. PriB proteins cooperatively bind to ssDNA in two steps: two PriB proteins independently interact with ssDNA and then interact with each other through His64 on the ssDNA. The ssDNA in the complex is shown in gold. The region in ssDNA that does not directly interact with PriB, proposed in this two-step binding model, is colored in yellow. (e) Proposed models for PriA-DNA-PriB structure. These models are based on these observations: (1) two PriB dimers are complexed with a single dT15; (2) PriA has a highly electropositive ssDNA-binding region in DBD, and the basic DBD in PriA may be involved in complex with PriB; (3) DBD of PriA alone in solution forms a dimer and not a monomer as the full-length PriA.

Figure 4(a) shows the alignment consensus of 111 sequenced PriB homologs by ConSurf [44]. The alignment indicates that the overall amino acid sequences among PriB proteins are not highly conserved; only 21 amino acid residues are significantly conserved: Asn3, Gly9, Ser20, Pro21, Gly23, Glu32, His33, Ser35, Glu39, Arg44, Ser55, Gly56, Gly69, Gly76, Phe77, Val91, Leu92, His93, Ala94, Ile97, and Gly103. Many residues important for ssDNA binding by *E. coli* PriB (EcPriB), such as Phe42 [64], Trp47 [64, 73], Lys82 [64, 73], Lys84 [73], and Lys89 [73], are not conserved. PriB may be a nonessential facilitating factor in DNA replication restart [53], and many prokaryotic genomes do not contain a recognizable homolog of *priB* [39]. Hence, we speculate that these residues among PriB proteins for binding ssDNA do not need to be precisely conserved.

We previously described the crystal structure of EcPriB in complex with ssDNA dT15 (Protein Data Bank entry: 2CCZ) [73]. A single dT15 ssDNA periodically interacts with two OB folds from two symmetrically related EcPriB dimers in the crystal, sandwiched by PriB dimers via their L_{45} loops (Figure 4(c)). Although the precise function of more than one PriB self-assembled on DNA to form a high-density nucleoprotein complex is still unclear, PriB binds DNA with strong cooperativity [70, 72, 73] in two steps (Figure 4(d)): two PriB proteins independently interact with ssDNA in primary binding mode, and then the proteins interact with each other through His64 on the ssDNA [77]. Whether the resultant ssDNA bound by more than one PriB forms a unique structure suitable for further assembly process for the primosome is not clearly known. The complex structure [73] and the thermodynamic analysis [72] indicate that the PriB dimer behaves like a protein with half-site reactivity, where only one monomer of the PriB dimer can engage in interactions with the DNA and the partner protein. The importance of the binding site on PriB for ssDNA to overlap the binding sites for PriA and DnaT needs to be investigated [15]. Each preprimosome may contain two PriB dimers [60]; whether or not this cocrystal structure, in which two PriB dimers are complexed with a single dT15 ssDNA, is an artificial or an actual binding mode for ssDNA by PriB also remains unclear. PriA may have a function similar to a monomer of the symmetrical PriB dimer in the crystal to stabilize the partially disordered ssDNA because the cooperation between PriB and PriA may be necessary to form a stable PriA-DNA-PriB complex. That is, the PriB-ssDNA-PriB complex (Figure 4(c)) may mimic the structure of the PriA-ssDNA-PriB complex (Figure 4(e)). We proposed three binding ways by use of the crystal structures of PriA and PriB. EcPriA has a highly electropositive ssDNA-binding region (amino acid residues 1–198) containing 8 Lys and 14 Arg residues in DBD; thus, the basic DBD in EcPriA may be involved in complex with EcPriB [73]. The DBD of EcPriA alone in solution forms a dimer and not a monomer as EcPriA [31], suggesting that another unknown stabilization factor is needed. The DBD of PriA and one of the monomers of PriB may bind to ssDNA cooperatively to decrease the dissociation rate of PriA from the DNA during helix unwinding [73]. The crystal structure of PriA in complex with PriB and DNA is necessary to elucidate the assembly mechanism of the replication restart primosome.

More than a mere ssDNA-binding protein, PriB can bind both ssDNA and dsDNA with comparable affinity [70]. SSB can also bind dsDNA but with far less affinity than ssDNA [78]. According to the crystal structures of some dimeric proteins complexed with dsDNA found in the Protein Data Bank, PriB binds dsDNA in three possible ways (Figure 5). First, PriB may bind to dsDNA via the replication terminator protein- (RTP-) binding mode (Protein Data Bank entry: 1F4K) [79]. RTP, a dimeric WH protein [80, 81], uses two recognition helices to bind the major grooves of dsDNA. The PriB dimer also has two helices but does not contain any aromatic or positively charged residues as RTP. Thus, PriB binds to dsDNA via the RTP-binding mode that can be ruled out. Second, PriB may bind to dsDNA via the HU-binding mode (Protein Data Bank entry: 1P51) [82, 83]. HU is a dimeric nucleoid-associated protein that mainly uses two β sheets to bind dsDNA. Third, PriB may bind dsDNA in a manner similar to binding ssDNA. The structure-based mutational analysis indicates that the residues in PriB crucial for ssDNA binding are also crucial for dsDNA binding [70]. These residues responsible for ssDNA and dsDNA binding are almost overlapped; thus, PriB may use a similar approach to bind to the phosphate backbone of ssDNA and dsDNA through several positively charged residues. This phenomenon may be the reason for the comparable binding affinities of PriB to ssDNA and dsDNA. We speculate that, during evolution [76], the conserved aromatic and other residues in the L_{45} loop of the OB fold in SSB are changed into nonconserved and positively charged residues in PriB to more precisely fit the requirement for assembly of the replication restart primosome at the stalled DNA forks.

2.3. DnaT Protein. DnaT is an essential protein in the assembly of the PriA-directed DNA replication restart primosome [6, 11–13, 15, 55, 57]. It provides a specific recognition site for loading the replicative DnaB helicase during the promosome assembly [15, 42]. DnaT, formerly known as the "protein i" [84–86], was originally discovered as a critical factor for the conversion of single-stranded circular DNA to the replicative-form DNA of ϕX174 single-stranded phage [9] and pBR322 plasmid replication, but not for R1 plasmid replication [87]. Genetic analysis for *E. coli* DnaT suggests that a replication protein is essential for bacterial cell growth because the colony size, cell morphology, inability to properly partition nucleoids, UV sensitivity, and basal SOS expression of the *dnaT822* mutant are similar to those of *priA2::kan* mutants [18]. DnaT is required for *E. coli* growth at elevated pressure [88] and for the lytic cycle of Mu growth [89]. DnaT is a homotrimer of ~22 kDa subunits [86, 90], but it also exists in solution as a monomer-trimer equilibrium system [91]. In a PriA-PriB-DnaT-dependent reaction, DnaT is the third protein to be assembled in the protein-DNA complex (Figure 2). The association of DnaT with PriA is facilitated by PriB [57]. Although the function of DnaT in the recruitment of DnaB helicase has been proposed, the fundamental function of DnaT for the replication restart primosome assembly is not widely known.

We have recently identified and characterized that DnaT is a ssDNA-binding protein [90]. Based on the alignment

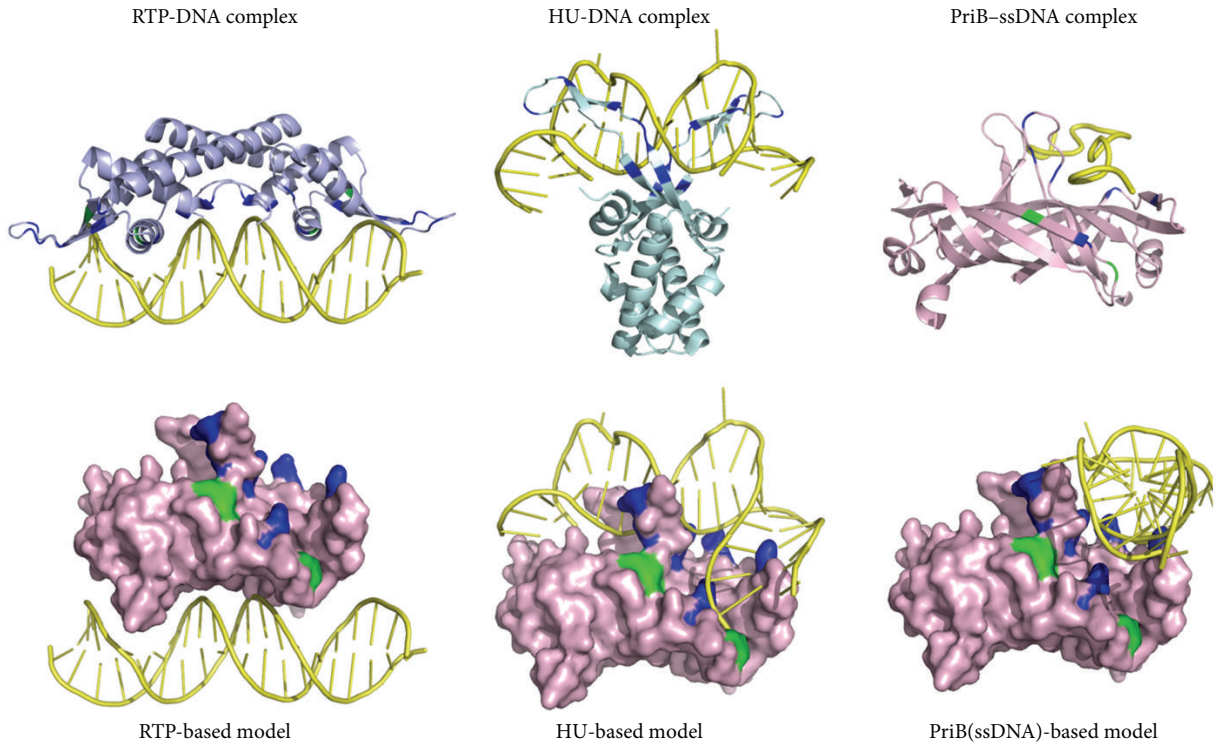

Figure 5: Putative dsDNA-binding mode of PriB. The DNA-binding models of PriB are directly constructed by manually superimposing the PriB dimer with DNA-bound crystal structure of RTP (Protein Data Bank entry: 1F4K), HU (Protein Data Bank entry: 1P51), and B-form dsDNA. The hydrophobic (green) and basic residues (blue) of RTP, Lys14, Arg16, Lys51, Arg59, Lys71, Lys74, Lys76, Lys77, Lys81, Lys91, Tyr58, and Tyr88, located on the dsDNA-binding surface, are indicated. The basic residues Arg53, Arg55, Lys56, Arg58, Arg61, Lys64, Lys68, and Arg75 of HU located on the dsDNA-binding surface are also indicated. Considering the known dsDNA-binding sites in PriB, PriB may use the HU-based model to bind dsDNA. Alternatively, PriB may use a similar approach to bind ssDNA and dsDNA because the residues responsible for ssDNA and dsDNA binding are almost overlapped.

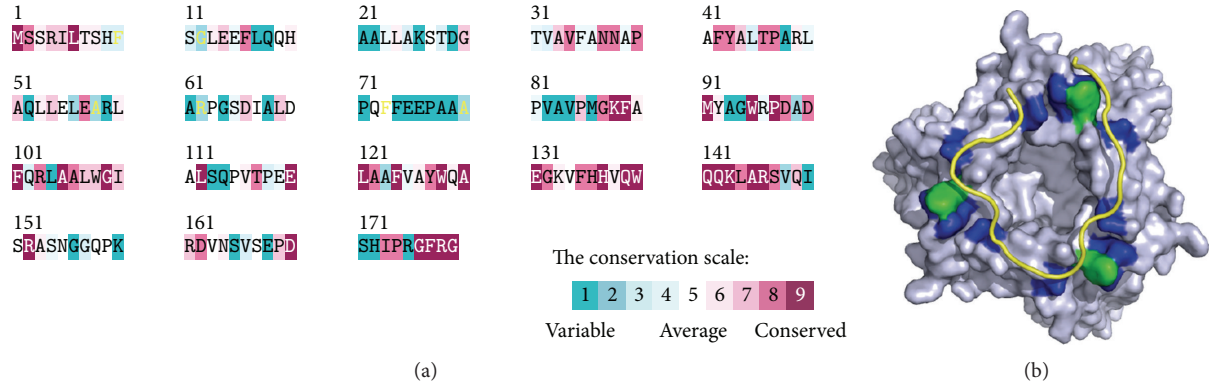

Figure 6: (a) Amino acid sequence alignment of KpDnaT. An alignment consensus of 29 sequenced DnaT homologs by the program ConSurf reveals the degree of variability at each position along the primary sequence. In general, the amino acid residues in the C-terminal region of KpDnaT are highly conserved. (b) Modeled structure of KpDnaT. The structure of KpDnaT is modeled by the bioinformatic program $(PS)^2$ and then manually built using threefold symmetry with a 25 mer ssDNA (gold). The highly conserved hydrophobic (green) and basic residues (blue) of KpDnaT, His136, His137, Trp140, Lys143, Arg146, and Arg151 located on the potential ssDNA-binding surface are indicated.

consensus of 29 sequenced DnaT homologs by ConSurf [44], we found that the amino acid residues in the C-terminal region of *K. pneumoniae* DnaT (KpDnaT) are highly conserved (Figure 6(a)) and that KpDnaT contains 10 Arg, 5 Lys, and 18 aromatic amino acid residues (11 Phe, 4 Trp, and 3 Tyr). We attempted to assess whether or not KpDnaT, especially at the C-terminal region, has ssDNA-binding activity because the aromatic stacking and electropositive interactions serve important functions in ssDNA binding by proteins [73, 75, 92–94]. KpDnaT can form distinct complexes with ssDNA of

different lengths, and the size of the binding site is 26 ± 2 nucleotides for a trimeric KpDnaT [90]. Although DnaT is not an OB-fold protein predicted from sequence analysis and structure modeling, the activity for ssDNA binding by DnaT, assayed in the same manner, is even higher than that of PriB, an OB-fold protein [90]. The two-domain structure for DnaT is characterized by the involvement of the N-terminal domain (amino acid residues 1–83) in PriB binding and the C-terminal domain (amino acid residues 84–179) in ssDNA binding [59].

To date, little is known about the ssDNA-binding mode of non-OB-fold proteins, particularly trimeric proteins. No protein with amino acid sequence similar to DnaT is found in the structure databank. Thus, homology modeling for the DnaT structure by several homology-based programs is not successful, including the use of SWISS-MODEL (http://swissmodel.expasy.org/) [95]. To obtain an indepth understanding of the structure-function relationship of KpDnaT, its 3D structure has been modeled by the bioinformatic program $(PS)^2$ [96, 97]. $(PS)^2$ (http://140.113.239.111/~ps2v2/docs.php) is an automatic homology modeling server that combines both sequence and secondary structure information to detect the homologous proteins with remote similarity and target-template alignment [96, 97]. The modeled structure of KpDnaT, manually built using threefold symmetry with a hit of alpha-aminotransferase from *Pyrococcus horikoshii* (Protein Data Bank entry: 1GD9) suggested from $(PS)^2$, is a ring-shaped trimer (Figure 6(b)) [59, 90]. Based on the structural model of KpDnaT, we suggested that the positively charged (blue) and aromatic residues (green) located in the C-terminus of DnaT are involved in ssDNA binding: H136, H137, W140, K143, R146, and R151 (Figure 6(b)). These residues in DnaT are significantly conserved among the 29 sequenced DnaT proteins (Figure 6(a)). F73 and F74 are also potential binding sites for ssDNA, but they are not completely conserved in DnaT family. The ring-like structure of KpDnaT is slightly similar to that of the hexameric (comprised of three dimers) DnaC helicase from *Geobacillus kaustophilus*, a DnaB-like helicase [92]. DnaT may bind to DnaB with a stoichiometry of 1 : 2, one DnaT monomer to a DnaB dimer. However, the DnaT structure is only a modeled structure, and these speculations, including the putative DNA and DnaB-binding modes of DnaT, must be further confirmed by additional biophysical studies.

3. Perspectives

Most DNA helicases of superfamily I and superfamily II are almost nonhexameric and have poor dsDNA unwinding activities when acting alone in vitro [98]. Some helicases might function as ssDNA translocases rather than helicases, and self-assembly and/or interactions with accessory proteins are required to activate helicase activity [98]. Several monomeric ssDNA translocases of superfamily I can potentially displace proteins that are bound to ssDNA by translocating along the ssDNA and be activated by self-assembly, removal of an autoinhibitory domain, or direct interactions with an accessory protein(s) [38, 40, 99–101]. For PriA, the self-assembly and removal of an autoinhibitory domain for higher helicase activity have not been reported. However, poor helicase activity for PriA, which can be significantly stimulated by PriB [40] and SSB [38], is found. Based on the structure of KpPriA bound to an SSB C-terminal peptide (Trp-Met-Asp-Phe-Asp-Asp-Asp-Ile-Pro-Phe) and the study of a single-molecule FRET (smFRET), Bhattacharyya et al. [45] proposed a pushing mechanism, which is similar to that for the RecA recombinase [102], for PriA-mediated replication restart. For SSB-bound DNA replication forks, PriA translocase activity may push SSB along the lagging-strand template to expose additional ssDNA for PriB and DnaT binding and that will ultimately serve as a binding site for DnaB [45]. This model provides structural insight into the molecular mechanism for initiating replication restart primosome assembly. The interaction of PriB with PriA is weak, and the stimulation of PriA by PriB via an interaction with ssDNA is not DNA structure-specific [40]. Thus, the targeting of stalled forks and recombination intermediates during replication restart likely correlates with PriA alone. More structural studies for these primosomal proteins are still necessary to elucidate the interaction between PriB and DnaT, as well as the release from the replication restart system. Several studies have raised new interesting questions as to whether or not PriA, PriB, and DnaT are always synchronically expressed for physiological needs and whether or not PriB and DnaT have additional functions for other systems. PriA and DnaT are required for *E. coli* growth at elevated pressure [88]; however, why PriB is not necessary to be synchronically expressed has yet to be determined. Many prokaryotic genomes do not contain a recognizable homolog of *priB* and *dnaT* (e.g., *P. aeruginosa*; Table 2). Thus, further operon and gene regulation analyses for PriB and DnaT expression, not limited to replication restart, should be also investigated in combination with the biochemical and structural investigations.

Table 2: Examples for some different PriA-directed primosome systems.

	PriA size (amino acid residues)	Partner proteins found in NCBI
Escherichia coli and *Klebsiella pneumoniae*	731	PriB, PriC, DnaT, DnaC, DnaB helicase, and DnaG
Staphylococcus aureus	802	DnaD, DnaB, DnaI, DnaC helicase, and DnaG
Pseudomonas aeruginosa	739	Only DnaB helicase and DnaG are found

PriA is conserved in bacteria, but its primosomal partners are not.

Conflict of Interests

The authors declare that there is no conflict of interests regarding the publication of this paper.

Acknowledgments

The authors would like to thank three anonymous reviewers and the editor for their comments. This research was supported by a grant from the National Science Council, Taiwan (NSC 102-2320-B-040-019 to C.Y. Huang).

References

[1] G. Smeenk and H. van Attikum, "The chromatin response to DNA breaks: leaving a mark on genome integrity," *Annual Review of Biochemistry*, vol. 82, pp. 55–80, 2013.

[2] S. Panier and D. Durocher, "Push back to respond better: regulatory inhibition of the DNA double-strand break response," *Nature Reviews Molecular Cell Biology*, vol. 14, pp. 661–672, 2013.

[3] R. C. Heller and K. J. Marians, "Replisome assembly and the direct restart of stalled replication forks," *Nature Reviews Molecular Cell Biology*, vol. 7, no. 12, pp. 932–943, 2006.

[4] R. L. Maher, A. M. Branagan, and S. W. Morrical, "Coordination of DNA replication and recombination activities in the maintenance of genome stability," *Journal of Cellular Biochemistry*, vol. 112, no. 10, pp. 2672–2682, 2011.

[5] P. McGlynn and R. G. Lloyd, "Recombinational repair and restart of damaged replication forks," *Nature Reviews Molecular Cell Biology*, vol. 3, no. 11, pp. 859–870, 2002.

[6] M. M. Cox, M. F. Goodman, K. N. Kreuzer, D. J. Sherratt, S. J. Sandler, and K. J. Marians, "The importance of repairing stalled replication forks," *Nature*, vol. 404, no. 6773, pp. 37–41, 2000.

[7] H. Masai, T. Tanaka, and D. Kohda, "Stalled replication forks: making ends meet for recognition and stabilization," *BioEssays*, vol. 32, no. 8, pp. 687–697, 2010.

[8] C. B. Gabbai and K. J. Marians, "Recruitment to stalled replication forks of the PriA DNA helicase and replisome-loading activities is essential for survival," *DNA Repair*, vol. 9, no. 3, pp. 202–209, 2010.

[9] K. J. Marians, "Prokaryotic DNA replication," *Annual Review of Biochemistry*, vol. 61, pp. 673–719, 1992.

[10] R. Schekman, A. Weiner, and A. Kornberg, "Multienzyme systems of DNA replication: proteins required for chromosome replication are resolved with the aid of a simple viral DNA template," *Science*, vol. 186, no. 4168, pp. 987–993, 1974.

[11] S. J. Sandler and K. J. Marians, "Role of PriA in replication fork reactivation in Escherichia coli," *Journal of Bacteriology*, vol. 182, no. 1, pp. 9–13, 2000.

[12] S. J. Sandler, "Multiple genetic pathways for restarting DNA replication forks in *Escherichia coli* K-12," *Genetics*, vol. 155, no. 2, pp. 487–497, 2000.

[13] K. J. Marians, "PriA-directed replication fork restart in *Escherichia coli*," *Trends in Biochemical Sciences*, vol. 25, no. 4, pp. 185–189, 2000.

[14] S. S. Patel, M. Pandey, and D. Nandakumar, "Dynamic coupling between the motors of DNA replication: hexameric helicase, DNA polymerase, and primase," *Current Opinion in Chemical Biology*, vol. 15, no. 5, pp. 595–605, 2011.

[15] M. Lopper, R. Boonsombat, S. J. Sandler, and J. L. Keck, "A hand-off mechanism for primosome assembly in replication restart," *Molecular Cell*, vol. 26, no. 6, pp. 781–793, 2007.

[16] R. Boonsombat, S. Yeh, A. Milne, and S. J. Sandler, "A novel dnaC mutation that suppresses priB rep mutant phenotypes in Escherichia coli K-12," *Molecular Microbiology*, vol. 60, no. 4, pp. 973–983, 2006.

[17] S. J. Sandler, "Requirements for replication restart proteins during constitutive stable DNA replication in Escherichia coli K-12," *Genetics*, vol. 169, no. 4, pp. 1799–1806, 2005.

[18] J. D. McCool, C. C. Ford, and S. J. Sandler, "A dnaT mutant with phenotypes similar to those of a priA2::kan mutant in Escherichia coli K-12," *Genetics*, vol. 167, no. 2, pp. 569–578, 2004.

[19] T. Hinds and S. J. Sandler, "Allele specific synthetic lethality between priC and dnaAts alleles at the permissive temperature of 30∘C in *E. coli* K-12," *BMC Microbiology*, vol. 4, article 47, 2004.

[20] S. J. Sandler, J. D. McCool, T. T. Do, and R. U. Johansen, "PriA mutations that affect PriA-PriC function during replication restart," *Molecular Microbiology*, vol. 41, no. 3, pp. 697–704, 2001.

[21] J. Liu, L. Xu, S. J. Sandler, and K. J. Marians, "Replication fork assembly at recombination intermediates is required for bacterial growth," *Proceedings of the National Academy of Sciences of the United States of America*, vol. 96, no. 7, pp. 3552–3555, 1999.

[22] A. H. Marceau, D. A. Bernstein, B. W. Walsh, W. Shapiro, L. A. Simmons, and J. L. Keck, "Protein interactions in genome maintenance as novel antibacterial targets," *PLoS ONE*, vol. 8, no. 3, Article ID e58765, 2013.

[23] D. Lu, D. A. Bernstein, K. A. Satyshur, and J. L. Keck, "Small-molecule tools for dissecting the roles of SSB/protein interactions in genome maintenance," *Proceedings of the National Academy of Sciences of the United States of America*, vol. 107, no. 2, pp. 633–638, 2010.

[24] K. Bush, "Alarming β-lactamase-mediated resistance in multidrug-resistant *Enterobacteriaceae*," *Current Opinion in Microbiology*, vol. 13, no. 5, pp. 558–564, 2010.

[25] H. W. Boucher, G. H. Talbot, J. S. Bradley et al., "Bad bugs, no drugs: no ESKAPE! An update from the Infectious Diseases Society of America," *Clinical Infectious Diseases*, vol. 48, no. 1, pp. 1–12, 2009.

[26] B. Sunchu, L. Berg, H. E. Ward, and M. E. Lopper, "Identification of a small molecule PriA helicase inhibitor," *Biochemistry*, vol. 51, no. 51, pp. 10137–10146, 2012.

[27] K. Arai and A. Kornberg, "Unique primed start of phage phi X174 DNA replication and mobility of the primosome in a direction opposite chain synthesis," *Proceedings of the National Academy of Sciences of the United States of America*, vol. 78, no. 1, pp. 69–73, 1981.

[28] H. Masai, T. Asai, Y. Kubota, K. Arai, and T. Kogoma, "Escherichia coli PriA protein is essential for inducible and constitutive stable DNA replication," *EMBO Journal*, vol. 13, no. 22, pp. 5338–5345, 1994.

[29] P. Nurse, K. H. Zavitz, and K. J. Marians, "Inactivation of the Escherichia coli PriA DNA replication protein induces the SOS response," *Journal of Bacteriology*, vol. 173, no. 21, pp. 6686–6693, 1991.

[30] A. Kornberg, "Replication deficiencies in priA mutants of Escherichia coli lacking the primosomal replication n' protein," *Proceedings of the National Academy of Sciences of the United States of America*, vol. 88, no. 8, pp. 3029–3032, 1991.

[31] M. R. Szymanski, P. J. Bujalowski, M. J. Jezewska, A. M. Gmyrek, and W. Bujalowski, "The N-terminal domain of the *Escherichia coli* pria helicase contains both the DNA- and nucleotide-binding sites. Energetics of domain-DNA interactions and allosteric effect of the nucleotide cofactors," *Biochemistry*, vol. 50, no. 43, pp. 9167–9183, 2011.

[32] H. Chen, S. H. North, and H. Nakai, "Properties of the PriA helicase domain and its role in binding PriA to specific DNA structures," *Journal of Biological Chemistry*, vol. 279, no. 37, pp. 38503–38512, 2004.

[33] T. Tanaka, T. Mizukoshi, C. Taniyama, D. Kohda, K. Arai, and H. Masai, "DNA binding of PriA protein requires cooperation of the N-terminal D-loop/arrested-fork binding and C-terminal helicase domains," *Journal of Biological Chemistry*, vol. 277, no. 41, pp. 38062–38071, 2002.

[34] C. A. Ouzounis and B. J. Blencowe, "Bacterial DNA replication initiation factor priA is related to proteins belonging to the "DEAD-box" family," *Nucleic Acids Research*, vol. 19, no. 24, article 6953, 1991.

[35] J. Y. Ng and K. J. Marians, "The ordered assembly of the phiX174-type primosome. I. Isolation and identification of intermediate protein-DNA complexes," *Journal of Biological Chemistry*, vol. 271, no. 26, pp. 15642–15648, 1996.

[36] P. Nurse, J. Liu, and K. J. Marians, "Two modes of PriA binding to DNA," *Journal of Biological Chemistry*, vol. 274, no. 35, pp. 25026–25032, 1999.

[37] P. McGlynn, A. A. Al-Deib, J. Liu, K. J. Marians, and R. G. Lloyd, "The DNA replication protein PriA and the recombination protein RecG bind D-loops," *Journal of Molecular Biology*, vol. 270, no. 2, pp. 212–221, 1997.

[38] C. J. Cadman and P. McGlynn, "PriA helicase and SSB interact physically and functionally," *Nucleic Acids Research*, vol. 32, no. 21, pp. 6378–6387, 2004.

[39] J. Dong, N. P. George, K. L. Duckett, M. A. P. DeBeer, and M. E. Lopper, "The crystal structure of *Neisseria gonorrhoeae* PriB reveals mechanistic differences among bacterial DNA replication restart pathways," *Nucleic Acids Research*, vol. 38, no. 2, Article ID gkp1031, pp. 499–509, 2009.

[40] C. J. Cadman, M. Lopper, P. B. Moon, J. L. Keck, and P. McGlynn, "PriB stimulates PriA helicase via an interaction with single-stranded DNA," *The Journal of Biological Chemistry*, vol. 280, no. 48, pp. 39693–39700, 2005.

[41] R. C. Heller and K. J. Marians, "Unwinding of the nascent lagging strand by Rep and PriA enables the direct restart of stalled replication forks," *Journal of Biological Chemistry*, vol. 280, no. 40, pp. 34143–34151, 2005.

[42] R. C. Heller and K. J. Marians, "The disposition of nascent strands at stalled replication forks dictates the pathway of replisome loading during restart," *Molecular Cell*, vol. 17, no. 5, pp. 733–743, 2005.

[43] K. Sasaki, T. Ose, N. Okamoto et al., "Structural basis of the 3′-end recognition of a leading strand in stalled replication forks by PriA," *EMBO Journal*, vol. 26, no. 10, pp. 2584–2593, 2007.

[44] M. Landau, I. Mayrose, Y. Rosenberg et al., "ConSurf 2005: the projection of evolutionary conservation scores of residues on protein structures," *Nucleic Acids Research*, vol. 33, no. 2, pp. W299–W302, 2005.

[45] B. Bhattacharyya, N. P. George, T. M. Thurmes et al., "Structural mechanisms of PriA-mediated DNA replication restart," *Proceedings of the National Academy of Sciences of the United States of America*, vol. 111, no. 4, pp. 1373–1378, 2014.

[46] A. Vindigni, F. Marino, and O. Gileadi, "Probing the structural basis of RecQ helicase function," *Biophysical Chemistry*, vol. 149, no. 3, pp. 67–77, 2010.

[47] A. C. W. Pike, B. Shrestha, V. Popuri et al., "Structure of the human RECQ1 helicase reveals a putative strand-separation pin," *Proceedings of the National Academy of Sciences of the United States of America*, vol. 106, no. 4, pp. 1039–1044, 2009.

[48] K. Büttner, S. Nehring, and K. Hopfner, "Structural basis for DNA duplex separation by a superfamily-2 helicase," *Nature Structural and Molecular Biology*, vol. 14, no. 7, pp. 647–652, 2007.

[49] B. Lucic, Y. Zhang, O. King et al., "A prominent β-hairpin structure in the winged-helix domain of RECQ1 is required for DNA unwinding and oligomer formation," *Nucleic Acids Research*, vol. 39, no. 5, pp. 1703–1717, 2011.

[50] S. S. Velankar, P. Soultanas, M. S. Dillingham, H. S. Subramanya, and D. B. Wigley, "Crystal structures of complexes of PcrA DNA helicase with a DNA substrate indicate an inchworm mechanism," *Cell*, vol. 97, no. 1, pp. 75–84, 1999.

[51] M. R. Singleton, S. Scaife, and D. B. Wigley, "Structural analysis of DNA replication fork reversal by RecG," *Cell*, vol. 107, no. 1, pp. 79–89, 2001.

[52] S. S. Patel and I. Donmez, "Mechanisms of helicases," *Journal of Biological Chemistry*, vol. 281, no. 27, pp. 18265–18268, 2006.

[53] S. J. Sandler, K. J. Marians, K. H. Zavitz, J. Coutu, M. A. Parent, and A. J. Clark, "dnaC mutations suppress defects in DNA replication- and recombination-associated functions in priB and priC double mutants in Escherichia coli K-12," *Molecular Microbiology*, vol. 34, no. 1, pp. 91–101, 1999.

[54] R. L. Low, J. Shlomai, and A. Kornberg, "Protein n, a primosomal DNA replication protein of *Escherichia coli*: purification and characterization," *Journal of Biological Chemistry*, vol. 257, no. 11, pp. 6242–6250, 1982.

[55] G. C. Allen Jr. and A. Kornberg, "Assembly of the primosome of DNA replication in Escherichia coli," *Journal of Biological Chemistry*, vol. 268, no. 26, pp. 19204–19209, 1993.

[56] C. Feng, B. Sunchu, M. E. Greenwood, and M. E. Lopper, "A bacterial PriB with weak single-stranded DNA binding activity can stimulate the DNA unwinding activity of its cognate PriA helicase," *BMC Microbiology*, vol. 11, article 189, 2011.

[57] J. Liu, P. Nurse, and K. J. Marians, "The ordered assembly of the φX174-type primosome. III. PriB facilitates complex formation between PriA and DnaT," *Journal of Biological Chemistry*, vol. 271, no. 26, pp. 15656–15661, 1996.

[58] M. R. Szymanski, M. J. Jezewska, and W. Bujalowski, "Binding of two PriA-PriB complexes to the primosome assembly site initiates primosome formation," *Journal of Molecular Biology*, vol. 411, no. 1, pp. 123–142, 2011.

[59] Y. H. Huang and C. Y. Huang, "The N-terminal domain of DnaT, a primosomal DNA replication protein, is crucial for PriB binding and self-trimerization," *Biochemical and Biophysical Research Communications*, vol. 442, pp. 147–152, 2013.

[60] J. Y. Ng and K. J. Marians, "The ordered assembly of the φX174-type primosome. II. Preservation of primosome composition from assembly through replication," *The Journal of Biological Chemistry*, vol. 271, no. 26, pp. 15649–15655, 1996.

[61] Y. H. Huang, M. J. Lin, and C. Y. Huang, "Yeast two-hybrid analysis of PriB-interacting proteins in replication restart primosome: a proposed PriB-SSB interaction model," *The Protein Journal*, vol. 32, no. 6, pp. 477–483, 2013.

[62] Y. H. Huang, H. H. Lin, and C. Y. Huang, "A single residue determines the cooperative binding property of a primosomal DNA replication protein, PriB, to single-stranded DNA," *Bioscience, Biotechnology and Biochemistry*, vol. 76, no. 6, pp. 1110–1115, 2012.

[63] S. Shioi, T. Ose, K. Maenaka et al., "Crystal structure of a biologically functional form of PriB from *Escherichia coli* reveals a potential single-stranded DNA-binding site," *Biochemical and*

Biophysical Research Communications, vol. 326, no. 4, pp. 766–776, 2005.

[64] M. Lopper, J. M. Holton, and J. L. Keck, "Crystal structure of PriB, a component of the *Escherichia coli* replication restart primosome," *Structure*, vol. 12, no. 11, pp. 1967–1975, 2004.

[65] J. H. Liu, T. W. Chang, C. Y. Huang et al., "Crystal structure of PriB, a primosomal DNA replication protein of *Escherichia coli*," *The Journal of Biological Chemistry*, vol. 279, no. 48, pp. 50465–50471, 2004.

[66] M. P. Horvath, "Structural anatomy of telomere OB proteins," *Critical Reviews in Biochemistry and Molecular Biology*, vol. 46, no. 5, pp. 409–435, 2011.

[67] R. L. Flynn and L. Zou, "Oligonucleotide/oligosaccharide-binding fold proteins: a growing family of genome guardians," *Critical Reviews in Biochemistry and Molecular Biology*, vol. 45, no. 4, pp. 266–275, 2010.

[68] I. D. Kerr, R. I. M. Wadsworth, L. Cubeddu, W. Blankenfeldt, J. H. Naismith, and M. F. White, "Insights into ssDNA recognition by the OB fold from a structural and thermodynamic study of *Sulfolobus*SSB protein," *The EMBO Journal*, vol. 22, no. 11, pp. 2561–2570, 2003.

[69] A. G. Murzin, "OB(oligonucleotide/oligosaccharide binding)-fold: common structural and functional solution for non-homologous sequences," *The EMBO Journal*, vol. 12, no. 3, pp. 861–867, 1993.

[70] Y. H. Huang, Y. H. Lo, W. Huang, and C. Y. Huang, "Crystal structure and DNA-binding mode of Klebsiella pneumoniae primosomal PriB protein," *Genes to Cells*, vol. 17, no. 10, pp. 837–849, 2012.

[71] H. C. Hsieh and C. Y. Huang, "Identification of a novel protein, PriB, in *Klebsiella pneumoniae*," *Biochemical and Biophysical Research Communications*, vol. 404, no. 1, pp. 546–551, 2011.

[72] M. R. Szymanski, M. J. Jezewska, and W. Bujalowski, "Interactions of the Escherichia coli Primosomal PriB Protein with the Single-stranded DNA. Stoichiometries, Intrinsic Affinities, Cooperativities, and Base Specificities," *Journal of Molecular Biology*, vol. 398, no. 1, pp. 8–25, 2010.

[73] C. Y. Huang, C. H. Hsu, Y. J. Sun, H. N. Wu, and C. D. Hsiao, "Complexed crystal structure of replication restart primosome protein PriB reveals a novel single-stranded DNA-binding mode," *Nucleic Acids Research*, vol. 34, no. 14, pp. 3878–3886, 2006.

[74] K. W. Chan, Y. J. Lee, C. H. Wang, H. Huang, and Y. J. Sun, "Single-stranded DNA-binding protein complex from *Helicobacter pylori* suggests an ssDNA-binding surface," *Journal of Molecular Biology*, vol. 388, no. 3, pp. 508–519, 2009.

[75] S. Raghunathan, A. G. Kozlov, T. M. Lohman, and G. Waksman, "Structure of the DNA binding domain of *E. coli* SSB bound to ssDNA," *Nature Structural Biology*, vol. 7, no. 8, pp. 648–652, 2000.

[76] V. A. Ponomarev, K. S. Makarova, L. Aravind, and E. V. Koonin, "Gene duplication with displacement and rearrangement: origin of the bacterial replication protein PriB from the single-stranded DNA-binding protein Ssb," *Journal of Molecular Microbiology and Biotechnology*, vol. 5, no. 4, pp. 225–229, 2003.

[77] S. Fujiyama, Y. Abe, T. Takenawa et al., "Involvement of histidine in complex formation of PriB and single-stranded DNA," *Biochimica et Biophysica Acta*, vol. 184, pp. 299–307, 2014.

[78] R. R. Meyer and P. S. Laine, "The single-stranded DNA-binding protein of Escherichia coli," *Microbiological Reviews*, vol. 54, no. 4, pp. 342–380, 1990.

[79] J. A. Wilce, J. P. Vivian, A. F. Hastings et al., "Structure of the RTP-DNA complex and the mechanism of polar replication fork arrest," *Nature Structural Biology*, vol. 8, no. 3, pp. 206–210, 2001.

[80] K. L. Tsai, Y. J. Sun, C. Y. Huang, J. Y. Yang, M. C. Hung, and C. D. Hsiao, "Crystal structure of the human FOXO3a-DBD/DNA complex suggests the effects of post-translational modification," *Nucleic Acids Research*, vol. 35, no. 20, pp. 6984–6994, 2007.

[81] K. L. Tsai, C. Y. Huang, C. H. Chang, Y. J. Sun, W. J. Chuang, and C. D. Hsiao, "Crystal structure of the human FOXK1a-DNA complex and its implications on the diverse binding specificity of winged helix/forkhead proteins," *Journal of Biological Chemistry*, vol. 281, no. 25, pp. 17400–17409, 2006.

[82] D. Kamashev, A. Balandina, A. K. Mazur, P. B. Arimondo, and J. Rouviere-Yaniv, "HU binds and folds single-stranded DNA," *Nucleic Acids Research*, vol. 36, no. 3, pp. 1026–1036, 2008.

[83] K. K. Swinger, K. M. Lemberg, Y. Zhang, and P. A. Rice, "Flexible DNA bending in HU-DNA cocrystal structures," *The EMBO Journal*, vol. 22, no. 14, pp. 3749–3760, 2003.

[84] H. Masai and K. Arai, "Initiation of lagging-strand synthesis for pBR322 plasmid DNA replication in vitro is dependent on primosomal protein i encoded by dnaT," *The Journal of Biological Chemistry*, vol. 263, no. 29, pp. 15016–15023, 1988.

[85] H. Masai, M. W. Bond, and K. Arai, "Cloning of the Escherichia coli gene for primosomal protein i: the relationship to dnaT, essential for chromosomal DNA replication," *Proceedings of the National Academy of Sciences of the United States of America*, vol. 83, no. 5, pp. 1256–1260, 1986.

[86] K. Arai, R. McMacken, S. Yasuda, and A. Kornberg, "Purification and properties of Escherichia coli protein i, a prepriming protein in ØX174 DNA replication," *The Journal of Biological Chemistry*, vol. 256, no. 10, pp. 5281–5286, 1981.

[87] H. Masai and K. Arai, "Escherichia coli dnaT gene function is required for pBR322 plasmid replication but not for R1 plasmid replication," *Journal of Bacteriology*, vol. 171, no. 6, pp. 2975–2980, 1989.

[88] S. L. Black, A. Dawson, F. B. Ward, and R. J. Allen, "Genes required for growth at high hydrostatic pressure in *Escherichia coli* K-12 identified by genome-wide screening," *PLoS One*, vol. 8, Article ID e73995, 2013.

[89] S. Jang, S. J. Sandler, and R. M. Harshey, "Mu insertions are repaired by the double-strand break repair pathway of *Escherichia coli*," *PLoS Genetics*, vol. 8, no. 4, Article ID e1002642, 2012.

[90] Y. H. Huang, M. J. Lin, and C. Y. Huang, "DnaT is a single-stranded DNA binding protein," *Genes Cells*, vol. 18, pp. 1007–1019, 2013.

[91] M. R. Szymanski, M. J. Jezewska, and W. Bujalowski, "The *Escherichia coli* primosomal dnat protein exists in solution as a monomer-trimer equilibrium system," *Biochemistry*, vol. 52, no. 11, pp. 1845–1857, 2013.

[92] Y. H. Lo, K. L. Tsai, Y. J. Sun, W. T. Chen, C. Y. Huang, and C. D. Hsiao, "The crystal structure of a replicative hexameric helicase DnaC and its complex with single-stranded DNA," *Nucleic Acids Research*, vol. 37, no. 3, pp. 804–814, 2009.

[93] D. L. Theobald, R. M. Mitton-Fry, and D. S. Wuttke, "Nucleic acid recognition by OB-fold proteins," *Annual Review of Biophysics and Biomolecular Structure*, vol. 32, pp. 115–133, 2003.

[94] C. Yang, U. Curth, C. Urbanke, and C. H. Kang, "Crystal structure of human mitochondrial single-stranded DNA binding protein at 2.4 A resolution," *Nature Structural Biology*, vol. 4, no. 2, pp. 153–157, 1997.

[95] K. Arnold, L. Bordoli, J. Kopp, and T. Schwede, "The SWISS-MODEL workspace: a web-based environment for protein structure homology modelling," *Bioinformatics*, vol. 22, no. 2, pp. 195–201, 2006.

[96] C.-C. Chen, J.-K. Hwang, and J.-M. Yang, "$(PS)^2$-v2: template-based protein structure prediction server," *BMC Bioinformatics*, vol. 10, article 366, 2009.

[97] C. C. Chen, J. K. Hwang, and J. M. Yang, "(PS)2: protein structure prediction server," *Nucleic Acids Research*, vol. 34, pp. W152–W157, 2006.

[98] T. M. Lohman, E. J. Tomko, and C. G. Wu, "Non-hexameric DNA helicases and translocases: mechanisms and regulation," *Nature Reviews Molecular Cell Biology*, vol. 9, no. 5, pp. 391–401, 2008.

[99] W. Zhang, M. S. Dillingham, C. D. Thomas, S. Allen, C. J. Roberts, and P. Soultanas, "Directional loading and stimulation of PcrA helicase by the replication initiator protein RepD," *Journal of Molecular Biology*, vol. 371, no. 2, pp. 336–348, 2007.

[100] R. D. Shereda, D. A. Bernstein, and J. L. Keck, "A central role for SSB in Escherichia coli RecQ DNA helicase function," *Journal of Biological Chemistry*, vol. 282, no. 26, pp. 19247–19258, 2007.

[101] S. W. Matson and A. B. Robertson, "The UvrD helicase and its modulation by the mismatch repair protein MutL," *Nucleic Acids Research*, vol. 34, no. 15, pp. 4089–4097, 2006.

[102] R. Roy, A. G. Kozlov, T. M. Lohman, and T. Ha, "SSB protein diffusion on single-stranded DNA stimulates RecA filament formation," *Nature*, vol. 461, pp. 1092–1097, 2009.

Hindawi Publishing Corporation
BioMed Research International
Volume 2014, Article ID 573936, 16 pages
http://dx.doi.org/10.1155/2014/573936

Research Article

C-Terminal Domain Swapping of SSB Changes the Size of the ssDNA Binding Site

Yen-Hua Huang[1] and Cheng-Yang Huang[1,2]

[1] *School of Biomedical Sciences, Chung Shan Medical University, No.110, Sec.1, Chien-Kuo N. Rd., Taichung City, Taiwan*
[2] *Department of Medical Research, Chung Shan Medical University Hospital, No.110, Sec.1, Chien-Kuo N. Rd., Taichung City, Taiwan*

Correspondence should be addressed to Cheng-Yang Huang; cyhuang@csmu.edu.tw

Received 26 May 2014; Accepted 9 July 2014; Published 4 August 2014

Academic Editor: Huangen Ding

Single-stranded DNA-binding protein (SSB) plays an important role in DNA metabolism, including DNA replication, repair, and recombination, and is therefore essential for cell survival. Bacterial SSB consists of an N-terminal ssDNA-binding/oligomerization domain and a flexible C-terminal protein-protein interaction domain. We characterized the ssDNA-binding properties of *Klebsiella pneumoniae* SSB (KpSSB), *Salmonella enterica* Serovar Typhimurium LT2 SSB (StSSB), *Pseudomonas aeruginosa* PAO1 SSB (PaSSB), and two chimeric KpSSB proteins, namely, KpSSBnStSSBc and KpSSBnPaSSBc. The C-terminal domain of StSSB or PaSSB was exchanged with that of KpSSB through protein chimeragenesis. By using the electrophoretic mobility shift assay, we characterized the stoichiometry of KpSSB, StSSB, PaSSB, KpSSBnStSSBc, and KpSSBnPaSSBc, complexed with a series of ssDNA homopolymers. The binding site sizes were determined to be 26 ± 2, 21 ± 2, 29 ± 2, 21 ± 2, and 29 ± 2 nucleotides (nt), respectively. Comparison of the binding site sizes of KpSSB, KpSSBnStSSBc, and KpSSBnPaSSBc showed that the C-terminal domain swapping of SSB changes the size of the binding site. Our observations suggest that not only the conserved N-terminal domain but also the C-terminal domain of SSB is an important determinant for ssDNA binding.

1. Introduction

Single-stranded DNA-binding protein (SSB) specifically binds to single-stranded DNA (ssDNA) and is known to have important functions in the DNA metabolic processes, such as DNA replication, repair, and recombination of both prokaryotes and eukaryotes [1–4]. During these reactions, SSB binds to and protects susceptible ssDNA from nucleolytic digestion and chemical attacks and also prevents secondary structure formation [5]. Many but not all bacterial and human mitochondrial SSBs are active as homotetramers [5–7], in which four oligonucleotide/oligosaccharide-binding folds (OB folds) form a DNA-binding domain [8–12]. However, SSB from the bacterial phylum Deinococcus-Thermus functions as a homodimer, in which each monomer contains two OB folds linked by a conserved spacer sequence [13–20]. SSB from *Sulfolobus solfataricus* is a monomer that includes one OB fold, which differentiates SSB from the bacterial form, and is likely to be a more ancestral "simple" SSB [21–25]. The DdrB protein from *Deinococcus radiodurans* is an alternative SSB and functions as a pentamer [26]. Recent studies found that a distinct SSB from hyperthermophilic Crenarchaea, termed ThermoDBP, has ssDNA-binding domains that are markedly different from the classical OB folds of bacterial SSB [27, 28].

Bacterial SSBs consist of two domains, namely, an N-terminal ssDNA-binding/oligomerization domain and a flexible C-terminal protein-protein interaction domain without a defined tertiary structure [3, 29]. Tyrosine phosphorylation of SSB increases binding to ssDNA by almost 200-fold in vitro [30, 31]. The N-terminal domain is separated from the highly conserved acidic tail of the last 10 C-terminal amino acid residues of SSB by a long proline- or glycine-rich hinge [3, 32]. SSB interacts with other auxiliary proteins that are essential for cell survival [33]. The C-terminal acidic tail of SSB, such as "DDDIPF," has been shown to bind to more than a dozen different proteins and the activity of some of these proteins is stimulated by their interactions with ssDNA-bound SSB [3].

The binding of SSB to ssDNA makes the glycine-rich region more easily accessible to other proteins such as proteases and DNA polymerase III [33, 34]. The C-terminus in SSB can also interact with the OB fold and regulate the ssDNA-binding activity of SSB itself [35, 36].

Studies on SSB from different organisms have grown rapidly during the past few years and knowledge on how SSBs interact with ssDNA has increased [22, 32, 37–46]. The most thoroughly studied SSB is that of *Escherichia coli* (EcSSB), which binds cooperatively to ssDNA [47]. The estimated binding site size of EcSSB is dependent on the salt concentration in fluorescence titrations with poly(dT) [47]. EcSSB mainly binds to 35- and 65-nucleotide- (nt) long ssDNA via the $(SSB)_{35}$- and $(SSB)_{65}$-binding modes, respectively. In the $(SSB)_{35}$-binding mode, two subunits of the EcSSB tetramer interact with ssDNA, whereas in the $(SSB)_{65}$-binding mode all four subunits participate in ssDNA binding. These different binding modes may be required during different stages of DNA metabolism for the in vivo function of SSB [48–50]. Although SSB binds to ssDNA via the highly conserved ssDNA-binding domain, the reason that the binding site sizes of SSBs from different organisms differ remains unclear. For example, differences are found among the binding site sizes of *Methanococcus jannaschii* SSB [51], the Gonococcal Genetic Island-encoded SSB from *Neisseria gonorrhoeae* [39], the thermostable *Thermotoga maritima* and *Thermotoga neapolitana* SSBs [32], and the psychrophilic bacterial SSBs [37]. In addition, the $(SSB)_{35}$- and $(SSB)_{65}$-binding modes are not found in some SSBs [32, 39, 42].

Previously, we have examined the electrophoretic mobility shift patterns of a His-tagged *Klebsiella pneumoniae* SSB (KpSSB) [40], a His-tagged *Salmonella enterica* serovar Typhimurium LT2 SSB (StSSB) [43], and a His-tagged *Pseudomonas aeruginosa* PAO1 SSB (PaSSB) [42] bound to different lengths of ssDNA. We also determined their corresponding binding site sizes, that is, 26, 22, and 29 nt per tetramer, respectively. The electrophoretic mobility shift assay (EMSA) is a well-established approach in studies of molecular biology [52], and the use of radioactive tracer in this assay allows visualization of the actual formation of the distinct protein-DNA complex(es)[53]. The expected result of EMSA is that when the length of the nucleotides is sufficient for the binding of two or more SSB molecules, the electrophoretic mobility of the higher SSB oligomer complex will be lower than that of the smaller SSB oligomer complex [52, 54]. Recent studies on SSB binding also reveal that determination of the ssDNA-binding site size by using EMSA is significantly consistent with that of the cocrystal structure of SSB with ssDNA [27].

KpSSB, StSSB, and PaSSB are similar proteins whose N-terminal ssDNA-binding domains are almost identical, except for different ssDNA-binding site sizes [40, 42, 43]. Thus, we should assess whether the glycine-rich hinge, which is not conserved among SSBs, is involved in the determination of the binding site size of SSB. In this study, we swapped the C-terminal domains of StSSB and PaSSB into that of KpSSB through protein chimeragenesis. Chimeras are proteins that contain segments from two or more different parent proteins and serve as valuable tools to understand enzyme mechanism and protein function [55]. The EMSA behavior (patterns) of the resultant chimeric proteins, namely, KpSSBnStSSBc and KpSSBnPaSSBc, was characterized and compared with untagged KpSSB, StSSB, and PaSSB (Figure 1). On the basis of the chimeragenesis results, the flexible C-terminal domain of SSB was found to be involved in determining the ssDNA-binding site sizes.

2. Materials and Methods

2.1. Materials. All restriction enzymes and DNA-modifying enzymes were purchased from New England Biolabs (Ipswich, MA, USA) unless explicitly stated otherwise. All chemicals were purchased from Sigma-Aldrich (St. Louis, MO, USA) unless explicitly stated otherwise. The *E. coli* strains TOP10F′ (Invitrogen, USA) and BL21(DE3)pLysS (Novagen, UK) were used for genetic construction and protein expression, respectively.

2.2. Construction of Plasmids for KpSSB, StSSB, and PaSSB Expression. The KpSSB [40], StSSB [43], and PaSSB [42] expression plasmids were constructed by the protocols described previously, with minor modification, to avoid having a His tag fused with the gene product. A fragment containing the coding sequence of KpSSB (*KPN04446*), StSSB (*STM4256*), and PaSSB (*PA4232*) (with the stop codon) was directly amplified by PCR by using the genomic DNA of *K. pneumoniae* subsp. *pneumoniae* MGH 78578, *S. enterica* serovar Typhimurium LT2, or *P. aeruginosa* PAO1 (Primers 1 to 6, resp.). During the process, NdeI and XhoI restriction sites were introduced at the 5′-end and the 3′-end of these genes, after which they were ligated into the pET21b vector (Novagen Inc., Madison, WI, USA) for protein expression in *E. coli* BL21. The expected gene product expressed by these plasmids does not contain any artificial residue, including a His tag. Primers used for construction of these plasmids are summarized in Table 1.

2.3. Construction of Plasmids for KpSSBnStSSBc and KpSSBnPaSSBc Expression through Protein Chimeragenesis. To investigate the effect of the C-terminal domain of SSB on the size of the ssDNA-binding site, the C-terminal domain of KpSSB was replaced by that of StSSB and PaSSB. pET21b-KpSSB (Primers 7 and 8), pET21b-StSSB (Primers 9 and 10), and pET21b-PaSSB (Primers 11 and 12) vectors were mutated to create a desired SacI site and to obtain the vectors for expression of the chimeric proteins KpSSBnStSSBc and KpSSBnPaSSBc. The D91E/Q92L-engineered pET21b-KpSSB vector, the D91E/Q92L-engineered pET21b-StSSB vector, and the G90E/Q91L-engineered pET21b-PaSSB vector were cut at NdeI and SacI sites. Subsequently, the KpSSBn, StSSBc-pET21b, and PaSSBc-pET21b fragments were purified. KpSSBn was ligated with StSSBc-pET21b and PaSSBc-pET21b fragments to generate the engineered pET21b-KpSSBnStSSBc and pET21b-KpSSBnPaSSBc vectors. To avoid artificial residues, positions 91 and 92 of the two plasmids were mutated back (Primers 13 to 16) to obtain pET21b-KpSSBnStSSBc and pET21b-KpSSBnPaSSBc vectors.

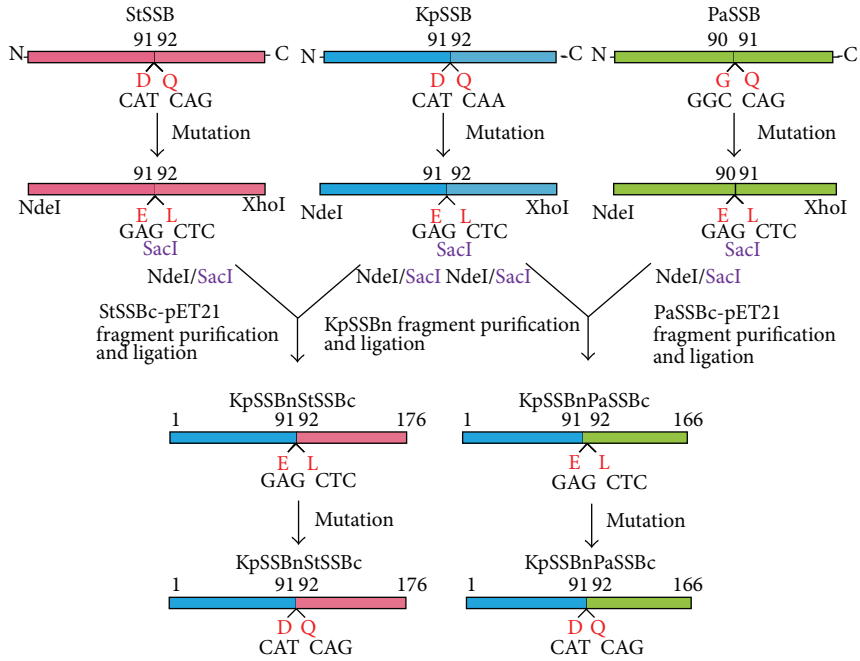

Figure 1: Construction of plasmids for expression of the chimeric KpSSBnStSSBc and KpSSBnPaSSBc proteins. To investigate the effect of the C-terminal domain of SSB on the size of the ssDNA-binding site, the C-terminal domain of KpSSB was replaced by that of StSSB and PaSSB. pET21b-KpSSB (Primers 7 and 8), pET21b-StSSB (Primers 9 and 10), and pET21b-PaSSB (Primers 11 and 12) vectors were mutated to create a desired SacI site and to obtain the vectors for expression of the chimeric proteins KpSSBnStSSBc and KpSSBnPaSSBc. The D91E/Q92L-engineered pET21b-KpSSB vector, the D91E/Q92L-engineered pET21b-StSSB vector, and the G90E/Q91L-engineered pET21b-PaSSB vector were cut at NdeI and SacI sites. Subsequently, the KpSSBn, StSSBc-pET21b, and PaSSBc-pET21b fragments were purified. KpSSBn was ligated with StSSBc-pET21b and PaSSBc-pET21b fragments to generate the engineered pET21b-KpSSBnStSSBc and pET21b-KpSSBnPaSSBc vectors. To avoid artificial residues, positions 91 and 92 of the two plasmids were mutated back (Primers 13 to 16) to obtain pET21b-KpSSBnStSSBc and pET21b-KpSSBnPaSSBc vectors. Thus, pET21b-KpSSBnStSSBc and pET21b-KpSSBnPaSSBc will express KpSSB1-91 fused StSSB92-176 and PaSSB91-165, respectively. Note that KpSSBnPaSSBc will have 166 amino acid residues.

Thus, pET21b-KpSSBnStSSBc and pET21b-KpSSBnPaSSBc will express KpSSB1-91 fused StSSB92-176 and PaSSB91-165, respectively. Note that KpSSBnPaSSBc will have 166 amino acid residues. Plasmids were verified by DNA sequencing. Underlined nucleotides indicate the designated site for mutation or the restriction site (Table 1).

2.4. Protein Expression and Purification. The recombinant SSBs were expressed using the protocol described previously [9, 40, 42, 43, 56–60]. Purification of these recombinant SSBs was carried out as described previously with the following modifications [61, 62]. Briefly, *E. coli* BL21(DE3) cells were individually transformed with the expression vector and grown to OD_{600} of 0.9 at 37°C in Luria-Bertani medium containing 250 μg/mL ampicillin with rapid shaking. Overexpression of the expression plasmids was induced by incubating with 1 mM isopropyl thiogalactoside (IPTG) for 3 h at 37°C. The cells overexpressing the protein were chilled on ice, harvested by centrifugation, resuspended in Buffer A (20 mM Tris-HCl, 5 mM imidazole, and 0.2 M ammonium sulfate, pH 7.9), and disrupted by sonication with ice cooling. The protein solution (50 mL) was precipitated from the supernatant of the cell lysate by incubation with 0.27 g/mL of ammonium sulfate for 30 min and centrifugation at 20000 g for 10 min. The pellets were washed twice with 2.0 mL of Buffer B (20 mM Tris-HCl, 5 mM imidazole, and 1.2 M ammonium sulfate, pH 7.9). After dialysis against Buffer C (20 mM Tris-HCl, 5 mM imidazole, 1 mM EDTA, and 100 mM NaCl, pH 7.9), the protein solution applied to the Q column (GE Healthcare Bio-Sciences, Piscataway, NJ, USA) was eluted with a linear NaCl gradient from 0.1 to 0.6 M with Buffer C using the AKTA-FPLC system (GE Healthcare Bio-Sciences, Piscataway, NJ, USA). The peak fractions with the ssDNA-binding activity were collected and dialyzed against Buffer D (20 mM potassium phosphate, 1 mM EDTA, and 100 mM NaCl, pH 7.0). The protein solution was then applied to the Heparin HP column (GE Healthcare Bio-Sciences, Piscataway, NJ, USA) and eluted with a linear NaCl gradient from 0.1 to 1.0 M with Buffer D. The peak fractions from this chromatographic step with the ssDNA-binding activity were collected and concentrated, and the purity of these SSBs was checked by Coomassie-stained SDS-PAGE (Mini-PROTEAN Tetra System, Bio-Rad, CA, USA; Figure 3).

2.5. Protein Concentration. The protein concentration of the solutions was determined by the Bio-Rad Protein Assay using bovine serum albumin as a standard (Bio-Rad, CA, USA). The Bio-Rad Protein Assay is a dye-binding assay in which a differential color change of a dye occurs in response to various concentrations of protein.

Table 1: Primers used for construction of plasmids.

Oligonucleotide	Primer
1 KpSSB-NdeI-N	GGGCATATGGCCAGCAGAGGCGTAAAC
2 KpSSB-XhoI-C	GGGCTCGAGTTAGAACGGGATGTCGTC
3 StSSB-NdeI-N	CTGAACATATGGCCAGCAGAGGCGTAA
4 StSSB-XhoI-C	TGGAACTCGAGTTAGAACGGAATGTCG
5 PaSSB-NdeI-N	TTGCTCATATGGCCCGTGGGGTTAACA
6 PaSSB-XhoI-C	TTGCACTCGAGTTAGAACGGAATGTCG
7 KpSSB(D91E/Q92L-SacI)-N	AAGTGGACCGAGCTCTCCGGTCAGGACA
8 KpSSB(D91E/Q92L-SacI)-C	GTCCTGACCGGAGAGCTCGGTCCACTT
9 StSSB(D91E/Q92L-SacI)-N	AAGTGGACCGAGCTCAGTGGCCAGGAA
10 StSSB(D91E/Q92L-SacI)-C	TTCCTGGCCACTGAGCTCGGTCCACTT
11 PaSSB(G90E/Q91L-SacI)-N	AAGTGGCAGGAGCTCGACGGTCAGGAT
12 PaSSB(G90E/Q91L-SacI)-C	ATCCTGACCGTCGAGCTCCTGCCACTT
13 KpSSBnStSSBc(E91D/L92Q)-N	AAGTGGACCGATCAGAGTGGCCAGGAA
14 KpSSBnStSSBc(E91D/L92Q)-C	TTCCTGGCCACTCTGATCGGTCCACTT
15 KpSSBnPaSSBc(E91D/L92Q)-N	AAGTGGACCGATCAGGACGGTCAGGAT
16 KpSSBnPaSSBc(E91D/L92Q)-C	ATCCTGACCGTCCTGATCGGTCCACTT

A fragment containing the coding sequence of KpSSB, StSSB, and PaSSB (with the stop codon) was cloned into the pET21b vector (using Primers 1–6). During the process, NdeI and XhoI restriction sites were introduced at the 5′-end and the 3′-end of these genes, after which they were ligated into the pET21b vector. To obtain the vectors for expression of the chimeric proteins KpSSBnStSSBc and KpSSBnPaSSBc, pET21b-KpSSB (Primers 7 and 8), pET21b-StSSB (Primers 9 and 10), and pET21b-PaSSB (Primers 11 and 12) vectors were mutated to create a desired SacI site. The D91E/Q92L-engineered pET21b-KpSSB vector, the D91E/Q92L-engineered pET21b-StSSB vector, and the G90E/Q91L-engineered pET21b-PaSSB vector were cut at NdeI and SacI sites. Subsequently, the KpSSBn, StSSBc-pET21b, and PaSSBc-pET21b fragments were purified. KpSSBn was ligated with StSSBc-pET21b and PaSSBc-pET21b fragments to generate the engineered pET21b-KpSSBnStSSBc and pET21b-KpSSBnPaSSBc vectors. To avoid artificial residues, positions 91 and 92 of the two plasmids were mutated back (Primers 13 to 16) to obtain pET21b-KpSSBnStSSBc and pET21b-KpSSBnPaSSBc vectors. Thus, pET21b-KpSSBnStSSBc and pET21b-KpSSBnPaSSBc will express KpSSB1-91 fused StSSB92-176 and PaSSB91-165, respectively. These plasmids were verified by DNA sequencing. Underlined nucleotides indicate the designated site for mutation or the restriction site.

2.6. Gel-Filtration Chromatography. Gel-filtration chromatography was carried out by the AKTA-FPLC system (GE Healthcare Bio-Sciences, Piscataway, NJ, USA). Briefly, purified protein (2 mg/mL) was applied to a Superdex 200 HR 10/30 column (GE Healthcare Bio-Sciences, Piscataway, NJ, USA) equilibrated with Buffer D. The column was operated at a flow rate of 0.5 mL/min, and 0.5 mL fractions were collected. The proteins were detected by measuring the absorbance at 280 nm. The column was calibrated with proteins of known molecular weight: thyroglobulin (670 kDa), γ-globulin (158 kDa), ovalbumin (44 kDa), and myoglobin (17 kDa). The K_{av} values for the standard proteins and the SSB variants were calculated from the equation: $K_{av} = (V_e - V_o)/(V_c - V_o)$, where V_o is column void volume, V_e is elution volume, and V_c is geometric column volume.

2.7. Electrophoretic Mobility Shift Assay (EMSA). EMSA [52] for these SSBs was carried out by the protocol described previously for DnaB [63], PriB [59, 64–66], DnaT [57, 67], and SSB proteins [40, 42, 43, 52]. Briefly, radiolabeling of various lengths of ssDNA oligonucleotides was carried out with [γ^{32}P]ATP (6000 Ci/mmol; PerkinElmer Life Sciences, Waltham, MA) and T4 polynucleotide kinase (Promega, Madison, WI, USA). The protein (0, 19, 37, 77, 155, 310, 630, 1250, 2500, and 5000 nM) was incubated for 30 min at 25°C with 1.7 nM DNA substrates (dT15–65) in a total volume of 10 μL in 20 mM Tris-HCl pH 8.0 and 100 mM NaCl. Aliquots (5 μL) were removed from each of the reaction solutions and added to 2 μL of gel-loading solution (0.25% bromophenol blue and 40% sucrose). The resulting samples were resolved on a native 8% polyacrylamide gel at 4°C in TBE buffer (89 mM Tris borate and 1 mM EDTA) for 1 h at 100 V and were visualized by autoradiography. Complexed and free DNA bands were scanned and quantified.

2.8. DNA-Binding Ability. The ssDNA-binding ability ($[\text{Protein}]_{50}$; $K_{d,\text{app}}$) for the protein was estimated from the protein concentration that binds 50% of the input ssDNA [52]. Each $[\text{Protein}]_{50}$ is calculated as the average of three measurements ± SD.

2.9. Bioinformatics. Sequence alignment of KpSSB, StSSB, and PaSSB was generated by CLUSTALW2 [68]. The structure of the C-terminal domain of these SSBs was modeled by $(\text{PS})^2$ (http://140.113.239.111/~ps2v2/docs.php/). The structures were visualized by using the program PyMol.

3. Results

3.1. Sequence Analysis. Based on the nucleotide sequence found, using a database search through the National Center for Biotechnology Information (NCBI), we predicted that KpSSB, StSSB, and PaSSB monomer proteins have lengths of 174, 176, and 165 amino acid residues, respectively. The size of the ssDNA-binding site of His-tagged KpSSB [40], StSSB

FIGURE 2: Multiple amino acid sequence alignment of SSB proteins. Sequence alignment of KpSSB, StSSB, and PaSSB was generated by CLUSTALW2. Identical amino acid residues are colored in red. Gly and Gln residues are shaded in cyan and gray. The N-terminal domains of these SSBs are significantly conserved.

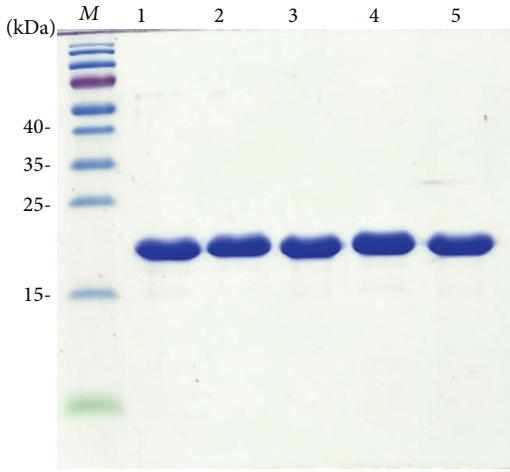

FIGURE 3: Protein purity. Coomassie Blue-stained SDS-PAGE (15%) of the purified KpSSB (lane 1), StSSB (lane 2), PaSSB (lane 3), KpSSBnStSSBc (lane 4), KpSSBnPaSSBc (lane 5), and molecular mass standards (*M*) are shown. The sizes of the standard proteins, from the top down, are as follows: 55, 40, 35, 25, 15, and 10 kDa. The purified SSBs migrated between the 25 and 15 kDa standards on the SDS-PAGE.

[43], and PaSSB [42] was determined to be 26 ± 1, 22 ± 1, and 29 ± 1 nt, respectively. The longer the length of the polypeptide chain, the smaller the size for ssDNA binding. Analysis of the primary structures of KpSSB, StSSB, and PaSSB by RPS-BLAST revealed the presence of a putative OB-fold domain that is common to all known SSBs. Figure 2 shows that the alignments of the amino acid sequences of KpSSB, StSSB, and PaSSB amino acid residues in their N-terminal domains are highly conserved (colored in red). In the *E. coli* SSB-ssDNA complex [11], four essential aromatic residues, namely, Trp40, Trp54, Phe60, and Trp88, participate in ssDNA binding via stacking interactions [11]. These residues are conserved in most SSB families, including KpSSB, StSSB, and PaSSB. The important motif in the C-terminal tail of *E. coli* SSB, DDDIPF residues, is also conserved in KpSSB, StSSB, and PaSSB. By contrast to those motifs, the residues found in the glycine-rich hinge of *E. coli* SSB are not conserved in KpSSB, StSSB, and PaSSB (Figure 2). Thus, the length and composition of the amino acid residues in the glycine-rich hinge may be responsible for the different ssDNA-binding site sizes of SSBs.

3.2. Expression and Purification of KpSSB, StSSB, and PaSSB. The N-terminal ssDNA-binding domain of SSB has been well-established to be highly conserved. However, SSBs possessing different ssDNA-binding site sizes have been reported. The reason that SSBs have similar ssDNA-binding domains but possess varying ssDNA-binding site sizes remains unclear. Although the ssDNA-binding site sizes of KpSSB, StSSB, and PaSSB have been reported, we reinvestigated the ssDNA-binding properties of KpSSB, StSSB, and PaSSB in the absence of a His tag to avoid the unknown effect of a His tag (hexahistidine) on the ssDNA binding of SSB.

3.3. KpSSB Bound to ssDNA. To investigate the length of nucleotides sufficient for the formation of the KpSSB-ssDNA complex and the ssDNA-binding ability of KpSSB, we studied the binding of KpSSB to dT20 (Figure 4(a)), dT25 (Figure 4(b)), dT35 (Figure 4(c)), dT45 (Figure 4(d)), dT50 (Figure 4(e)), dT55 (Figure 4(f)), and dT60 (Figure 4(g)) with different protein concentrations. As shown in Figure 4(a), no band shift was observed when KpSSB was incubated with dT20, indicating that KpSSB could not form a stable complex with this homopolymer. By contrast to dT20, longer dT homopolymers, which include dT25–50, produced a significant band shift (C, complex), that is, formation of a stable protein-DNA complex in solution. Furthermore, two different complexes for dT55 were formed by KpSSB (Figure 4(f)). At lower protein concentrations, KpSSB formed a single complex (C1) with dT55, similar to that observed with dT50 (Figure 4(e)). However, when the KpSSB concentration was increased, another slower migrating complex (C2) was observed.

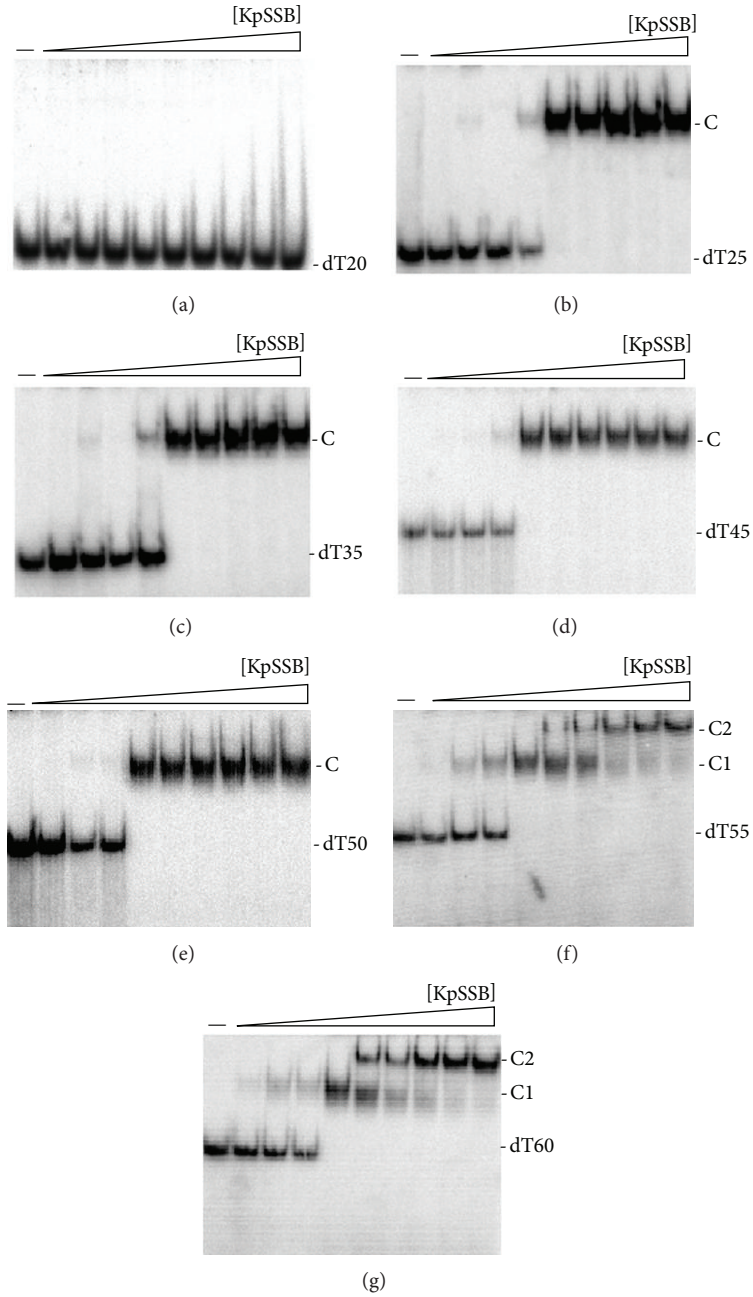

Figure 4: Binding of KpSSB to dT20–60. KpSSB (0, 19, 37, 77, 155, 310, 630, 1250, 2500, and 5000 nM) was incubated for 30 min at 25°C with 1.7 nM of (a) dT20, (b) dT25, (c) dT35, (d) dT45, (e) dT50, (f) dT55, or (g) dT60 in a total volume of 10 μL in 20 mM Tris-HCl pH 8.0 and 100 mM NaCl. Aliquots (5 μL) were removed from each reaction solution and added to 2 μL of gel-loading solution (0.25% bromophenol blue and 40% sucrose). The resulting samples were resolved on a native 8% polyacrylamide gel at 4°C in TBE buffer (89 mM Tris borate and 1 mM EDTA) for 1 h at 100 V and visualized by autoradiography. Complexed and free DNA bands were scanned and quantified.

Two different complexes of KpSSB were also observed to bind to dT60 (Figure 4(g)). The appearance of the second complex resulted from the increased KpSSB concentration, suggesting that two KpSSB proteins may be present per oligonucleotide. Although dT55 is only 5 nt longer than dT50 is, the presence of an extra 5 nt in dT55 compared with that of dT50 provides enough interaction space for the binding of two KpSSB proteins. Therefore, one KpSSB occupies 25 (50/2 = 25) nt to 27.5 (55/2 = 27.5) nt of the ssDNA. The EMSA results suggest that the length of an ssDNA (or the binding site size) [52] required for KpSSB binding is 26 ± 2 nt.

3.4. StSSB Bound to ssDNA. The binding of StSSB to dT15 (Figure 5(a)), dT20 (Figure 5(b)), dT30 (Figure 5(c)), dT40 (Figure 5(d)), dT45 (Figure 5(e)), and dT50 (Figure 5(f)) was

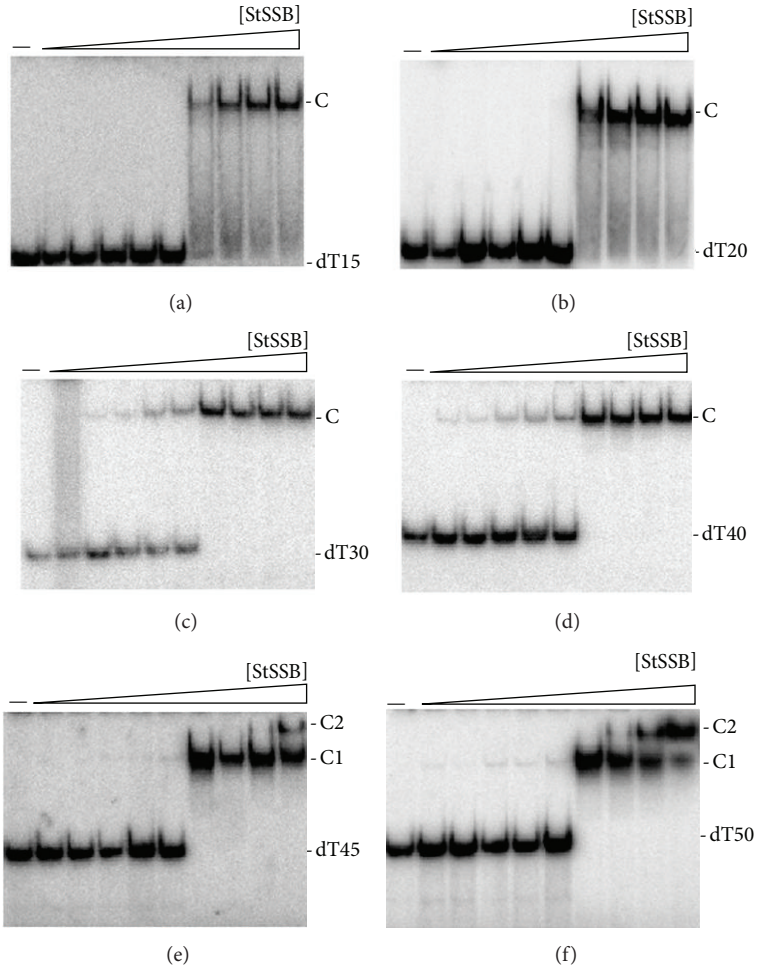

Figure 5: Binding of StSSB to dT15–50. StSSB (0, 19, 37, 77, 155, 310, 630, 1250, 2500, and 5000 nM) was incubated for 30 min at 25°C with 1.7 nM of (a) dT15, (b) dT20, (c) dT30, (d) dT40, (e) dT45, or (f) dT50 in a total volume of 10 μL in 20 mM Tris-HCl pH 8.0 and 100 mM NaCl. Aliquots (5 μL) were removed from each reaction solution and added to 2 μL of gel-loading solution (0.25% bromophenol blue and 40% sucrose). The resulting samples were resolved on a native 8% polyacrylamide gel at 4°C in TBE buffer (89 mM Tris borate and 1 mM EDTA) for 1 h at 100 V and visualized by autoradiography. Complexed and free DNA bands were scanned and quantified.

examined using EMSA. StSSB can bind and form a single complex with dT15 (Figure 5(a)) and dT20 (Figure 5(b)), but KpSSB cannot (Figure 4(a)). StSSB bound to dT15–40 and formed a single complex. For dT45 and dT50, two different complexes of StSSB appeared at high protein concentrations (Figures 5(e) and 5(f)). Therefore, one StSSB occupies 20 (40/2 = 20) nt to 22.5 (45/2 = 22.5) nt of the ssDNA. The EMSA results suggest that the length of an ssDNA (or the binding site size) [52] required for StSSB binding is 21 ± 2 nt.

3.5. PaSSB Bound to ssDNA. The binding of PaSSB to dT20 (Figure 6(a)), dT25 (Figure 6(b)), dT35 (Figure 6(c)), dT45 (Figure 6(d)), dT55 (Figure 6(e)), dT60 (Figure 6(f)), and dT65 (Figure 6(g)) was studied by EMSA. Unlike StSSB, no complex was observed when PaSSB was incubated with dT20. Some smears were observed, indicating that PaSSB interacts with dT20. However, the ssDNA may be too short to be fully wrapped by PaSSB. PaSSB could form a single complex with dT25–55 and form two distinct complexes with dT60 and dT65 (Figures 6(f) and 6(g)), respectively. Therefore, one PaSSB occupies 27.5 (55/2 = 27.5) nt to 30 (60/2 = 30) nt of the ssDNA. These results from EMSA suggest that the length of an ssDNA (or the binding site size) [52] required for PaSSB binding is 29 ± 2 nt. Although the SSBs, that is, KpSSB, StSSB, and PaSSB, have significantly similar ssDNA-binding domains, their binding site sizes are different and range from 19 (21 ± 2; StSSB) to 31 (29 ± 2; PaSSB) nt. The obtained EMSA results (Figures 4–6) also show that the binding site sizes of the untagged SSBs (KpSSB, StSSB, and PaSSB) were found to be almost identical to those of the His-tagged ones [40, 42, 43].

3.6. Design of the Chimeric KpSSB Proteins KpSSBnStSSBc and KpSSBnPaSSBc. The N-terminal ssDNA-binding domain of KpSSB, StSSB, and PaSSB is highly conserved (Figure 2), but their binding site sizes are different (Figures 4–6) and range from 19 nt to 31 nt. The C-terminal acidic tails, DDDIPF, are conserved (Figure 2), and these features led us to assess

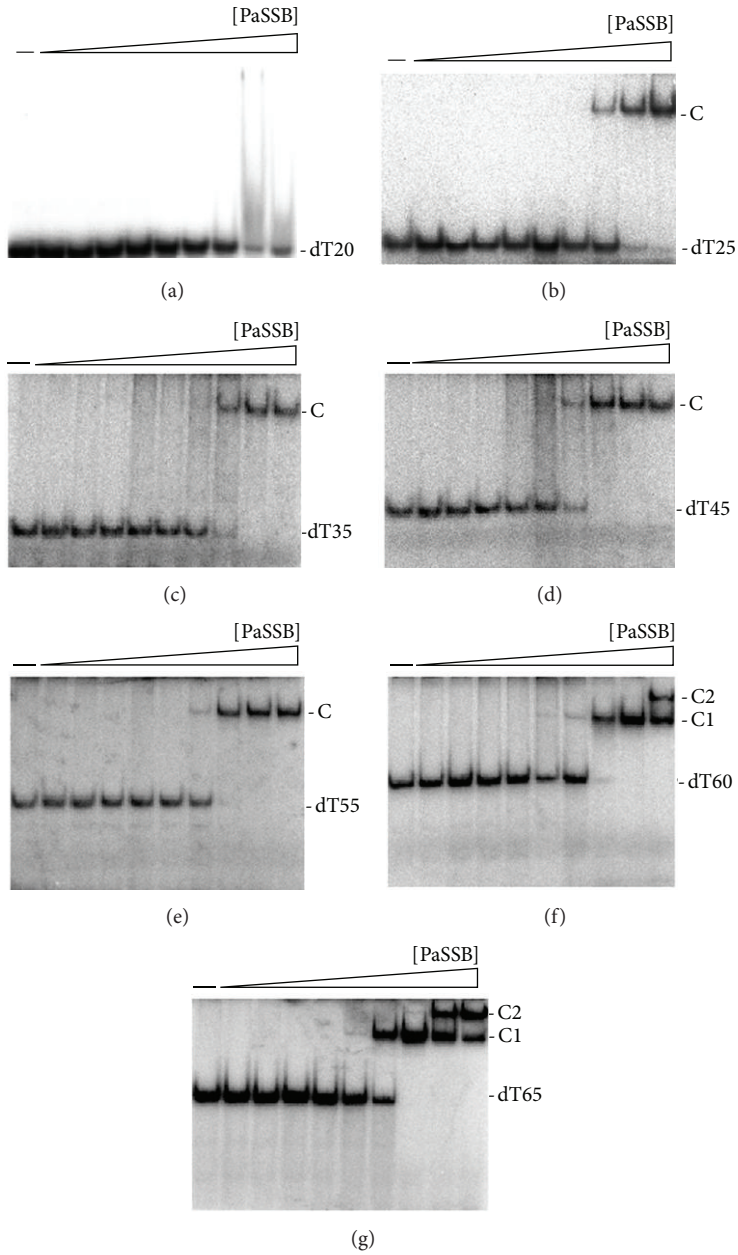

Figure 6: Binding of PaSSB to dT20–65. PaSSB (0, 19, 37, 77, 155, 310, 630, 1250, 2500, and 5000 nM) was incubated for 30 min at 25°C with 1.7 nM of (a) dT20, (b) dT25, (c) dT35, (d) dT45, (e) dT55, (f) dT60, or (g) dT65 in a total volume of 10 μL in 20 mM Tris-HCl pH 8.0 and 100 mM NaCl. Aliquots (5 μL) were removed from each reaction solution and added to 2 μL of gel-loading solution (0.25% bromophenol blue and 40% sucrose). The resulting samples were resolved on a native 8% polyacrylamide gel at 4°C in TBE buffer (89 mM Tris borate and 1 mM EDTA) for 1 h at 100 V and visualized by autoradiography. Complexed and free DNA bands were scanned and quantified.

whether the flexible glycine-rich hinge in the C-terminal domain, which is not conserved among SSBs, is involved in the determination of the binding site size of SSB. Thus, the C-terminal domains of StSSB and PaSSB were swapped with KpSSB through protein chimeragenesis.

3.7. KpSSBnStSSBc Bound to ssDNA. The binding of KpSSBnStSSBc to dT15 (Figure 7(a)), dT20 (Figure 7(b)), dT40 (Figure 7(c)), and dT45 (Figure 7(d)) was examined using EMSA. KpSSBnStSSBc exhibited significantly different ssDNA-binding properties from those of KpSSB. Unlike KpSSB (Figure 4), both KpSSBnStSSBc (Figure 8) and StSSB (Figure 5) can bind and form a single complex with dT15 and dT20. Similar to StSSB, KpSSBnStSSBc binds to dT15–40 and forms a single complex. For dT45, two different complexes of KpSSBnStSSBc appeared at high protein concentrations (Figure 8(d)); this EMSA feature was also similar to that of StSSB. One KpSSBnStSSBc occupies 20 (40/2 = 20) nt to 22.5 (45/2 = 22.5) nt of the ssDNA. These EMSA results suggest that the length of an ssDNA (or the binding site

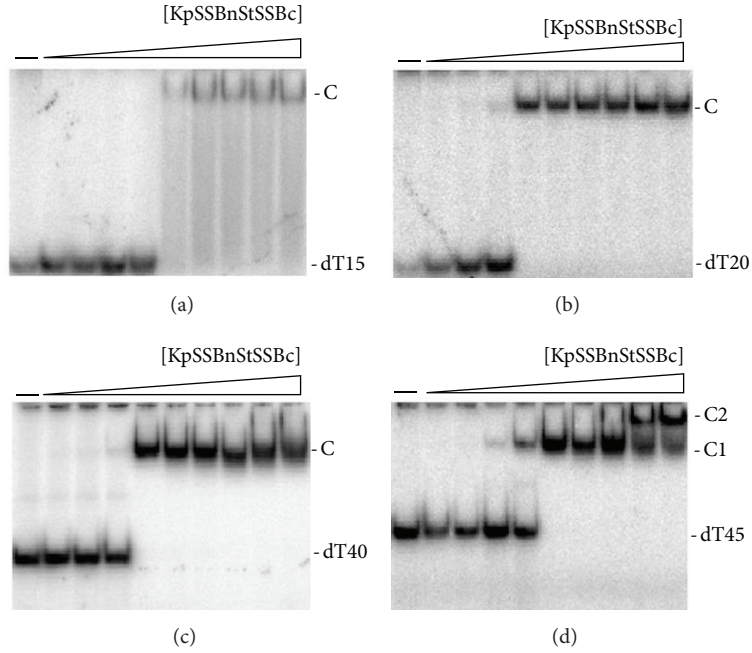

Figure 7: Binding of KpSSBnStSSBc to dT15–45. KpSSBnStSSBc (0, 19, 37, 77, 155, 310, 630, 1250, 2500, and 5000 nM) was incubated for 30 min at 25°C with 1.7 nM of (a) dT15, (b) dT20, (c) dT40, or (d) dT45 in a total volume of 10 μL in 20 mM Tris-HCl pH 8.0 and 100 mM NaCl. Aliquots (5 μL) were removed from each reaction solution and added to 2 μL of gel-loading solution (0.25% bromophenol blue and 40% sucrose). The resulting samples were resolved on a native 8% polyacrylamide gel at 4°C in TBE buffer (89 mM Tris borate and 1 mM EDTA) for 1 h at 100 V and visualized by autoradiography. Complexed and free DNA bands were scanned and quantified.

size) [52] required for KpSSBnStSSBc binding is 21 ± 2 nt, a value identical to that for StSSB (Figure 5). Swapping of the C-terminal domain of StSSB with KpSSB changes the size of the ssDNA-binding site from 26 nt to 21 nt.

3.8. KpSSBnPaSSBc Bound to ssDNA. The binding features of KpSSBnPaSSBc with dT20 (Figure 8(a)), dT25 (Figure 8(b)), dT40 (Figure 8(c)), dT55 (Figure 8(d)), and dT60 (Figure 8(e)) were studied by EMSA. Similar to the cases of KpSSB and PaSSB, no complex was observed when KpSSBnPaSSBc was incubated with dT20. However, KpSSBnPaSSBc still exhibited dramatically different ssDNA-binding properties from those of KpSSB. KpSSB can form two distinct complexes with dT55 (Figure 4(f)), but both KpSSBnPaSSBc (Figure 9) and PaSSB (Figure 6) cannot. One KpSSBnPaSSBc occupies 27.5 (55/2 = 27.5) nt to 30 (60/2 = 30) nt of the ssDNA. The above EMSA results suggest that the length of an ssDNA (or the binding site size) [52] required for KpSSBnPaSSBc binding is 29 ± 2 nt, a value identical to that of PaSSB. Swapping of the C-terminal domain of PaSSB to KpSSB changes the size of the ssDNA-binding site from 26 nt to 29 nt. Although these SSBs, namely, KpSSB, StSSB, PaSSB, KpSSBnStSSBc, and KpSSBnPaSSBc, have nearly identical ssDNA-binding domains, their binding site sizes are different (Table 2). Thus, the size of the ssDNA-binding site required for second SSB binding is likely to be dependent on the C-terminal domain of SSB.

3.9. Binding Constants of the SSB-ssDNA Complexes Determined from EMSA. To compare the ssDNA-binding abilities of KpSSB, StSSB, PaSSB, KpSSBnStSSBc, and KpSSBnPaSSBc, the midpoint values for input ssDNA binding, calculated from the titration curves of EMSA and referred to as $[\text{Protein}]_{50}$ (monomer), were quantified and are summarized in Table 2. Although the N-terminal ssDNA-binding domains of these SSB proteins are highly similar (Figure 2), their ssDNA-binding activities and binding site sizes are different (Table 2). $[\text{KpSSB}]_{50}$ values ranged from 100 nM to 220 nM; $[\text{StSSB}]_{50}$ values ranged from 420 nM to 650 nM; $[\text{PaSSB}]_{50}$ values ranged from 550 nM to 1700 nM; $[\text{KpSSBnStSSBc}]_{50}$ values ranged from 110 nM to 260 nM; and $[\text{KpSSBnPaSSBc}]_{50}$ values ranged from 220 nM to 390 nM. The ssDNA-binding ability is as follows, in the order of decreasing affinity: KpSSB > KpSSBnStSSBc > KpSSBnPaSSBc > StSSB > PaSSB. Results from the above analyses indicate that the exchange of the C-terminal domain in SSB significantly changed the ssDNA-binding ability and the DNA-binding behavior (complex number). The reason as to why swapping of the C-terminal domain can affect the ssDNA-binding activity of SSB remains unclear. The C-terminal domain of SSB is suggested to be involved in ssDNA binding. However, this relation is not evident in the results of the cocrystal structure.

3.10. Oligomeric State of KpSSBnStSSBc and KpSSBnPaSSBc in Solution. Gel-filtration chromatography was used to confirm

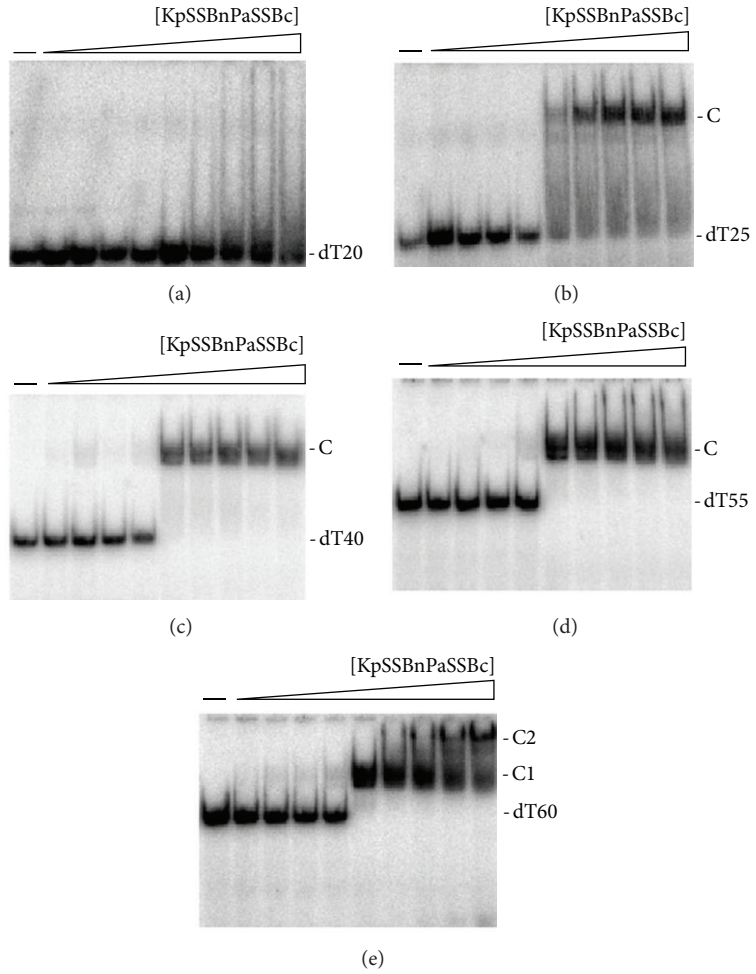

Figure 8: Binding of KpSSBnPaSSBc to dT20–60. KpSSBnPaSSBc (0, 19, 37, 77, 155, 310, 630, 1250, 2500, and 5000 nM) was incubated for 30 min at 25°C with 1.7 nM of (a) dT20, (b) dT25, (c) dT40, (d) dT55, or (e) dT60 in a total volume of 10 μL in 20 mM Tris-HCl pH 8.0 and 100 mM NaCl. Aliquots (5 μL) were removed from each reaction solution and added to 2 μL of gel-loading solution (0.25% bromophenol blue and 40% sucrose). The resulting samples were resolved on a native 8% polyacrylamide gel at 4°C in TBE buffer (89 mM Tris borate and 1 mM EDTA) for 1 h at 100 V and visualized by autoradiography. Complexed and free DNA bands were scanned and quantified.

that the oligomeric state of KpSSBnStSSBc and KpSSBnPaSSBc remains as tetramers after chimeragenesis. The analysis of purified KpSSBnStSSBc and KpSSBnPaSSBc (2 mg/mL) using a Superdex 200 HR 10/30 column revealed a single peak with elution volumes of 78.6 and 78.9 mL, respectively. Assuming that KpSSBnStSSBc and KpSSBnPaSSBc both have shapes and partial specific volumes similar to the standard proteins, the native molecular masses of KpSSBnStSSBc and KpSSBnPaSSBc were estimated to be 76641 and 74827 Da, as calculated from a standard linear regression equation, $K_{av} = -0.3684(\log Mw) + 2.2707$ (Figure 9). The native molecular masses for KpSSBnStSSBc and KpSSBnPaSSBc are approximately four times the mass of the monomer (~19 kDa). Therefore, KpSSBnStSSBc and KpSSBnPaSSBc under the above chromatographic conditions are stable tetramers in solution. Although the exchange of the C-terminal domain in SSB significantly changed the ssDNA-binding ability and DNA-binding behavior (complex number), protein chimeragenesis did not cause any change in the oligomeric state of SSB.

3.11. Summary of Gly, Gln, and Pro Number in SSBs. To analyze the C-terminal amino acid composition of SSBs, we further counted the number of Gly, Gln, and Pro residues in different SSB segments. SSB is abundant in Gly, Gln, and Pro (GQP) (Table 3). The GQP contents of KpSSB1–91, StSSB1–91, and PaSSB1–90 are similar. However, the Gly number of PaSSB116–165 is significantly lower than that of KpSSB116–174 and StSSB117–176; PaSSB116–165 contains only 1 Gly, but KpSSB116–174 and StSSB117–176 contain 11 and 12 Gly, respectively. In addition, we found different distribution patterns among KpSSB, StSSB, and PaSSB. Although they contain similar number of Gln (Q), the QQQ pattern is frequently found in PaSSB (Table 3).

3.12. Structural Modeling of SSBs. Given its disordered C-terminal domain, the crystal structure of the full-length SSB is lacking, even when SSB can be crystallized with DNA [69]. We attempted to model the structure by homology modeling using the bioinformatics program $(PS)^2$ to obtain an

Table 2: ssDNA binding properties of KpSSB, StSSB, PaSSB, KpSSBnStSSBc, and KpSSBnPaSSBc as analyzed by EMSA.

Protein	DNA	$[\text{Protein}]_{50}$ (nM)	Complex number
KpSSB	dT20	ND	0
	dT25	200 ± 20	1
	dT35	220 ± 30	1
	dT45	100 ± 10	1
	dT50	110 ± 20	1
	dT55	100 ± 20	2
	dT60	100 ± 10	2
StSSB	dT15	650 ± 120	1
	dT20	450 ± 80	1
	dT30	420 ± 60	1
	dT40	420 ± 80	1
	dT45	440 ± 60	2
	dT50	440 ± 50	2
PaSSB	dT20	ND	0
	dT25	1700 ± 250	1
	dT35	950 ± 180	1
	dT45	780 ± 160	1
	dT55	820 ± 90	1
	dT60	810 ± 110	2
	dT65	550 ± 70	2
KpSSBnStSSBc	dT15	260 ± 60	1
	dT20	110 ± 20	1
	dT40	120 ± 20	1
	dT45	160 ± 20	2
KpSSBnPaSSBc	dT20	ND	0
	dT25	390 ± 60	1
	dT40	220 ± 30	1
	dT55	230 ± 30	1
	dT60	230 ± 30	2

$[\text{Protein}]_{50}$ was calculated from the titration curves of EMSA by determining the concentration of the protein (μM) needed to achieve the midpoint value for input ssDNA binding. For some oligonucleotides, input ssDNA binding was the sum of the intensities from the two separate ssDNA-protein complexes. Errors are standard deviations determined by three independent titration experiments.

Table 3: Summary of Gly, Gln, and Pro number in SSB.

SSB segment	G	Q	P
KpSSB1–91	10	5	2
StSSB1–91	10	5	2
PaSSB1–90	11	6	2
KpSSB92–174	18	16	9
StSSB92–176	17	18	11
PaSSB91–165	5	15	11
KpSSB116–174	11	12	9
StSSB117–176	12	13	10
PaSSB116–165	1	12	11

in-depth understanding of the structure-function relationship of the C-terminal domains of these SSBs [70, 71].

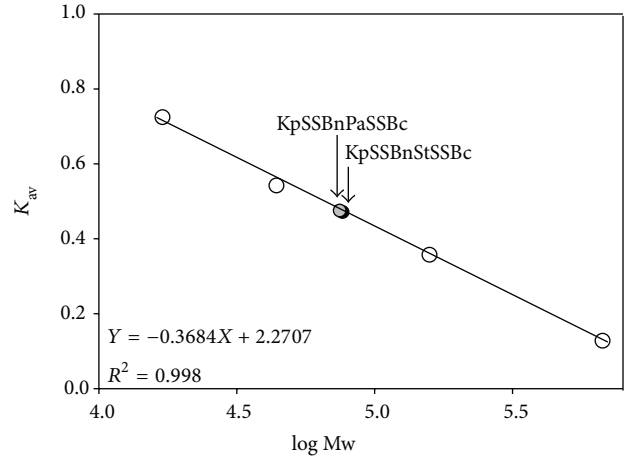

Figure 9: Gel-filtration chromatographic analyses of KpSSBnStSSBc and KpSSBnPaSSBc. Purified protein (2 mg/mL) was applied to a Superdex 200 HR 10/30 column (GE Healthcare Bio-Sciences, Piscataway, NJ, USA) equilibrated with Buffer D. The column was operated at a flow rate of 0.5 mL/min, and 0.5 mL fractions were collected. The proteins were detected by measuring the absorbance at 280 nm. The column was calibrated with proteins of known molecular weight: thyroglobulin (670 kDa), γ-globulin (158 kDa), ovalbumin (44 kDa), and myoglobin (17 kDa). The K_{av} values for the standard proteins and the SSB variants were calculated from the equation: $K_{av} = (V_e - V_o)/(V_c - V_o)$, where V_o is column void volume, V_e is elution volume, and V_c is geometric column volume.

$(\text{PS})^2$ (http://140.113.239.111/~ps2v2/docs.php/) is an automatic homology modeling server that combines both sequence and secondary structure information to detect the homologous proteins with remote similarity and the target-template alignment. After pasting the amino acid sequence to the website of $(\text{PS})^2$, only one hit (Protein Data Bank entry: 1QVC; EcSSB) for the C-terminal domains of KpSSB and StSSB was suggested. For the C-terminal domain of PaSSB, only one hit, that is, CstF-77 (Protein Data Bank entry: 2OOE; cleavage stimulation factor, CstF), but not EcSSB, was suggested as the template for modeling. Figure 10 shows that modeled structures of these SSB C-terminal domains are highly disordered but that of PaSSB is more ordered than that of other domains.

4. Discussion

In this study, we examined the sizes of the binding site of the untagged SSB and the chimeric SSB from the ubiquitous opportunistic pathogens *K. pneumoniae*, *S. enterica* serovar Typhimurium LT2, and *P. aeruginosa* PAO1. Many clinical strains of the abovementioned bacteria are highly resistant to antibiotics [72–75]. The development of clinically useful small-molecule antibiotics has been a seminal event in the field of infectious diseases [48]. Nucleic acid metabolism is one of the most basic biological functions and should be a prime target in antibiotic development [76–78]. Many bacterial SSBs form conserved protein interaction "hubs" that are essential to recruit many proteins involved in DNA

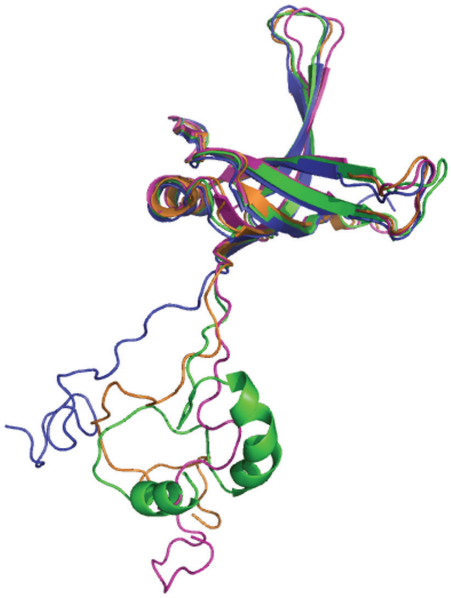

Figure 10: Structure modeling of SSB. The structures of KpSSB1–115, StSSB1–115, and PaSSB1–115 (the N-terminal domain of SSB) were modeled by SWISS-MODEL. The structures of KpSSB116–142, StSSB116–142, and PaSSB121–160 (the C-terminal domain of SSB) were modeled by $(PS)^2$. Other regions of SSBs could not be modeled by these two programs. The structures of the N-terminal domain and the C-terminal domain of these SSBs were manually linked (KpSSB1–142, blue; StSSB1–142, pink; PaSSB1–160, green) and superimposed with the crystal structure of EcSSB1–142 (orange) (PDB entry: 1QVC) for comparison. For clarity, only one subunit of the tetramer was shown for each SSB.

replication, recombination, and repair SSB/DNA nucleoprotein substrates [79]. Thus, SSBs may be promising targets in antibiotic development [80]. As a first step toward achieving this goal, we investigated why SSBs possess highly conserved N-terminal ssDNA-binding domain but exhibit varying binding site sizes. One significant clue is that their flexible hinges and the length at the C-terminus are different as revealed by sequence alignment (Figure 2).

The interactions of various SSBs with ssDNA have been analyzed using a variety of techniques such as tryptophan-fluorescence quenching [47], filter binding [81], EMSA [52, 82], analytical ultracentrifugation [83], electron microscopy [84], nuclease digestion [44], single-molecule fluorescence microscopy [48], and crystallographic analyses [11]. In this study, we have examined the electrophoretic mobility shift patterns of KpSSB, StSSB, PaSSB, KpSSBnStSSBc, and KpSSBnPaSSBc bound to different lengths of ssDNA and determined the corresponding binding site sizes to be 26, 21, 29, 22, and 29 nt per tetramer, respectively (Figures 4–8). PaSSB and KpSSBnPaSSBc have the largest sizes for ssDNA binding among the SSBs studied. We also identified His-tagged and untagged SSBs that have similar ssDNA-binding site sizes [40, 42, 43]. EMSA is a well-established approach in studies of molecular biology [52], and the use of radioactive tracer in this assay allows detection of the actual formation of the distinct protein-DNA complex(es) [53]. For example, DNase protection assay and footprinting assay using radioactive tracer can determine the specific DNA sequence complexed by a protein. In EMSA, when the length of the nucleotides is sufficient for the binding of two or more SSB molecules, the electrophoretic mobility of the higher SSB oligomer complex will be lower than that of the smaller SSB oligomer complex [52, 54]. In addition, results of the ssDNA-binding site size from EMSA and cocrystal structure of SSB were consistent [27]. Thus, throughout this paper, we determined the ssDNA-binding site sizes of SSB from the EMSA behavior.

Many SSBs bind to ssDNA with some degree of positive cooperativity. Cooperativity can result from direct protein-protein interactions between the nearest neighbors, such as the LAST motif in the T4 gene-32 protein [85] and the arginine-mediated interaction motif in *Thermus* SSB [86, 87]. Cooperativity can also result from the protein-induced distortion of adjacent DNA, as demonstrated in *Sulfolobus* SSB, PriB, and FOXK1a proteins [23, 60, 88]. In the cases of KpSSB, StSSB, and PaSSB (Figures 4–6), binding appeared to be nearly noncooperative for several DNAs because all DNA mainly shifts into the first complex (C1) before the appearance of the second complex (C2) when subjected to increasing protein concentrations. The length dependence of the $[SSB]_{50}$ values suggests that the amount of spacing is optimum for steric considerations (Table 2).

Because bacteria have varying genomic DNA sizes, their SSBs may need to evolve to have different binding site sizes for DNA metabolism. Results from protein chimeragenesis showed the C-terminal domain dependence of the binding site sizes of SSB (Figure 11). The experimental data showed that the binding site size of KpSSBnStSSBc was similar to that of StSSB and the size of the binding site of KpSSBnPaSSBc was similar to that of PaSSB. The reason for which the binding site size of SSB changed, followed by swapping of the C-terminal domain, remains unclear. Flexibility, number of glycine residues, and/or different QQQ patterns of the C-terminal domain of SSB (Figure 2 and Table 3) may be important factors for determining the ssDNA-binding site size. In fact, the C-terminal domain of PaSSB, that is, PaSSB116–165, has only 1 Gly residue, which is significantly less than that of KpSSB (11 Gly) and StSSB (12 Gly). Gly (and Pro) is an important component of the flexible region; a protein that contains low Gly content is predicted to have low flexibility. Unlike typical SSB [35, 69], PaSSB116–165 has a partial structure (Figure 10). Although KpSSB, StSSB, and PaSSB contain similar number of Gln (Q), the QQQ pattern is frequently found in PaSSB (Figure 2 and Table 3). PolyQ and repeated sequences GAGAG are commonly found in the structures of amyloids, silk fibers, and neurodegradation proteins [89–92]. Considering that the simple coil polyQ, the heptapeptide GNNQQNY, and the hexapeptide NNQQNY can cause protein aggregation and nucleation [93–95], the distribution of Gln in the C-terminal domain of a tetrameric SSB may also be an important determinant of the ssDNA-binding site size of SSB by some steric hindrances (Figure 11). However, the above speculation must be confirmed by further biochemical experiments.

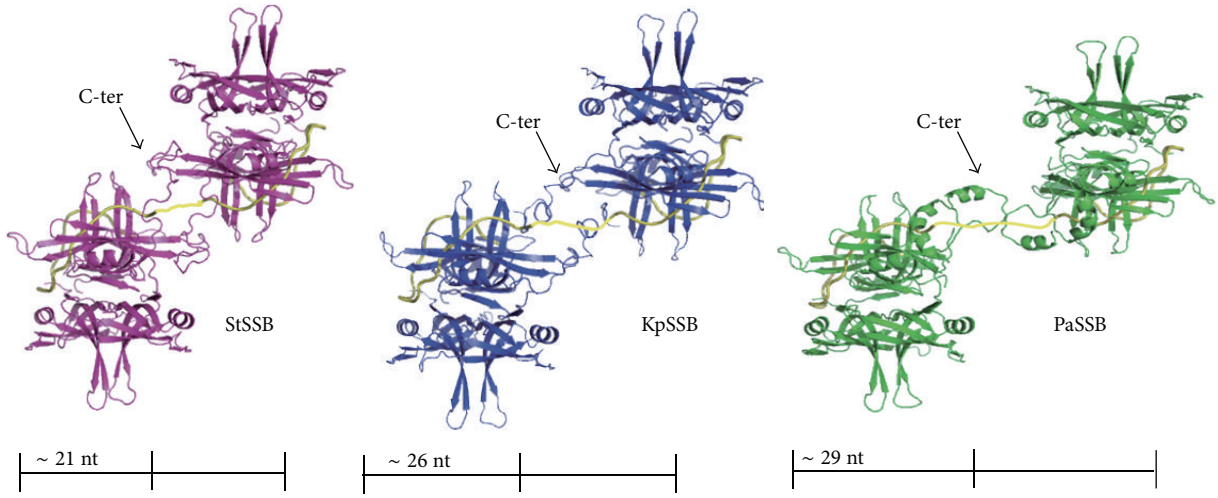

Figure 11: Possible models for explaining why SSBs are with different binding site sizes. Two modeled structures of KpSSB1–142 (blue), StSSB1–142 (pink), and PaSSB1–160 (green) complexed with ssDNA (gold) are shown. For clarity, only one C-terminal domain was shown for each SSB tetramer. By using the electrophoretic mobility shift assay and the protein chimeragenesis, we characterized that the binding site sizes of KpSSB, StSSB, PaSSB, KpSSBnStSSBc, and KpSSBnPaSSBc were 26, 21, 29, 21, and 29 nt per tetramer, respectively. KpSSB, StSSB, and PaSSB are similar proteins whose N-terminal ssDNA-binding domains are almost identical. Thus, the C-terminal domain of SSB may indirectly contribute to ssDNA binding and wrapping and affects the binding site size by the steric hindrance.

5. Conclusion

In this study, we characterized the ssDNA-binding properties of untagged SSBs from *K. pneumoniae*, *S. enterica* serovar Typhimurium LT2, and *P. aeruginosa* PAO1 and proposed a role of the C-terminal flexible domain for ssDNA binding from the protein chimeragenesis and EMSA results. The amino acid sequence of the N-terminal ssDNA-binding/oligomerization domain in these pathogenic SSBs is highly conserved, but their apparent binding site sizes are different. This finding indicates that the C-terminal protein-protein interaction domain may also indirectly contribute to ssDNA binding and wrapping.

Conflict of Interests

The authors declare that there is no conflict of interests regarding the publication of this paper.

Acknowledgment

This research was supported by a Grant from the National Science Council, Taiwan (NSC 102-2320-B-040-019 to Cheng-Yang Huang).

References

[1] R. Reyes-Lamothe, D. J. Sherratt, and M. C. Leake, "Stoichiometry and architecture of active DNA replication machinery in escherichia coli," *Science*, vol. 328, no. 5977, pp. 498–501, 2010.

[2] D. J. Richard, E. Bolderson, and K. K. Khanna, "Multiple human single-stranded DNA binding proteins function in genome maintenance: structural, biochemical and functional analysis," *Critical Reviews in Biochemistry and Molecular Biology*, vol. 44, no. 2-3, pp. 98–116, 2009.

[3] R. D. Shereda, A. G. Kozlov, T. M. Lohman, M. M. Cox, and J. L. Keck, "SSB as an organizer/mobilizer of genome maintenance complexes," *Critical Reviews in Biochemistry and Molecular Biology*, vol. 43, no. 5, pp. 289–318, 2008.

[4] D. J. Richard, E. Bolderson, L. Cubeddu et al., "Single-stranded DNA-binding protein hSSB1 is critical for genomic stability," *Nature*, vol. 453, no. 7195, pp. 677–681, 2008.

[5] R. R. Meyer and P. S. Laine, "The single-stranded DNA-binding protein of Escherichia coli," *Microbiological Reviews*, vol. 54, no. 4, pp. 342–380, 1990.

[6] C. Yang, U. Curth, C. Urbanke, and C. Kang, "Crystal structure of human mitochondrial single-stranded DNA binding protein at 2.4 Å resolution," *Nature Structural Biology*, vol. 4, no. 2, pp. 153–157, 1997.

[7] G. Webster, J. Genschel, U. Curth, C. Urbanke, C. Kang, and R. Hilgenfeld, "A common core for binding single-stranded DNA: structural comparison of the single-stranded DNA-binding proteins (SSB) from E. coli and human mitochondria," *FEBS Letters*, vol. 411, pp. 313–316, 1997.

[8] R. L. Flynn and L. Zou, "Oligonucleotide/oligosaccharide-binding fold proteins: a growing family of genome guardians," *Critical Reviews in Biochemistry and Molecular Biology*, vol. 45, no. 4, pp. 266–275, 2010.

[9] K. Chan, Y. Lee, C. Wang, H. Huang, and Y. Sun, "Single-Stranded DNA-Binding Protein Complex from Helicobacter pylori Suggests an ssDNA-Binding Surface," *Journal of Molecular Biology*, vol. 388, no. 3, pp. 508–519, 2009.

[10] D. L. Theobald, R. M. Mitton-Fry, and D. S. Wuttke, "Nucleic acid recognition by OB-fold proteins," *Annual Review of Biophysics and Biomolecular Structure*, vol. 32, pp. 115–133, 2003.

[11] S. Raghunathan, A. G. Kozlov, T. M. Lohman, and G. Waksman, "Structure of the DNA binding domain of *E. coli* SSB bound to

ssDNA," *Nature Structural Biology*, vol. 7, no. 8, pp. 648–652, 2000.

[12] A. G. Murzin, "OB(oligonucleotide/oligosaccharide binding)-fold: common structural and functional solution for non-homologous sequences," *EMBO Journal*, vol. 12, no. 3, pp. 861–867, 1993.

[13] N. P. George, K. V. Ngo, S. Chitteni-Pattu et al., "Structure and cellular dynamics of deinococcus radiodurans single-stranded DNA (ssDNA)-binding protein (SSB)-DNA complexes," *The Journal of Biological Chemistry*, vol. 287, no. 26, pp. 22123–22132, 2012.

[14] P. Filipkowski and J. Kur, "Identification and properties of the Deinococcus grandis and Deinococcus proteolyticus single-stranded DNA binding proteins (SSB)," *Acta Biochimica Polonica*, vol. 54, no. 1, pp. 79–87, 2007.

[15] P. Filipkowski, A. Duraj-Thatte, and J. Kur, "Identification, cloning, expression, and characterization of a highly thermostable single-stranded-DNA-binding protein (SSB) from *Deinococcus murrayi*," *Protein Expression and Purification*, vol. 53, no. 1, pp. 201–208, 2007.

[16] P. Filipkowski, M. Koziatek, and J. Kur, "A highly thermostable, homodimeric single-stranded DNA-binding protein from Deinococcus radiopugnans," *Extremophiles*, vol. 10, no. 6, pp. 607–614, 2006.

[17] P. Filipkowski, A. Duraj-Thatte, and J. Kur, "Novel thermostable single-stranded DNA-binding protein (SSB) from Deinococcus geothermalis," *Archives of Microbiology*, vol. 186, no. 2, pp. 129–137, 2006.

[18] G. Witte, C. Urbanke, and U. Curth, "Single-stranded DNA-binding protein of Deinococcus radiodurans: a biophysical characterization," *Nucleic Acids Research*, vol. 33, no. 5, pp. 1662–1670, 2005.

[19] D. A. Bernstein, J. M. Eggingtont, M. P. Killoran, A. M. Misic, M. M. Cox, and J. L. Keck, "Crystal structure of the Deinococcus radiodurans single-stranded DNA-binding protein suggests a mechanism for coping with DNA damage," *Proceedings of the National Academy of Sciences of the United States of America*, vol. 101, no. 23, pp. 8575–8580, 2004.

[20] S. Dabrowski, M. Olszewski, R. Piatek, A. Brillowska-Dabrowska, G. Konopa, and J. Kur, "Identification and characterization of single-stranded-DNA-binding proteins from Thermus thermophilus and Thermus aquaticus—new arrangement of binding domains," *Microbiology*, vol. 148, no. 10, pp. 3307–3315, 2002.

[21] R. Gamsjaeger, R. Kariawasam, C. Touma, A. H. Kwan, M. F. White, and L. Cubeddu, "Backbone and side-chain ^{1}H, ^{13}C and ^{15}N resonance assignments of the OB domain of the single stranded DNA binding protein from *Sulfolobus solfataricus* and chemical shift mapping of the DNA-binding interface," *Biomolecular NMR Assignments*, 2013.

[22] M. L. Rolfsmeier and C. A. Haseltine, "The single-stranded DNA binding protein of Sulfolobus solfataricus acts in the presynaptic step of homologous recombination," *Journal of Molecular Biology*, vol. 397, no. 1, pp. 31–45, 2010.

[23] I. D. Kerr, R. I. M. Wadsworth, L. Cubeddu, W. Blankenfeldt, J. H. Naismith, and M. F. White, "Insights into ssDNA recognition by the OB fold from a structural and thermodynamic study of Sulfolobus SSB protein," *EMBO Journal*, vol. 22, no. 11, pp. 2561–2570, 2003.

[24] C. A. Haseltine and S. C. Kowalczykowski, "A distinctive single-stranded DNA-binding protein from the Archaeon Sulfolobus solfataricus," *Molecular Microbiology*, vol. 43, no. 6, pp. 1505–1515, 2002.

[25] R. I. M. Wadsworth and M. F. White, "Identification and properties of the crenarchaeal single-stranded DNA binding protein from Sulfolobus solfataricus," *Nucleic Acids Research*, vol. 29, no. 4, pp. 914–920, 2001.

[26] S. Sugiman-Marangos and M. S. Junop, "The structure of DdrB from *Deinococcus*: a new fold for single-stranded DNA binding proteins," *Nucleic Acids Research*, vol. 38, no. 10, Article ID gkq036, pp. 3432–3440, 2010.

[27] H. Ghalei, H. V. Moeller, D. Eppers et al., "Entrapment of DNA in an intersubunit tunnel system of a single-stranded DNA-binding protein," *Nucleic Acids Research*, vol. 42, no. 10, pp. 6698–6708, 2014.

[28] S. Paytubi, S. A. McMahon, S. Graham et al., "Displacement of the canonical single-stranded DNA-binding protein in the thermoproteales," *Proceedings of the National Academy of Sciences of the United States of America*, vol. 109, no. 7, pp. E398–E405, 2012.

[29] T. H. Dickey, S. E. Altschuler, and D. S. Wuttke, "Single-stranded DNA-binding proteins: multiple domains for multiple functions," *Structure*, vol. 21, no. 7, pp. 1074–1084, 2013.

[30] D. Vujaklija and B. Macek, "Detecting posttranslational modifications of bacterial SSB proteins," *Methods in Molecular Biology*, vol. 922, pp. 205–218, 2012.

[31] I. Mijakovic, D. Petranovic, B. Macek et al., "Bacterial single-stranded DNA-binding proteins are phosphorylated on tyrosine," *Nucleic Acids Research*, vol. 34, no. 5, pp. 1588–1596, 2006.

[32] M. Olszewski, A. Grot, M. Wojciechowski, M. Nowak, M. Mickiewicz, and J. Kur, "Characterization of exceptionally thermostable single-stranded DNA-binding proteins from Thermotoga maritima and Thermotoga neapolitana," *BMC Microbiology*, vol. 10, article 260, 2010.

[33] U. Curth, J. Genschel, C. Urbanke, and J. Greipel, "In vitro and in vivo function of the C-terminus of Escherichia coil single-stranded DNA binding protein," *Nucleic Acids Research*, vol. 24, no. 14, pp. 2706–2711, 1996.

[34] G. Witte, C. Urbanke, and U. Curth, "DNA polymerase III chi subunit ties single-stranded DNA binding protein to the bacterial replication machinery," *Nucleic Acids Research*, vol. 31, pp. 4434–4440, 2003.

[35] D. Shishmarev, Y. Wang, C. E. Mason et al., "Otting, Intramolecular binding mode of the C-terminus of Escherichia coli single-stranded DNA binding protein determined by nuclear magnetic resonance spectroscopy," *Nucleic Acids Research*, vol. 42, pp. 2750–2757, 2014.

[36] A. G. Kozlov, M. M. Cox, and T. M. Lohman, "Regulation of single-stranded DNA binding by the C termini of Escherichia coli single-stranded DNA-binding (SSB) protein," *Journal of Biological Chemistry*, vol. 285, no. 22, pp. 17246–17252, 2010.

[37] M. Nowak, M. Olszewski, M. Spibida, and J. Kur, "Characterization of single-stranded DNA-binding proteins from the psychrophilic bacteria *Desulfotalea psychrophila, Flavobacterium psychrophilum, Psychrobacter arcticus, Psychrobacter cryohalolentis, Psychromonas ingrahamii, Psychroflexus torquis, and Photobacterium profundum*," *BMC Microbiology*, vol. 14, article 91, 2014.

[38] T. Paradzik, N. Ivic, Z. Filic et al., "Structure-function relationships of two paralogous single-stranded DNA-binding proteins from Streptomyces coelicolor: implication of SsbB in chromosome segregation during sporulation," *Nucleic Acids Research*, vol. 41, no. 6, pp. 3659–3672, 2013.

[39] S. Jain, M. Zweig, E. Peeters et al., "Characterization of the single stranded DNA binding protein SsbB encoded in the gonoccocal genetic island," *PLoS ONE*, vol. 7, no. 4, Article ID e35285, 2012.

[40] Y. H. Huang and C. Y. Huang, "Characterization of a single-stranded DNA-binding protein from Klebsiella pneumoniae: mutation at either Arg73 or Ser76 causes a less cooperative complex on DNA," *Genes to Cells*, vol. 17, no. 2, pp. 146–157, 2012.

[41] E. Antony, E. A. Weiland, S. Korolev, and T. M. Lohman, "Plasmodium falciparum SSB tetramer wraps single-stranded DNA with similar topology but opposite polarity to E. Coli SSB," *Journal of Molecular Biology*, vol. 420, no. 4-5, pp. 269–283, 2012.

[42] H. Jan, Y. L. Lee, and C. Y. Huang, "Characterization of a single-stranded DNA-binding protein from *pseudomonas aeruginosa* PAO1," *Protein Journal*, vol. 30, no. 1, pp. 20–26, 2011.

[43] Y.-H. Huang, Y.-L. Lee, and C.-Y. Huang, "Characterization of a single-stranded DNA binding protein from *Salmonella enterica* serovar typhimurium LT2," *Protein Journal*, vol. 30, no. 2, pp. 102–108, 2011.

[44] S. K. Bharti, K. Rex, P. Sreedhar, N. Krishnan, and U. Varshney, "Chimeras of *Escherichia coli* and *Mycobacterium tuberculosis* single-stranded DNA binding proteins: characterization and function in *Escherichia coli*," *PLoS ONE*, vol. 6, no. 12, Article ID e27216, 2011.

[45] M. T. Oliveira and L. S. Kaguni, "Functional roles of the N- and C-terminal regions of the human mitochondrial single-stranded DNA-binding protein," *PLoS ONE*, vol. 5, no. 10, Article ID e15379, 2010.

[46] A. G. Kozlov, J. M. Eggington, M. M. Cox, and T. M. Lohman, "Binding of the dimeric Deinococcus radiodurans single-stranded DNA binding protein to single-stranded DNA," *Biochemistry*, vol. 49, no. 38, pp. 8266–8275, 2010.

[47] T. M. Lohman and M. E. Ferrari, "Escherichia coli single-stranded DNA-binding protein: multiple DNA-binding modes and cooperatives," *Annual Review of Biochemistry*, vol. 63, pp. 527–570, 1994.

[48] R. Zhou, A. G. Kozlov, R. Roy et al., "SSB functions as a sliding platform that migrates on DNA via reptation," *Cell*, vol. 146, pp. 222–232, 2011.

[49] R. Roy, A. G. Kozlov, T. M. Lohman, and T. Ha, "SSB protein diffusion on single-stranded DNA stimulates RecA filament formation," *Nature*, vol. 461, pp. 1092–1097, 2009.

[50] R. Roy, A. G. Kozlov, T. M. Lohman, and T. Ha, "Dynamic structural rearrangements between DNA binding modes of E. coli SSB protein," *Journal of Molecular Biology*, vol. 369, no. 5, pp. 1244–1257, 2007.

[51] T. J. Kelly, P. Simancek, and G. S. Brush, "Identification and characterization of a single-stranded DNA-binding protein from the archaeon Methanococcus jannaschii," *Proceedings of the National Academy of Sciences of the United States of America*, vol. 95, no. 25, pp. 14634–14639, 1998.

[52] C. Y. Huang, *Determination of the Binding Site-Size of the Protein-DNA Complex by Use of the Electrophoretic Mobility Shift Assay*, InTech Press, Rijeka, Croatia, 2012.

[53] A. Kornberg, "Ten commandments of enzymology, amended," *Trends in Biochemical Sciences*, vol. 28, no. 10, pp. 515–517, 2003.

[54] W. Zhang, X. Lü, and J. Shen, "EMSA and single-molecule force spectroscopy study of interactions between bacillus subtilis single-stranded DNA-binding protein and single-stranded DNA," *Langmuir*, vol. 27, no. 24, pp. 15008–15015, 2011.

[55] M. Ostermeier and S. J. Benkovic, "Evolution of protein function by domain swapping," *Advances in Protein Chemistry*, vol. 55, pp. 29–77, 2000.

[56] W. F. Peng and C. Y. Huang, "Allantoinase and dihydroorotase binding and inhibition by flavonols and the substrates of cyclic amidohydrolases," *Biochimie*, vol. 101, pp. 113–122, 2014.

[57] Y. H. Huang, M. J. Lin, and C. Y. Huang, "DnaT is a single-stranded DNA binding protein," *Genes to Cells*, vol. 18, no. 11, pp. 1007–1019, 2013.

[58] Y. Y. Ho, Y. H. Huang, and C. Y. Huang, "Chemical rescue of the post-translationally carboxylated lysine mutant of allantoinase and dihydroorotase by metal ions and short-chain carboxylic acids," *Amino Acids*, vol. 44, no. 4, pp. 1181–1191, 2013.

[59] Y. H. Huang, Y. Lo, W. Huang, and C. Y. Huang, "Crystal structure and DNA-binding mode of Klebsiella pneumoniae primosomal PriB protein," *Genes to Cells*, vol. 17, no. 10, pp. 837–849, 2012.

[60] C. Y. Huang, C. Y. Hsu, Y. Sun, H. Wu, and C. Hsiao, "Complexed crystal structure of replication restart primosome protein PriB reveals a novel single-stranded DNA-binding mode," *Nucleic Acids Research*, vol. 34, no. 14, pp. 3878–3886, 2006.

[61] T. Kinebuchi, H. Shindo, H. Nagai, N. Shimamoto, and M. Shimizu, "Functional domains of Escherichia coli single-stranded DNA binding protein as assessed by analyses of the deletion mutants," *Biochemistry*, vol. 36, no. 22, pp. 6732–6738, 1997.

[62] N. Shimamoto, N. Ikushima, H. Utiyama, H. Tachibana, and K. Horie, "Specific and cooperative binding of *E. coli* single-stranded DNA binding protein to mRNA," *Nucleic Acids Research*, vol. 15, no. 13, pp. 5241–5250, 1987.

[63] H. Lin and C. Y. Huang, "Characterization of flavonol inhibition of DnaB helicase: Real-time monitoring, structural modeling, and proposed mechanism," *Journal of Biomedicine and Biotechnology*, vol. 2012, Article ID 735368, 2012.

[64] Y. H. Huang, H. H. Lin, and C. Y. Huang, "A single residue determines the cooperative binding property of a primosomal DNA replication protein, PriB, to single-stranded DNA," *Bioscience, Biotechnology and Biochemistry*, vol. 76, no. 6, pp. 1110–1115, 2012.

[65] H. C. Hsieh and C. Y. Huang, "Identification of a novel protein, PriB, in *Klebsiella pneumoniae*," *Biochemical and Biophysical Research Communications*, vol. 404, no. 1, pp. 546–551, 2011.

[66] J. H. Liu, T. W. Chang, C. Y. Huang et al., "Crystal structure of PriB, a primosomal DNA replication protein of *Escherichia coli*," *The Journal of Biological Chemistry*, vol. 279, no. 48, pp. 50465–50471, 2004.

[67] Y. H. Huang and C. Y. Huang, "The N-terminal domain of DnaT, a primosomal DNA replication protein, is crucial for PriB binding and self-trimerization," *Biochemical and Biophysical Research Communications*, vol. 442, pp. 147–152, 2013.

[68] M. A. Larkin, G. Blackshields, N. P. Brown et al., "Clustal W and Clustal X version 2.0," *Bioinformatics*, vol. 23, no. 21, pp. 2947–2948, 2007.

[69] S. N. Savvides, S. Raghunathan, K. Fütterer, A. G. Kozlov, T. M. Lohman, and G. Waksman, "The C-terminal domain of full-length *E. coli* SSB is disordered even when bound to DNA," *Protein Science*, vol. 13, no. 7, pp. 1942–1947, 2004.

[70] C.-C. Chen, J.-K. Hwang, and J.-M. Yang, "(PS)2-v2: template-based protein structure prediction server," *BMC Bioinformatics*, vol. 10, article 366, 2009.

[71] C. Chen, J. Hwang, and J. Yang, "(PS)2: protein structure prediction server," *Nucleic Acids Research*, vol. 34, pp. W152–W157, 2006.

[72] K. Bush and J. F. Fisher, "Epidemiological expansion, structural studies, and clinical challenges of new β-lactamases from gram-negative bacteria," *Annual Review of Microbiology*, vol. 65, pp. 455–478, 2011.

[73] K. K. Kumarasamy, M. A. Toleman, T. R. Walsh et al., "Emergence of a new antibiotic resistance mechanism in India, Pakistan, and the UK: a molecular, biological, and epidemiological study," *The Lancet Infectious Diseases*, vol. 10, no. 9, pp. 597–602, 2010.

[74] K. Bush and M. J. MacIelag, "New β-lactam antibiotics and β-lactamase inhibitors," *Expert Opinion on Therapeutic Patents*, vol. 20, no. 10, pp. 1277–1293, 2010.

[75] K. Bush, "Alarming β-lactamase-mediated resistance in multidrug-resistant *Enterobacteriaceae*," *Current Opinion in Microbiology*, vol. 13, no. 5, pp. 558–564, 2010.

[76] A. Srivastava, M. Talaue, S. Liu et al., "New target for inhibition of bacterial RNA polymerase: "switch region"," *Current Opinion in Microbiology*, vol. 14, no. 5, pp. 532–543, 2011.

[77] K. Chono, K. Katsumata, T. Kontani et al., "ASP2151, a novel helicase-primase inhibitor, possesses antiviral activity against varicella-zoster virus and herpes simplex virus types 1 and 2," *Journal of Antimicrobial Chemotherapy*, vol. 65, no. 8, pp. 1733–1741, 2010.

[78] M. T. Black and K. Coleman, "New inhibitors of bacterial topoisomerase GyrA/ParC subunits," *Current Opinion in Investigational Drugs*, vol. 10, no. 8, pp. 804–810, 2009.

[79] A. H. Marceau, D. A. Bernstein, B. W. Walsh, W. Shapiro, L. A. Simmons, and J. L. Keck, "Protein interactions in genome maintenance as novel antibacterial targets," *PLoS ONE*, vol. 8, no. 3, Article ID e58765, 2013.

[80] D. Lu, D. A. Bernstein, K. A. Satyshur, and J. L. Keck, "Small-molecule tools for dissecting the roles of SSB/protein interactions in genome maintenance," *Proceedings of the National Academy of Sciences of the United States of America*, vol. 107, no. 2, pp. 633–638, 2010.

[81] I. Wong and T. M. Lohman, "A double-filter method for nitrocellulose-filter binding: application to protein-nucleic acid interactions," *Proceedings of the National Academy of Sciences of the United States of America*, vol. 90, no. 12, pp. 5428–5432, 1993.

[82] M. Mitas, J. Y. Chock, and M. Christy, "The binding-site sizes of Escherichia coli single-stranded-DNA-binding protein and mammalian replication protein A are 65 and $\geq$ 54 nucleotides respectively," *Biochemical Journal*, vol. 324, no. 3, pp. 957–961, 1997.

[83] C. Urbanke, G. Witte, and U. Curth, "Sedimentation velocity method in the analytical ultracentrifuge for the study of protein-protein interactions," *Methods in Molecular Biology*, vol. 305, pp. 101–114, 2005.

[84] S. Chrysogelos and J. Griffith, "Escherichia coli single-strand binding protein organizes single-stranded DNA in nucleosome-like units," *Proceedings of the National Academy of Sciences of the United States of America*, vol. 79, no. 19, pp. 5803–5807, 1982.

[85] J. R. Casas-Finet, K. R. Fischer, and R. L. Karpel, "Structural basis for the nucleic acid binding cooperativity of bacteriophage T4 gene 32 protein: the (Lys/Arg)3(Ser/Thr)2 (LAST) motif," *Proceedings of the National Academy of Sciences of the United States of America*, vol. 89, pp. 1050–1054, 1992.

[86] G. Witte, R. Fedorov, and U. Curth, "Biophysical analysis of *Thermus aquaticus* single-stranded DNA binding protein," *Biophysical Journal*, vol. 94, no. 6, pp. 2269–2279, 2008.

[87] R. Fedorov, G. Witte, C. Urbanke, D. J. Manstein, and U. Curth, "3D structure of Thermus aquaticus single-stranded DNA-binding protein gives insight into the functioning of SSB proteins," *Nucleic Acids Research*, vol. 34, no. 22, pp. 6708–6717, 2006.

[88] K. L. Tsai, C. Y. Huang, C. H. Chang, Y. J. Sun, W. J. Chuang, and C. D. Hsiao, "Crystal structure of the human FOXK1a-DNA complex and its implications on the diverse binding specificity of winged helix/forkhead proteins," *Journal of Biological Chemistry*, vol. 281, no. 25, pp. 17400–17409, 2006.

[89] A. H. Mao, N. Lyle, and R. V. Pappu, "Describing sequence-ensemble relationships for intrinsically disordered proteins," *Biochemical Journal*, vol. 449, no. 2, pp. 307–318, 2013.

[90] R. Wetzel, "Physical chemistry of polyglutamine: Intriguing tales of a monotonous sequence," *Journal of Molecular Biology*, vol. 421, no. 4-5, pp. 466–490, 2012.

[91] H. T. Orr, "Polyglutamine neurodegeneration: expanded glutamines enhance native functions," *Current Opinion in Genetics and Development*, vol. 22, no. 3, pp. 251–255, 2012.

[92] M. Figiel, W. J. Szlachcic, P. M. Switonski, A. Gabka, and W. J. Krzyzosiak, "Mouse models of polyglutamine diseases: review and data table. Part I," *Molecular Neurobiology*, vol. 46, no. 2, pp. 393–429, 2012.

[93] J. Nasica-Labouze and N. Mousseau, "Kinetics of amyloid aggregation: a study of the GNNQQNY prion sequence," *PLoS Computational Biology*, vol. 8, no. 11, Article ID e1002782, 2012.

[94] J. Nasica-Labouze, M. Meli, P. Derreumaux, G. Colombo, and N. Mousseau, "A multiscale approach to characterize the early aggregation steps of the amyloid-forming peptide gnnqqny from the yeast prion sup-35," *PLoS Computational Biology*, vol. 7, no. 5, Article ID e1002051, 2011.

[95] J. R. Lewandowski, P. C. A. van der Wel, M. Rigney, N. Grigorieff, and R. G. Griffin, "Structural complexity of a composite amyloid fibril," *Journal of the American Chemical Society*, vol. 133, no. 37, pp. 14686–14698, 2011.

科技部補助專題研究計畫出席國際學術會議心得報告

日期：103 年 10 月 29 日

計畫編號	NSC 102-2320-B-040-019		
計畫名稱	DnaT 與 DNA 結合性質之研究		
出國人員 姓名	黃晟洋	服務機構 及職稱	中山醫學大學/生物醫學科學系/ 副教授
會議時間	103 年 6 月 25 日至 103 年 6 月 27 日	會議地點	日本/橫濱
會議名稱	(中文)第 14 回日本蛋白質科學年會 (英文) The 14th Annual Meeting of the Protein Science Society of Japan		
發表題目	(中文)類黃醇對二氫乳清酸水解酶與尿囊素水解酶之抑制 (英文) Inhibition of dihydroorotase and allantoinase by flavonols		

一、參加會議經過

The 14th Annual Meeting of the Protein Science Society of Japan was held from Jun 25 to 27, 2014 in Yokohama, Japan. As the meeting is mainly based on biophysics for the main shaft, so lots of the participating researchers are in the fields of macromolecular interactions in which I am rather interested. In the lecture sections of Prof. Soichi Wakatsuki, Prof. Kohsuke Inomata, and Prof. Takashi Fujii, I am deeply attracted to learn more about new and efficient strategies to develop my research scenario. I also contributed a post presentation (1P-026) at Day 1 (June 25). The title is “Inhibition of dihydroorotase and allantoinase by flavonols.”

二、與會心得

I would briefly elucidate those summaries of my most impressive lectures as following:

1). The talk by Dr. Noritaka Nishida, entitled “NMR observation of protein-protein interactions in living mammalian cells using a gel-encapsulated bioreactor system”, discusses the latest topics of in-cell NMR for obtaining structural information within living cells. They developed a novel bioreactor system, in which fresh culture medium is supplied to cells encapsulated in thermoreversible Mebiol gels inside the NMR tube, to

overcome the problem, that is, the rapid increase of the dead cells has limited the application of various NMR methods with a long experimental time. They introduced a 9 kDa microtubule-binding domain (Cap-Gly domain 1) into HeLa S3 cells by using the reversible membrane permeabilizing toxin streptolysin O. The binding site of CG1 for the endogenous microtubules was identified as a stronger signal intensity reduction of the NMR signals.

2). The talk by Dr. Atsushi Matsumoto, entitled “Atomic model building from low resolution electron microscopy images”, in which they developed a computational technique to build an atomic model from an electron microscopy (EM) image of a biological molecule. In this technique, many atomic models with different conformations of the molecule are prepared by deforming the X-ray crystal structure or the modeled structure.

3). The talk by Dr. Satoshi Takahashi, entitled “Protein folding dynamics observed by microsecond resolved single molecule fluorescence spectroscopy”, in which they developed a line-confocal microscope combined with fast sample flow system. By imaging the path while flowing samples at fast speed, they can trace a time evolution of fluorescence intensity and FRET efficiency from single molecules. The single molecule measurements at different denaturant concentrations suggested the presence of intermediate states in solution.

4). The talk by Dr. Susumu Uchiyama, entitled “Analytic ultracentrifugation for quantitative intermolecular interaction studies”, in which the protein-protein interaction (PPI) analysis includes the determinations of dissociation constant and stoichiometry is able to be studied by ultracentrifugation. I think that this is a very important and convenient method for us to study the protein-protein interactions, such as DnaT-primosomal protein interactions.

5). The talk by Dr. Atsushi Suenaga, entitled “All-atom molecular dynamics analysis of peptide aggregation”. Non-amyloidogenic protein aggregation is an important issue in several areas of biochemical research and biopharmaceutical industries, particularly in the production and maintenance of protein pharmaceuticals or industrial enzymes. They used molecular dynamics simulation for understanding of peptide aggregation.

三、發表論文全文或摘要

ID: 1P-026

Inhibition of dihydroorotase and allantoinase by flavonols

Huang, Cheng-Yang*
Biomed. Sci., Chung Shan Med. Univ.

Bacterial dihydroorotase (DHOase) and allantoinase (ALLase), members of the cyclic amidohydrolases family, possess very similar binuclear metal centers in the active site. In this study, the inhibition of DHOase and ALLase by chelators, nucleotides, triazole derivatives, flavonols, and the substrates of other cyclic amidohydrolases were investigated. Both DHOase and ALLase were only

slightly inhibited by several chelators, nucleotides, triazole derivatives, and the substrates of other cyclic amidohydrolases. We further investigated the effects of the flavonols myricetin, quercetin, kaempferol, and galangin, on the inhibition of DHOase and ALLase. DHOase and ALLase were both significantly inhibited by kaempferol; kaempferol was a competitive inhibitor for ALLase but an uncompetitive inhibitor for DHOase. A structural study using PatchDock showed that kaempferol was docked in the active site pocket of ALLase but outside the active site pocket of DHOase. These results constituted a first study that naturally occurring product flavonols inhibit the cyclic amidohydrolases, DHOase and ALLase, even more than the substrate analogues. Thus, flavonols may serve as drug leads for designing compounds that target several cyclic amidohydrolases.

四、攜回資料名稱及內容

The 14th Annual Meeting of the Protein Science Society of Japan abstracts book.

科技部補助計畫衍生研發成果推廣資料表

日期:2014/10/29

科技部補助計畫	計畫名稱: DnaT與DNA結合性質之研究
	計畫主持人: 黃晟洋
	計畫編號: 102-2320-B-040-019- 學門領域: 微生物及免疫學

無研發成果推廣資料

102 年度專題研究計畫研究成果彙整表

計畫主持人：黃晟洋	計畫編號：102-2320-B-040-019-
計畫名稱：DnaT 與 DNA 結合性質之研究	

成果項目			量化			單位	備註（質化說明：如數個計畫共同成果、成果列為該期刊之封面故事...等）
			實際已達成數（被接受或已發表）	預期總達成數(含實際已達成數)	本計畫實際貢獻百分比		
國內	論文著作	期刊論文	0	0	100%	篇	
		研究報告/技術報告	0	0	100%		
		研討會論文	0	0	100%		
		專書	0	0	100%		
	專利	申請中件數	0	0	100%	件	
		已獲得件數	0	0	100%		
	技術移轉	件數	0	0	100%	件	
		權利金	0	0	100%	千元	
	參與計畫人力（本國籍）	碩士生	1	1	100%	人次	
		博士生	0	0	100%		
		博士後研究員	0	0	100%		
		專任助理	1	1	100%		
國外	論文著作	期刊論文	5	5	100%	篇	
		研究報告/技術報告	0	0	100%		
		研討會論文	0	0	100%		
		專書	0	0	100%	章/本	
	專利	申請中件數	0	0	100%	件	
		已獲得件數	0	0	100%		
	技術移轉	件數	0	0	100%	件	
		權利金	0	0	100%	千元	
	參與計畫人力（外國籍）	碩士生	0	0	100%	人次	
		博士生	0	0	100%		
		博士後研究員	0	0	100%		
		專任助理	0	0	100%		

其他成果 (無法以量化表達之成果如辦理學術活動、獲得獎項、重要國際合作、研究成果國際影響力及其他協助產業技術發展之具體效益事項等，請以文字敘述填列。)	無

	成果項目	量化	名稱或內容性質簡述
科教處計畫加填項目	測驗工具(含質性與量性)	0	
	課程/模組	0	
	電腦及網路系統或工具	0	
	教材	0	
	舉辦之活動/競賽	0	
	研討會/工作坊	0	
	電子報、網站	0	
	計畫成果推廣之參與（閱聽）人數	0	

科技部補助專題研究計畫成果報告自評表

請就研究內容與原計畫相符程度、達成預期目標情況、研究成果之學術或應用價值（簡要敘述成果所代表之意義、價值、影響或進一步發展之可能性）、是否適合在學術期刊發表或申請專利、主要發現或其他有關價值等，作一綜合評估。

1. 請就研究內容與原計畫相符程度、達成預期目標情況作一綜合評估

■達成目標

□未達成目標（請說明，以 100 字為限）

□實驗失敗

□因故實驗中斷

□其他原因

說明：

2. 研究成果在學術期刊發表或申請專利等情形：

論文：■已發表 □未發表之文稿 □撰寫中 □無

專利：□已獲得 □申請中 ■無

技轉：□已技轉 □洽談中 ■無

其他：（以 100 字為限）

此次計畫之執行共發表 5 篇 SCI 論文(含 1 篇 review article),本人皆為通訊作者

3. 請依學術成就、技術創新、社會影響等方面，評估研究成果之學術或應用價值（簡要敘述成果所代表之意義、價值、影響或進一步發展之可能性）（以 500 字為限）

此次研究除在學術研究上揭露了新的反應機轉,在抗生素研發上亦有新發現的標靶可供進一步探討與開發